

HETEROGENEOUS CATALYST MICROWAVE ASSISTED PRODUCTION OF  
BIODIESEL FUEL FOR COMPRESSION IGNITION ENGINES

NUR HAMZAH SAID

UNIVERSITI TEKNOLOGI MALAYSIA

## UNIVERSITI TEKNOLOGI MALAYSIA

**DECLARATION OF THESIS / POSTGRADUATE COPYRIGHT**

Author's full name : NUR HAMZAH SAID

Date of birth : 11<sup>th</sup> NOVEMBER 1963

Title : HETEROGENEOUS CATALYST MICROWAVE  
ASSISTED PRODUCTION OF BIODIESEL  
FOR COMPRESSION IGNITION ENGINES

Academic Session : 2017/2018

classified as :

- CONFIDENTIAL** (Contains confidential information under the Official Secret Act 1972)\*
- RESTRICTED** (Contains restricted information as specified by the organization where research was done)\*
- OPEN ACCESS** I agree that my thesis to be published as online open access (full text)

I acknowledged that Universiti Teknologi Malaysia reserves the right as follows:

1. The thesis is the property of Universiti Teknologi Malaysia.
2. The Library of Universiti Teknologi Malaysia has the right to make copies for the purpose of research only.
3. The Library has the right to make copies of the thesis for academic exchange.

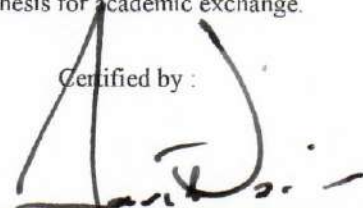
Certified by :


**SIGNATURE**

B2601611

**(NEW IC NO. /PASSPORT NO.)**

Date : 26 JULY 2018


**SIGNATURE OF SUPERVISOR**PROF. IR. DR. FARID NASIR BIN  
HAJI ANI**NAME OF SUPERVISOR**

Date : 26 JULY 2018

NOTES:\* If the thesis is CONFIDENTIAL or RESTRICTED, please attach with the letter from the organization with period and reasons for confidentiality or restriction

We hereby declare that we have read this thesis and in our opinion this thesis is sufficient in terms of scope and quality for the award of the degree of Doctor of Philosophy (Mechanical Engineering)

Signature

:   
.....

Name of Supervisor I : PROF. IR. DR. FARID NASIR BIN HAJI ANI

Date : 26 JULY 2018

Signature

:   
.....

Name of Supervisor II: ASSOC. PROF. DR. MOHD FARID BIN MUHAMAD SAID

Date : 26 JULY 2018

## **BAHAGIAN A – Pengesahan Kerjasama\***

Adalah disahkan bahawa projek penyelidikan tesis ini telah dilaksanakan melalui kerjasama antara \_\_\_\_\_ dengan \_\_\_\_\_

Disahkan oleh:

Tandatangan : ..... Tarikh : .....

Nama : .....

Jawatan : .....

(Cop rasmi)

*\* Jika penyediaan tesis/projek melibatkan kerjasama.*

---

---

## **BAHAGIAN B – Untuk Kegunaan Pejabat Sekolah Kejuruteraan Mekanikal**

Tesis ini telah diperiksa dan diakui oleh:

Nama dan Alamat Pemeriksa Luar : **Prof. Dato' Dr. Rosli bin Abu Bakar**  
**Fakulti Kejuruteraan Mekanikal**  
**Universiti Malaysia Pahang**  
**26600 Pekan**  
**Pahang**

Nama dan Alamat Pemeriksa Dalam : **Prof. Dr. Mazlan bin Abdul Wahid**  
**Sekolah Kejuruteraan Mekanikal**  
**Fakulti Kejuruteraan**  
**Universiti Teknologi Malaysia**  
**Johor Bahru**

Disahkan oleh Naib Pengurus di Sekolah Kejuruteraan Mekanikal:

Tandatangan : ..... Tarikh : .....

Nama : .....

HETEROGENEOUS CATALYST MICROWAVE ASSISTED PRODUCTION OF  
BIODIESEL FUEL FOR COMPRESSION IGNITION ENGINES

NUR HAMZAH SAID

A thesis submitted in fulfilment of the  
requirements for the award of the degree of  
Doctor of Philosophy (Mechanical Engineering)

School of Mechanical Engineering  
Faculty of Engineering  
Universiti Teknologi Malaysia

JULY 2018

I declare that this thesis entitled "*Heterogeneous Catalyst Microwave Assisted Production of Biodiesel Fuel for Compression Ignition Engines*" is the result of my own research except as cited in the references. The thesis has not been accepted for any degree and is not concurrently submitted in candidature of any other degree.

Signature :  .....

Name : NUR HAMZAH SAID

Date : 26 JULY 2018

To my beloved mother and father,  
Hj. Nurmiah Nurdin and H. Muhammad Said Mahmud Suaib (Alm)

To my honored mother and father in law,  
Hj. Syatiah Ahmad and H. Muhammad Djafar Kampo

To my lovely wife and sons  
Haryanti Djafar  
Muhammad Ihsan Shalihin  
Muhammad Ikram Fauzan  
Muhammad Aiman Syawal

## ACKNOWLEDGEMENTS

First of all, Alhamdulillah, I am grateful to Allah s.w.t. for giving me the will, strength, patience and health so that I could complete this research. Special thanks go to my helpful supervisor Professor Ir. Dr. Farid Nasir bin Hj. Ani and Assoc. Prof. Dr. Mohd Farid Bin Muhamad Said for their supervision, valuable and critical ideas, comments and guidance throughout my research.

I would like to thank Dr. H. Syahrul Yasin Limpo, SH, M.Si, MH as Governor of South Sulawesi, Indonesia for the scholarship to attend the Faculty of Mechanical Engineering Universiti Teknologi Malaysia.

My deepest thanks to my wonderful mother, Hj. Nurmiah, my lovely wife Haryanti Djafar and my sons, who have always given me encouragement and support in completing this thesis. I am also grateful to my brothers, sister, and other family members for their love, constant support, understanding, and caring for all these years.

I am also indebted to my fellow postgraduate students and colleagues especially Mukhamadi Nurhadi, Muhammad Anshar, Rusdi Nur, Ahmad Zubair Sultan, Ahmad Haya, Encik Mohammad, Puan Mahanum, Puan Rubiah and Mr. Abioye who have provided assistance on various occasions. My thanks also go to all the technicians from the Combustion Laboratory and Automotive Laboratory for their valued assistance during my experimental work. My sincere appreciation also extends to all my colleagues and others who have provided assistance directly or indirectly throughout this research. Their views and tips are useful indeed. Unfortunately, it is not possible to list all of them in this limited space.



## ABSTRACT

Biodiesel is a viable alternative fuel used in compression ignition (CI) engines because of its non-toxicity, biodegradability and renewability. Raw material and production process are factors that affect the cost of biodiesel. The use of waste cooking oil (WCO) as the fuel feedstock and microwave heating technology is able to reduce the cost of biodiesel. In this study a continuous flow transesterification of WCO by microwave irradiation for biodiesel production using calcium oxide (CaO) from cockle shell as the catalyst has been investigated. The catalyst was packed inside a plastic container that is mounted on a stirrer shaft and inserted inside the reactor. Response surface methodology (RSM) and Box–Behnken design were employed to study the relationships of power input, stirrer speed and liquid hourly space velocity (LHSV) on waste cooking oil methyl ester (WCOME) conversion. The WCOME produced was tested on a small-unmodified direct injection diesel engine to investigate the performance and exhaust emissions and then compared with the commercial diesel fuel (Petron diesel max, PDM) and commercial biodiesel (palm oil methyl ester, POME). Experimental measurements of engine performances, exhaust emissions, cylinder pressure and heat rate release were performed as a function of engine load at a constant engine speed. The optimum conditions of the transesterification of WCO have been found to be power input 445 W, stirrer speed 380 rpm and LHSV 71.5 h<sup>-1</sup> and yielded a maximum WCOME conversion of 72.5%. The performance, emission and combustion of a one-cylinder Yanmar Diesel engine L70 using PDM containing 7% methyl ester, two blends of PDM with POME and two blends of PDM with WCOME equivalent to B10 and B20, respectively, were investigated. The performance, emission and combustion test results of five test fuel PDM, BP10, BP20, BW10 and BW20 were then compared with the simulation results by using GT-SUITE V6.0 software. The experimental results indicated that using POME and WCOME blends resulted in increment in break specific fuel consumption (BSFC) up to 5.9% and reduction in brake thermal efficiency (BTE) up to 29.3% compared to PDM. These biodiesel blends also increased NO<sub>x</sub> emissions and decreased CO<sub>2</sub>, CO and uHC emissions for all engine loads at constant speed of 2500 rpm. Both experiment and simulation of the maximum cylinder pressure increase significantly with the increase of engine load for each test fuel. All the simulation graphs show the similar trend compared to experiment.

## ABSTRAK

Biodiesel adalah bahan bakar alternatif yang boleh digunakan dalam enjin pencucuhan mampatan (CI) kerana tidak bertoksin, mudah terurai dan boleh diperbaharui. Bahan mentah dan proses penghasilan adalah faktor yang mempengaruhi kos biodiesel. Penggunaan sisa minyak masak (WCO) sebagai bahan bakar dan teknologi pemanasan gelombang mikro mampu mengurangkan kos pengeluaran biodiesel. Dalam kajian ini transesterifikasi aliran terus oleh WCO menggunakan sinaran gelombang mikro untuk menghasilkan biodiesel menggunakan kalsium oksida (CaO) dari kulit kerang sebagai mangkin telah dikaji. Mangkin dibungkus dalam bekas plastik yang diletakkan pada besi pengaduk dan dimasukkan ke dalam reaktor. *Response surface methodology (RSM)* dan reka bentuk Box-Behnken digunakan untuk mengkaji hubungan antara masukan kuasa, kelajuan pengaduk dan halaju ruang muatan cecair (LHSV) dalam penukaran metil ester sisa minyak masak (WCOME). WCOME yang terhasil diuji dalam enjin diesel suntikan langsung yang tidak diubahsuai untuk mengkaji prestasi dan pelepasan ekzos dan kemudian dibandingkan dengan bahan api diesel komersial (Petron diesel max, PDM) dan biodiesel komersial (metil ester minyak sawit, POME). Kajian pengukuran prestasi enjin, pelepasan ekzos, tekanan silinder dan pelepasan kadar haba dilakukan sebagai fungsi beban enjin pada kelajuan enjin yang tetap. Keadaan optimum bagi transesterifikasi WCO telah dikenalpasti pada masukan kuasa 445 W, kelajuan pengaduk 380 rpm dan LHSV 71.5 h<sup>-1</sup> dan menghasilkan WCOME maksimum sebanyak 72.5%. Prestasi, pelepasan dan pembakaran satu silinder enjin Diesel Yanmar L70 menggunakan PDM yang mengandungi 7% metil ester, dua adunan PDM dan POME dan dua adunan PDM dan WCOME bersamaan dengan B10 dan B20 masing-masing dikaji. Prestasi pelepasan dan pembakaran lima bahan uji PDM, BP10, BP20, BW10 dan BW20 kemudian dibandingkan dengan hasil simulasi dengan menggunakan perisian GT-SUITE V6.0. Keputusan eksperimen menunjukkan bahawa penggunaan campuran POME dan WCOME menghasilkan peningkatan penggunaan bahan bakar khusus (BSFC) sehingga 5.9% dan pengurangan dalam kecekapan terma brek (BTE) sehingga 29.3% berbanding dengan PDM. Campuran biodiesel ini juga meningkatkan pelepasan NO<sub>x</sub> dan mengurangkan pelepasan CO<sub>2</sub>, CO dan uHC untuk semua beban enjin pada kelajuan tetap 2500 rpm. Kedua-dua kajian dan simulasi tekanan silinder maksimum meningkat dengan ketara dengan peningkatan beban enjin, bagi setiap bahan uji. Semua simulasi grafik menunjukkan tren yang sama berbanding dengan ujikaji.

## TABLE OF CONTENTS

CHAPTER	TITLE	PAGE
	DECLARATION	iii
	DEDICATION	vi
	ACKNOWLEDGEMENTS	viii
	ABSTRACT	ix
	ABSTRAK	x
	TABLE OF CONTENTS	xi
	LIST OF TABLES	xvi
	LIST OF FIGURES	xix
	LIST OF SYMBOLS	xxvi
	LIST OF ABBREVIATIONS	xxviii
	LIST OF APPENDICES	xxxii
<b>1</b>	<b>INTRODUCTION</b>	<b>1</b>
	1.1 Background of Study	1
	1.2 Problem Statement	3
	1.3 Objectives	6
	1.4 Scope of the Study	7
	1.5 Organization of Thesis	8
<b>2</b>	<b>LITERATURE REVIEW</b>	<b>9</b>
	2.1 Biodiesel from Transesterification Process of Waste Cooking Oil	9
	2.1.1 Heterogeneous Catalyst	19
	2.1.1.1 Catalyst Preparation	21
	2.1.1.2 Catalyst Characterization	22

2.1.2	Biodiesel Production from Waste Cooking Oil Using Heterogeneous Catalyst	24
2.1.3	Continuous Production of Biodiesel	33
2.1.4	Reactor	35
2.1.4.1	Space-time and Space Velocity	35
2.1.4.2	Microwave Irradiation	36
2.1.5	Design of Experiments	37
2.2	Utilization of Biodiesel from Waste Cooking Oil in Diesel Engines	37
2.2.1	Diesel Engine Performance	38
2.2.2	Diesel Engine Combustion	41
2.2.3	Diesel Engine Emission	41
2.2.3.1	Carbon Monoxide	43
2.2.3.2	Carbon Dioxide	44
2.2.3.3	Unburned Hydrocarbons	45
2.2.3.4	Nitrogen Oxides	46
2.3	Modelling Direct Injection Diesel Engine in GT-SUITE	47
2.3.1	Overview	47
2.3.2	Mathematical Modelling	49
<b>3</b>	<b>RESEARCH METHODOLOGY</b>	<b>50</b>
3.1	Transesterification Process of Waste Cooking Oil	52
3.1.1	Materials and Methods	52
3.1.2	Experimental Design and Optimization	53
3.1.3	Experimental Set-up and Procedure	57
3.2	Characterization of Biodiesel Fuel	59
3.2.1	Determination of the Acidity Value and Free Fatty Acid of the Oil	60
3.2.2	Determination of Fatty Acids Conversion	60
3.3	Diesel Engine Test	61
3.3.1	Test Fuels	61
3.3.2	Experiment Set-up and Procedure	62

3.3.2.1	Engine Speed and Torque Measurement	64
3.3.2.2	Air Flow Measurement	65
3.3.2.3	Fuel Flow Measurement	66
3.3.2.4	Temperature Measurement	67
3.3.2.5	In-cylinder Pressure and Crank Angle Measurement	68
3.3.2.6	Data acquisition	69
3.3.2.7	Gas Emission Analyser and Exhaust Smoke	69
3.3.2.8	Support Measurement Tools	70
3.3.3	Experimental Method	70
3.3.4	Data Analysis	71
3.3.4.1	Engine Test Parameters	71
3.3.4.2	Analysis of Gaseous Emissions	74
3.3.4.3	Heat Release Rate Analysis	75
3.4	Simulation Methodology	79
3.4.1	Introduction	79
3.4.2	Gas Dynamic – One-Dimensional Model	80
3.4.3	Flows in Cylinder Valve	82
3.4.4	The Engine Cylinder	84
3.4.5	Injection and Combustion	87
3.4.6	Input Parameters for Simulation	88
3.4.6.1	Defined value for environment and pipe objects	88
3.4.6.2	Fuel Injector	89
3.4.6.3	Engine	90
3.4.6.4	Fuel properties	91
3.4.6.5	Case Setup	92
<b>4</b>	<b>RESULT AND DISCUSSION</b>	<b>96</b>
4.1	Catalyst Characterisation	96

4.2	Transesterification of Waste Cooking Oil Using Calcium Oxide Catalyst	97
4.2.1	Temperature Profile	97
4.2.2	Physical Properties	98
4.2.3	Chemical Properties	99
4.2.4	Model Fitting and Statistical Analysis of Biodiesel Conversion	101
4.2.4.1	ANOVA and mathematical model for time collected to space-time ratio = 1/3	103
4.2.4.2	ANOVA and Mathematical Model for Time Collected to Space-time Ratio= 2/3	108
4.2.4.3	ANOVA and Mathematical Model for Time Collected to Space-time Ratio = 1	112
4.2.5	Optimisation and Validation	116
4.3	Diesel Engine Test	117
4.3.1	Fuel Test	117
4.3.2	Diesel Engine Performance	118
4.3.2.1	Brake Specific Fuel Consumption	118
4.3.2.2	Brake Thermal Efficiency	119
4.3.2.3	Engine Performance Statistical Analysis	120
4.3.2.4	Air Fuel Ratio	121
4.3.3	Diesel Engine Exhaust Emissions	122
4.3.3.1	Carbon Monoxide Emissions	122
4.3.3.2	Carbon Dioxide Emissions	124
4.3.3.3	Unburned Hydrocarbon Emissions	125
4.3.3.4	Oxides of Nitrogen Emissions	126
4.3.4	Combustion Characteristics	128
4.3.4.1	Pressure in Cylinder and Heat Release Rate	128

4.3.4.2	Burned Fuel Fraction and Combustion Duration	137
4.3.5	Comparison with Simulation	141
<b>5</b>	<b>CONCLUSIONS AND RECOMENDATIONS</b>	<b>169</b>
5.1	Conclusions	169
5.2	Recommendations for Future Work	170
	<b>REFERENCES</b>	<b>171</b>
	<b>APPENDICES A - O</b>	<b>181-213</b>

## LIST OF TABLES

TABLE NO.	TITLE	PAGE
2.1	ASTM standards of biodiesel and diesel fuels (Demirbas, 2008)	10
2.2	Comparison of properties between virgin soybean oil and waste cooking oil (Birla <i>et al.</i> , 2012)	14
2.3	Selected physical properties of waste cooking oil	15
2.4	Percentage of fatty acid composition in waste cooking oil	16
2.5	Comparison of properties of waste cooking oil, biodiesel from waste cooking oil and commercial diesel fuel (Demirbas, 2009; Yaakob <i>et al.</i> , 2013)	17
2.6	Properties of diesel and biodiesel fuel and biodiesel produced from waste cooking oil according to ASTM standards (Birla <i>et al.</i> , 2012)	18
2.7	Characterization of heterogeneous testing catalyst in waste cooking oil transesterification	23
2.8	Selected heterogeneous catalyst used in biodiesel production of waste cooking oil and its condition and performance	26
2.9	The advantages and drawbacks of heterogeneous catalyst used in transesterification of waste cooking oil (Borges and Díaz, 2013; M. K. Lam <i>et al.</i> , 2010)	30
3.1	Independent variables in transesterification of waste cooking oil used for Box–Behnken experiment design	53



3.2	Simplification of independent variables in the transesterification of waste cooking oil used for Box–Behnken experiment design	55
3.3	Proportion blends in fuel test	62
3.4	Yanmar L70N6-engine specifications made in Italy	63
3.5	The components that can be measured by EMS model 5002	70
3.6	Defined value for environment and pipe objects	88
3.7	Defined value intake and exhaust for valve	89
3.8	Defined value for injector	89
3.9	Defined value for engine geometry and inertia	90
3.10	Enthalpy constant for all fuels	91
3.11	Transport properties	91
3.12	Defined value for fuel property	93
3.13	Case setup	94
4.1	Physico-chemical properties of waste cooking oil and waste cooking oil methyl ester	99
4.2	Fatty acid composition of biodiesel from waste cooking oil	100
4.3	Experimental data of waste cooking oil transesterification for three level of time collected to space-time ratio	102
4.4	Box-Behnken design matrix of three-factor-three levels with experimental result for time collected to space-time ratio = 1/3	103
4.5	Table analysis of variance (ANOVA) for response surface quadratic model for conversion at time collected to space-time ratio =1/3	104
4.6	Responses for transesterification of WCOME at time collected to space-time ratio =1/3	106
4.7	Box-Behnken design matrix of three-factor-three level with experimental result for time collected to space-time ratio = 2/3	108

4.8	Analysis of variance (ANOVA) for response surface quadratic model for conversion at time collected to space-time ratio =2/3	109
4.9	Box Behnken design matrix of three-factor-three level with experimental result for time collected to space-time ratio = 1	112
4.10	Table analysis of variance for response surface quadratic model for conversion at time collected to space-time ratio =1	113
4.11	Properties of test fuels	117

## LIST OF FIGURES

FIGURE NO.	TITLE	PAGE
2.1	Fatty acid composition of waste cooking oil before and after transesterification	18
2.2	Schematic flow diagram of biodiesel production from WCO (Maddikeri <i>et al.</i> , 2012)	19
2.3	Classification of catalyst (Chouhan and Sarma, 2011)	21
2.4	Continuous heterogeneous catalyzed process diagram (Hillion <i>et al.</i> , 2003)	25
2.5	Ideal reactor type (Levenspiel, 1999)	35
2.6	Average mission impact of biodiesel fuel in heavy-duty highway engine (United States Environmental Protection Agency (EPA), 2002)	42
3.1	The research methodology flowchart	51
3.2	The experiment design and optimization of conversion of WCO biodiesel flowchart	56
3.3	The experimental set-up for single step transesterification continues process with catalyst container stirrer	58
3.4	Schematic diagram of the engine test setup	63
3.5	Engine was coupled to an Eddy current dynamometer on test-bed	65
3.6	The 19" Magtrol DSP6001 Dynamometer Controller	65
3.7	Fuel flow measurement using burette method	67
3.8	Temperature scanner	68
3.9	Typical combustion phases in DI engine heat release rate diagram (Heywood, 1988)	76

3.10	Direct Injection diesel engine model using one dimensional model	81
3.11	Valve lift profile	83
3.12	Cylinder geometry	85
3.13	Four stroke cycle (Challen and Baranescu, 1999)	87
3.14	Graph of valve lift of inlet and exhaust versus crank angle (Said, 2006)	90
4.1	The XRD of the cockle shell calcined at 900 °C for 3.5 h	97
4.2	Typical temperature profile power input 180 W and 450 W for single step transesterification continuous process	98
4.3	Typical analysis of fatty acid methyl ester from biodiesel of waste cooking oil using Gas Chromatography Mass Spectrometry	100
4.4	3 D response surface showing the power input speed, stirrer speed and <i>LHSV</i> on WCOME conversion at time collected to space-time ratio = 1/3	107
4.5	3 D response surface showing the power input speed, stirrer speed and <i>LHSV</i> on WCOME conversion at time collected to space-time ratio = 2/3	111
4.6	3 D response surface showing the power input speed, stirrer speed and <i>LHSV</i> on WCOME conversion at time collected to space-time ratio = 1	115
4.7	The variation of brake specific fuel consumption with brake mean effective pressure at five different loads	119
4.8	The variation of brake mean effective pressure with engine brake thermal efficiency	120
4.9	The variation of brake mean effective pressure with air fuel ratio	122
4.10	The variation of carbon monoxide with brake mean effective pressure	123
4.11	The variation of brake specific carbon monoxide with brake mean effective pressure	123

4.12	The variation of carbon dioxide with brake mean effective pressure	124
4.13	The variation of brake specific carbon dioxide with brake mean effective pressure	125
4.14	The variation of unburned hydrocarbon with engine brake mean effective pressure	126
4.15	The variation of brake specific unburned hydrocarbon with engine brake mean effective pressure	126
4.16	The variation of oxide of nitrogen with engine brake mean effective pressure	127
4.17	The variation of brake specific oxide of nitrogen with engine brake mean effective pressure	127
4.18	The profiles of pressure cylinder against crank angle for all fuels at brake mean effective pressure 1.18 bar	130
4.19	The profiles of pressure cylinder against crank angle for all fuels at brake mean effective pressure 1.96 bar	130
4.20	The profiles of pressure cylinder against crank angle for all fuels at brake mean effective pressure 2.75 bar	131
4.21	The profiles of pressure cylinder against crank angle for all fuels at brake mean effective pressure 3.53 bar	131
4.22	The profiles of pressure cylinder against crank angle for all fuels at brake mean effective pressure 3.93 bar	132
4.23	The comparison Petron Diesel Max and biodiesel blends on peak cylinder pressure	132
4.24	The profiles of heat release rate against crank angle at brake mean effective pressure at 1.18 bar	134
4.25	The profiles of heat release rate against crank angle at brake mean effective pressure at 1.96 bar	135
4.26	The profiles of heat release rate against crank angle at brake mean effective pressure at 2.75 bar	135
4.27	The profiles of heat release rate against crank angle at brake mean effective pressure at 3.53 bar	136

4.28	The profiles of heat release rate against crank angle at brake mean effective pressure at 3.93 bar	136
4.29	The peak heat release rate against brake mean effective pressure at various fuels	137
4.30	The profile of burned fuel fraction at brake mean effective pressure 1.18 bar	138
4.31	The profile of burned fuel fraction at brake mean effective pressure 1.96 bar	138
4.32	The profile of burned fuel fraction at brake mean effective pressure 2.75 bar	139
4.33	The profile of burned fuel fraction at brake mean effective pressure 3.53 bar	139
4.34	The profile of burned fuel fraction at brake mean effective pressure 3.93 bar	140
4.35	The comparison PDM and biodiesel blends on combustion duration	140
4.36	Experiment and simulated data of brake specific fuel consumption and brake thermal efficiency versus brake mean effective pressure for PDM fuel	141
4.37	Experiment and simulated data of brake specific fuel consumption and brake thermal efficiency versus brake mean effective pressure for BP10 fuel	142
4.38	Experiment and simulated data of brake specific fuel consumption and brake thermal efficiency versus brake mean effective pressure for BP20 fuel	142
4.39	Experiment and simulated data of brake specific fuel consumption and brake thermal efficiency versus brake mean effective pressure for BW10 fuel	143
4.40	Profiles of pressure in cylinder against crank angle using Petron Diesel Max fuel at BMEP=1.18 bar	145
4.41	Profiles of pressure in cylinder against crank angle at various brake mean effective pressure using Petron Diesel Max fuel at BMEP=1.96 bar	145

4.42	Profiles of pressure in cylinder against crank angle at various brake mean effective pressure using Petron Diesel Max fuel at BMEP= 2.75 bar	146
4.43	Profiles of pressure in cylinder against crank angle at various brake mean effective pressure using Petron Diesel Max fuel at BMEP= 3.53 bar	146
4.44	Profiles of pressure in cylinder against crank angle at various brake mean effective pressure using Petron Diesel Max fuel at BMEP=3.93 bar	147
4.45	Profiles of pressure in cylinder against crank angle at 1.18 bar brake mean effective pressure using BP10 fuel	147
4.46	Profiles of pressure in cylinder against crank angle at 1.96 bar brake mean effective pressure using BP10 fuel	148
4.47	Profiles of pressure in cylinder against crank angle at 2.75 bar brake mean effective pressure using BP10 fuel	148
4.48	Profiles of pressure in cylinder against crank angle at 3.53 bar brake mean effective pressure using BP10 fuel	149
4.49	Profiles of pressure in cylinder against crank angle at 3.93 bar brake mean effective pressure using BP10 fuel	149
4.50	Profiles of pressure in cylinder against crank angle at 1.18 bar brake mean effective pressure using BP20 fuel	150
4.51	Profiles of pressure in cylinder against crank angle at 1.96 bar brake mean effective pressure using BP20 fuel	150
4.52	Profiles of pressure in cylinder against crank angle at 2.75 bar brake mean effective pressure using BP20 fuel	151
4.53	Profiles of pressure in cylinder against crank angle at 3.53 bar brake mean effective pressure using BP20 fuel	151
4.54	Profiles of pressure in cylinder against crank angle at 3.93 bar brake mean effective pressure using BP20 fuel	152
4.55	Profiles of pressure in cylinder against crank angle at 1.18 bar brake mean effective pressure using BW10 fuel	152
4.56	Profiles of pressure in cylinder against crank angle at 1.96 bar brake mean effective pressure using BW10 fuel	153

4.57	Profiles of pressure in cylinder against crank angle at 2.75 bar brake mean effective pressure using BW10 fuel	153
4.58	Profiles of pressure in cylinder against crank angle at 3.53 bar brake mean effective pressure using BW10 fuel	154
4.59	Profiles of pressure in cylinder against crank angle at 3.93 bar brake mean effective pressure using BW10 fuel	154
4.60	Profiles of pressure in cylinder against crank angle at 1.18 bar brake mean effective pressure using BW20 fuel	155
4.61	Profiles of pressure in cylinder against crank angle at 1.96 bar brake mean effective pressure using BW20 fuel	155
4.62	Profiles of heat release rate against crank angle at 1.18 bar brake mean effective pressure using PDM fuel	157
4.63	Profiles of heat release rate against crank angle at 1.96 bar brake mean effective pressure using PDM fuel	158
4.64	Profiles of heat release rate against crank angle at 2.75 bar brake mean effective pressure using PDM fuel	158
4.65	Profiles of heat release rate against crank angle at 3.53 bar brake mean effective pressure using PDM fuel	159
4.66	Profiles of heat release rate against crank angle at 3.93 bar brake mean effective pressure using PDM fuel	159
4.67	Profiles of heat release rate against crank angle at 1.18 bar brake mean effective pressure using BP10 fuel	160
4.68	Profiles of heat release rate against crank angle at 1.96 bar brake mean effective pressure using BP10 fuel	160
4.69	Profiles of heat release rate against crank angle at 2.75 bar brake mean effective pressure using BP10 fuel	161
4.70	Profiles of heat release rate against crank angle at 3.53 bar brake mean effective pressure using BP10 fuel	161
4.71	Profiles of heat release rate against crank angle at 3.93 bar brake mean effective pressure using BP10 fuel	162
4.72	Profiles of heat release rate against crank angle at 1.18 bar brake mean effective pressure using BP20 fuel	162



4.73	Profiles of heat release rate against crank angle at 1.96 bar brake mean effective pressure using BP20 fuel	163
4.74	Profiles of heat release rate against crank angle at 2.75 bar brake mean effective pressure using BP20 fuel	163
4.75	Profiles of heat release rate against crank angle at 3.53 bar brake mean effective pressure using BP20 fuel	164
4.76	Profiles of heat release rate against crank angle at 3.93 bar brake mean effective pressure using BP20 fuel	164
4.77	Profiles of heat release rate against crank angle at 1.18 bar brake mean effective pressure using BW10 fuel	165
4.78	Profiles of heat release rate against crank angle at 1.96 bar brake mean effective pressure using BW10 fuel	165
4.79	Profiles of heat release rate against crank angle at 2.75 bar brake mean effective pressure using BW10 fuel	166
4.80	Profiles of heat release rate against crank angle at 3.53 bar brake mean effective pressure using BW10 fuel	166
4.81	Profiles of heat release rate against crank angle at 3.93 bar brake mean effective pressure using BW10 fuel	167
4.82	Profiles of heat release rate against crank angle at 1.18 bar brake mean effective pressure using BW20 fuel	167
4.83	Profiles of heat release rate against crank angle at 1.96 bar brake mean effective pressure using BW20 fuel	168

## LIST OF SYMBOLS

$A_o$	-	Orifice area
$A_T$	-	Curtain Area
$\text{CH}_4$	-	Methane
$C_D$	-	Orifice discharge coefficient
$D$	-	Valve head diameter
$d_o$	-	Orifice plate diameter (airbox)
$g$	-	Acceleration due to gravity
$H$	-	Height
$L$	-	Valve lift
$L$	-	Connecting rod length
$M$	-	Mass
$\dot{i}$	-	Air mass flow rate
$\dot{i}$	-	Exhaust mass flow rate
$\dot{i}$	-	Fuel mass flow rate
$N$	-	Engine speed
$N_s$	-	Stirrer speed
$n_c$	-	Number of cylinder
$N_m$	-	Minimum engine speed at which measurements are required
$P$	-	Pressure
$P_a$	-	Ambient pressure
$P_m$	-	Power input of microwave
$\bar{P}$	-	Average cylinder pressure
$p_{sr}$	-	Standard reference saturated water vapor pressure
$p_{st}$	-	Ambient saturated water vapor pressure during test
$p_t$	-	Ambient total barometric pressure during test

$Q$	-	Heat release rate
$Q_{HV}$	-	Heating value
$R$	-	Specific gas constant for air
$rel_H$	-	Relative humidity
$S$	-	Stroke
$S_m$	-	Standard error of the mean
$T$	-	Temperature
$T$	-	Torque
$T_a$	-	Atmospheric temperature
$T_t$	-	Ambient air thermodynamic temperature during test
$\bar{T}$	-	Average cylinder temperature
$V_c$	-	Clearance volume
$V_c$	-	Catalyst Volume
$V_d$	-	Engine displacement volume
$V_s$	-	Swept volume
$\dot{W}$	-	Rate of work
$W_c$	-	Catalyst weight
$\rho$	-	Density
$\rho_c$	-	Catalyst density
$\tau$	-	The space-time
$\tau_i$	-	Ignition delay
$\Phi$	-	Equivalence ratio
$\Omega$	-	Non-dimensional crank angle
$x_D$	-	Diffusion burning
$x_P$	-	Pre-mix burning
$\Phi$	-	Engine operating equivalence ratio
$\Theta$	-	Angle
$\rho_a$	-	Air density
$\Delta p$	-	Pressure drop across the orifice plate

## LIST OF ABBREVIATIONS

AD	-	Analogue to Digital
AFR	-	Air Fuel Ratio
AR	-	Analytical Reagent
ASTM	-	American Society for Testing and Material
ANOVA	-	Analysis of variance
B10	-	Biodiesel (10%)
B20	-	Biodiesel (20%)
BP	-	Brake Power
BP10	-	POME equivalent to B10
BP20	-	POME equivalent to B20
BW10	-	WCOME equivalent to B10
BW20	-	WCOME equivalent to B20
BBD	-	Box-Behnken Design
BDC	-	Bottom Dead Center
BDUR	-	Burn Duration
BET	-	Brunauer- Emmer-Teller
BMEP	-	Brake Mean Effective Pressure
BSCO	-	Brake Specific Carbon Monoxide
BSCO <sub>2</sub>	-	Brake Specific Carbon Dioxide
BSFC	-	Brake Specific Fuel Consumption
BSHC	-	Brake Specific Hydrocarbon
BSNO <sub>x</sub>	-	Brake Specific Nitrogen Oxides

BTE	-	Brake Thermal Efficiency
C	-	Conversion
CA	-	Crank Angle
CAI	-	Crank Angle Ignition
CaO	-	Calcium Oxide
CFD	-	Computational Fluid Dynamic
CO	-	Carbon Monoxide
CO <sub>2</sub>	-	Carbon Dioxide
CR	-	Compression ratio
CSR	-	Time collection to space time ratio
CSTR	-	Continuously Stirred Tank Reactor
DAQ	-	Data Acquisition System
DI	-	Direct Injection
DTA	-	Differential Thermal Analysis
EDAX	-	Energy Dispersive Analysis
EDX	-	Energy Dispersive X-ray Spectrophotometer
EGR	-	Exhaust Gas Recirculation
EU	-	European Union
EVC	-	Exhaust Valve Closing
EVO	-	Exhaust Valve Opening
F	-	Flowrate
<i>g</i>	-	Gram
FAME	-	Fatty Acid Methyl Esters
FESEM	-	Field-Emission Scanning Electron Microscope
FFA	-	Free Fatty Acid
FID	-	Flame-Ionization Detector

FTIR	-	Fourier Transform Infra-Red
GC	-	Gas Chromatography
GCMS	-	Gas Chromatography Mass Spectrometry
HC	-	Hydrocarbon
HRR	-	Heat Release Rate
IC	-	Internal Combustion
IDI	-	Indirect Injection
IVO	-	Intake Valve Opening
JCPDS	-	Joint Committee on Powder Diffraction Standards
IVC	-	Intake Valve Closing
LHSV	-	Liquid Hourly Space Velocity
ml	-	Millilitre
min	-	Minute
NO	-	Nitric Oxide
N	-	Speed
NO <sub>2</sub>	-	Nitrogen Dioxide
NO <sub>x</sub>	-	Nitrogen Oxides
O <sub>2</sub>	-	Oxygen
PBDF	-	Petroleum Based Diesel Fuel
POME	-	Palm Oil Methyl Ester
PDM	-	Petron Diesel Max
PM	-	Particulate Matter
ppm	-	Parts per Million
RMS	-	Response Surface Methodology
rpm	-	Revolution Per Minute
uHC	-	Unburned Hydrocarbon

SEM	-	Scanning Electron Microscopy
SEM-EDS	-	Scanning Electron Microscopy - Energy Dispersive Spectra
T	-	Torque
TCD	-	Thermal conductivity detector
TDC	-	Top Dead Centre
TGA	-	Thermogravimetric analysis
THC	-	Total Hydrocarbon
TPD	-	Temperature-programmed desorption
WCO	-	Waste Cooking Oil
WCOME	-	Waste Cooking Oil Methyl Ester
XPS	-	X-ray Photoelectron Spectroscopy
XRD	-	X-ray Diffraction
XRF	-	X-ray Fluorescence

## LIST OF APPENDICES

APPENDIX	TITLE	PAGE
A	Titration of waste cooking oil	181
B	Test report of waste cooking oil	182
C	Biodiesel Production Experimental Apparatus	183
D	Reactor and Stirrer Drawing	185
E	Peristaltic Pump Calibration	186
F	Equipment Used for Biodiesel Processing and Measuring of Raw Material and Biodiesel Product	187
G	Standard JCPDS Card No.00-021-0917	191
H	Fatty acid composition from biodiesel waste cooking oil	192
I	Petron Diesel Max (PDM) specification	195
J	Biodiesel from palm oil (POME) specification	196
K	Standard Hexadecanoid Calibration	197
L	Experimental Procedure of Diesel Engine Test	198
M	Experimental Data of Engine Performance Test	201
N	Analysis Result Data of Engine Performance Test	208
O	List of Publication	213



# CHAPTER 1

## INTRODUCTION

### 1.1 Background of Study

In recent years, the number of prime movers for power plant and transformation, especially ones that use diesel fuel as fuel, is increasing rapidly. Diesel fuel has the biggest share among the users of petroleum fuels and this ratio continues to increase annually. An alternative diesel fuel is becoming more attractive because of the increasing utilization of diesel fuel and the generation of atmospheric pollution. In addition, alternative diesel fuels are locally available, renewable and environmentally- friendly (Balat and Balat, 2008; Canakci and Sanli, 2008; Demirbas, 2008).

Biodiesel is an alternative diesel fuel that is produced using raw materials derived from renewable biological sources such as vegetable oils and animal fats. The process of producing biodiesel involves the use of modern technology and skilled researchers. This is related to the issue of rising fuel prices derived from petroleum and environmental pollution. Also of interest to researchers is the increasing use of fuel, so the risk of environmental pollution is also increasing. The researchers stated that the use of biodiesel blend fuels could reduce global warming levels such as carbon dioxide CO<sub>2</sub> (Balat and Balat, 2010).

The waste cooking oil (WCO), a non-edible vegetable oil, was used as raw material to produce an alternative fuel for diesel engine (Pugazhvadivu and Jeyachandran, 2005). Compared with neat vegetable oils, WCO is much cheaper.

Utilization of waste cooking oil is very promising to be used as a substitute for vegetable oils in the process of biodiesel production (Kulkarni and Dalai, 2006). From environmental point of view, the use of WCO might decrease disposal problem.

Transesterification reaction using microwave irradiation technology offers a reliable, minimum energy consumption, powerful heat source with modern equipment operating at over 90% efficiency. The application of microwave irradiation technology is also environmentally friendly compared to conventional heating in various chemical processes (Choedkiatsakul *et al.*, 2015; M. K. Lam *et al.*, 2010; S. S. Lam *et al.*, 2010).

Several works have been conducted using continuous production of biodiesel from WCO in a packed-bed catalytic reactor in a recirculation system (Borges and Díaz, 2013) and the continuous-flow transesterification using a rotating packed bed (RPB) using a rotating packed bed (Chen *et al.*, 2010).

A number of researchers have tested diesel engines using WCO and its blends as fuel (Abu-Jrai *et al.*, 2011; Kalam *et al.*, 2011; Ozsezen *et al.*, 2009; Senthil Kumar and Jaikumar, 2014).

However, studies of continuous flow transesterification WCO using microwave technology in biodiesel production, where solid catalyst was put in a stirring packed-bed reactor, have never been published. Therefore, it is interesting to obtain and characterize biodiesel fuel with WCO as feedstock in continuous flow transesterification reaction using heterogeneous catalyst on microwave irradiation technology at laboratory scale. Also of interest is the application of the Box–Behnken response surface methodology for optimizing the biodiesel from production. The performance and emission of direct injection diesel engine using several proportions of biodiesel fuel WCO methyl ester and commercial Palm Oil methyl ester with commercial diesel fuel was performed.

## 1.2 Problem Statement

Worldwide demand for energy has increased in recent decades. Most of the world's energy demand is met by conventional energy sources known as oil-based fuels such as coal, petroleum, and natural gas. These oil-based fuels can only be found in certain regions of the world in limited reserves (Demirbas, 2008). In addition, environmental issues need to be considered seriously. Therefore, the use of an alternative diesel fuel that is locally available, renewable and environmentally friendly, is necessary and important (Balat and Balat, 2008; Canakci and Sanli, 2008).

Biodiesel is one of the alternative fuels to replace ordinary petroleum fuels that are still in use, having biodegradable and renewable properties. This biodiesel is a mono alkyl ester of long chain fatty acids whose raw materials are sourced from renewable feed oil (edible or inedible oil), animal fat, waste materials and algae (Marchetti, 2011; No, 2011).

Compared to petroleum diesel, biodiesel fuel has several advantages. In terms of its environmental use, biodiesel has lower pollutant emissions, lower toxicity, no particulate pollutants, biodegradable and contains almost no sulphur contaminants. As for technical aspects, this biodiesel has a higher cetane number than petroleum diesel, better CO<sub>2</sub> combustion, no aromatics, can improve engine lubrication, 10-11% heavy oxygen content and contributes to sustainability (Chhetri *et al.*, 2008). Unfortunately, it has some major problems such as high raw material costs, inferior storage and oxidative stability, lower calorific value, lesser temperature operability and higher NO<sub>x</sub> emissions.

The use of low-cost raw materials is one of the main issues, apart from improving the efficiency of production processes, developing effective catalysts and managing agricultural land. One effort to reduce the cost of raw material aspects, and hence the presentation of an economic opportunity, is the use of waste cooking oil. The use of waste cooking oil as a raw material in biodiesel production can reduce overall costs, as raw material costs constitute about 70-95% of the total cost of biodiesel production. Hence, the use of former high-priority cooking oil is higher than

vegetable oils as raw materials of biodiesel (Chhetri *et al.*, 2008). Therefore, one of the key areas of current and future research is the development of low-cost feedstocks for biodiesel production, so the total cost can be reduced. Utilization of non-edible vegetable oils is also important because of the need for vegetable oils as food (No, 2011).

The Energy Information Administration (EIA) in the United States (US) estimates that 100 million gallons of waste cooking oil is produced per day in the United States, while around 0.49-0.7 million gallons is produced per day in Europe. The estimated total waste cooking oil produced in Canada about 135,000 tons in a year. Similarly, in European Union (EU) countries, the total production of waste cooking oil is around 700,000-1,000,000 tons a year. The United Kingdom (UK) produces over 200,000 tons waste cooking oil annually. The amount is very large as the opportunity for utilization and management of WCO oil as a substitute fuel is very large, thus leading to large difficulty in overcoming problems that threaten the environment. Most waste cooking oil is illegally dumped into rivers and landfills, causing environmental pollution. To prevent pollution from rising as a result of this waste, some countries are paying close attention to this issue, including some developed countries that have adopted policies that punish the disposal of WCO into drainage. Both economic and environmental aspects strongly support the use of waste cooking oil to produce biodiesel as a substitute for fuel from petroleum (Chhetri *et al.*, 2008; Patil *et al.*, 2012).

There are four ways to convert oils and fats into biodiesel namely transesterification, mixing, micro emulsions and pyrolysis. The most commonly used method is transesterification. Based on the catalysts used, the process of producing biodiesel by transesterification reaction can be divided into alkali, acidic or enzymatic catalysts. The transesterification process using alkali catalyst and catalyst acid requires less reaction time at lower processing costs compared to enzyme catalyst processes. The transesterification process with an alkaline catalyst produces large amounts of biodiesel and shorter reaction times. However, for raw materials with high fatty acid content (FFA), this method cannot be used. Therefore, to produce biodiesel from raw materials with high FFA content, a two-stage process transesterification is used, esterification process of acid followed by alkaline transesterification. The first process

is used to remove high FFA content and to improve biodiesel yield. Drawbacks of the two-stage process include longer reaction time and lower recovery of the catalyst. Transesterification with microwave irradiation assistance is the right solution for energy saving and time accelerating to produce biodiesel from different raw materials. Previous study showed that alkaline process with microwave irradiation assisted produces biodiesel with high quantity and in shorter reaction time (Patil *et al.*, 2012).

Although transesterification using an alkaline catalysis process can convert triglycerides to biodiesel in short reaction times with high conversion, this reaction has several drawbacks. One of the transesterification processes using a homogenous catalyst based is a hydroxide reaction with methanol. This reaction will produce a certain amount of water that causes ester hydrolysis and soap formation. The soap formation in products can reduce biodiesel yields and also complicate the separation between esters and glycerol.. In addition, in this conventional homogeneous method, the catalyst separation process in the production currently uses a washing process, which requires large amounts of water and hence the potential to pollute the environment. Therefore, heterogeneous catalysts are particularly suitable for biodiesel transesterification processes because these catalysts have many advantages over homogeneous catalysts. They are noncorrosive, environmentally friendly, present fewer disposal problems, much more easily separated from liquid products, reusable and can be designed to provide higher catalyst activity, selectivity and durability. In addition, the use of heterogeneous catalysts does not produce soap through the neutralization of free fatty acids or triglycerides saponification (Basumatary, 2013).

Several works have been performed using continuous process to produce biodiesel using conventional heating. Melero *et al.* (2014) used material bentonite clay to form a macroscopic structured with particle sizes of 1.5 mm as heterogeneous catalyst in the continuous production of biodiesel waste cooking oil on a packed bed reactor. Borges and Diaz (2013) used the packed-bed catalytic reactor configuration in a recirculation system to minimize catalyst mechanical damage occurring in the slurry reactor due to continuous stirring. They found that potential reaction rate decreased when a packed-bed reactor configuration was used compared with using a slurry batch reactor for vegetable oil transesterification reaction. Chen *et al.* (2010) employed a novel transesterification reactor, namely the continuous-flow

transesterification, using a rotating packed bed (RPB). They performed experiment using soybean oil with methanol and KOH as catalysts to produce biodiesel. Li *et al.* (2013) used continuously stirred tank reactor (CSTR) for transesterification of soybean oil. The soybean oil and methanol were mixed in separate reactor. Then, the mixture was pumped to the second reactor which consisted of a stirring packed-bed reactor, preheating equipment. However, while these experiments have produced biodiesel with adequate yield and conversion, the reaction time is still relatively long. The reaction time can be reduced using microwave assisted irradiation (Choedkiatsakul *et al.*, 2015; Motasemi and Ani, 2012).

Production of biodiesel from WCO as raw materials using heterogeneous catalysts, especially calcined cockle shell in microwave irradiation, can reduce the current high cost of biodiesel production, thus making biodiesel production competitive compared to petroleum-based diesel fuel. Therefore, the purpose of this study was to investigate the production of biodiesel using raw materials of WCO and CaO as a heterogeneous catalyst for performing continuous transesterification reaction with assisted microwave irradiation and to investigate the effect of various WCO biodiesel fuel on direct injection (DI) diesel engine.

### 1.3 Objectives

The objectives of this study are to produce biodiesel using heterogeneous catalyst transesterification reaction microwave irradiation and to investigate the effect of a various WCO biodiesel blends fuels on direct injection (DI) diesel engine.

The specific objectives of the study are as follows:

- i. To characterize calcium oxide (CaO) from cockle shells as solid catalyst.
- ii. To characterize biodiesel fuel with WCO as feedstock in transesterification reaction using a heterogeneous catalyst and methanol on microwave irradiation technology.

- iii. To determine the performance and emission of diesel engine using several proportions of a commercial biodiesel fuel Palm Oil Methyl Ester and Waste Cooking Oil Methyl Ester with a commercial diesel fuel.

#### 1.4 Scope of the Study

Based on several considerations of the methods used and the establishment of limitations, the scope of the study focused on the following:

- i. The WCO as raw material of biodiesel was obtained from fried banana having FFA content less or equal 0.5 %.
- ii. Process parameters for transesterification reaction include power input (180-450 watt), catalyst weight (10-20 gram), stirrer speed (200-400 rpm) and flowrate (5.25-6.97 ml/min).
- iii. Design of experiment (DOE) with response surface method (RMS) using Box-Behnken design (BBD) was used to determine the experiment plans.
- iv. Five test fuels were used including one commercial diesel fuel Petron Diesel Max Fuel (PDM) and four biodiesel blends of commercial palm oil methyl ester (POME), waste cooking oil methyl ester (WCOME) and diesel fuel PDM at several volumetric proportions. These biodiesel blends are equivalent to B10 and B20, respectively.
- v. The brake power, the air and fuel consumption were measured to determine the performance of the engine and its thermal efficiency. For the exhaust emissions, nitric oxide ( $\text{NO}_x$ ), carbon monoxide (CO), carbon dioxide ( $\text{CO}_2$ ) and unburned hydrocarbon (uHC) were measured. The heat release rate for biodiesel blends were calculated based on the in-cylinder data and were compared to PDM as reference fuel.
- vi. The engine performance and emissions of direct injection (DI) diesel engine were measured using software tools GT-SUITE version 6.0.

## 1.5 Organization of Thesis

This thesis comprises of five chapters with each chapter a specific area of research. Chapter 1 (this chapter) described background of the study, objectives of this research and scope of the study.

In Chapter 2, the literature review is described, including the heterogeneous catalysts, biodiesel transesterification using heterogeneous catalyst, irradiation microwave reactor in transesterification, design experiment using Box Behnken design. Utilization of biodiesel from WCO in Diesel engine for engine performance, emission and combustion and modelling Diesel engine with a popular engine simulation tool was also described.

In Chapter 3, the techniques for continuous biodiesel processing using WCO as raw material of oil and CaO as catalysts in irradiation microwave as well as materials preparation, collecting data, data analysis, and experimental design are presented. Further, engine tests using WCOME and POME blended as well as fuel properties, performance, emission and combustion were examined. Simulation using GT-SUITE V6.0 software is used.

In Chapter 4, the catalyst characterization and biodiesel product are discussed. Optimization of biodiesel conversion using BBD and its validation are discussed as well. The effect of fuel tests on the brake thermal efficiency, specific fuel consumption, exhaust gas emission and combustion characteristics of diesel engine is discussed. Comparison of experimental result and simulation of diesel engine is described.

Finally, the findings and contributions of this thesis are summarized and recommendations for future work are presented in Chapter 5.



## CHAPTER 2

### LITERATURE REVIEW

#### 2.1 Biodiesel from Transesterification Process of Waste Cooking Oil

Biodiesel is an ester-based oxygen fuel whose material is biologically renewable. In chemistry, biodiesel is defined as a monoalkyl ester of long chain fatty acids derived from renewable biolipids. Fatty acids (m) ethyl ester (FAME) or biodiesel from processed organic oils are produced from vegetable oils, animal fats, used cooking oil, including triglycerides with methanol or ethanol by using a catalyst. (Demirbas, 2008; Pandey, 2009). In terms of chemical and physical properties, the properties of biodiesel have many similarities with fuel derived from petroleum. The use of biodiesel as a substitute for petroleum-derived fuel is profitable with regard to engine performance and fuel consumption of diesel engine (Bajpai and Tyagi, 2006). Table 2.1 shows diesel standards with ASTM D975 and biodiesel according to ASTM D6751 designated B100.

The advantages of neat vegetable oil and biodiesel as a diesel fuel are its portability, ready obtainability, renewability, biodegradability, lower aromatic content, non-toxicity, higher flash point, better lubrication, higher cetane number, non-flammable, non-explosive, negligible sulphur content, higher combustion efficiency and lower overall exhaust emissions with the exception of  $\text{NO}_x$  (Canakci and Sanli, 2008; Demirbas, 2008; Graboski and McCormick, 1998; Moser, 2011; Rakopoulos *et al.*, 2011).

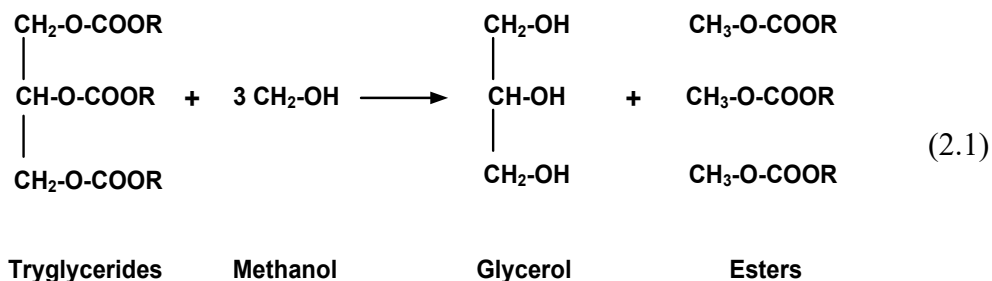
**Table 2.1 :** ASTM standards of biodiesel and diesel fuels (Demirbas, 2008)

Properties	Test Method	ASTM D975 (diesel)	ASTM D6751 (biodiesel, B100)
Flash point	D 93	325 K	Min 403 K
Water and sediment	D 2709	0.05 max % vol	0.05 max % vol
Kinematic viscosity (at 313 K)	D 445	1.3-4.1 mm <sup>2</sup> /s	1.9-6.0 mm <sup>2</sup> /s
Sulfated ash	D 874	-	0.02 max %wt
Ash	D 482	0.01 max %wt	-
Sulfur	D 5453	0.05 max %wt	-
Sulfur /129	D 2622	-	0.05 max %wt
Copper strip corrosion	D 130	No 3 max	No 3 max
Aromaticity	D 1319	35 max % vol	-
Carbon residue	D 4530	-	0.05 max %mass
Cetane number	D 613	40 min	47 min
Carbon residue	D 524	0.35 max %mass	-
Distillation temperature (90% volume recycle)	D 1160	555 K min–611 K max	-

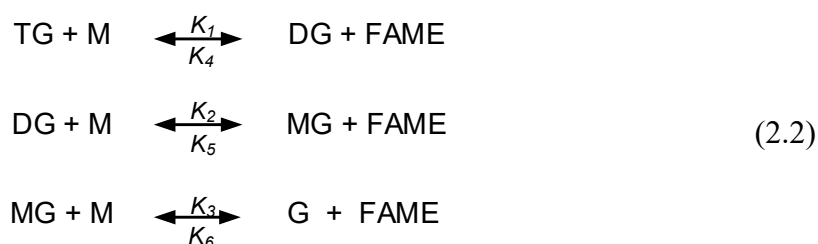
The main disadvantages of vegetable oil and neat biodiesel are in terms of properties such as higher viscosity, lower calorific value, higher cloud point and pour point. One important issue in the selection of biodiesel as a substitute for diesel fuel is the high production cost (Demirbas, 2008; Ma and Hanna, 1999; Rakopoulos *et al.*, 2011; United States Department of Energy, 2006).

Transesterification process is influenced by several factors such as molar ratio of oil or glycerides to alcohols, type of alcohol, type and amount of catalyst, reaction temperature, reaction time, and water content in oils or fats and FFA in oil (Ma and

Hanna, 1999). The reversible reaction sequence in the transesterification process is shown in Eq. 2.1 and Eq. 2.2 (Sharma *et al.*, 2008).



In the first step, triglycerides (TG) is converted to diglycerides (DG) and fatty methyl ester (FAME) by using methanol (M). Furthermore, the diglycerides are reacted with methanol to produce monoglycerides (MG) and FAME. In the third and final step, monoglycerides (MG) are converted with methanol-assisted to produce glycerol (G) and FAME. Each step produces an ester. The rate constants for forward reactions are  $K_1$ ,  $K_2$  and  $K_3$ , while the rate constants of backward are  $K_4$ ,  $K_5$ , and  $K_6$ . Thus, one triglyceride molecule produces three esters.



The selection of process used in biodiesel production depends on the fundamental factors affecting the reaction of transesterification and the ester result. In terms of raw material and reactants, factors include the water content in oil and the value of acid or FFA and type of alcohol, type of catalyst, respectively. Operating factors include molar ration of alcohol to oil, catalyst load, reaction temperature and pressure during process, heating process methods, reaction time and mixing density.

In the process of transesterification, reaction can be catalysed by using base, acid, or enzyme. This transesterification reaction can be catalysed homogeneously or heterogeneously. The choice of catalyst depends on the solubility of the chemical catalyst in the reaction mixture. Consideration must be paid to process used, since each process has its own advantages and disadvantages (Banković-Ilić *et al.*, 2012; Maddikeri *et al.*, 2012).

Biodiesel can be produced using the transesterification process under lower temperature reaction conditions and shorter reaction times, and can obtain higher yields with alkali catalysts than acid catalysts (Chen *et al.*, 2012; Mazubert *et al.*, 2013; Pandey, 2009). Generally, to improve the reaction rate and increase process yield, industries use alkaline catalyst such as NaOH, KOH in the transesterification process of vegetable oil into biodiesel (Borges and Díaz, 2013; Pandey, 2009).

Biodiesel from vegetable oils is considered as the first generation biofuel since it is exclusively produced from energy crops using the conventional transesterification technology. Using vegetable oil from seeds of various crops as feedstock raise economic and social implications due to the associated “food versus fuel” debate and problematic glycerine disposal. Nevertheless, the growing need for biodiesel has directed research that is focused on finding alternative technologies that can exploit residual biomass (Bezergianni and Dimitriadis, 2013).

In the second generation, Banković-Ilić *et al.* (2012) discussed the possibility of optimization, kinetics, and increased biodiesel production from non-edible oils by considering a number of different methods relating to operating conditions and yield ester. A new technology was developed for biodiesel production by improving the transesterification process to produce Fischer–Tropsch diesel, hydrotreated green diesel, hybrid diesel and white diesel (Bezergianni and Dimitriadis, 2013). Hydrotreating (petroleum hydroprocessing) technology is a modification of classical transesterification with the aim of producing hydrocarbons (green hydrocarbon) instead of oxygenates. This process employ different catalysts, reactants and harsher conditions to allow complete deoxygenation of triglycerides (TGs) (Serrano-Ruiz *et al.*, 2012).

The substitution of vegetable neat oil with WCO is very promising because the price of WCO is very much cheaper than a neat vegetable oil. Thus, it can significantly improve the economic feasibility of biodiesel production (Chhetri *et al.*, 2008; Kulkarni and Dalai, 2006). The WCO is produced from the frying process. It may come from vegetable oils such as soybeans, cotton seeds, peanuts, sunflower, rapeseed, sesame, maize, olive, palm oil, palm kernel, coconut, flaxseed, castor, soybeans or various sources plants and animals fats/oils such as butter, lard, fat, vegetable oil and fish oil (M. K. Lam *et al.*, 2010; No, 2011; Zhou *et al.*, 2007).

In the frying process, the change of cooking oil at a temperature of 160-190° C under atmospheric conditions for a long period of time cause changes in chemical and physical properties in the oil. Fried foods absorb between 5% and 20% of used oil. This value can significantly increase the number of harmful compounds that degraded oil provide to fried foods (Stoytcheva and Montero, 2011). Oil undergoes several changes in physical and chemical properties, depending on the type of oil and oil composition. Some physical changes observed in vegetable oil after frying are: an increase in viscosity, a change in surface tension, an increase in specific heat and a change in color. In addition, oil is subject to three types of reaction when frying, namely thermolytics, oxidative, and hydrolytic. This reaction causes unwanted and dangerous formation if oil is used repeatedly (M. K. Lam *et al.*, 2010).

Table 2.2 shows the comparison of properties between virgin soybean oil and WCO. Due to frying, properties of WCO such as density, specific gravity, viscosity, suspended solid, acid value and FFA content have increased.

**Table 2.2 :** Comparison of properties between virgin soybean oil and waste cooking oil (Birla *et al.*, 2012)

Properties	Virgin soybean oil	WCO
Density (kg/m <sup>3</sup> )	890	896
Specific gravity at (30 °C)	0.894	0.899
Viscosity (cSt) at (40 °C)	28.08	35.06
Suspended solids (g/l)	Nil	9.272
Acid value (mg of KOH/g of oil)	0.709	1.948
Free fatty acid (%)	0.3545	0.974
Color	Pale yellow	Golden yellow

From an environmental point of view, cooking oil that has been used for deep frying can no longer be used, which creates disposal problems. The use of inappropriate methods of disposal may cause water pollution and is also harmful to humans. In fact, inappropriate methods of disposal are not only harmful to humans, but to farm animals as well. Therefore, the European Union (EU) has imposed a ban on the use of all waste oils as domestic fodder. To prevent environmental pollution from disposing of waste oil through drainage, some developed countries have established policies that punish anyone who does so (Kulkarni and Dalai, 2006; M. K. Lam *et al.*, 2010).

Several physical and chemical properties of WCO used as feedstocks for biodiesel production are shown in Table 2.3. The table shows that the acid value for WCO varies from 0.98 -7.45 mg KOH/g, while viscosity ranges from 47.58 to 82.2 mm<sup>2</sup>/s at 40 °C.

Table 2.4 shows fatty acid composition of various WCO as biodiesel feedstock that have been reported by several investigators. It shows that most of the WCO contain monosaturated oleic acid (C18:1) and polyunsaturated linoleic (C18:2).

**Table 2.3 :** Selected physical properties of waste cooking oil

Properties							Reference
Density at 25 °C (kg /m <sup>3</sup> )	Mean molecular weight (g/mol)	Acid value (mg KOH/ g)	Free fatty acid (%)	Moisture content (%)	Saponification value (mg KOH/g)	Viscosity at 40 °C (mm <sup>2</sup> /s)	
900	-	5.08	-	0	-	47.58	(Wan Omar and Amin, 2011)
918	856.5	0.98	0.87	0.124	183.4	-	(Molaei Dehkordi and Ghasemi, 2012)
926	-	7.45	-	1	206	49.93	(Noshadi et al., 2012)
963.51	-	0.587	-	-	-	-	(Uzun et al., 2012)
918	272.27	-	-	-	-	82.2	(Boffito et al., 2013)
930	-	4.3	-	-	198	54.3	(Maddikeri et al., 2013)
918	-	4.06	-	-	-	66.5	(Melero et al., 2014)

In the process of producing biodiesel, four main processes are known, namely direct use with mixing, micro emulsion, thermal cracking (pyrolysis) and finally transesterification. Transesterification of triglycerides or esterification of FFA with low molecular weight alcohols is the most commonly used process, in which the raw materials are purified vegetable oils, animal oils, and WCO (Farag *et al.*, 2011; Ramadhas *et al.*, 2004).

The technical properties of commercial diesel fuel, WCO and biodiesel from WCO are given in Table 2.5. The table indicates that viscosity of WCO is higher than its source but decreased significantly after transesterification. This value is in the range of the viscosity of diesel fuel. Density, flash point, and pour point also decreased after transesterification process, whereas calorific value and cetane number increased.

**Table 2.4 :** Percentage of fatty acid composition in waste cooking oil

Myristic acid (C14:0)	Palmitic acid (C16:0)	Palmitoleic acid (C16:1)	Stearic acid (C18:0)	Oleic acid (C18:1)	Linoleic acid (C18:2)	Linolenic acid (C18:3)	Arachidic acid (C20:0)	Eicosanoic acid (C20:1)	Docasanoic acid (C22:0)	Lignoceric acid (C24:0)	Others	Reference
-	8.4	0.2	3.7	34.6	50.5	0.6	0.4	0.4	0.8	0.3	-	(Dias <i>et al.</i> , 2008)
0.4	1.1	25.8	4.7	34.6	29.4	2.5	0.2	0.3	-	-	1.0	(Charoenchaitrakool and Thienmethangkoon, 2011)
-	29.5	-	-	61.4	9.1	-	-	-	-	-	-	(Wan Omar and Amin, 2011)
-	32.4	-	3.8	42.5	15.3	-	-	-	-	-	5.9	(Molaei Dehkordi and Ghasemi, 2012)
1.1	22.5	-	4.1	54.7	11.2	1.1	-	-	-	-	5.3	(Noshadi <i>et al.</i> , 2012)
-	7.07	-	2.42	36.68	52.20	-	-	-	0.83	-	0.8	(Uzun <i>et al.</i> , 2012)
-	38.8	4.1	0.0	47.9	0.2	-	-	-	-	-	9.0	(Boffito <i>et al.</i> , 2013)
-	6.7	-	1.6	18.3	73.4	-	-	-	-	-	-	(Maddikeri <i>et al.</i> , 2013)
-	8.5	-	3.1	21.2	55.2	5.9	-	-	-	-	4.2	(Sanjid <i>et al.</i> , 2013)
-	26.5	-	10.9	21.4	1.7	-	-	-	-	-	39.6	(Talebian-Kiakalaieh <i>et al.</i> , 2013)
-	11.8	-	5.4	26.3	48.6	5.9	-	-	-	-	1.4	(Muciño <i>et al.</i> , 2014)
0.1	11.55	0.08	5.88	67.41	12.16	0.13	0.48	0.39	0.59	0.23	1.0	(Mulinari <i>et al.</i> , 2017)



**Table 2.5 :** Comparison of properties of waste cooking oil, biodiesel from waste cooking oil and commercial diesel fuel (Demirbas, 2009; Yaakob *et al.*, 2013)

Fuel properties	Units	WCO	Biodiesel from WCO	Commercial diesel fuel
Kinematic viscosity at 313K	mm <sup>2</sup> /s	36.4	5.31	1.9–4.1
Density at 288K	kg/L	0.924	0.897	0.075–0.840
Flash point	K	485	469	340-358
Pour point	K	284	262	254-260
Cetane number	-	49	54	40-46
Ash content	%	0.006	0.004	0.008-0.010
Sulfur content	%	0.09	0.06	0.35-0.55
Carbon residue	%	0.46	0.33	0.35-0.40
Water content	%	0.42	0.04	0.02-0.05
Higher heating value	MJ/kg	41.40	42.65	45.62–46.48
Free Fatty Acid (FFA)	mgKOH/g	1.32	0.10	-
Saponification value	-	188.2	-	-
Iodine value	-	141.5	-	-

Table 2.5 presents a comparison of biodiesel properties produced from WCO to commercial diesel fuel. The higher heating value (HHV) of WCO biodiesel is slightly lower than commercial diesel fuel, but kinematic viscosity, density, and flash point of biodiesel are in accordance with ASTM D 6751 specifications. A comparison of WCO before and after transesterification is shown in Figure 2.1. It indicates that palmitic acid (C16:0) and oleic acid (C18:1) in WCO decrease after transesterification, whereas others are converted to linoleic acid (C18:2) significantly.

**Table 2.6 :** Properties of diesel and biodiesel fuel and biodiesel produced from waste cooking oil according to ASTM standards (Birla *et al.*, 2012)

Fuel properties	Unit	Diesel fuel	Biodiesel range	Biodiesel from WCO
Fuel standard		ASTM D 975	ASTM D 6751	ASTM D 6751
Calorific value	kJ/kg	41,800–44,800	–	35,305.87
Acid value	mg KOH/g oil	–	≤0.5	0.48
Kinematic viscosity at 40 °C	(m <sup>2</sup> /s) × 10 <sup>-6</sup>	1.3–4.1	1.9–6.0	5.4
Density	kg/m <sup>3</sup>	800–860	860–894	865
Flash point	°C	60–80	100–170	169
Cloud point	°C	–35 to 5	–3 to 15	1
Pour point	°C	–35 to –15	–5 to 10	–4.0

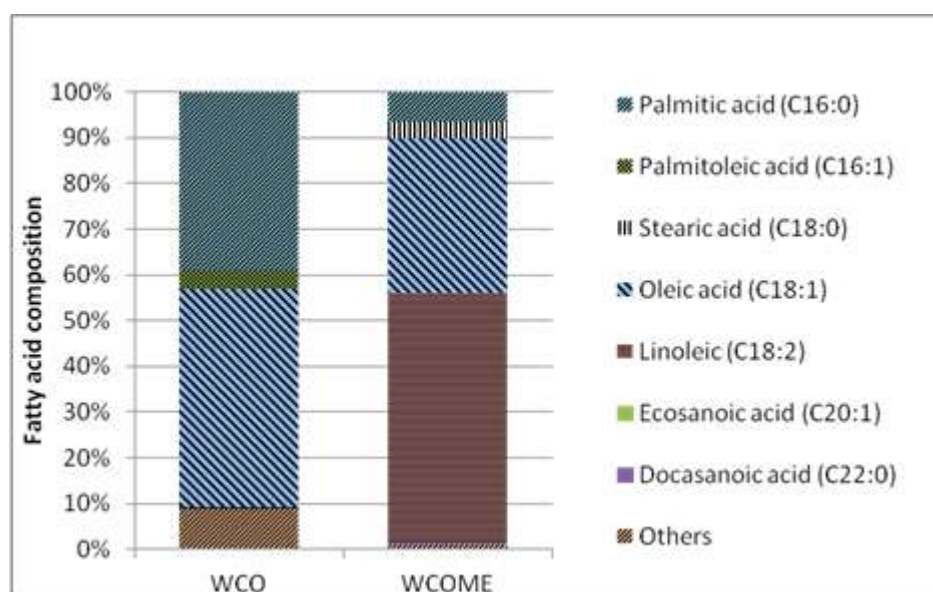


**Figure 2.1** Fatty acid composition of waste cooking oil before and after transesterification

The schematic flow diagram process of biodiesel production from WCO is shown in Figure 2.2. The method used for biodiesel production from WCO is similar to conventional transesterification process after WCO is processed by the right

method. The selection of processes used in biodiesel production depends on the fundamental factors affecting the transesterification reaction and the ester results. As shown in the diagram, the role of testing with titration method is very important to determine the acid value or FFA. Transesterification process can be done if the value of FFA <1%; if not, pre-treatment process should be done.

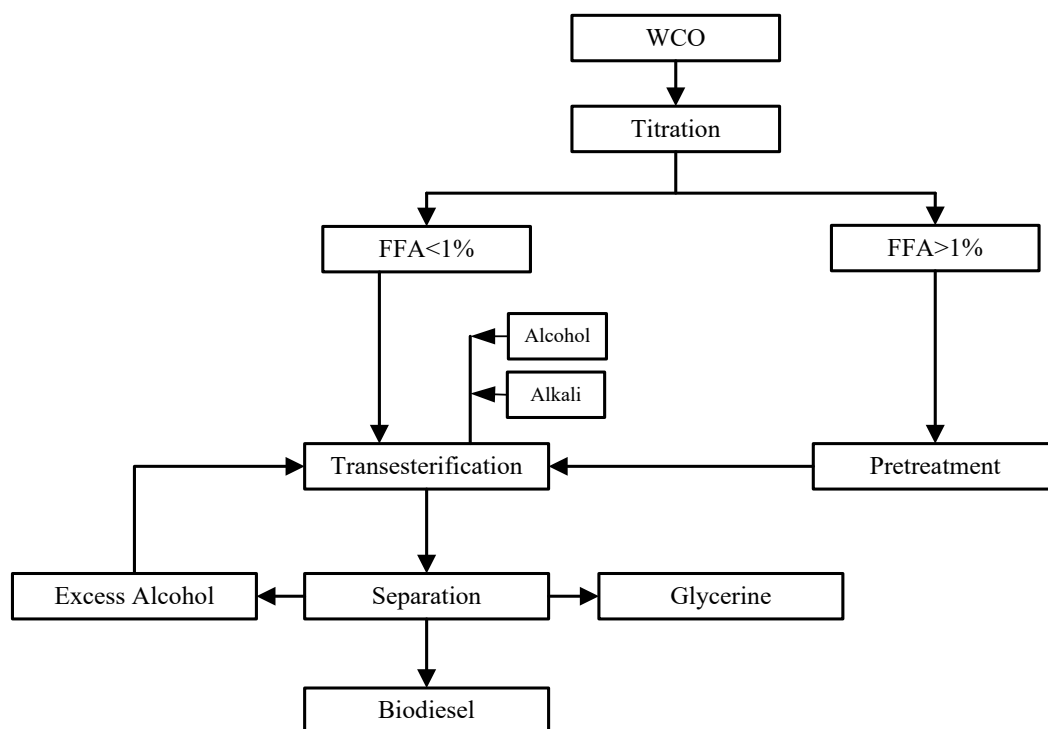


**Figure 2.2** Schematic flow diagram of biodiesel production from WCO (Maddikeri *et al.*, 2012)

### 2.1.1 Heterogeneous Catalyst

According to Hill (1977), catalysts are substances that affect the rate or direction of chemical reaction processes, but which cannot be consumed in the process. Although by definition the catalyst cannot change the transformations of matter and energy (the thermodynamic equilibrium) of the reaction during process, in industry the role of the catalyst is in addition to accelerating the reaction rate to the chemical equilibrium in the process as well as to improve the economic process (Lloyd, 2011).

Heterogeneous catalysts are classified as solid base and solid acid. The solid base catalyst can be classified into broad compounds in categories such as alkaline earth metal hydroxides, hydrotalcites hydroxides, alumina loaded with compounds zeolites, calcium oxide, magnesium oxide, solid superbase and various other compounds. Heterogeneous acid catalysts can be classified into resins and membranes, superacid catalysts, polyaniline sulphate, heteropoly acid (HPA), pyrone complexes with metals, metal oxides, zeolite, acidic ionic liquids, and sulphated zirconia (Nair *et al.*, 2012; Sharma *et al.*, 2011). Enzymes are one of the heterogeneous catalyst groups that can act on groundwater interface phases. This enzyme can also be immobilized with support materials such as resins or other matrices. Recent research has shown that the cost of biodiesel synthesis can be greatly reduced by the use of lipase compounds as a catalyst (Nair *et al.*, 2012).

Chouhan and Sarma (2011) reviewed recent discoveries and the use of heterogeneous acid catalysts, bases and biocatalysts for those used in biodiesel production processes. They also reviewed the suitability of this catalyst group not only from laboratory use but also in industrial use. The classification of this catalyst including their sub-classification is shown in Figure 2.3.

Talebian-Kiakalaieh *et al.* (2013) stated that a good solid catalyst for use in the catalytic process should have characteristics such as interconnection systems of large pores, moderate concentrations to high concentrations of strong acid sites, hydrophobic surfaces, and the ability to regulate surfaces to prevent deactivation (poisoning).

The catalytic reaction process of metolysis by using heterogeneous catalysts is complicated. This is caused by this process involving three phases, namely a solid catalyst (heterogeneous) and two liquid phases of oil and methanol which cannot be mixed (immiscible). Along with the process of metolysis, there are also additional reactions or side reactions such as the formation of soap (saponification) of glycerides and methyl esters, and alkali refining (neutralization) of FFA by the catalyst (Refaat, 2011).

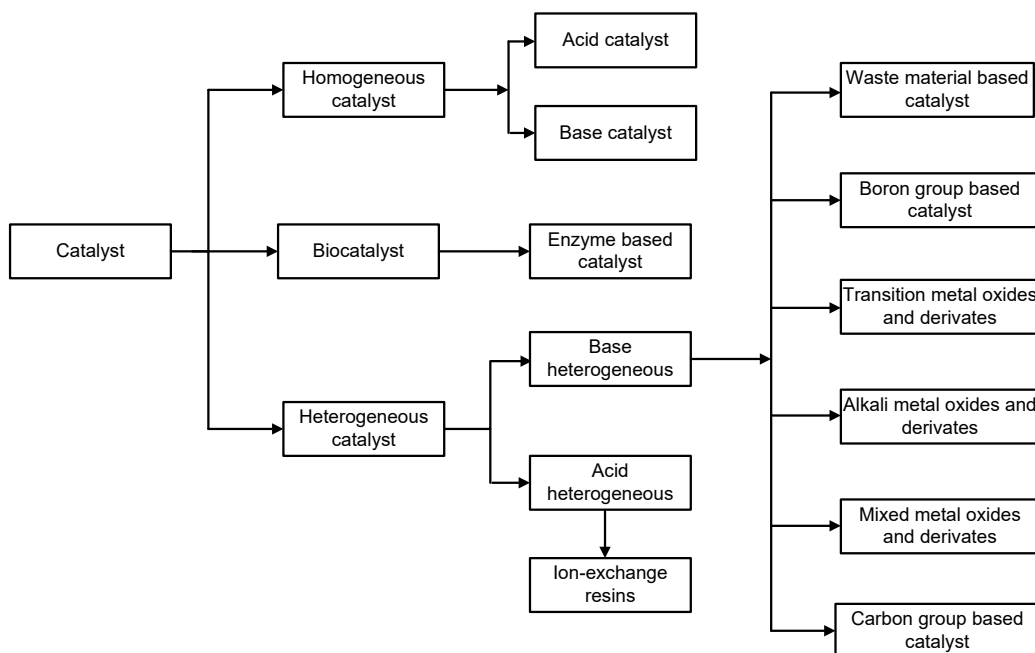


**Figure 2.3** Classification of catalyst (Chouhan and Sarma, 2011)

Lam *et al.* (2010) reviewed the transesterification of high FFA oil to biodiesel using homogeneous, heterogeneous, and enzymatic catalysis. They claimed that some acid catalytic systems and heterogeneous acid catalysis are not suitable for industrial applications caused by mass transfer problems. Zabeti *et al.* (2009) reviewed the application of metal oxides such as magnesium oxide, calcium oxide, strontium oxide and zirconium oxide, alumina, zinc oxide, silicate, and zirconium oxide and supported the use of metal oxides in biodiesel production.

### 2.1.1.1 Catalyst Preparation

Many catalysts can be prepared by one of two methods, namely precipitation and impregnation. Precipitation is usually selected when a support material is not sufficiently porous. It can be impregnated by loading its surface by active metal. It is necessary to control the reaction conditions carefully to obtain consistent quality during the catalyst-making process (Lloyd, 2011).

An effective catalyst may consist of having many types of active surface species, and each catalyst will be able to catalyse either a single reaction or an entire reaction. Metals, oxides and sulphides are the most commonly encountered species, but many other materials have also been shown to have catalytic activity. Another factor that can increase the rate of catalytic reactions is the particles. Small particle (nano) molecules have full access to the surface of the reactants (Ross, 2012).

Generally, the catalyst can be produced in various ways such as conversion to oxides by calcinations (Birla *et al.*, 2012; Roschat *et al.*, 2012), impregnated amounts of base metals, precipitation (Brito *et al.*, 2009), co-precipitation, heteropolyacid (Cao *et al.*, 2008), pyrolyzed rice husk (Li *et al.*, 2014) and modified impregnation method (Farooq *et al.*, 2013; Mahesh *et al.*, 2015). Some authors applied non-conventional catalysts using conversion natural source to oxide by calcination such as waste mud crab (*Scylla serrata*) shell (Boey *et al.*, 2009), waste coral fragments (Roschat *et al.*, 2012), sea sand (Muciño *et al.*, 2014), barium meliorated construction site waste marble (Balakrishnan *et al.*, 2013), clamshells (*M. mereterix*) (Nair *et al.*, 2012), snail shell (Birla *et al.*, 2012) and eggshell (Niju *et al.*, 2015).

#### **2.1.1.2 Catalyst Characterization**

Catalyst characterization is essential to be conducted after a catalyst has been prepared. The purpose of catalyst characterization is to determine the characteristics of the catalyst and to enable the reproduction of any preparations performed. It is also possible to demonstrate that physical and chemical properties will be similar, as long as the prepared sample has the same chemical composition and is in the same condition. Characterization of catalysts includes chemical composition, physical texture, catalytic activity, selectivity and stability (Ross, 2012).

Table 2.7 presents the characterization of solid catalysts testing and its objectives used by researchers for the biodiesel production from WCO.

**Table 2.7 :** Characterization of heterogeneous testing catalyst in waste cooking oil transesterification

Characterization testing	Objective testing	Typical procedure	References
Micrometrics adsorption equipment	Measure the specific surface area and pore size	Performed using Micrometrics adsorption equipment (Model ASAP 2000) at 78 K using liquid nitrogen.	(Jacobson <i>et al.</i> , 2008)
Thermal conductivity detector (TCD)	Measure the desorption profile of NH <sub>3</sub>	-	(Lou <i>et al.</i> , 2008)
Elemental Analysis (EA)	Determine the elemental composition	Elementar vario EL $\beta$ apparatus is applied.	(Lou <i>et al.</i> , 2008)
Energy dispersive analysis (EDAX)	Monitor the surface morphology of the catalyst particles	The scanning electron microscope (SEM) coupled with an Oxford Link (ISIS L200Cs) detector	(Brito <i>et al.</i> , 2009)
Field-emission scanning electron microscope (FESEM)	Observe surface morphology	The sample was placed in a sample grid and coated with gold-palladium	(Chin <i>et al.</i> , 2009)
Fourier transform infrared (FTIR)	Determine determine the surface functional groups	-	(Chin <i>et al.</i> , 2009)
Scanning electron microscopy (SEM)	Evaluate the surface morphology of the catalyst particles	SEM (Jeol LTD, JSM-6300) coupled with a detector to perform energy dispersive analysis (EDAX)	(Brito <i>et al.</i> , 2009)
Thermogravimetric analysis (TGA)	Evaluate the thermal decomposition of the catalyst	Perform on a Rigaku TGDTA 8120 thermal analyzer under air flow condition with a temperature ramp rate of 10 °C/min.	(Brito <i>et al.</i> , 2009)
X-ray fluorescence (XRF)	Determine the chemical composition of the main elements present in the material	Samples emit secondary X-rays following bombardment with hard X-rays which allow complete elemental analysis.	(Lloyd, 2011)
Hammett indicators	Determine the basic catalyst strengths	About 25 mg of the catalyst was agitated with 5 ml volume of methanol solution	(Birla <i>et al.</i> , 2012)
Temperature-programmed desorption (TPD)	Measure the total basicity of the catalysts	Using CO <sub>2</sub> as the probe molecule. These experiments were carried out using BELCAT-A.	(Molaei Dehkordi and Ghasemi, 2012)
X-ray diffraction (XRD)	Identifies crystalline compounds by reference to standard tables. The proportion of each phase present in the sample can be calculated	Carried out using a Bruker D8 Advance X-ray diffractometer,	(Molaei Dehkordi and Ghasemi, 2012)
X-ray photoelectron spectroscopy (XPS)	Determine the surface and composition of catalysts	Using Al anode of a V.G. Microtech XR3E2 X-ray source and a concentric hemispherical analyzer	(Molaei Dehkordi and Ghasemi, 2012)

### **2.1.2 Biodiesel Production from Waste Cooking Oil Using Heterogeneous Catalyst**

The methods applied in the use of catalysts in the biodiesel production process of WCO as a feedstock can be classified into three main groups; (a) homogeneous, (b) heterogeneous, and (c) non-catalytic transesterification (Talebian-Kiakalaieh *et al.*, 2013; Yaakob *et al.*, 2013).

The chemical conversion of biodiesel can be carried out by two stages of reaction and separation of glycerol, successively, in order to replace the equilibrium reaction of heterogeneous-catalyzed continuous process as shown in Figure 2.4. The catalyst portion consists of two fixed bed reactors. They are fed by oil and methanol mixture at a certain ratio. Each reactor releases excess methanol with partial flash. Further ester and glycerol were separated in the settlers. The glycerol phase is incorporated and the final trace of methanol is removed by evaporation. Biodiesel is recovered after evaporation process to recover methanol and then purified to remove the last glycerol.



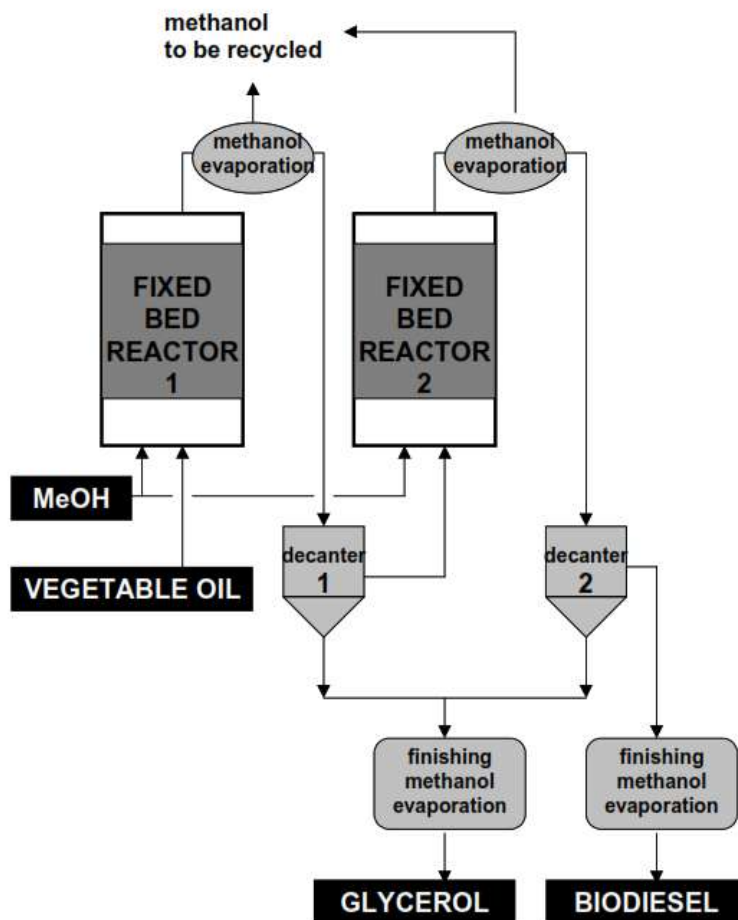


**Figure 2.4** Continuous heterogeneous catalyzed process diagram (Hillion *et al.*, 2003)

Table 2.8 presented several studies using a catalyst in the WCO transesterification process and its condition and performance. Table 2.8 clearly shows that only a few of them used catalyst material from natural resource through calcinations, while others use synthesized mixed, whereas Table 2.9 lists their advantages and drawbacks.

**Table 2.8 :** Selected heterogeneous catalyst used in biodiesel production of waste cooking oil and its condition and performance

Catalyst	Methods or technologies	WCO properties	Reaction condition				Reference	
			Temperature	Type of alcohol (alcohol to oil molar ratio)	Catalyst loading	Reaction time		Performance
<i>Heterogeneous base catalyst</i>								
Calcium oxide (CaO) Ca(OH) <sub>2</sub> , CaCO <sub>3</sub>	Batch process with reflux of methanol in a nitrogen gas flow	Acid value=5.1 mg-KOH/g	60 °C	Methanol – 25 ml	25 g	1h	Yield=93% Yield=12% Yield=0%	(Kouzu <i>et al.</i> , 2008)
Powdered calcined clamshell (Mereterix-mereterix)	Batch process		60 °C	Methanol (6.03)	3.0 g in 100 ml of oil	3 h	Yield>89% Conversion>97%	(Nair <i>et al.</i> , 2012)
Calcined waste coral fragments	Batch process	1.15 mg KOH/g	65 °C	Methanol (15)	100 wt.%;	2 h	Yield>98%	(Roschat <i>et al.</i> , 2012)
Calcined snail shell	Batch process	Acid value = 1.948 mgKOH/g	60 °C	Methanol (6.03)	2.0 wt.%	8 h	Yield=99.58%	(Birla <i>et al.</i> , 2012)
Calcium oxide (CaO)	Batch process	Acid value= 3.2 mgKOH/g (FFA=1.6 %)	60 °C	Methanol (9.14)	3.49%	60.49 min	Yield=94.10%	(Aworanti <i>et al.</i> , 2013)

**Table 2.8:** Selected heterogeneous catalyst used in biodiesel production of waste cooking oil and its condition and performance (cont'd)

Catalyst	Methods or technologies	WCO properties	Reaction condition					Reference
			Temperature	Type of alcohol (alcohol to oil molar ratio)	Catalyst loading	Reaction time	Performance	
Barium meliorated construction site waste marble	Batch process	Acid value =0.04 mgKOH/g	65 °C	Methanol (9)	3.0 wt. %.	3 h	Yield = 88%	(Balakrishnan <i>et al.</i> , 2013)
Heterogeneous catalyst from potassium-loaded pumice material	A packed-bed catalytic reactor – recirculation - continue system. Conventional heating	Acid value =0.04 mgKOH/g	55 °C	Methanol (20)	129.2 g for 18 cm bed length	2 h	Yield = 96.5% Conversion= 99.5 %	(Borges and Díaz, 2013)
Calcined Sea sand	a two-step reaction system was performed	Acid value =0.31 mg of KOH/g	60 °C	Methanol (12)	7.5wt%	6 h	Yield=97.5%	(Muciño <i>et al.</i> , 2014)
Na-loaded SiO <sub>2</sub> from waste sponge skeletons	ultrasonic bath (42 kHz) with the power dissipation 100 W	Acid value= 3.54 mg KOH/g,	55 °C	Methanol (9)	3 wt. %	90 min	Yield=98.4 %	(Hindryawati and Maniam, 2015)
KBr impregnated CaO	Batch process	Acid value =2.34 mgKOH/g FFA=1.176 (%)	65 °C	Methanol (12)	3 wt%	1.8 h	Yield=83.6%	(Mahesh <i>et al.</i> , 2015)

**Table 2.8:** Selected heterogeneous catalyst used in biodiesel production of waste cooking oil and its condition and performance (cont'd)

Catalyst	Methods or technologies	WCO properties	Reaction condition					Reference
			Temperature	Type of alcohol (alcohol to oil molar ratio)	Catalyst loading	Reaction time	Performance	
Calcined egg shell	Batch process	Acid value =2.14 mg of KOH/g	65 °C	Methanol (9)	3 wt %	3 h	Yield = 95.05% Conversion=96.11%	(Niju <i>et al.</i> , 2015)
Calcined scallop shell (CSS)	Batch process	Acid value = 1.23 mgKOH/g saponification =212.2 mgKOH/g	65°C	Methanol (6)	5 wt%	2 h	Yield=86%	(Sirisomboonchai <i>et al.</i> , 2015)
Calcined waste chicken bones	Batch process	Acid value =1.86 mg of KOH/g	55 °C	Methanol (15)	5 wt%	4 h	Yield=89.33	(Farooq <i>et al.</i> , 2015)
Activated carbon produced from oil palm biomass was calcined with potassium phosphate tri-basics (K <sub>3</sub> PO <sub>4</sub> )	Batch process using a 1 l three-neck round-bottom flask equipped with magnetic stirrer bar	-	60 °C	Methanol (12)	5 wt%	4 h	Yield=98%	(Ahmad Farid <i>et al.</i> , 2017)

**Table 2.8:** Selected heterogeneous catalyst used in biodiesel production of waste cooking oil and its condition and performance (cont'd)

Catalyst	Methods or technologies	WCO properties	Reaction condition				Reference	
			Temperature	Type of alcohol (alcohol to oil molar ratio)	Catalyst loading	Reaction time		Performance
<i>Heterogeneous acid catalyst</i> WO <sub>3</sub> /ZrO <sub>2</sub> .	A packed-bed continuous flow reactor		70 °C	Methanol to Oleic acid(19.4:)	4 wt.%	1 h	Conversion=80%	(Park <i>et al.</i> , 2008)
Tri-potassium phosphate	Batch process	Acid value =7.7 mg KOH/g	60 °C	Methanol (6)	4 wt.%	2 h	Yield-97.3%	(Guan <i>et al.</i> , 2009)
Mixed oxides of TiO <sub>2</sub> -MgO	Batch process	Acid value =3.6mg KOH/g Saponification value=207 mg KOH/g	60 °C	Methanol (50)	10 wt%,	6 h	Yield= 91.6%	(Wen <i>et al.</i> , 2010)
Solid acidic mixed oxide catalysts Mn <sub>3.5x</sub> Zr <sub>0.5y</sub> Al <sub>x</sub> O <sub>3</sub>	Batch process	Acid value =2.45mg KOH/g	150 °C	Methanol (14)	2.5 % wt	5 h	Yield>93%	(Amani <i>et al.</i> , 2014)

**Table 2.9 :** The advantages and drawbacks of heterogeneous catalyst used in transesterification of waste cooking oil (Borges and Díaz, 2013; M. K. Lam *et al.*, 2010)

Advantages	Drawbacks
<p><i>Heterogeneous base catalyst</i></p> <p>The relative rate of reaction is faster than transesterification of the acid catalyst</p> <p>Does not require heavy reaction and high energy for reaction process</p> <p>The process of separating biodiesel from the reaction mixture is easier and without using water as a cleaning agent</p> <p>The possibility to reuse and regenerate the catalyst is high</p> <p>Characters that are less corrosive</p> <p>Leading to safer, cheaper</p> <p>More environmentfriendly</p>	<p>The catalyst may be partially or totally deactivated (poisoning) due to contact with ambient air</p> <p>Sensitive to FFA content in oil</p> <p>Forming soap if the oil content contains FFA greater than 2 wt.%</p> <p>The biodiesel yields decreased and caused problems during product purification due to soap formation</p> <p>Product contamination due to leaching of catalyst active sites</p>
<p><i>Heterogeneous acid catalyst</i></p> <p>Not sensitive to oil with FFA and water content</p> <p>Suitable for low grade oil</p> <p>The process of esterification and transesterification take place simultaneously</p> <p>Separating the catalyst from the product is easier</p>	<p>Higher costs due to complicated catalytic synthesis processes</p> <p>Usually, the process requires long reaction time, high temperature of reaction and high alcohol to oil molar ratio.</p> <p>It takes a lot of energy</p> <p>Active site leaching of the catalyst may cause contamination of the product</p>

Some literature reports a number of uses of heterogeneous basic catalysts for biodiesel production from WCO. Kouzu *et al.* (2008) used calcium oxide (CaO) as a solid base catalyst for transesterifying WCO with the acid value of 5.1 mg-KOH/g. The result of FAME reaches above 99% at 2 hours reaction time, but unfortunately, some of the catalysts are converted into calcium soap by reacting with the FFA present in the

WCO during the initial stages of transesterification. They concluded that CaO could be implemented by multi-step transesterification in biodiesel production with WCO raw material. An appropriate process for pre-treatment is esterification of FFA using cation exchange resins combined with the removal of by-produced moisture.

Chin *et al.* (2009) carried out transesterification of WCO palm oil using oil palm ash as a catalyst at 10 bar. The optimum conditions were obtained under reaction conditions: 5.35% by weight of the catalyst (based on the weight of the oil), the temperature 60 °C, the molar ratio of methanol to oil of 18.0 and the reaction time of 0.5 hours. Using surface response methodology and quadratic polynomial equations predicted result of 60.07% wt and experiment of 71.74% wt.

Roschat *et al.* (2012) performed transesterification to produce biodiesel and glycerol by-product using solid catalysts obtained from the waste coral fragments using calcination process. They used WCO, palm oil, soybean oil, and rice bran as raw materials. The optimum value of biodiesel obtained with FAME result is more than 98% if using coral fragments calcined at temperature of 700 °C for 1 hour under reaction condition, catalyst to oil ratio 100% weight, molar ratio methanol to oil of 15 and reaction temperature 65 °C for 2 hours with constant stirring rate.

Nair *et al.* (2012) produced biodiesel using clamshell (*Meretrix meretrix*) as the raw material for producing heterogeneous catalysts. The clamshell was powdered then calcined at 1173 K for 2.5 hours and 3.5 hours to determine the effect of time on catalytic activity. The results of the catalyst testing of the WCO transesterification process showed that the catalyst calcined for 3.5 hours had higher activity and reduced transesterification reaction time. From a number of experiments, the optimization values were catalyst weight of 3.0 g, molar ratio of methanol oil of 6.03, reaction temperature of 333 K and reaction time 3 hours. In addition, high yields over 89% and conversions over 97% were reported.

Anastopoulos *et al.* (2012) studied ethanolysis of four different vegetable oils (WCO, sunflower, cottonseed, and olive oil) using calcium ethoxide ( $(\text{Ca}(\text{OCH}_2\text{CH}_3)_2)$ ) as a heterogeneous catalyst. They found the optimal conditions for the first stage

transesterification were ethanol-to-oil molar ratio of 12:1, catalyst amount of 3.5% wt., and temperature of 80 °C, where the maximum yield of ethyl ester reached 80.5%. In the second stage, the ethyl ester yields 16% improvement in relation to one-stage transesterification, obtained by optimum reaction conditions is 0.75% catalyst concentration, and an ethanol-to-oil molar ratio of 6: 1. Some properties such as density, the viscosity, and the calorific value of ethyl ester produced have values close to the no. 2 diesel. Conversely, the cold filter plugging point was higher than conventional diesel.

Birla *et al.* (2012) used snail shell as a raw material for the production of heterogeneous base catalyst. Optimised results of yield and conversion were obtained from a number of variations in the amount of catalyst (1.0-3.5 wt% of oil), the methanol-to-oil molar ratio (4.83 to 9.65), reaction temperature (50-65°C), and reaction time (5-8 hours). The result of biodiesel were 87.28% and 99.58% for yield and conversion, respectively. In this condition, energy of activation was 79 kJ/mol, and frequency factor (A) was  $2.98 \times 10^{10}/\text{min}$  in first-order kinetics. Biodiesel properties obtained were in accordance with ASTM D 6751.

Balakrishnan *et al.* (2013) studied the application of barium waste construction sites melioration of marble waste as a raw material in producing the solid base catalyst. The construction waste material was calcined at 830 °C for 4 hours to increase the activity of the catalyst with large pores. The results of the catalyst testing of the WCO transesterification process showed that at a reaction temperature of 65 °C and reaction time of 3 hours, the methanol-to-oil molar ratio was 9, and the catalyst mass ratio of oil to 3.0 wt. % obtained methyl ester yield of 88%. In this process, the catalyst can be reused more than three times in the reaction process, offering a low operating reaction, and reducing energy consumption and environmental pollution from waste.

Niju *et al.* (2015) studied the transesterification WCO using CaO as a heterogeneous base catalyst derived from calcination of egg shells. Dried egg shells were crushed into small pieces. The calcination process was then performed in a muffler furnace under temperature at 900 °C for 2.5 hours in static air conditions. The results obtained from this test are high biodiesel yields of 95.05%, and 96.11%



conversion can be achieved under catalyst reaction conditions of 3% by weight of oil, methanol-to-oil molar ratio of 9, a reaction temperature of 65 °C, and reaction time of 3 hours.

### 2.1.3 Continuous Production of Biodiesel

Several works have been performed using continuous process to produce biodiesel using conventional heating such as Melero *et al.* (2014), Borges and Diaz (2013), Buasri *et al.* (2012) and Chen *et al.* (2010), while using microwave irradiation such as Choedkiatsakul *et al.* (2015), Encinar *et al.* (2012) and Barnard *et al.* (2007).

Encinar *et al.* (2012) investigated the production of methyl esters from soybean transesterification by the use of a modified microwave as a biodiesel reactor for continuous transesterification. They used KOH as the homogeneous catalyst. For comparison, the conventional heating systems were also employed in transesterification in homogeneous batch and flow processes. The transesterification reaction under microwave radiation yielded similar results but with very fast heating rates.

A continuous transesterification of an acidified WCO with methanol was carried out by Buasri *et al.* (2012). In this process, used calcium oxide is supported on an activated carbon catalyst (CaO/AC). This catalyst was prepared according to the new wet impregnation starting from aqueous calcium nitrate ( $\text{Ca}(\text{NO}_3)_2 \cdot 4\text{H}_2\text{O}$ ) aqueous solution on the activated carbon support of coconut shell in fixed bed reactor with outside diameter 60 mm and height 345 mm. Results showed that FFA conversion increases with increasing alcohol-to-oil molar ratio, catalyst bed height, and temperature, and decreases with increasing flow rate and initial moisture content in raw materials. FAME yield reached 94% at 60 °C reaction temperature, 25: 1 methanol-to-oil molar ratio and 8 hours residence time.

Borges and Díaz (2013) used heterogeneous catalyst from potassium-loaded pumice material (K-Pumice) in sunflower oil and WCO to produce biodiesel by

transesterification using a packed-bed catalytic reactor. This system is equipped with recirculation system to improve biodiesel production. To achieve potassium exchange and create some base sites on natural materials, pumice particles ranging in size from 1.40 to 3.0 mm were introduced into KOH solution. The reaction conversion increased slightly at elevated temperature from 50 to 60 °C, at reaction temperature at 55 °C, reaction time of 2 hours, methanol to oil molar ratio of 20:1, and catalytic packed-bed length of 8.2 cm, the value of FAME content of the biodiesel is 96.5% and conversion value of 99.5 %.

Li *et al.* (2013) performed the transesterification of soybean oil with methanol to synthesize biodiesel using  $\text{Ca}(\text{C}_3\text{H}_7\text{O}_3)_2/\text{CaO}$  solid-base catalyst in a stirring packed-bed reactor. The shell–core  $\text{Ca}(\text{C}_3\text{H}_7\text{O}_3)_2/\text{CaO}$  was prepared from a mechanically durable core CaO which reacted with glycerol to form thin layer of active  $\text{Ca}(\text{C}_3\text{H}_7\text{O}_3)_2/\text{CaO}$  on the outer surface. They used a stirring reactor by packing catalyst pellets inside four static columns and then stirred to mix soybean oil and methanol in the reactor. The oil/methanol mixture was forced to flow through the space between catalysts. Thus mass-transfer resistance is decreased by reducing the boundary layer, which improves the contact between reactants and catalyst. A biodiesel yield of 96.75% was achieved when the residence time was 123 min.

Melero *et al.* (2014) performed a continuous production of biodiesel from WCO in a packed bed reactor using a catalyst with a particle size formed from an agglomerated Zr-SBA-15 with bentonite clay. Under operating conditions, the mixture methanol to oil molar ratio of 50:1, temperature of 210 °C and pressure of 70 bar and a residence time of 30 minutes could produce FAME yield of around 96%.

Choedkiatsakul *et al.* (2015) used a commercial FlowSynth microwave reactor for the continuous production of biodiesel from palm oil. They applied homogeneous catalyst NaOH loading of 1% wt oil to produce a high ester content of 99.4%. The operating parameters are 1.75 min residence time, methanol to oil molar ratio of 12, microwave heating power of 400 W, reaction temperature of 70 °C. The energy consumption of palm oil transesterification as low as 0.1167 kWh/L of biodiesel was

required, proving that microwave reactors need less energy consumption as compared to conventional processes.

## 2.1.4 Reactor

Ideal reactor types are shown in Figure 2.5. Commonly, ideal reactors have three flow or contacting patterns, namely batch, plug and mixed flow.

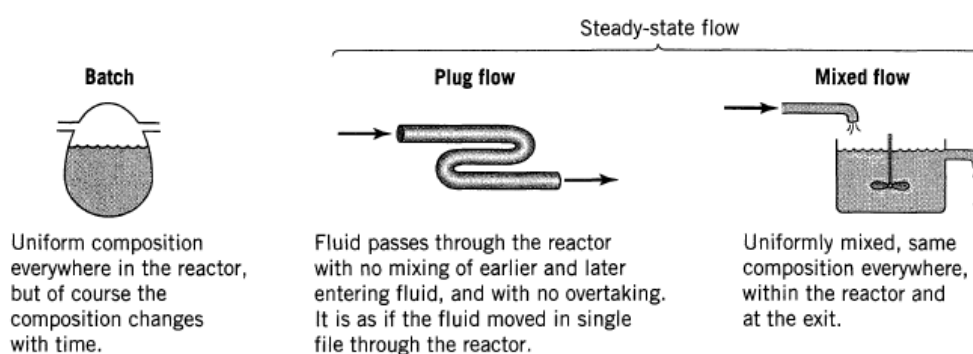


**Figure 2.5** Ideal reactor type (Levenspiel, 1999)

### 2.1.4.1 Space-time and Space Velocity

According to Levenspiel (1999) the reaction time is a measure of the natural performance for the batch reactor, as well as the space-time and space velocity of the exact performance measurement of the flow reactor. This term is defined as follows:

The space-time,  $\tau$  is time required to process one reactor volume of feed measured. In the ideal tubular reactor, space-time is the same as the residence time in the batch reactor only if volume changes are neglectable.

$$\tau = \frac{\text{volume mixture in reactor (ml)}}{\text{flowrate (ml/min)}} \quad (2.3)$$

$$\begin{aligned}
 \text{Volume mixture in reactor} & \\
 &= \text{Reactor volume} - \text{container volume} \\
 &\quad - \text{catalyst volume}
 \end{aligned}
 \tag{2.4}$$

The inverse of the space time is called the *space velocity* (Ancheyta, 2011).

$$\text{Space Velocity} = \frac{1}{\tau} = \left( \begin{array}{c} \text{number of reactor volume of feed at specified condition} \\ \text{which can be treated in unit time} \end{array} \right)
 \tag{2.5}$$

Measure of feed rate is well-known Liquid Hourly Space Velocity (*LHSV*),  $\text{h}^{-1}$

#### 2.1.4.2 Microwave Irradiation

Microwave irradiation is the electromagnetic wave that has a wavelength range from 0.01 m to 1 m or equivalent to a frequency range from 0.3 to 300 GHz. All microwave reactors for chemical synthesis and all domestic microwave ovens work at a frequency of 2.45 GHz corresponding to a wavelength of 12.25 cm (Motasemi, 2011).

Microwave heating of the dielectric material is a process of converting electromagnetic energy into heat in the irradiated material. Compared to conventional heating that has been used, microwave has advantages in many aspects such as: (i) no contact occurs during heating process (ii) energy transfer is more dominant than heat transfer; (iii) selectively heated materials, (iv) faster heating process; (v) heating based on volumetric; (vi) higher levels of safety and automation; (vii) heating of the inner parts of the material body; and (viii) faster to start and stop. Because of the many advantages in this microwave, it can be used in various scientific and technological fields for the heating process of various materials (Menéndez *et al.*, 2010).

### 2.1.5 Design of Experiments

Response surface methodology (RSM) is an empirical statistical technique used for multiple regression analysis by using quantitative data. This solves the multivariate data obtained from a well-designed experiment to solve the multivariate equations simultaneously (Sultania *et al.*, 2011). This method has been applied successfully to optimise the production of biodiesel in fat and oil feedstocks, including mahua oil, jatropha oil, waste rapeseed oil and animal fat (Mansourpoor and Shariati, 2012) and waste cooking palm oil (Charoenchaitrakool and Thienmethangkoon, 2011; Wan Nor Nadyaini and Nor Aishah, 2011).

Among a number of experimental designs, the Box-Behnken is a good design applied to the surface response methodology because it allows: (i) estimation of quadratic model parameters; (ii) construct sequential designs; (iii) can detect the lack of suitability of the model; and (iv) the use of blocks. Some advantages of the Box-Behnken design compared to other response surface designs such as central composites design (CCD), Doehlert matrices and full-level factorial designs are Box Behnken designs and Doehlert matrices are slightly more efficient than CCD. Box Behnken designs and Doehlert matrices are more efficient than the three-level factorial. The efficiency of an experimental design is defined as the number of coefficients in the approximate model divided by the number of experiments (Ferreira *et al.*, 2007). Applications of the Box–Behnken design in the optimization of chromatographic methods was reported by Ferreira *et al.*(2007) and optimization of biodiesel yield using Pongamia oil as raw material and its stability analysis was applied by Dwivedi and Sharma (2015).

## 2.2 Utilization of Biodiesel from Waste Cooking Oil in Diesel Engines

Several authors have investigated the use of WCOME in combination with diesel fuel in diesel engine such as blending with biodiesel. They examined the effect of using this combination of fuel on diesel engines relating to characteristics of

performance and emissions, characteristics of the combustion and characteristic of injection.

### 2.2.1 Diesel Engine Performance

Özsezen *et al.* (2009) performed DI diesel engine testing using waste palm oil (WPOME) and canola oil biodiesel (COME) to investigate its performance, combustion characteristics and diesel engine injection. They report that by using WPOME and COME as fuel, maximum engine torque declined slightly compared to petroleum-based diesel fuel (PBDF), while BSFC was 7.48% and 6.18% higher than PBDF. The reason for the increase of BSFC from biodiesel is the heating value of biodiesel is 8-10% lower than PBDF. Crankshaft advances to start of injection (SOI) for WPOME and COME are  $0.75^\circ$  and  $1.25^\circ$  CA earlier than PBDF. This is due to the high density and viscosity and the low of compressibility of the biodiesel blend. They conclude that combustion characteristics such as the start of combustion (SOC) time, maximum in-cylinder pressure ( $P_{\max}$ ), combustion duration (CD) and in-cylinder gas temperature are affected by shorter ignition delay (ID) and progress on SOI time. Also, the use of biodiesel can improve HC, CO and smoke emissions, unless  $\text{NO}_x$  has increased.

Muralidharan and Vasudevan (2011) examined the effect of four waste cooking oil biodiesel blends from 20% to 80% by volume to diesel fuel and five different compression ratios (18 to 22) on a single cylinder, four-stroke. They investigated the effect of several parameters on performance, emissions and combustion characteristics of this engine. The engine is tested at 50% speed and engine speed is 1500 rpm. The test results showed that the maximum BTE was obtained with a mixture containing 40% biodiesel and a 21: 1 compression ratio. Under the same conditions, BSFC was obtained minimum. However, there was a slight increase in  $\text{NO}_x$  and HC emissions. It was also shown that the mixture causes higher combustion pressures on higher compression ratios due to longer IDs, lower maximum pressure gain ( $dP_{\max}$ ) and  $\text{HRR}_{\max}$  levels compared to diesel fuel. However, other studies have reported different results than this study, for example on HC emissions.

Hwang *et al.* (2014) performed testing on a single-cylinder, common-rail, direct injection diesel engine using WCO biodiesel fuel. They investigated the combustion and combustion characteristics of engines on two different engine loads to determine the effects of injection pressures on 80 and 160 MPa and variations of injection timings from -25 to 0°CA BTDC. They found that the peak cylinder pressure ( $P_{max}$ ) and peak heat release rate ( $HRR_{max}$ ) were slightly lower due to biodiesel fuel injection timing, while the ignition delay (ID) was slightly longer. In addition, it was found that high fuel injection pressures it can improve smoke, CO, HC emissions, while  $NO_x$  emissions increase.

The effects of WCO biodiesel on the Euro IV diesel engine have been investigated by An *et al.* (2013) with different engine speeds, i.e. standby speed, 1200-3600 rpm at 1200 rpm intervals. Loads are varied at 25%, 50% and 100%. The results of the combustion characteristics indicate that the  $HRR_{max}$  value is lower with slightly shorter ignition delay (ID) for biodiesel fuel compared to diesel fuel No.2 on testing engine at low loads, indicating that the addition of biodiesel fuel significantly increases CO emissions and reduces  $CO_2$ , HC and  $NO_x$  emissions. However, the opposite trend occurs in lower engine revolutions and higher engine load. In general, the addition of biodiesel fuel to diesel fuel No. 2 leads to considerable reductions in emissions of HC, PM,  $SO_2$  and CO, while  $NO_x$  emissions have increased slightly.

Abu-Jrai *et al.* (2011) performed diesel engine testing using biodiesel from WCO, where the WCO used as raw material for producing of biodiesel fuel came from a restaurant. In testing, the engine used biodiesel blends with diesel fuel No. 2 with the proportion of 50% (vol) and mixture tested on different engine loads. The result of this experiment is the reduction of smoke emissions and HC and  $CO_2$  with increased load. The emissions test results indicated that the increase of  $NO_x$  emissions in the use of biodiesel fuel occurs in the more advanced fuel injection time in consequence of higher modulus of biodiesel fuel bulk. Also, they decided that the application of exhaust gas recirculation can reduce the emission of  $NO_x$  and exhaust gas with 50% exhaust gas recirculation (EGR) level rate.

Lapuerta *et al.* (2008) tested direct injection diesel engines using biodiesel fuel produced from WCO. With EU 70/220 emission directives, they tested the effect of 30%, 70% and 100% (in vol) mixtures on five selected machine operation modes. They concluded that the addition of biodiesel in the mixture could reduce smoke emissions and PM emissions as well as average particle diameter.

Can (2014) performed an investigation of biodiesel blends with No. 2 diesel fuel on single cylinder diesel engines, direct injection, four-stroke, naturally aspirated diesel engines. The engine was operated with four different engine loads, equivalent to BMEP from 0.12 to 0.48 MPa with interval 0.12 MPa and 2200 rpm engine speed. For this test, two types of WCO were mixed with 5% and 10% with No.2 diesel fuel. Test results show that higher fuel cetane number values lead to ignition of biodiesel fuel burning delays. In addition, the maximum heat release rate and increased pressure level in the cylinder slightly increased and the duration of combustion was lengthened by the addition of biodiesel.

Ozsezen and Canakci (2011) used canola oil methyl ester (COME), waste frying palm oil methyl ester (WPOME) and petroleum based diesel fuel (PBDF) as fuel to study performance characteristics, burning and injection of injection diesel engines. The results show that with the use of WPOME or COME, brake power decreases 4-5%, while BSFC increases by 9-10% compared with PBDF. In addition, WPOME and COME biodiesel leads to the reduction of emissions such as CO, CO<sub>2</sub>, unburned hydrocarbons (HC), and smoke opacity compared to machines that use PBDF. However, the use of both methyl esters increased NO<sub>x</sub> emissions by 11-22% compared to PBDF over the speed range.

The SFC of biodiesel or biodiesel blended is higher than diesel fuel (DF) for the same power (Altun *et al.*, 2008; Rakopoulos *et al.*, 2006). This can be attributed to the fact that biodiesel has a lower calorific value and lower density than diesel fuel. Also, its inability to mix well with air cause complete combustion in the diesel engine (Altun *et al.*, 2008; Mahanta *et al.*, 2006).



### **2.2.2 Diesel Engine Combustion**

Diesel combustion is a process of ignition of fuel that occurs shortly after fuel is injected into a cylinder containing pressurized air that has high temperature and high pressure. The combustion process does not occur immediately when fuel is injected inside the engine cylinder containing turbulent compressed air, but there is a period of time called the ignition delay, where the fuel droplets evaporate and ignite and undergo chemical reaction that make the chemical species needed for spontaneous ignition in the air inside the cylinder (Challen and Baranescu, 1999).

After a considerable time lapse, ignition will occur spontaneously in a mixed air-fueled area that has a fuel ratio approaching stoichiometry. The combustion takes place very quickly because the mixture of air with fuel occurs during the ignition delay period. The temperature rises rapidly and pressure of the fuel-air mixture inside the cylinder will accelerate uncontrolled combustion until the backlog runs out. The fuel in the core spray is still too rich to burn, while the fuel on the perimeter of the spray is leaner to burn, so the burning process becomes slower. In this process, the combustion is controlled by the rate at which air enters and a combustible mixture is formed. The first stage of combustion is known as the premix phase, in which the combustible fuel burns quickly, and the second phase is mixing (diffusion) phase. The level of combustion during the mixed-controlled phase depends heavily upon the motion of the air and the momentum of the fuel spray. The burn rate starts high enough because there is enough excess air and the fuel spray carries the air quickly. After the end of fuel injection, especially at high loads in the absence of excess air as in light loads, the combustion rate will decrease gradually to zero (Challen and Baranescu, 1999).

### **2.2.3 Diesel Engine Emission**

Emissions produced in diesel engine combustion depend heavily on engine types, operating conditions of the engine, fuel formulations, after-treatment technology, engine wear and maintenance, and many other factors (Chin, 2011). Therefore, sub-

sections of the chapter will provide some research in which the role of fuel is very influential on exhaust emissions.

The assessment impacts of biofuels in the diesel engine exhaust gas are mainly carbon monoxide (CO), carbon dioxide (CO<sub>2</sub>), Nitrogen Dioxide (NO<sub>2</sub>), unburned hydrocarbons (uHC), nitrogen oxide (NO<sub>x</sub>), particulate matter (PM) and smoke (Rutz and Janssens, 2007; Said, 2006). This is relevant because one of the main greenhouse gases (CHG) is CO<sub>2</sub> (Rutz and Janssens, 2007). Most researchers concluded that the emissions of PM, HCs and CO were reduced in all cases when the biodiesel or biodiesel-blended fuels were used in the diesel engine; in contrast, the NO<sub>x</sub> emission increases (Lee *et al.*, 2005). These states are also relevant to the results of evaluations by the EPA of the United States on the impact of biodiesel use on pollutant emissions for heavy-duty highway engines as shown in Figure 2.6.

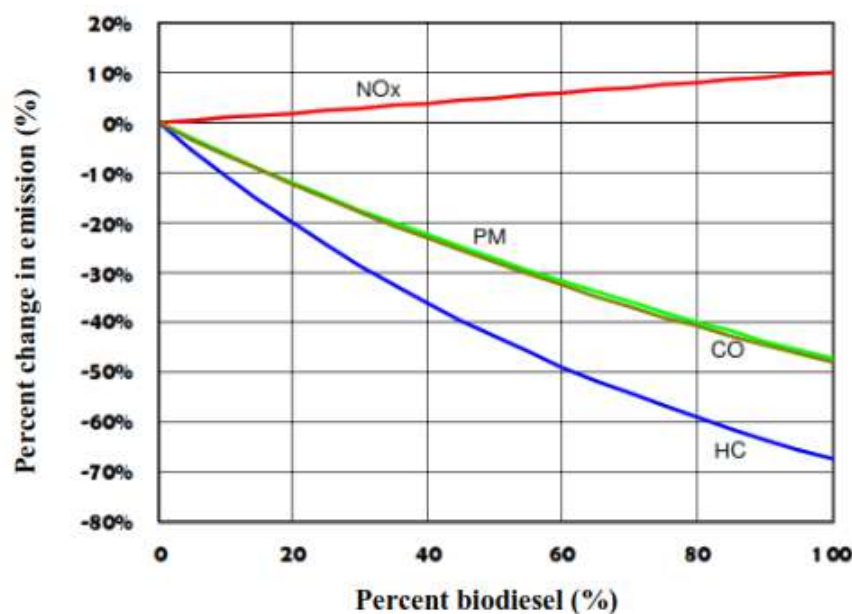


**Figure 2.6** Average mission impact of biodiesel fuel in heavy-duty highway engine (United States Environmental Protection Agency (EPA), 2002)

Compared with biodiesel oil, the CO emitted by all the vegetable oil blends of various origins is higher than biodiesel oil produced by the corresponding DF case (Rakopoulos *et al.*, 2006). The use of biodiesel in diesel engines has an impact on the reduction of exhaust emissions; about CO of 20%, HC of 30%, PM of 40% and soot

emissions of 50%. In contrast, NO<sub>x</sub> emissions increase by about 10-15% (Canakci and Sanli, 2008; Graboski and McCormick, 1998). However, retarding the injection timing can be implemented to solve the high NO<sub>x</sub> problem (Canakci and Sanli, 2008).

The increase in engine speed and engine load causes NO<sub>x</sub> emissions to decrease. The smaller calorific value of the blend could reduce NO<sub>x</sub> emissions (Altun *et al.*, 2008). Although some researchers reported that NO<sub>x</sub> emissions were concluded to be insensitive to ignition delay, others stated that the increase of NO<sub>x</sub> emissions could be affected by ignition delay (Altun *et al.*, 2008).

The CO emission is influenced by many parameters such as air-fuel ratio and the engine temperature. Diesel engines that use biodiesel blends will produce low CO<sub>2</sub> emissions with lower engine speed compared to diesel fuel (Altun *et al.*, 2008). If the fuel is burned completely in the engine, then only the water content (H<sub>2</sub>O) and carbon dioxide (CO<sub>2</sub>) will form in the exhaust gas. However, in reality, the combustion process is always incomplete, producing species in the exhaust of the presence of unburned hydrocarbons from fuels and partial oxidation processes such as carbon monoxide (Challen and Baranescu, 1999).

### **2.2.3.1 Carbon Monoxide**

Carbon monoxide is colourless, tasteless, and odourless, but toxic. This gas does not irritate the skin or mucous membranes, but it can bind the haemoglobin in the blood up to 210 times the power of oxygen. As the contact between blood and CO increases, the more haemoglobin is bound to CO and the oxygen carrying capacity in the blood decreases, which can cause unconsciousness and ultimately death. In the diesel engine exhaust, this product is a product of incomplete hydrocarbon fuel combustion. Therefore, CO emissions are heavily dependent on the ratio of air fuel compared to the ratio of stoichiometric air-fuel. Fuel-rich combustion always generates CO and emissions increase almost linearly with deviations from stoichiometry. In diesel engines operating with a fuel-lean mixture, their CO emissions are usually well below the specified limits and not too apprehensive. The CO products in diesel engine

exhaust gases occur due to incomplete mixing where combustion takes place in rich local conditions. To reduce CO and unburned hydrocarbon emissions, oxidation catalyst can be used in the exhaust. This process is assisted by excess air in the exhaust gases. In general, CO emissions from diesel engines are very low as they always operate under fuel-lean conditions (Challen and Baranescu, 1999).

### **2.2.3.2 Carbon Dioxide**

Ideally, the perfect combustion process in hydrocarbon fuels produces only carbon dioxide (CO<sub>2</sub>) and water. The proportion of CO<sub>2</sub> and water depends on the ratio of carbon-hydrogen content to fuel, to ordinary diesel. This value is about 1: 1.75. In other words, carbon dioxide emissions from engine exhaust gases can be reduced by lowering the carbon content of fuel per unit of energy, or by increasing the engine fuel efficiency.

Recently, CO<sub>2</sub> emissions from burning fossil fuels has attracted much attention. Solar energy reaches the earth after passing a layer containing water vapour, CO<sub>2</sub> and other gases, but this layer traps some thermal radiation which is then released by the earth. This phenomenon is called 'Greenhouse effect', which causes the earth's temperature to be warmer than it should be. The CO<sub>2</sub> levels in the atmosphere have increased since the start of the Industrial Revolution, apparently due to the widespread and growing burning of fossil fuels. The results prove that the global climate is affected by this change. This problem can be known by increasing the world average temperature, a phenomenon known as 'global warming'.

As an inevitable end point of combustion, CO<sub>2</sub> cannot practically be reduced only by the after-treatment process (as with catalytic converters). Indeed, catalytic oxidation of CO and HC will increase CO<sub>2</sub> emissions slightly (Challen and Baranescu, 1999).

### 2.2.3.3 Unburned Hydrocarbons

Constituents in unburned hydrocarbons (uHC) can cause strong irritation of mucous membranes in the eyes and throat. Unburned hydrocarbons participate in the smoke haze-forming reaction that produces ozone and other irritating substances. Unburned hydrocarbon emissions (uHC) in fuel is comprised of completely unburned and only partially burned. In the cylinder engine occurred the widespread distribution of fuel-air ratio due to the heterogeneous nature of diesel combustion. Unburned hydrocarbon emissions are attributed to the fuel mixture to air that is too lean to ignite the fire automatically or to support a spreading flame, or fuel into the air mixture that is too rich to ignite, such as the core of the fuel spray core (Challen and Baranescu, 1999).

The chemical composition of the fuel can significantly affect the composition and the amount of organic emissions. Fuel can escape from the main combustion process with two main mechanisms, namely over-mixed over-lean regions and under-mixed region. The first mechanism is the over-mixed over-lean region whose process takes place before ignition. Diesel fuel is injected into a cylinder containing hot pressurized air when the piston approaches the top dead centre. The chemical reaction begins with spontaneous ignition of the fuel occurring after a short delay period-during mixing of fuel and hot air. Not all fuels burned in the cylinder, only a mixture of air and fuel within flammable limits will burn. The mixture of freshly-injected fuel injected is too rich, thus it takes time to mix with enough air to support the combustion.

The fuel injected prior to ignition causes the mixture to be too rich to burn, so it needs mixing with too much hot air to make the lean mixture. Further mixing is not probable to reverse this condition. A slower thermal oxidation reaction can occur, but it is too slow to consume in accordance with the time available. Fuel injected after ignition occurs cannot over-mix with air. In this process, the fuel will burn because it is still within flammable limits. Thus, the over-mixed over-lean fuel injected within a period of ignition delay escapes from the main combustion and is a significant non-burning fuel source. The process of extending the ignition delay will increase uHC emissions (Challen and Baranescu, 1999).

The second major source of unburnt hydrocarbon emissions from diesel engines is the mixed fuel that is injected close the end of combustion. The mixing rate with air depends on relatively strong movement when fuel is injected. After the injection ends, the secondary injection may occur, or the fuel left in a small volume at the tip of the nozzle (the 'sac' volume) can enter the combustion chamber. With the latter, there are some delays while the fuel is evaporated. Alternatively, some fuels in the vapour phase or liquid phase enter at low speed into the rapidly cooling combustion chamber. At that time, the fuel is not mixed with air effectively, and some fuel leaves the cylinder without burning or only partial burning. This uHC source can be controlled by designing a fuel injection system that has a fast and clean tip for injection (so-called 'spill rate'). Injectors with minimum sac volumes are now standard (Challen and Baranescu, 1999).

#### **2.2.3.4 Nitrogen Oxides**

Nitrogen oxides ( $\text{NO}_x$ ) are comprised of nitric oxide (NO) and nitrogen dioxide ( $\text{NO}_2$ ), and typically over 90% of the  $\text{NO}_x$  from diesel engine is NO (Moser, 2011). However, NO will then oxidize to  $\text{NO}_2$  after the engine exhaust gas is emitted into the atmosphere. The NO gas is not a strong irritant, but binds to haemoglobin in the same way as CO. The  $\text{NO}_x$  emissions are unexpected result of combustion, not an incomplete stage in the combustion process (Challen and Baranescu, 1999).

Chemical kinetics results show that  $\text{NO}_x$  emissions are strongly influenced by the temperature of combustion, length of time and concentration of oxygen in the combustion zone. The highest NO concentration in exhaust gas was obtained for a slightly lean mixture and rapid combustion (Heywood, 1988). Also, several factors affecting  $\text{NO}_x$  diesel engine emissions are fuel properties especially cetane number, fuel injection timings, speed and exhaust gas recirculation rates (Said, 2006).

The formation of NO emissions in the exhaust gas depends on the high temperature and the amount of oxygen. High temperature occurs after the combustion process. Thus, the initial portion of combustion is essential to control the formation of

NO<sub>x</sub>, since almost all NO<sub>x</sub> is formed at the first 20 °CA after the start of combustion. Therefore, the application of techniques to control NO<sub>x</sub> is focused on this combustion stage. However, most of these techniques can decrease temperatures of combustion and increase in hydrocarbon emissions, particulate emissions, and fuel consumption. For this reason, it is common to refer to the 'trade-offs' curve between NO<sub>x</sub> and particulate emissions and fuel consumption of diesel engines operation (Challen and Baranescu, 1999; Said, 2006).

## **2.3 Modelling Direct Injection Diesel Engine in GT-SUITE**

### **2.3.1 Overview**

GT-SUITE is a simulation software that has a multi-use platform with many physical libraries, which contain both basic and high-level components. By using this component, engineers are empowered to build a model system with almost unlimited variation. This application covers many industries, and has grown, and continues to develop special tools and components for many industries, one of them on-highway vehicles. The engine system analysis of this software is based on the dynamics of one-dimensional gas representing flow and heat transfer both on pipes and other components. In addition, many other special models can be applied for many kinds of system analysis (Gamma Technologies, 2003). The detailed model information related to the present work is described in sub-sections 3.4.

Several researchers have used this GT-SUITE software to analyse performance, emission and combustion of diesel engine (King, 2002; Liu *et al.*, 2010; Meyer, 2011; Said, 2006; Shah *et al.*, 2014; Yang, 2011).

Liu *et al.* (2010) performed modelling and testing of a four-stroke single cylinder diesel engine using pure soybean, cottonseed, and algae biodiesel as test fuels. An engine simulation tool developed by Gamma Technologies, GT Power, has been used to perform predictive engine combustion simulations using direct-injection jet modelling technique. Various physical and thermodynamic properties of the test fuels

in both liquid and vapour states are required as fuel property in combustion simulations. The engine emissions of the conventional diesel and biodiesel fuels have been predicted from combustion simulations to investigate emission impacts of the biodiesel fuels using the calculated biodiesel fuel properties and an assumed fuel injector sac pressure profile.

Yang (2011) studied the modelling and control of the combustion mode transition problem for a multi-cylinder engine with dual-stage valve lift and electrical variable valve timing (VVT) systems. The developed engine model was calibrated and validated using the simulation results from the corresponding one-dimensional GT-Power engine model in the dSPACE based HIL engine simulation environment. The continuous dynamics of engine air-handling system and crankshaft were modelled by traditional time-based mean value models, while the engine combustion process is modelled as a crank-based (crank-based) modelling function using a two-zone combustion modelling approach. The developed combustion model is capable of simulating the SI, HCCI, and SI-HCCI hybrid combustion modes. This unique modelling approach made it possible for the engine model to be simulated in real-time in a dSPACE based hardware-in-the-loop (HIL) system due to its low computational throughput.

Shah *et al.* (2014) used GT Power as a simulating tool to study the development of a turbocharged direct-injection compression ignition (CI) engine model using fluid-dynamic engine simulation. The model was fuelled with diesel, and then with various blends of biodiesel and diesel by allotting suitable parameters to predict an optimum blended fuel. During the optimization, the main focus was on the engine performance, combustion, and one of the major regulated gaseous pollutants known as oxides of nitrogen (NO<sub>x</sub>). They stated that this simulation tool has the potential for use in turbocharging analysis, gas exchange, combustion, simple and complex heat release model for turbocharger matching, thermal analysis, engine performance, and exhaust emissions.



### 2.3.2 Mathematical Modelling

In GT-SUITE, using some reference objects such as gas is usually described with the composition C: H: O: N, low heating value, critical temperature and pressure, enthalpy, and transport properties that include viscosity and thermal conductivity. As for fluids, the necessary inputs are enthalpy, density, and transport properties. In addition, usually, every liquid reference object must be associated with the reference object of the gas to know the evaporation of the liquid. The fluid flow in the pipeline is simplified as a transient one-dimensional problem involving simultaneous solutions of continuity equations, momentum and energy only in the flow direction. All the average quantities cross the flow direction as this is a one-dimensional problem.

The study presents a developed modelling to predict the performance and exhaust gas emissions of a compression ignition engine fuelled by PDM, POME blend with PDM and WCOME blend with PDM. This modelling is carried out from the first law of thermodynamics. A thermodynamic model is developed with the aid of Matlab code, Zero-dimensional flow conditions inside the cylinder, single zone, a closed cycle model.

## **CHAPTER 3**

### **RESEARCH METHODOLOGY**

In this research there are two main activities namely (1) experimental biodiesel fuel was produced from the WCO by transesterification process in microwave heating using solid catalyst and diesel engine test using POME blends and WCOME blends as fuel (2) numerical approach which includes modelling and simulation with GT SUITE software on diesel engine one-cylinder direct injection and comparison of this result with experimental result. The research methodology flowchart is shown in Figure 3.1.

In experimental biodiesel fuel, the Box-Behnken experimental design was used to study the interaction between variables on the response and to determine the optimum combination of variables. Design Expert version 7.0 was used to solve the above problem. This software applies ANOVA to test significance because it can be used to test for means for more than two populations, but the mean test can be used to test only for a single population or at most two populations.

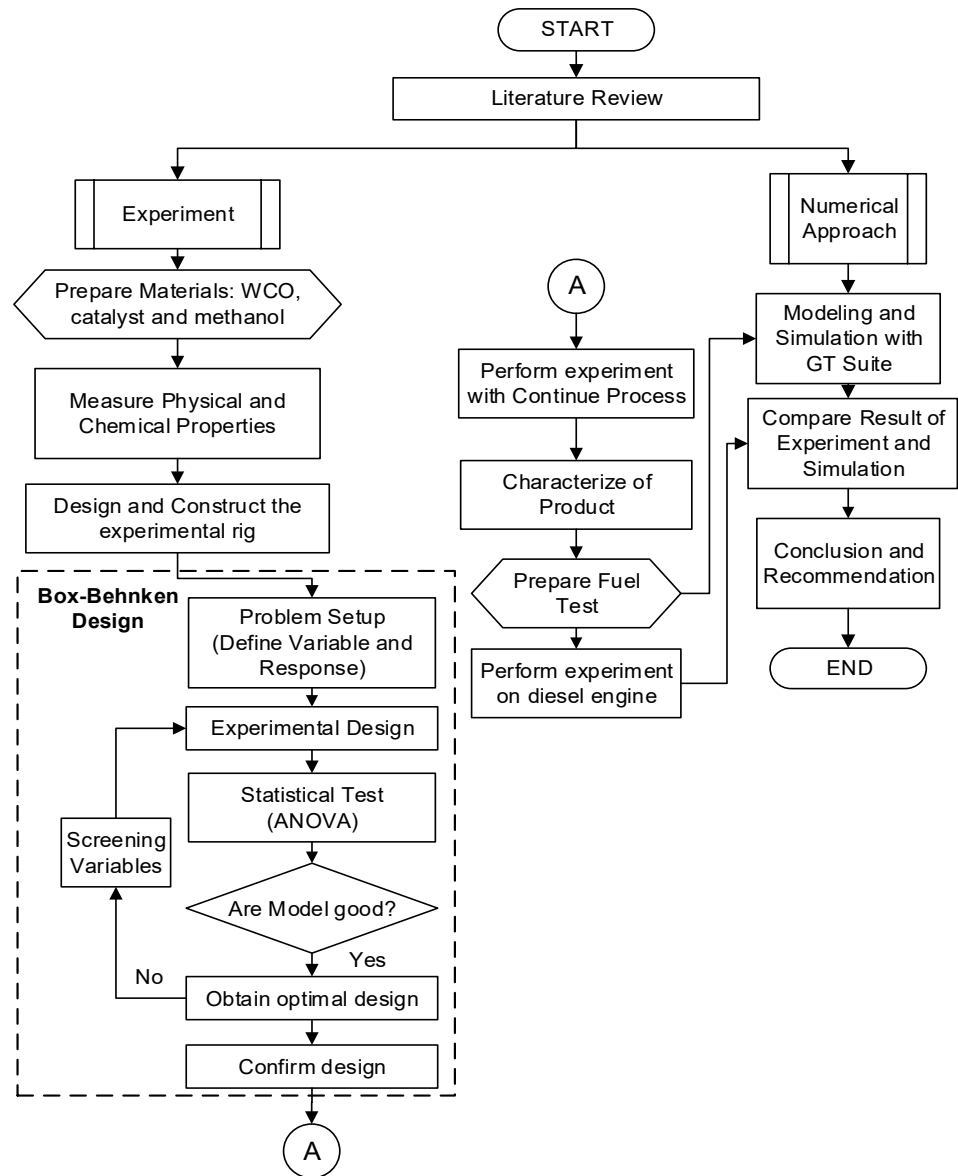


**Figure 3.1** The research methodology flowchart

### **3.1 Transesterification Process of Waste Cooking Oil**

#### **3.1.1 Materials and Methods**

WCO as the raw material of biodiesel was obtained from fried banana commonly found around the university. This usually contains food waste in the form of solids, therefore filtering is necessary. In addition, water content contained in the WCO needs to be removed by evaporation. Evaporation of water was performed by heating in an electric oven at 110 °C for 4 hours. A small part of the WCO was taken as a sample to determine the FFA content by titration. The result of FFA analysis was used to select catalyst and the transesterification process. Methanol analytical reagent (AR) Grade was obtained from QRċC, New Zealand, and used as alcohol in the transesterification process.

The raw material for catalyst is cockle shells washed with tap water and distilled water to remove sand and seaweed deposited on its surface and then dried naturally. The cockle shells were crushed using a hammer and sieved to the size of 2 mm to 4 mm. Furthermore, cockle shells were decomposed in the furnace at a temperature of 900 °C for 3.5 hours in accordance with the method performed by Nair (2012). After the decomposed cockle shells become cold and then stored in the desiccator before it use in transesterification process. Characterization was performed using X-ray diffraction (XRD) to see the structure of the oxide formed. The characterization results obtained are compared with data JCPDS, which is standard for XRD diffraction pattern data.

### 3.1.2 Experimental Design and Optimization

The Box-Behnken experimental design was used to study the interaction between variables on the response and to determine the optimum combination of variables. Table 3.1 shows the independent variables in the WCO transesterification process used for Box-Behnken experimental design. There are four variables namely power input, catalyst weight, stirrer speed and flowrate, where each variable uses three-level design levels.

**Table 3.1 :** Independent variables in transesterification of waste cooking oil used for Box-Behnken experiment design

Variables	Unit	Levels	
		Low	High
Power Input ( $P_m$ )	watt	180	450
Catalyst weight ( $W_c$ )	gram	10	20
Stirrer speed ( $N_s$ )	rpm	200	400
Flowrate ( $F$ )	ml/min	5.22	6.97

The regression and graphical analysis of the data was analysed using the Design Expert version 7.0 software. For each experiment, samples were taken three times. The first sample was taken from one-third of the space-time, the second sample was from the two-thirds of the space-time and the last sample was taken when the value was similar with the space-time. The conversion values of WCO biodiesel for all three samples were taken in response to the design experiment. Experimental data from the implementation of above experimental design were analysed by surface

response regression using second-order polynomial function as in Eq. 3.1 (Dwivedi and Sharma, 2015).

$$y = \beta_o + \sum_{j=1}^k \beta_j X_j + \sum_{j=1}^k \beta_{jj} X_{j^2} + \sum_{i=1}^{j-1} \sum_{j=2}^k \beta_{ij} X_i X_j + \varepsilon \quad (3.1)$$

where  $y$  is the predicted response,  $\beta_o$  stands for the constant term,  $k$  is the number of variables,  $\beta_i$  stands for the coefficient of the linear parameters,  $x_i$  and  $x_j$  are the uncoded independent variables,  $i$  and  $j$  are the linear and quadratic coefficients respectively, and  $\varepsilon$  is the residual associated with the experiment.

Independent variables in Table 3.1 can be simplified by knowing the relationship between the  $LHSV$ , catalyst weight and flowrate as shown in the Eq. (3.2).

$$LHSV = \frac{60 \times F}{V_c} \quad (3.2)$$

where  $V_c$  is volume of catalyst, so that Eq. 3.2 can be expressed in equation as follows:

$$LHSV = \frac{60 \times F}{\frac{W_c}{\rho}} \quad (3.3)$$

Thus, the four variables in Table 3.1 can be simplified by three variables as shown in Table 3.2.

**Table 3.2 :** Simplification of independent variables in the transesterification of waste cooking oil used for Box–Behnken experiment design

Variables	Unit	Symbols	Levels		
			-1	0	1
Power Input ( $P_m$ )	watt	A	180	315	450
Stirrer speed ( $N_s$ )	rpm	B	200	300	400
$LHSV$	$h^{-1}$	C	31.19	17.83	83.19

The experiment design and optimisation process for this experiment used Design Expert software. Design Expert is a piece of software designed to help with the design and interpretation of multi-factor experiments. The software covers a wide range of designs, including factorials, fractional factorials, response surface design and composite designs. Box-Behnken designs are response surface designs specifically made to require only 3 levels. Box-Behnken designs are available for 3 to 10 factors. They are formed by combining two-level factorial designs with incomplete block designs. This procedure creates designs with desirable statistical properties but, most importantly, with only a fraction of the experiments required for a three-level factorial. Because there are only three levels, the quadratic model is appropriate. The analysis of variance (ANOVA) can be used to access various techniques for analysing and interpreting the fitted models.

The flowchart for experiment design and optimization of WCO biodiesel is shown in Figure 3.2.

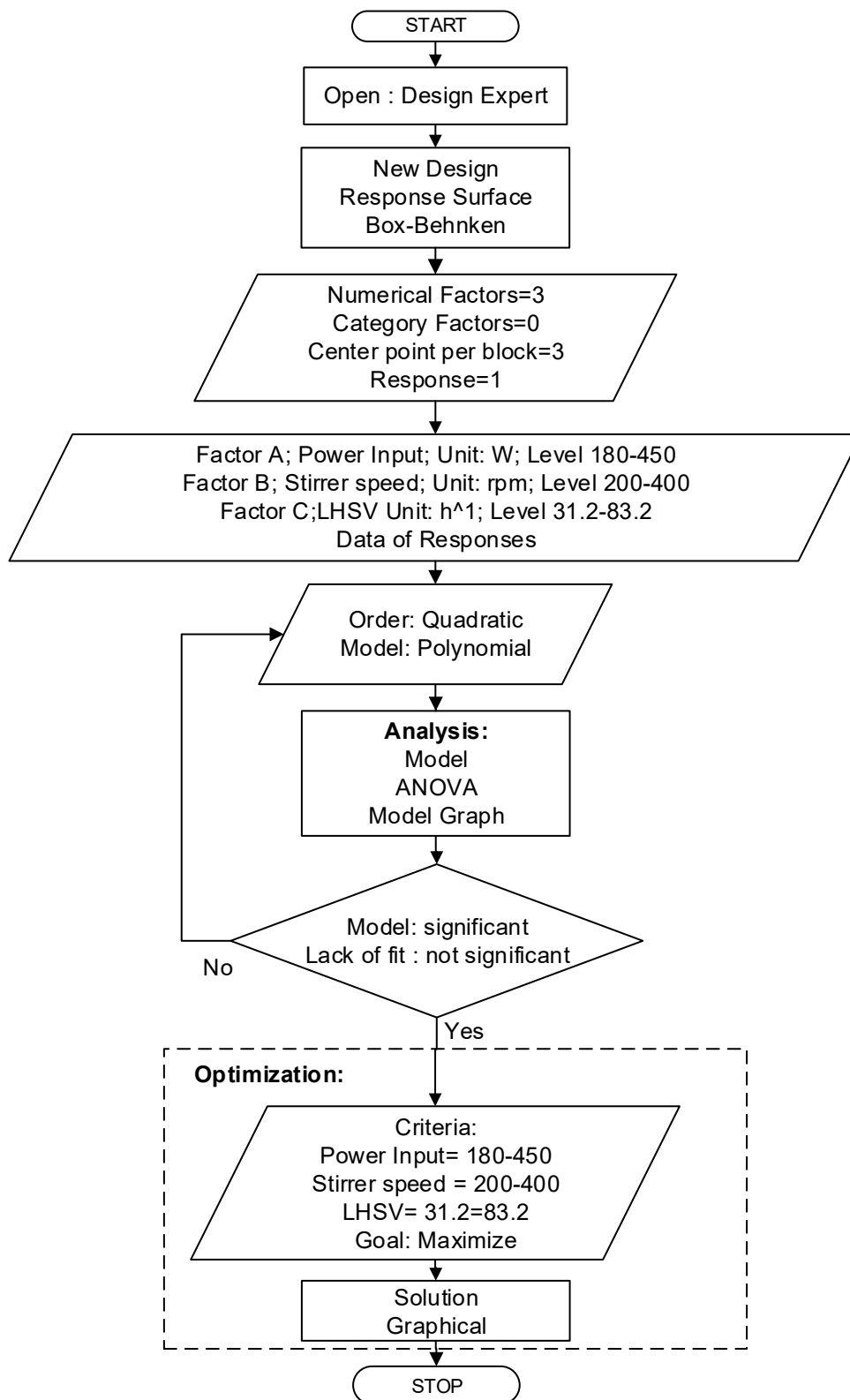


**Figure 3.2** The experiment design and optimization of conversion of WCO biodiesel flowchart



### 3.1.3 Experimental Set-up and Procedure

This transesterification reaction process is carried out by using a modified 1 kW domestic microwave system that has a frequency of 2450 MHz. The microwave power can be selected at different levels from 100 to 1000 W and for various exposure times (1-90 minutes). The catalyst was packed inside a perforated plastic container mounted on a stirrer shaft and inserted inside the reactor. The stirrer speed was controlled by an overhead high-speed stirrer with a digital regulator (WiseStir model HS-30D) placed at the top of the microwave. Stirrer speed 200, 300 and 400 rpm were used in this research. Three holes were drilled at the top reactor cover of the domestic microwave oven for placing the reactor inside the microwave. Two K-type metallic thermocouples are used as the temperature transducers. One of the transducers is mounted on the bottom of the reactor (T1), while the other is mounted on the top of the reactor (T2). Both transducers are used to measure the temperature of the oil mixture and methanol in the reactor. Thermocouples connect to Pico's data acquisition system and then connect to a personal computer. For recording temperatures during the reaction process, a picolog is required and should be installed in a personal computer. The thermocouple (T1) is also connected to temperature controller and microwave power input to maintain the temperature. Microwaves and thermocouples must be grounded to avoid sparks that can ignite the oil and methanol mixture in the reactor, otherwise preventing the difference between the read temperatures. The experimental set-up for single step transesterification continues the process with catalyst container stirrer as shown in Figure 3.3. Detailed specification and drawing are shown in Appendix C and D.

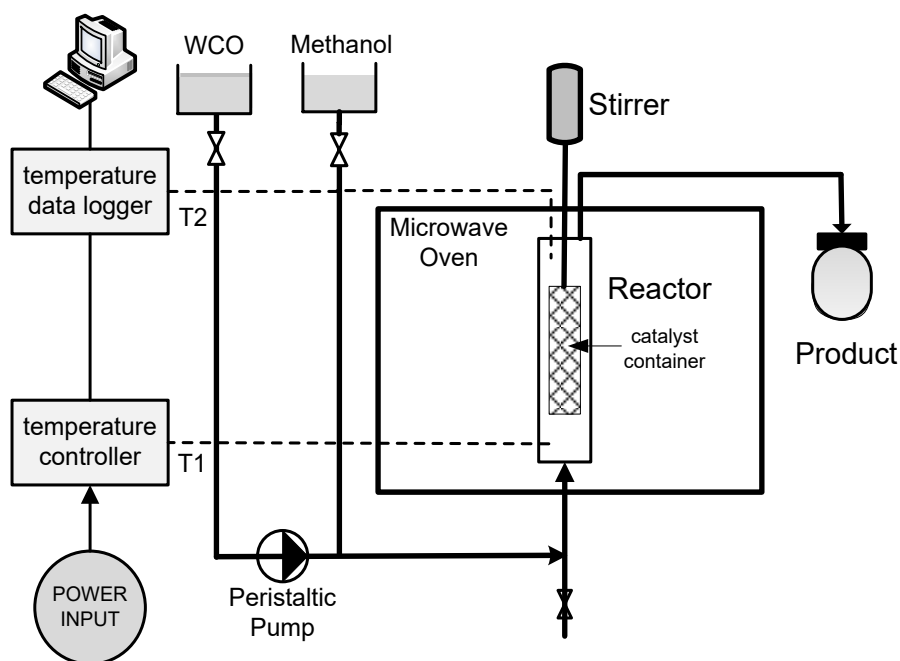


**Figure 3.3** The experimental set-up for single step transesterification continues process with catalyst container stirrer

A peristaltic pump was used to feed WCO in a reactor. The flow rate of this pump can be adjusted using speed regulator in peristaltic pump unit. The relationship between pump speed is directly proportional to the flow rate. The calibration result from this pump is shown in Appendix E.

The molar ratio of alcohol to oil and reaction temperature in this study were fixed at 9:1 (Aworanti *et al.*, 2013; Buasri *et al.*, 2013; Niju *et al.*, 2015) and 65 °C (Buasri *et al.*, 2013). The weight of catalyst was varied 10.00, 12.73 and 20.00 gram. The flow rate of WCO is regulated by setting the speed of a peristaltic pump of 24, 28 and 32 rpm. The alcohol was put into the reactor using a syringe for certain volume every minute.

The data retrieval procedure is as follows:

- i. Weigh catalyst and insert catalyst into the container.
- ii. Fix a container on the stirrer shaft and insert it into the glass reactor.
- iii. Pour methanol into the glass reactor. Attach the movable cover for the top of a reactor.
- iv. Set stirrer speed and temperature controller.
- v. Make the process of dispersing of methanol and catalyst at 65 °C for 20 minutes. Then stream the WCO through the bypass valve until the reactor is full.
- vi. Close the valve bypass and turn on the peristaltic pump.
- vii. Take sample every third of the space-time. The sample was collected in 10 ml glass vials.
- viii. Centrifuge sample at 4000 rpm for 10 minutes.
- ix. Evaporate excess methanol in product mixture by exposure to open air for 30 minutes (Aworanti *et al.*, 2013).
- x. Then, the samples were analysed chemical and physical properties.

### **3.2 Characterization of Biodiesel Fuel**

The effect of different parameters on the production of biodiesel that were investigated are catalyst weight, flowrate, stirrer speed, power input and space-time on WCO methyl ester conversion, where molar ratio and reaction temperature are kept constant.

### 3.2.1 Determination of the Acidity Value and Free Fatty Acid of the Oil

Determination of the amount of free fatty acid (FFA) in WCO as a raw material for producing biodiesel is important to ensure that the selected transesterification method is suitable. The determination of the amount of FFA is done by titration. A 5 g oil sample was mixed with 10 ml of isopropyl alcohol and five drops of phenolphthalein pH indicator. This mixture was then titrated with 0.1 NaOH concentration. The amount of added solution represents the degree of the acidity of the oil. The reaction continues until completion when all FFA is neutralized, which is indicated by the colour change of the phenolphthalein indicator. Acid value and FFA are calculated by using Eq. 3.4 and Eq. 3.5 (Abd Rabu *et al.*, 2013).

$$AV = \frac{Vol_{NaOH}(ml) \times Conc_{NaOH}N \times MW_{NaOH}}{sample\ weight\ (g)} \quad (3.4)$$

where  $Conc_{NaOH}N$  = Normality of NaOH

$$\% Free\ Fatty\ Acid\ (FFA) = AV \times 0.503 \quad (3.5)$$

### 3.2.2 Determination of Fatty Acids Conversion

Samples of reaction products in the form of waste cooking oil methyl ester (WCOME) were analysed by gas chromatography Perkin Elmer Auto GS FID system equipped with fire ionisation (FID) detector through G5 capillary BPC column 30

meters long, 0.25 mm ID and 0.25 micrometre. Reactants and samples are identified by comparing with the original sample. Hexadecanoid acid methyl ester (palmitic acid) was used as the internal standard. The conversion of palmitic acid may be derived from Eq. 3.6 (Han *et al.*, 2016).

$$Conversion (\%) = \left( 1 - \frac{a_1}{a_2} \right) \times 100\% \quad (3.6)$$

where  $a_1$  and  $a_2$  represent the palmitic acid in raw material and palmitic acid in product, respectively.

### 3.3 Diesel Engine Test

#### 3.3.1 Test Fuels

The Malaysian grade 2 diesel fuel (D2) was commonly used for testing of diesel engines. However, the D2 fuel is now replaced by diesel fuel that has already been mixed with biodiesel fuel. A commercial diesel fuel that was used in this experiment is Petron B7 Diesel Max, labelled PDM, containing 7% methyl ester (detailed specifications are shown in Appendix I). This is one of diesel fuels that is commercially available in Malaysia. There are two blends of PDM with Palm Oil Methyl Ester (POME) (detailed specifications are shown in Appendix J), labelled BP10 and BP20, while blend of PDM and WCOME were labelled BW10 and BW20. These fuel blends are equivalent with B10 and B20. The fuel test determination is based on some of previous studies such as (Elshaib *et al.*, 2014; Ozsezen *et al.*, 2009).

The proportion of volume of these biodiesels in blends is shown in Table 3.3. The major properties for the PDM and its blends were tested in the Laboratory Centre UTM, Mechanical Engineering Universiti Teknologi Malaysia (UTM). All fuels were tested for viscosity, density, calorific value and elemental analysis.

**Table 3.3 :** Proportion blends in fuel test

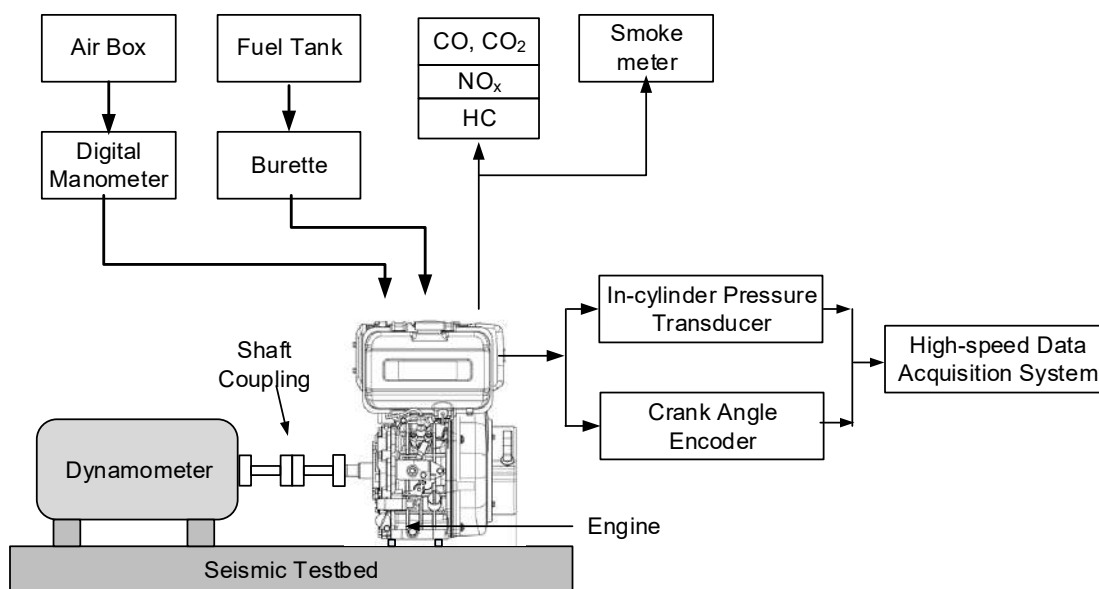
<b>Fuel Type</b>	<b>Methyl ester content</b>	<b>Percentage of biodiesel in blends by volume (%)</b>	<b>Remarks</b>
Petron B7 Diesel Max (PDM)	7	-	Commercial
Palm Oil Methyl Ester (POME)	100	-	Commercial
Waste Cooking Methyl Ester (WCOME)	97.9	-	Previous experiment
BP10 (PDM+POME)	10	2.23	Equivalent to B10
BP20 (PDM+POME)	20	13.98	Equivalent to B20
BW10 (PDM+WCOME)	10	3.30	Equivalent to B10
BW20 (PDM+WCOME)	20	14.30	Equivalent to B20

### 3.3.2 Experiment Set-up and Procedure

An experiment to examine performance was conducted using direct injection, single-cylinder, and four-stroke diesel engine. The main engine specifications are given in Table 3.4. The schematic diagram of the diesel engine test setup is shown in Figure 3.4. The experimental test was done in the Automotive Laboratory at University of Technology of Malaysia (UTM) for a variety of fuel tests.

**Table 3.4 :** Yanmar L70N6-engine specifications made in Italy

Engine Parameter	Specification
4-stroke, vertical cylinder diesel	
No. of cylinder	1
Bore × stroke	78 × 67mm
Displacement	0.320 litre
Continuous Rated output	4.4kW @3600 rpm
Max Rated output	4.9kW @3600 rpm
Combustion system	Direct injection
Cooling system	Forced air by flywheel fan
Maximum engine speed	3600 (rpm)
Starting system	Electric start/Recoil start

**Figure 3.4** Schematic diagram of the engine test setup

The measurement instrumentation used in the test system is described in the following sub-sub section:

### 3.3.2.1 Engine Speed and Torque Measurement

To measure the torque of the diesel engine, Eddy-current brake dynamometer directly coupled with the shaft and a flexible coupling shaft was used. For the load setting, the Eddy-current brake dynamometer is equipped with a load controller as shown in Figure 3.5. The package contained a *Magtrol* dynamometer with an absorption capacity of 30 kW (100 Nm @ 2865 rpm) with a maximum of 18000 rpm. The load cell utilises strain gauge as a transducer mounted on Magtrol dynamometer, where its output is an analogue signal. The analogue signal output is then displayed on a digital display meter located at the Controller Dynamometer Magtrol DSP6001. The dynamometer is a device which allows the engine to develop torque by resisting the rotation of the engine crankshaft. The force generated by the torque arm dynamometer will press the load cell. Hence the torque brake can be obtained.

To control the speed of the engine, throttle actuator that activates the servo motor is used, while to control the load Controller Dynamometer Magtrol DSP6001 unit is used. Figure 3.6 shows that the load controller units are capable of reading 120 per second, and can thus provide superior resolution for curve potting and data acquisition.

The capabilities of Magtrol DSP6001 controller is supported by M-TEST 4.0 software from Magtrol. This software is the most sophisticated software testing program for the needs of Windows-based data acquisition because of overall accuracy and efficiency. The software can also store, display and print data in tabular or graphic formats and can be easily imported into spreadsheet software.



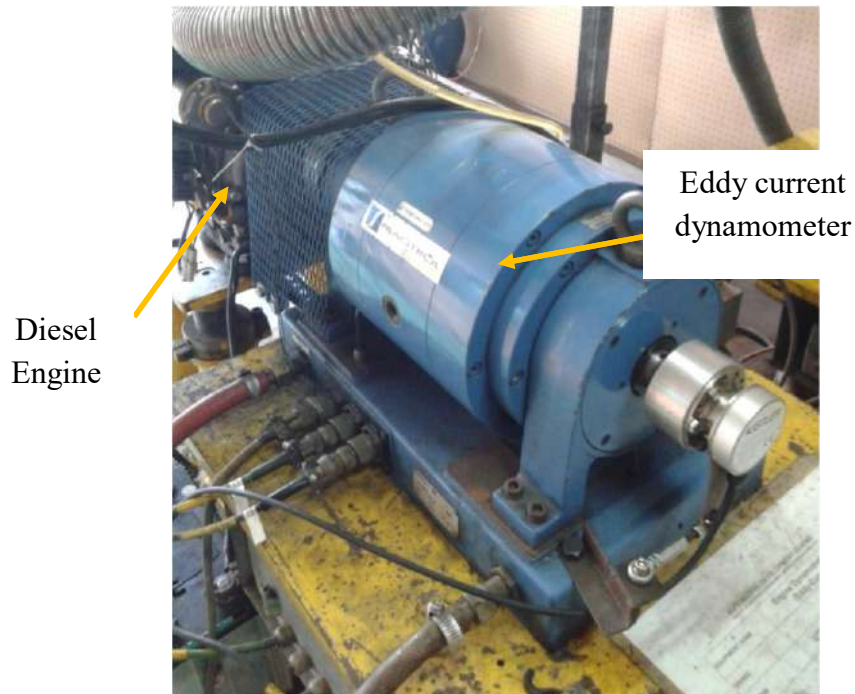


**Figure 3.5** Engine was coupled to an Eddy current dynamometer on test-bed



**Figure 3.6** The 19" Magtrol DSP6001 Dynamometer Controller

### 3.3.2.2 Air Flow Measurement

In order to determine the air fuel ratio (AFR) and to analyse the engine fuel consumption, metering of the air flow and fuel flow are necessary. The air induced

into the engine was measured using a special-made airbox with a 30 mm diameter sharp-edged orifice mounted in the side of an airbox. The engine intake system is connected to the airbox. A digital manometer is used to measure the differential pressure between upstream and downstream orifice. The air mass flow rate through the orifice plate for air box volume is given by Michael and Anthony and cited by Said (2006), and is written as follows:

$$\dot{m} = C_D A_o \sqrt{2\rho_u \Delta p} \quad (3.7)$$

where  $\Delta p$  is pressure differential in orifice plate in mmH<sub>2</sub>O,  $C_D$  is coefficient discharge = 0.6.

### 3.3.2.3 Fuel Flow Measurement

Figure 3.7 shows the glass burette that was used to measure the engine fuel consumption. The burette method for measuring average fuel consumption depends on recording the time it takes for the engine to consume a certain volume of fuel. The measurement results of this device provide data on volumetric fuel consumption. To convert this measurement into the gravimetric rate, it must be calculated by involving the fuel density. The accuracy of burette and stopwatch are 0.1 ml and 0.01 second, respectively.

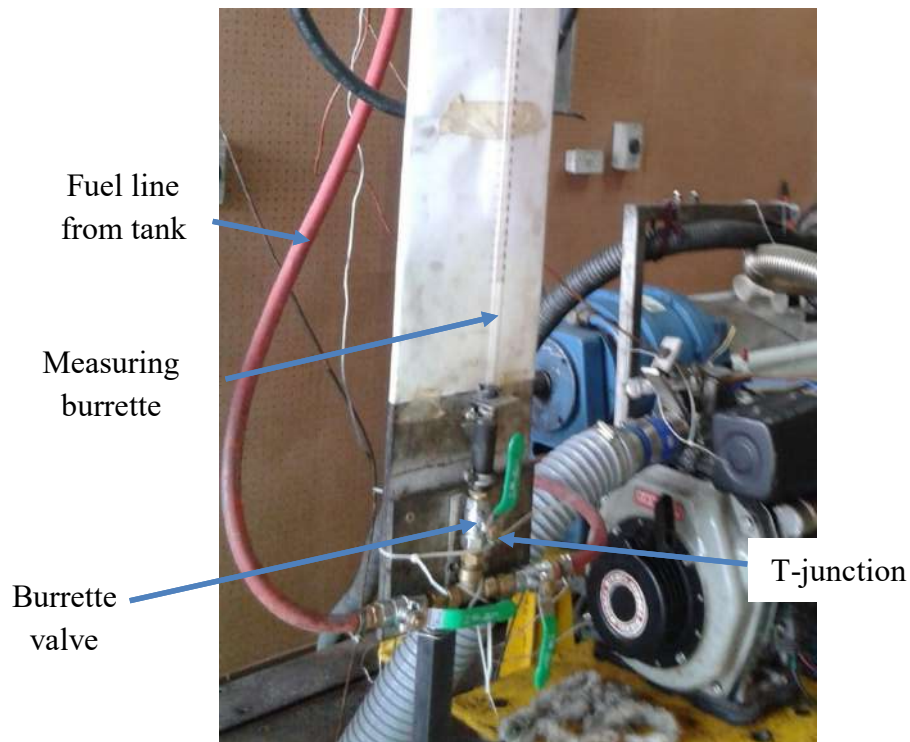


**Figure 3.7** Fuel flow measurement using burette method

#### 3.3.2.4 Temperature Measurement

To monitor the various operating temperatures, in particular, the temperature of intake air, engine block, exhaust manifold and exhaust gas, temperature scanner is used. Figure 3.8 shows temperature scanner used the K-type thermocouples as temperature transducers. The display on the monitor is obtained from readings scanned simultaneously. This temperature scanner has accuracy of 1 °C.



**Figure 3.8** Temperature scanner

### 3.3.2.5 In-cylinder Pressure and Crank Angle Measurement

Measurement of pressure in cylinder using piezoelectric pressure transducer mounted on the cylinder head. The cylinder pressure data is averaged over 120 successive engine cycles with a crank angle encoder resolution of  $0.2^\circ$  C for Kistler 2613B. Measurement of crank angle position was performed by Kistler's CAM crank angle encoder, which is an optical sensing device specially developed for internal combustion engine applications. It provides exact correlation between pressure measurement signal and crank angle position. These data are intended to be used in plotting profiles of pressure versus crank angle, calculating the heat release rate and plotting its profiles to crank angle.

### 3.3.2.6 Data acquisition

Data acquisition is a process of sampling a signal that measures the physical state and converts the resulting sample into a digital numerical value that can be manipulated by a computer. Data acquisition systems, abbreviated by acronym DAS or DAQ, usually convert analogue waveforms into digital values for processing. The components of the data acquisition system consist of sensors, signal conditioning circuits, and analog-to-digital converters. For that required data logging capabilities to record signal pressure and crank angle with 9600 bit /sec sampling rates. The computer-based data acquisition system is the SPECTRUM card installed on a DEWE-5000 portable data acquisition system. Data acquired during the experiment work were retrieved using software provided by *Dewetron*. For crank angle data, DEWECa was used while DEWESoft used data which are not dependant on crank angle. The data were processed using MS Excel and GT SUITE for further analysis.

### 3.3.2.7 Gas Emission Analyser and Exhaust Smoke

EMS Model 5002 gas emission was used to measure the emission of exhaust gas of engine. A sample of exhaust gas was taken through a probe mounted inside the exhaust pipe. A filter system is installed on the sampling line to safeguard this emission gas analyser from damage due to the entry of solid particles to the equipment. The exhaust sample measured by the analyser is dry gas, therefore to remove the moisture content in the exhaust gas, the sample must be passed through a water vapour filter. This analyser can be operated in temperatures ranging from 2 to 45 °C, relative humidity ranging from 0 to 98%. This analyser is multi-component gas measurement and provides for the display of five gases and AFR. Features of the exhaust gas

analysis components are listed as shown in Table 3.5. For smoke density, a dedicated Smokemeter of sampling pump type (EFAW 65 BOSCH) was used. An adequate amount of exhaust gas is drawn from the exhaust tail pipe of the diesel engine passing through a filter paper.

**Table 3.5 :** The components that can be measured by EMS model 5002

<b>Component</b>	<b>Range</b>	<b>Display resolution</b>
CO	0 – 10%	0.01% vol.
NO	0 – 5000 ppm	1 ppm
O <sub>2</sub>	0 – 25%	0.01% vol.
CO <sub>2</sub>	0 – 20%	0.1 % vol.
HC	0 – 2000 ppm	1 ppm vol.

### 3.3.2.8 Support Measurement Tools

Support measurement tools used are stopwatch and remote weather station. A stopwatch is used to measure the time spent on fuel consumption. The remote weather station is used to measure atmospheric conditions around the test such as room temperature, atmospheric pressure and humidity.

### 3.3.3 Experimental Method

In the present study, the experiments were carried out on steady-state conditions at 2,500 rpm constant engine speed, while the load is varied to describe the actual condition of the engine. All engine parameters related to performance, emission

and combustion in this test are recorded based on constant engine speed mode. In this way, variations in performance, exhaust emissions and combustion behaviour can be analysed at each load change.

To obtain accurate data, the experimental test procedure for engine performance, emissions on compression ignition must follow guidelines in preparing the instrumentation and experiment runs recommended by the Society of Automotive Engineers Standard (Said, 2006). The experimental test procedure is presented in Appendix L. Because this study attempts to compare performance and emissions between PDM, POME blends and WCOME blends used on engine, some key parameters are measured such as brake torque, air and fuel consumption, in-cylinder pressure and exhaust emissions. In this experiment, the temperature of air entering the engine is ambient temperature. The final result is obtained from the average of three stable and continuous values.

### **3.3.4 Data Analysis**

#### **3.3.4.1 Engine Test Parameters**

Fuel containing chemical energy undergoes combustion process in the combustion chamber. Combustion results in high-pressure and temperature. High pressure gas acts to push the piston from translational motion into mechanical work rotation.

To evaluate engine performance required some relevant parameters such as speed, brake torque, air consumption and fuel consumption. From the experimental data, the engine performance parameters were analysed using a number of equations. Some performance parameters are brake power, brake mean effective pressure, brake specific fuel consumption and thermal brake efficiency. They are further explained as follows:

**Brake Power, BP (kW)** – Net power produced by an engine at its crankshaft.

**Brake Mean Effective Pressure, BMEP (bar)** – This parameter is widely used to compare the performance of different machines, where the average pressure works on the piston that produces the same amount of work.

**Brake Specific Fuel Consumption, BSFC (kg/kWh)** – The amount of fuel consumed by the engine produces a certain amount of work. In other words, the rate of fuel consumed to generate kilowatts of power. This parameter is to compare fuel consumption among different engines especially in economic aspects.

**Brake Thermal Efficiency, BTE (%)** – The ratio of net power generated by the engine (also called shaft power) to the heat rate supplied from the combustion of the fuel. This shows the percentage of heat energy from the fuel that is converted to work on the shaft.

**Air Fuel Ratio, AFR** – The mass ratio of air and fuel consumed by the combustion process in engine. The ratio of this value to the stoichiometric conditions will indicate whether the mixture is rich or lean.



The following equations have been used to calculate for engine performance. Based on Heywood (1988) , the brake power is defined by:

$$BP = \frac{2 \pi \times N \times T}{60 \times 10^3} \quad (kW) \quad (3.8)$$

where  $N$  = Engine Speed (rpm),  $T$  = Torque (N.m)

The brake mean effective pressure can be calculated using:

$$BMEP = \frac{1.2 \times BP}{N \times V_d} \quad (\text{bar}) \quad (3.9)$$

where  $V_d$  is displacement ( $\text{m}^3$ )

The brake specific fuel consumption was then formulated as:

$$BSFC = \frac{3.6 \times \dot{m}_f}{BP} \quad (\text{kg/kWh}) \quad (3.10)$$

where  $\dot{m}_f$  is mass flowrate of fuel in g/s.

The brake thermal efficiency (BTE) is defined as:

$$BTE = \frac{BP}{10^{-3} \times Q_{HV} \dot{m}_f} \quad (3.11)$$

where  $Q_{HV}$  is calorific value of fuel in kJ/kg.

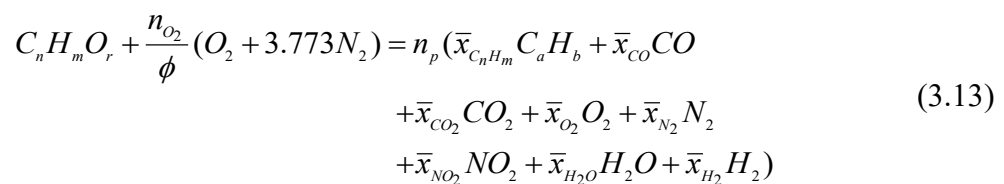
The air fuel ratio is defined as:

$$AFR = \frac{\dot{m}_a}{\dot{m}_f} \quad (3.12)$$

where  $\dot{m}_a$  is mass flowrate of combustion air in g/s.

### 3.3.4.2 Analysis of Gaseous Emissions

Exhaust gas emission depends on the relative proportion of fuel and air fed to the engine, fuel composition, and completeness of combustion. The general formula for the composition of fuel can be presented as  $C_nH_mO_r$ , while the air as oxidizer is presented as  $(O_2+3.773N_2)$  (Heywood, 1988). The overall combustion reaction can be written explicitly as



where  $\phi$  is a measured equivalence ratio  $\left[ \left( \frac{F}{A} \right)_{actual} / \left( \frac{F}{A} \right)_{stoichiometric} \right]$ ,  $n_{O_2}$  is the number of  $O_2$  molecules required for complete combustion  $(n+m/4-r/2)$ ,  $n_p$  is the total number of moles of exhaust products, and  $\bar{x}_i$  is the mole fraction of the  $i$ th component.

The emissions data were obtained for each fuel test according to similar operating condition. Each test was run three times. The observation data were then averaged to obtain the emissions data (Appendix L). This is a common practice of exhaust emissions data and can be expressed in 'specific brakes'. The specific brake

of emission is the mass flow rate of the pollutant divided by the engine power. From the measurements of exhaust emissions, mass flow rate of exhaust gas and brake power generated by the engine, the specific basis of the brake (BS) can be calculated. Brake specific equations are as follows (Said, 2006).

$$BS_{CO_2} (g/kWh) = 9.90 \times 10^{-2} \times \dot{m}_{exh} \times CO_2(ppm)/BP(kW) \quad (3.14)$$

$$BS_{CO} (g/kWh) = 5.79 \times 10^{-2} \times \dot{m}_{exh} \times CO(ppm)/BP(kW) \quad (3.15)$$

$$BS_{NO_x} (g/kWh) = 9.50 \times 10^{-2} \times \dot{m}_{exh} \times NO_x(ppm)/BP(kW) \quad (3.16)$$

$$BS_{uHC} (g/kWh) = 2.87 \times 10^{-2} \times \dot{m}_{exh} \times uHC(ppm)/BP(kW) \quad (3.17)$$

where

$$\dot{m}_{exh} \left( \frac{kg}{min} \right) = \dot{m}_{inlet} \times \left( 1 - \frac{F}{A} \right) \quad (3.18)$$

### 3.3.4.3 Heat Release Rate Analysis

The analysis of the heat release rate (HRR) is usually applied to the combustion process on a diesel engine. It calculates how much heat should be added to the cylinder content to produce observed pressure variations against crank angle. In the combustion process, there will be four distinct phases. They are identified in a typical heat release rate diagram for the direct injection diesel engine in Figure 3.9.

**Ignition delay (ab).** The period between the start of the fuel injection process into the cylinder and the beginning of the combustion process. This period can be determined from changes in tilt at pressure versus the crank angle diagram or from heat release.

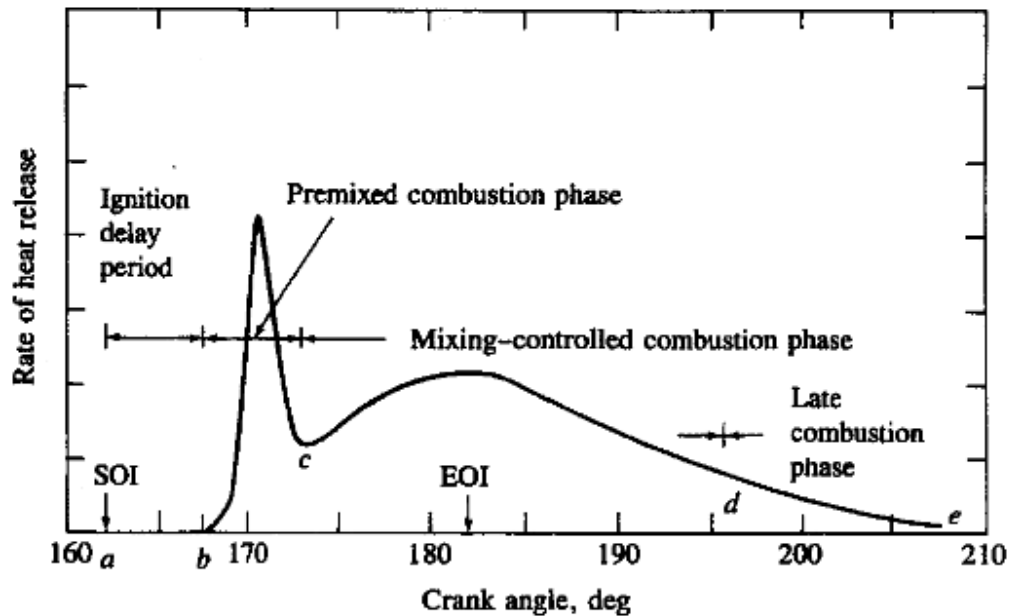


**Figure 3.9** Typical combustion phases in DI engine heat release rate diagram (Heywood, 1988)

***Premixed or rapid combustion phase (bc).*** The phase where the combustion of fuels that have been mixed with air into flammable limits during the ignition delay period occurs rapidly in several degrees of crank angle. The high heat release level characteristic of the phase yield occurs when the combustion mixture is added to the burning fuel and burns during this phase.

***Mixing-controlled combustion phase (cd).*** During the ignition delay, premixed air and fuel have been consumed, the combustion rate (or rate of heat release) is controlled by the level at which the mixture is available for combustion. In this phase, several processes involved include atomization of liquid fuels, evaporation, mixing of fuel vapor with air, pre-flame chemical reaction. In this phase, the level of combustion is controlled by the process of mixing the air of fuel vapour.

**Late combustion phase (de).** The heat release still continues at a lower rate well into the expansion stroke. This can happen because a small proportion of the fuel may not yet have burned and a small portion of the fuel energy is present in soot and rich products of combustion that can still be released. Charging on the cylinder is not uniform and mixing during this period encourages more complete combustion and less dissociated products. The final burnout kinetics becomes slower due to the drop in temperature of the cylinder gas during the expansion process.

The calculation of the heat release rate on combustion process in cylinder is very useful to investigate the combustion of diesel engines. The most basic model used in the calculation of this heat release rate begins with the application of the first law of thermodynamics. The calculation of a simple heat release rate is sufficient, as the beginning of the combustion process. A simple method of analysis of the rate of release of chemical energy of fuel (often called heat release) through the combustion process of diesel engines is described in this sub section. The analytical method begins with the three basic assumptions used in the first law of thermodynamics. The first assumption is that the trapped charge inside the cylinder is contained in a single uniform zone of constant composition of the inlet valve that is closed until the exhaust valve is open. The second assumption is that the charge in the form of a mixture of fuel and air inside the cylinder behaves as an ideal gas. A third assumption is that the energy released in the combustion process can be modelled as additional heat to the cylinder (Said, 2006).

Using these three assumptions, the heat release rate equations can be derived. This heat release rate is equated with heat loss. From the first law:

$$\frac{dUT}{dt} = Q - W \quad (3.19)$$

$$mC_v \frac{dT}{dt} = Q - P \frac{dv}{dt} \quad (3.20)$$

The ideal gas assumption can be used to simplify Eq.3.19.

$$PV = mRT \quad (3.21)$$

which can be differentiated to give:

$$\frac{dT}{dt} = \frac{1}{mR} \left[ P \frac{dV}{dt} + V \frac{dP}{dt} \right] \quad (3.22)$$

After combining these two equations, the heat release rate equation becomes:

$$Q = \left[ \frac{C_v}{R} + 1 \right] P \frac{dV}{dt} + \frac{C_v}{R} V \frac{dP}{dt} \quad (3.23)$$

Replacing time ( $t$ ) with crank angle ( $\theta$ ), the above equation becomes

$$\frac{dQ}{d\theta} = \frac{\gamma}{\gamma - 1} P \frac{dV}{d\theta} + \frac{1}{\gamma - 1} V \frac{dP}{d\theta} \quad (3.24)$$

where  $\gamma$  is the ratio of specific heats,  $C_p/C_v$ . A suitable range for diesel heat-release analysis is 1.3 to 1.35. Eq. 3.23 is often used with a constant value of  $\gamma$  within this range (Heywood, 1988). The corresponding  $\gamma$  values during combustion that will provide the most accurate heat release information is not clearly expressed, but the equation is more than sufficient to predict the beginning of combustion.

### **3.4 Simulation Methodology**

#### **3.4.1 Introduction**

The task of simulation is to build machine models and parameter values that can predict engine performance. The simulation allows users to imagine unimaginable things by being able to see temporal variations of pressure, volume and gas flow rates that occur during the engine cycle on the computer screen. Many parametric changes are observed in this visual way, along with their net effect on power output and fuel consumption, giving designers a lot of things to think about. The results of the calculation process are presented in numerical form and graph analysis.

The theory of performance of diesel engines with computer modelling of thermodynamic engine simulations is increasingly complete and increasingly widely used. Modelling of engine is a very large subject, in part because of possible engine configuration ranges and variations of alternative analysis techniques, or sub-models, which can be used on the whole model. The main reason for the growth of modelling of engine activity is the benefit of the economic aspect. Using a computer model allows tremendous savings for expensive experimental works.

Although the model cannot replace real engine testing, at least it can provide a good performance change forecast due to possible engine modifications. Using modelling can help in selecting the best option for further development, thereby reducing the amount of hardware development and saving a lot of money. Expenditures by helping optimization, for example, component control and matching strategies, are an increasingly important area as engine sub-systems have become increasingly complex and difficult to optimize on machine test sites. Finally, they can

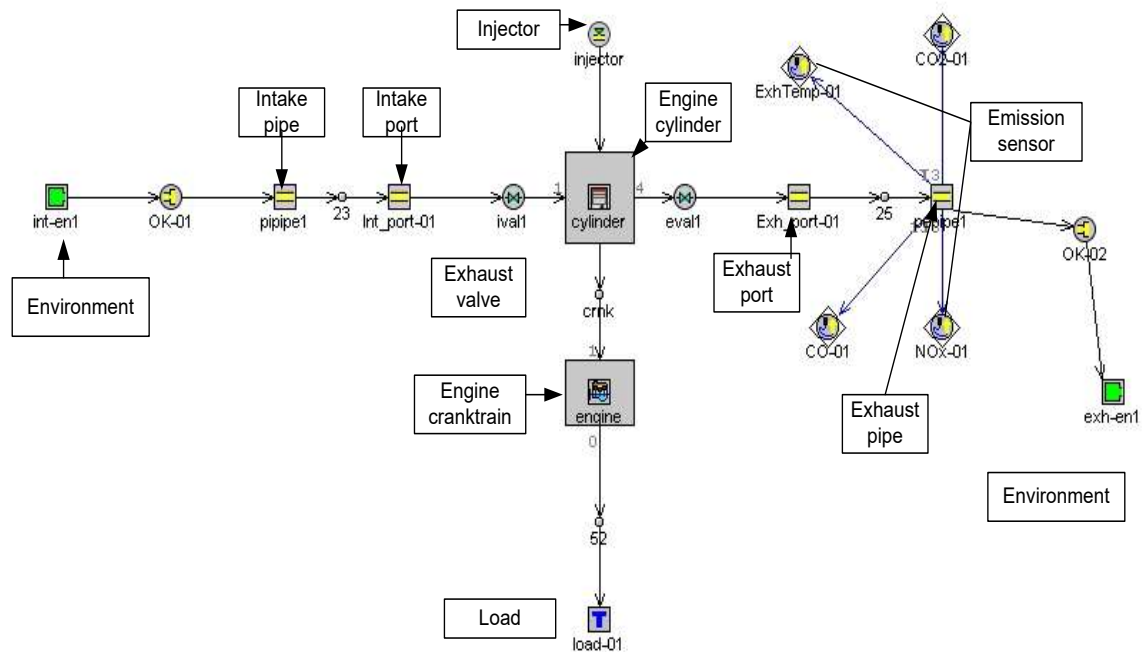
provide sufficient insight into certain aspects of engine behaviour that may not be felt from experimental work. The more advanced models are very large and complex, while the basics of the thermodynamic model of engine are quite easy to understand and are easily understood and described in detail by Heywood (1988). The GT-SUITE uses one-dimensional gas dynamics model to simulate the performance and emission of direct injection (DI) diesel engines. The results of this modeling work are validated with experimental data as discussed in sub-sections 4.3.5.

Figure 3.10 shows the DI diesel engine model that was developed using one-dimensional model. The inputs of engine geometry, diesel combustion model, fuels properties, injection parameter, combustion parameter, valve timing and ambient conditions were used in the simulation program in order to predict the performances, combustion and exhaust emissions. The details of inputs of engine model are presented in section 3.4.6. As shown in the figure, the component of load-01 was used to apply the brake torque to the engine. Sensor in the exhaust pipe was used to measure  $\text{NO}_x$ , CO and  $\text{CO}_2$ .

### **3.4.2 Gas Dynamic – One-Dimensional Model**

In one-dimensional model the gas dynamics model is based on one dimension, which represents the flow and heat transfer in the components of the engine system as in the pipeline. In addition to fluid flow and heat transfer capability, this software application contains many other special models required for system-related analysis of the machine, so it has the ability to model various aspects of the machine (Gamma Technologies, 2003).





**Figure 3.10** Direct Injection diesel engine model using one dimensional model

The flow model involves simultaneous solutions of continuity equations, momentum and energy. This equation is solved in the form of one dimension, which means that all the average quantities cross the direction of the flow. The gas dynamics model takes into account mass transfer, energy and momentum between the finite elements of the pipeline flow. Improved precision can be done by increasing the complexity of the program and the model run time. The gas dynamics are very important and have been widely used in machine models and also produce large amounts of literature. In addition, gas dynamics is appropriate for presenting basic equations and for demonstrating alternative methods of solutions. The following are limited to the one-dimensional gases dynamics that are usually used in complete machine cycle simulations. The three-dimensional method of computational fluid dynamics (CFD) is widely used in machine research, but is used to look at a small number of machines for very limited periods of time. Although the CFD method takes a lot of effort to prepare (day) and has a relatively long period of time (hours), it can

provide very detailed flow information. The intake system and exhaust system are modelled using pipe components. The long input, inlet and outlet diameters of the pipe are required during modelling. In a one-dimensional gas dynamics equation, the pipe is divided into several finite elements or mesh elements, usually of the same length, and by applying mass conservation laws, momentum and energy conservation laws to each element. There are several ways to manipulate the resulting equation, namely the basic conservation equations and the derived conservation equations (Said, 2006).

### **3.4.3 Flows in Cylinder Valve**

In GT-SUITE, data is needed for simulation such as the inputs of the valve lift profile as shown in Figure 3.11. The valve reference diameter and cam timing angle are also considered. All of the above variables are measured. The variation of valve lift for inlet and exhaust valve is determined by the cam profile of the crank angle curves. The discharge coefficient ( $C_D$ ) is another important input that was required in the simulation. The discharge coefficient for valves is calculated with reference to the valve reference diameter by using an isentropic flow equation (Gamma Technologies, 2003). Equation 3.24 is widely used to calculate the air flow ( $\dot{m}_a$ ) of orifices such as flow through the valves and throttle.

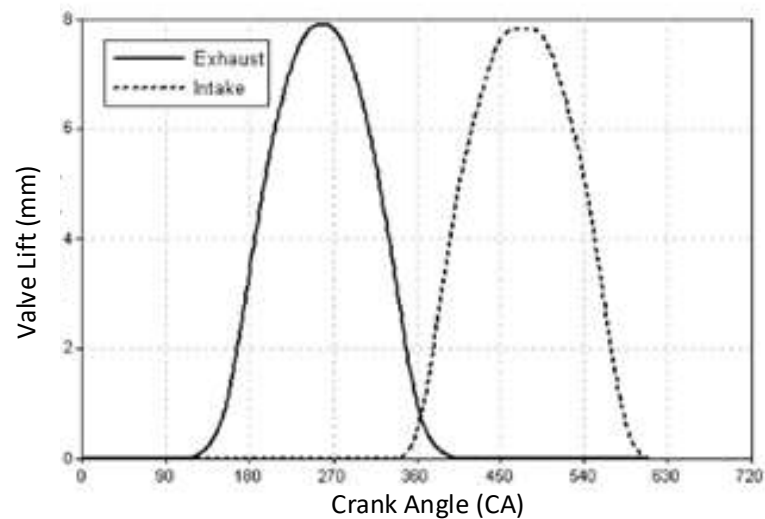


**Figure 3.11** Valve lift profile

$C_D$  values are generally obtained from experimental results. This equation is most appropriate for sudden holes such as valves and throttles where there is a pressure loss before and after the flow through the throat due to the separation of the flow after the throat, so it is not so well suited to a smooth hole like Venturi. In smooth holes there is pressure recovery and therefore no complete head loss requires a larger  $C_D$  than unity.

$$\dot{m}_a = C_D A_T P_1 \sqrt{\left(\frac{2\gamma}{\gamma-1}\right) \frac{1}{RT_1} \left[ \left(\frac{P_2}{P_1}\right)^{2/\gamma} - \left(\frac{P_2}{P_1}\right)^{\frac{\gamma+1}{\gamma}} \right]} \quad (3.25)$$

The flow data should generally be measured on a flow bench. From this data the discharge coefficients can be calculated (Eq. 3.25). In this study, the  $C_D$  was calculated using spreadsheet that was included in the GT-SUITE installation directory. In the spreadsheet, the approximation to flow area was used, the associated  $C_D$  values then calculated for the approximation. The ‘curtain area’ is a simply common approach.

$$\text{Curtain Area} = \pi DL \quad (3.26)$$

where  $D$  is valve head diameter and  $L$  the valve lift. It is important to understand that these  $C_D$  values may be included in the curtain area equations in Eq. 3.25 and should not be used with other definitions of the flow area, requiring a set of their own  $C_D$  lift curves. In the model, the effective flow area for Eq. 3.25 is obtained at each time step of the lift and crank corner table with the corresponding lift table using linear interpolation. To determine the pressure ratio required pressure data on the cylinder and inlet or exhaust manifold at the time step.

#### 3.4.4 The Engine Cylinder

The data such as the variables for bore diameter, stroke and connected rod length, TDC clearance height and compression ratio are needed to perform the simulation. In order for the energy equation for the cylinder to be solved, it needs the rate the volume change required volume change rate. Similarly, the rate of heat transfer will depend on the surface area of the combustion chamber. At this stage, it is appropriate to handle the cylindrical geometry as seen on Eq. 3.27.

$$CR = \frac{(V_s + V_c)}{V_c} \quad (3.27)$$

where  $V_s$  is the swept volume and  $V_c$  is the clearance volume. The volume of the combustion chamber is calculated from the moment the piston from the bottom dead center (BDC) to the peak dead centre (TDC),  $V_s$  is of course written by,

$$V_s = \frac{\pi}{4} B^2 S \quad (3.28)$$

where bore  $B$  and stroke  $S$ , the stroke or twice of the crankshaft throw ( $r$ ).

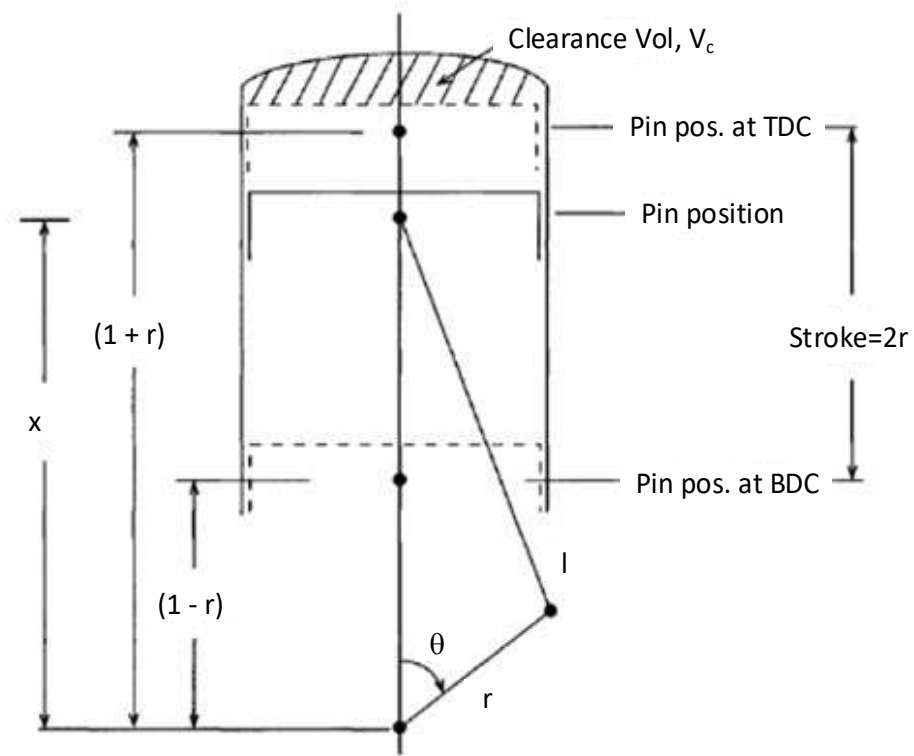


**Figure 3.12** Cylinder geometry

Referring to Figure 3.12, the instantaneous combustion chamber volume  $V$  as function of the  $x$  and its rate of change  $\dot{V}$ , are given by,

$$V = V_c + (\pi B^2/4)(l + r - x); \quad \dot{V} = -(\pi B^2/4)\dot{x} \quad (3.29)$$

where  $l$  is the connecting rod length. Similarly, the surface area of the combustion chamber can be calculated by,

$$A = A_p + A_H + A_L = A_p + A_H + \pi B(l + r - x) \quad (3.30)$$

where subscripts  $P$  refer to areas of the piston crown, H for cylinder head and L for exposed liner area. Eq. 3.29 and Eq. 3.30 can be used for A, when crank angle is  $\theta$  requires only the values of  $x$  and  $\dot{x}$ . From Figure 3.12,

$$x = r \cos \theta \sqrt{(l^2 - r^2 \sin^2 \theta)} \quad (3.31)$$

and differentiating:

$$\dot{x} = [r \sin \theta + (l^2 - r^2 \sin^2 \theta)^{-1/2} r^2 \sin \theta \cos \theta] \left( \frac{d\theta}{dt} \right) \quad (3.32)$$

where  $\left( \frac{d\theta}{dt} \right)$  is related to engine speed  $N$  (rpm) by,

$$\left( \frac{d\theta}{dt} \right) = \pi N / 30 \quad (3.33)$$

so that chamber volume, change volume rate and exposed surface area for any engine speed and crank angle can be calculated.

To solve the energy equation for the cylinder, data is needed. The data, depending on the point where the cylinder is on the engine rotation, is illustrated in Figure 3.13 for the 720° four-stroke crank cycle. The inlet line is immediately closed shortly after the piston reaches BDC during compression stroke, remaining air and residual gas is then compressed and fuel injections begin towards the end of compression pressure. After a short delay, the combustion process begins, generally towards the end of the compression stroke then continues well into the expansion stroke. In the late stroke expansion process, the open exhaust valve usually remains open right through exhaust stroke and closes immediately after TDC in induction or intake stroke. Toward the end of the exhaust gas exhaust process, the inlet valve is

usually opened, so the inlet and exhaust valves simultaneously open around the flotation TDC. The inlet valve then remains open throughout the induction stroke to the beginning of the compression stroke. The solution of energy equations for the cylinders for each phase cycle is described in detail by Challen and Baranescu (1999).

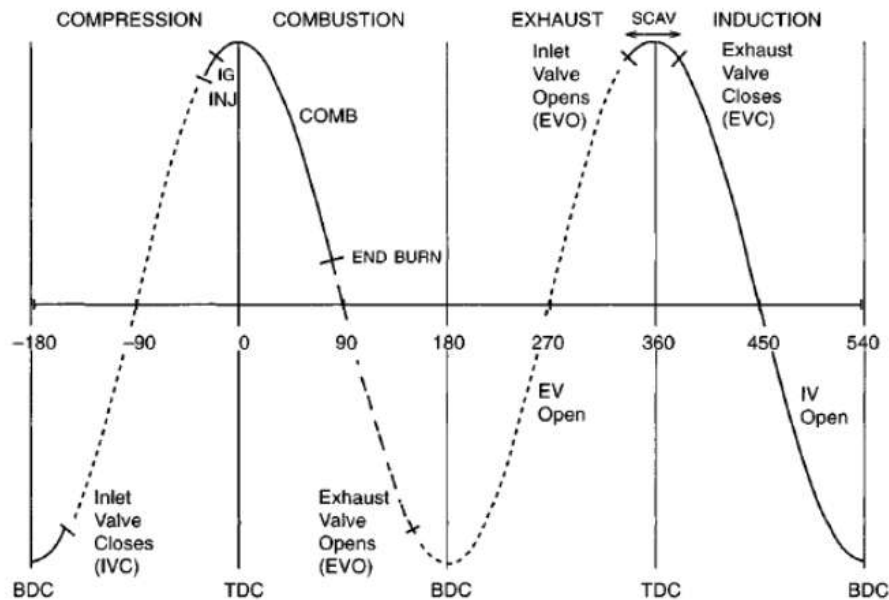


**Figure 3.13** Four stroke cycle (Challen and Baranescu, 1999)

### 3.4.5 Injection and Combustion

The parameters required for simulation are the input of injection parameters such as injected mass per cycle, start of injection, nozzle hole diameter, number of hole per nozzle and fuel injection pressure rate profile. The others inputs are fuel properties such as density, heat of vaporization, heating value, cetane number and distillation temperature. To model the combustion process for the purpose of cycle simulation, two key parameters are required. There is an ignition delay from starting the injection

to the start of combustion and the variation of the fuel fraction burned to the crank angle after ignition occurs. If these two key parameters are known, then the use of the fuel gas activity routine and the energy equations in the ordinary time-step process, then calculation of cylinder pressure and temperature variation can be calculated through the combustion process.

### 3.4.6 Input Parameters for Simulation

There are several objects to be defined, such as inlet environments, outlet environments, intake ports, exhaust ports, intakes and exhaust valves, cylinders, fuel injectors, and engine crank train. Some object values are of reference and measurement other than experimental data. A number of input parameters are presented in Table 3.6 to Table 3.13.

#### 3.4.6.1 Defined value for environment and pipe objects

**Table 3.6 :** Defined value for environment and pipe objects

<b>Attribute</b>	<b>Unit</b>	<b>Intake</b>	<b>Exhaust</b>
Pressure (absolute)	bar	1	2
Temperature	K	302.15	312.15
Pressure Flag		standard	standard
Composition		air	air
Diameter at Inlet End	mm	32	26
Diameter at Outlet End	mm	32	26
Length	mm	60	50
Discretization Length	mm	30	30
Imposed Wall Temperature	K	350	550
Heat Transfer Multiplier	-	1.5	1.5



**Table 3.7 :** Defined value intake and exhaust for valve

<b>Attribute</b>	<b>Unit</b>	<b>Intake</b>	<b>Exhaust</b>
Valve Reference Diameter	mm	30.5	25.5
Valve Lash	mm	0.1	0.15
Cam Timing Angle	°CA	360°	180°
Cam Timing Anchor Reference		TDCFiring	TDCFiring
Cam Timing Anchor Reference		Theta=0	Theta=0

### 3.4.6.2 Fuel Injector

This injection connection allows for injection of a periodic pressure or mass rate profile. It may be used to inject fluid into any cylinder, pipe, or flowsplit, but it is typically used for direct-injection diesel engines. Defined value for injector is shown in Table 3.8.

**Table 3.8 :** Defined value for injector

<b>Attribute</b>	<b>Unit</b>	<b>Object Value</b>
Nozzle Hole Diameter	mm	0.21
Number of Hole per Nozzle	-	4
Injected Fluid Temperature	K	313

Injection profile is the fuel pressure in the fuel line before the fuel enters the injector as shown in the graph in Figure 3.14.

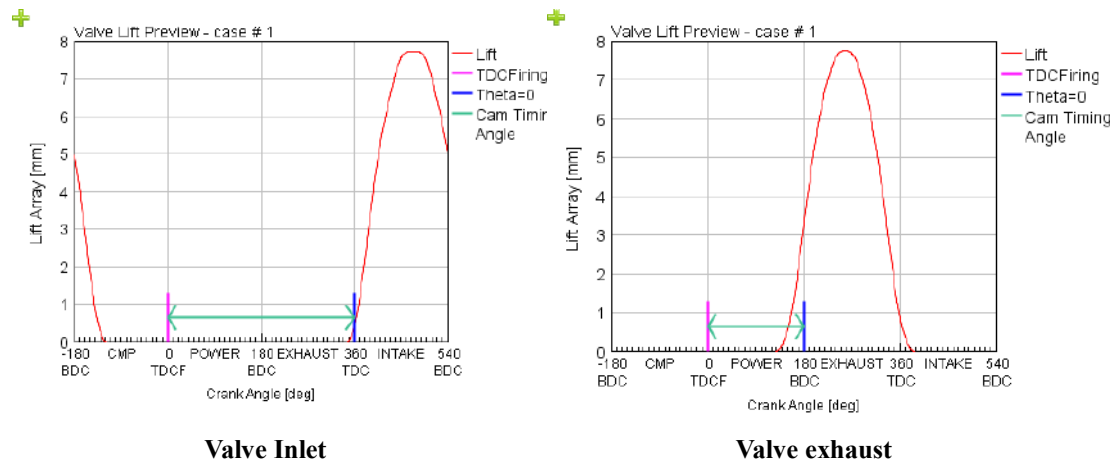


**Figure 3.14** Graph of valve lift of inlet and exhaust versus crank angle (Said, 2006)

### 3.4.6.3 Engine

This object specifies the attributes of the Engine Cranktrain part which is used to model the kinematics and rigid dynamics of common reciprocating IC engine cranktrain configurations. The resulting engine torque is reported at various "stations" such as cylinder, crankpin, shaft, brake. The net torque acting on the engine after inertia and friction may also be used to calculate acceleration of a free engine cranktrain (Gamma Technologies, 2003).

**Table 3.9 :** Defined value for engine geometry and inertia

Attribute	Unit	Object Value
Bore	mm	78
Stroke	mm	62
Connecting Rod Length	mm	102
Compression Ratio	-	20
TDC Clearance Height	mm	0.5
Engine Effective Rotating Inertia	kg-m <sup>2</sup>	17
Number of Periods at Initial Speed		Def(=4)

### 3.4.6.4 Fuel properties

Fuel properties were defined in fuel reference to describe the properties of incompressible liquids. It is only intended to be used in circuits which are primarily composed of gases, where the mass fraction of the liquid in the liquid/gas mixture is very small. In this case, the effect of the compressibility of the liquid may be negligible and can be ignored. This object should not and cannot be used as the working fluid in a liquid circuit. “FluidGas” is used to describe the properties of gases or vapours. The attribute and defined value for fuel property are shown in Table 3.10 to Table 3.12.

**Table 3.10 :** Enthalpy constant for all fuels

State	Attribute	PDM	BP10	BP20	BW10	BW20
Vapour	(T-Tref) Coefficient, a1	1634.3	1675	1675	1675	1675
	(T-Tref) Coefficient, a2	1.8191	1	1	1	1
	(T-Tref) Coefficient, a3	0	0	0	0	0
	(T-Tref) Coefficient, a4	0	0	0	0	0
	(T-Tref) Coefficient, a4	0	0	0	0	0
Liquid	(T-Tref) Coefficient, a1	2050	2050	-	-	-
	(T-Tref) Coefficient, a2	0	-	-	-	-
	(T-Tref) Coefficient, a3	0	-	-	-	-

**Table 3.11 :** Transport properties

Temperature array K	Pressure Array bar	Dynamic Viscosity kg/m-s	Thermal conductivity W/m-K
303.15	default	8.02e-006	0.00829904
373.55		6.75e-006	0.00829904
475.35		8.48e-006	0.00829904

### 3.4.6.5 Case Setup

The case setup, found under the under the "Run" pull-down menu or by clicking on the Case Setup icon on the toolbar, is used to specify values for each parameter. Parameters are variables that have been assigned by the user to attributes as the model was being built. An attribute that will be changed frequently should be made a parameter so that it can be entered conveniently in case setup. Case setup provides a common window to enter such data as well as provide a means of submitting several simulations at one time by assigning several different values to a given parameter. The case setup of this simulation is shown in Table 3.13.

The SOI and SOC parameters were included in case setup for each fuel test as shown in Table 3.13. To determine the SOI and SOC parameters, the HRR peak point location for simulation was then compared with the HRR peak point location for experimental. Both of these parameters will be appropriate when the HRR peak point location for simulation approaches the HRR peak point location for experiment.

This table shows the existence of file1 and file2 as the combustion rate data as well. They were obtained from the experimental results. Each case has a different combustion rate.

**Table 3.12** : Defined value for fuel property

State	Item	PDM	BP10	BP20	BW10	BW20
Vapour	Molecular Weight	ign	ign	ign	ign	ign
	Carbon Atoms per Molecule	7.11876	7.0866	7.08128	7.04408	6.9238
	Hydrogen Atoms per Molecule	13.98155	13.99365	14.04495	13.9726	13.95085
	Oxygen Atoms per Mole	0.002827	0.03575	0.037	0.06748	0.15818
	Nitrogen Atoms per Molecule	0.02561	0.02679	0.02605	0.02703	0.0243
	Sulfur Atoms per Molecule	0	0.000063	0.00072	0.00126	0.0014
	Argon Atoms per Molecule	0	0	0	0	0
	Lower Heating Value, kJ/kg	45488	45311	44624	44016	43801
	Critical Temperature, K	569.4	569.4	569.4	569.4	569.4
	Critical Pressure, bar	24.6	24.6	24.6	24.6	24.6
	Absolute Entropy at 298K	3445.47	ign	ign	ign	ign
Liquid	Heat of Vaporization, kJ/kg	250000				
	Density, kg/m <sup>3</sup>	830	832	835	835	855
	Enthalpy, kJ/kg					
	Viscosity, kg/m-s					
	Thermal Conductivity, W/m-K					

**Table 3.13 : Case setup**

Parameter	Unit	Description	1	2	3	4	5	6	7	8	9	10
Case No.			1	2	3	4	5	6	7	8	9	10
Case Label			PDM_1	PDM_2	PDM_3	PDM_4	PDM_5	BP10_1	BP10_2	BP10_3	BP10_4	BP10_5
SOI	deg		-13	-13	-13	-13	-13	-13	-13	-13	-13	-13
SOC			-7.7	-7.9	-8	-8.5	-8.6	-8.2	-8.55	-8.8	-9	-9.2
RPM	RPM		2500	2500	2500	2500	2500	2500	2500	2500	2500	2500
pist_tmp	K	Piston Temperature	540	540	540	540	540	540	540	540	540	540
pist_area		Piston bore/area ratio	1.26	1.26	1.26	1.26	1.26	1.26	1.26	1.26	1.26	1.26
load	N-m		3	5	7	9	10	3	5	7	9	10
head_tmp	K	Head temperature	570	570	570	570	570	570	570	570	570	570
fuelmass	mg		5.8463	7.0273	8.5092	9.9352	11.6084	6.2132	7.7028	9.3175	11.2646	12.8718
fuel			PDM	PDM	PDM	PDM	PDM	BP10	BP10	BP10	BP10	BP10
file1			<HR PDM.tx#1#1#0#98>				<HR BP10.tx#1#1#0#98>					
file2			<HR PDM.tx#0#0#0#98>				<HR BP10.tx#0#0#0#98>					
cyl_tmp	K		570	570	570	570	570	570	570	570	570	570
CA_ICV	deg		-110	-110	-110	-110	-110	-110	-110	-110	-110	-110

**Table 3.13. Case setup (cont'd)**

Parameter	Unit	Description	11	12	13	14	15	16	17	18	19	20	21	22		
Case No.			11	12	13	14	15	16	17	18	19	20	21	22		
Case Label			BP20_1	BP20_2	BP20_3	BP20_4	BP20_5	BW10_1	BW10_2	BW10_3	BW10_4	BW10_5	BW20_1	BP20_2		
SOI	deg		-13	-13	-13	-13	-13	-13	-13	-13	-13	-13	-13	-13		
SOC			-8.5	-8.7	-9.3	-9.35	-8.4	-8.55	-8.6	-9.65	-8.65	-8.7				
RPM	RPM		2500	2500	2500	2500	2500	2500	2500	2500	2500	2500	2500	2500		
pist_tmp	K	Piston Temperature	540	540	540	540	540	540	540	540	540	540	540	540		
pist_area		Piston bore/area ratio	1.26	1.26	1.26	1.26	1.26	1.26	1.26	1.26	1.26	1.26	1.26	1.26		
load	N-m		3	5	7	9	10	3	5	7	9	10	3	5		
head_tmp	K	Head temperature	570	570	570	570	570	570	570	570	570	570	570	570		
fuelmass	mg		6.3063	7.8506	9.6288	11.6693	13.3482	6.5800	8.1984	10.0364	12.1806	13.8207	6.6201	8.3882		
fuel			BP20	BP20	BP20	BP20	BP20	BW10	BW10	BW10	BW10	BW10	BW20	BW20		
file1			<HR BP10.tx#1#1#0#98>					<HR BW10.tx#1#1#0#98>					<HR BW20.tx#1#1#0#98>			
file2			<HR BP10.tx#0#0#0#98>					<HR BW10.tx#0#0#0#98>					<HR BW20.tx#0#0#0#98>			
cyl_tmp	K		570	570	570	570	570	570	570	570	570	570	570	570		
CA_ICV	deg		-110	-110	-110	-110	-110	-110	-110	-110	-110	-110	-110	-110		

## CHAPTER 4

### RESULT AND DISCUSSION

#### 4.1 Catalyst Characterisation

The catalyst characterisation used the X-ray diffraction (XRD). In the X-ray diffraction (XRD), the detector moves in a circle around the sample. The detector position is recorded as the angle  $2\theta$  ( $2\theta$ ). The detector records the number of X-rays observed at each angle  $2\theta$ . The X-ray intensity is usually recorded as “counts” or as “counts per second”.

The X-ray diffraction (XRD) pattern of the cockle shell calcined at  $900^{\circ}\text{C}$  for 3.5 h is shown in Figure 4.1. It indicated the sharp peaks at  $2\Theta = 32.53^{\circ}$ ,  $37.78^{\circ}$ ,  $54.48^{\circ}$ ,  $64.88^{\circ}$  and  $68.20^{\circ}$  which are characteristics of Calcium Iron Oxide phase, with composition 72.6 % CaO, 21.9 % FeO and 4.9 %  $\text{Fe}_2\text{O}_3$ . The Miller indices (hkl) of the diffraction peaks demonstrated in the top of each peak indicated that this catalyst is crystalline. The peaks were compared with the Standards JCPDS card No. 00-021-0917 in Appendix G.



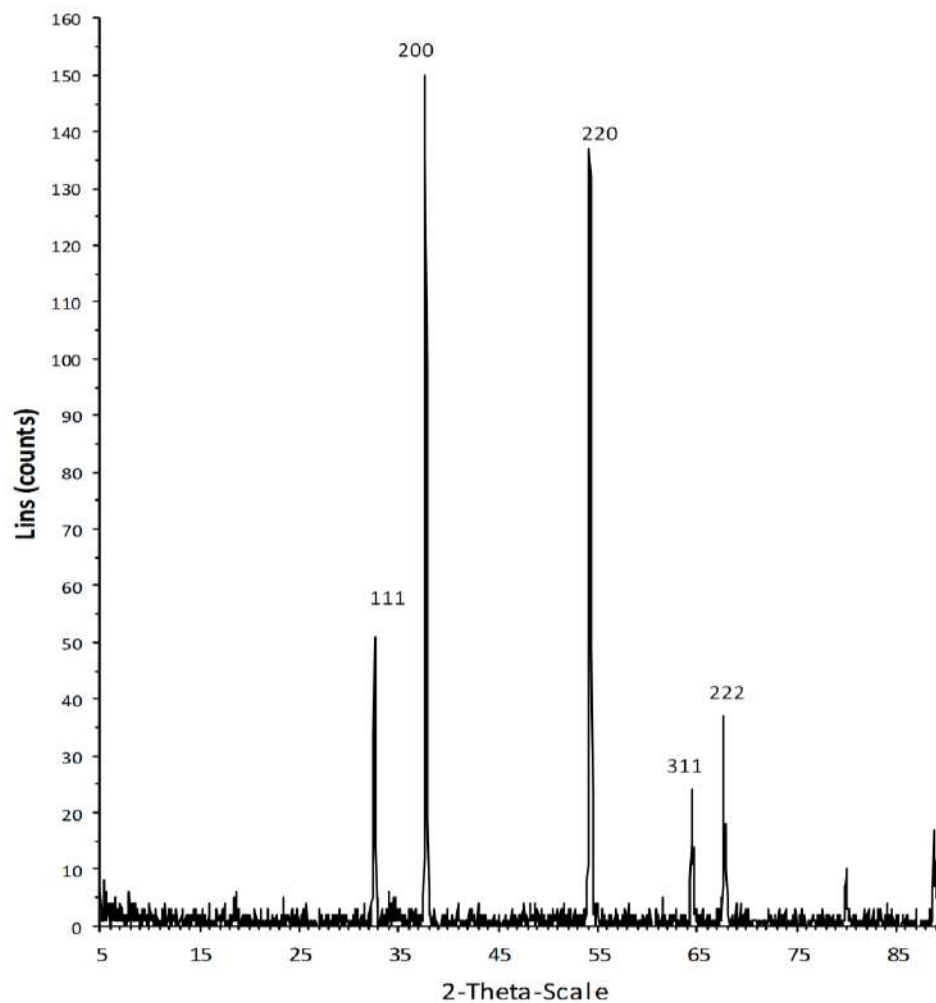


**Figure 4.1** The XRD of the cockle shell calcined at 900 °C for 3.5 h

## 4.2 Transesterification of Waste Cooking Oil Using Calcium Oxide Catalyst

### 4.2.1 Temperature Profile

Figure 4.2 depicts the real-time temperature profiles under microwave power input of 180 W and 450 W. It can be observed that the average temperature T2 is higher than the average temperature T1, which is caused by the heat transfer process that leads to the top of the reactor and an injection of methanol through the bottom of

the reactor. The average difference between T1 and T2 for 450 W input power is greater than 180 W.

In the dispersion of methanol and catalyst process (i), the time required to reach the temperature set point for power input 450 W is faster than 180 W because the heat rate at 450 W is higher than 180 W. The temperature record shows the fluctuations of the temperature of the mixture during mixing process of WCO, methanol and catalyst (ii). In the next process (iii), the temperature T2 fluctuated due to the input flow of methanol intermittently. These temperature profiles represent several temperature profiles that have the same trend.

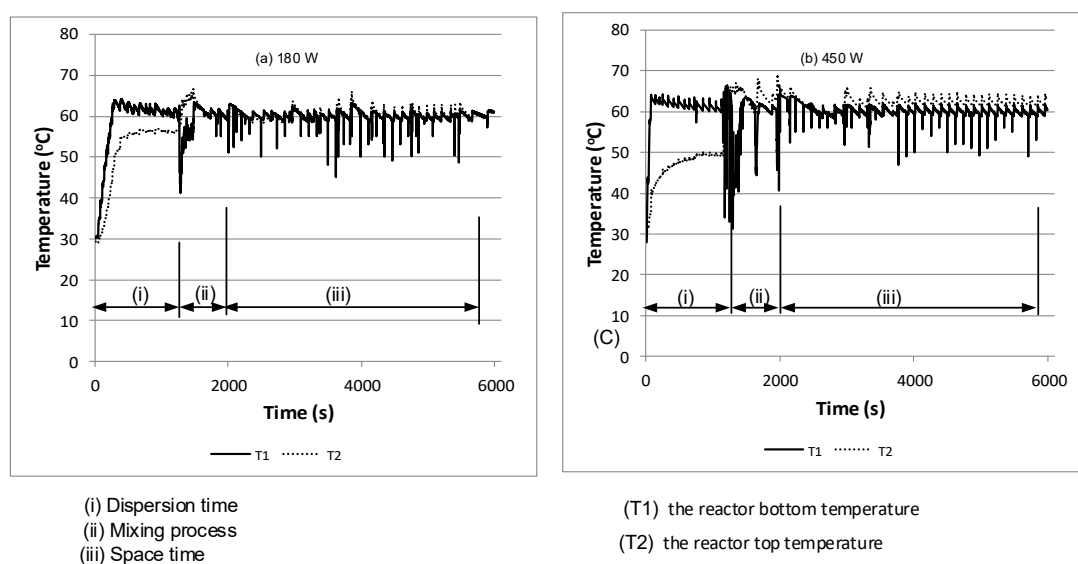


**Figure 4.2** Typical temperature profile power input 180 W and 450 W for single step transesterification continuous process

#### 4.2.2 Physical Properties

The data of physical properties of WCO and WCOME such as caloric value, density, flash point and kinematic are shown in Table 4.1. The data was processed at the Combustion Laboratory Mechanical Engineering and Laboratory Service Unit Faculty of Chemical Engineering UTM (see Appendix B).

**Table 4.1 :** Physico-chemical properties of waste cooking oil and waste cooking oil methyl ester

<b>Properties</b>	<b>ASTM Method</b>	<b>Units</b>	<b>WCO</b>	<b>WCOME</b>
Calorific value		kJ/kg	43,522	38,049
Density at 15 °C	ASTM D1298-85	kg/l	0.917	0.870
Flash Point	ASTM D92-90	°C	318.0	158.5
Kinematic Viscosity at 40 °C	ASTM D445-94	cSt	47.51	5.48
Free Fatty Acid		%	0.37-0.5	

#### 4.2.3 Chemical Properties

The WCO samples have FFA content 0.37-0.50 %. Detail of titration of these samples is presented in Appendix A. The results of the test using GCMS is shown in Figure 4.3 and Table 4.2. It showed that one sample contained 97.91% methyl ester. One of the biggest components of the sample is hexadecanoic acid methyl ester which is then to be used in the calculation of calibration.

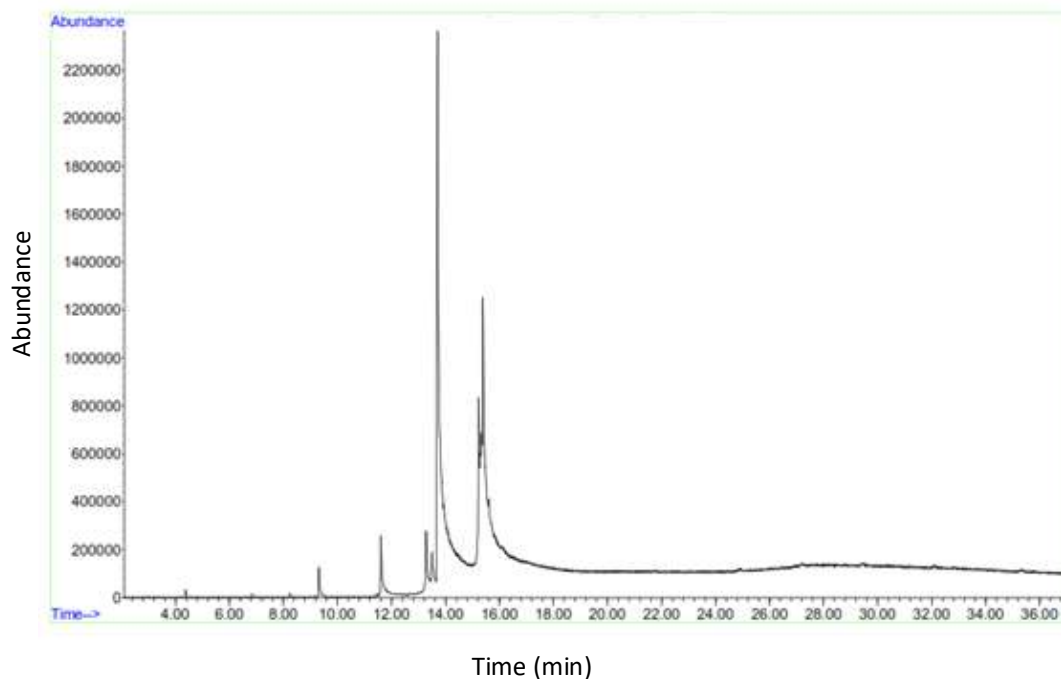


**Figure 4.3** Typical analysis of fatty acid methyl ester from biodiesel of waste cooking oil using Gas Chromatography Mass Spectrometry

**Table 4.2** : Fatty acid composition of biodiesel from waste cooking oil

Compound Name (CAS)	Percentage
Hexadecanoic acid, methyl ester	51.569
6-Octadecenoic acid, methyl ester	12.924
11-Octadecenoic acid, methyl ester	7.708
Pentadecanoic acid, 14-methyl-, methyl ester	4.629
Octasiloxane, 1,1,3,3,5,5,7,7,9,9,11,11,13,13,15,15-hexadecamethyl-	3.856
9-Octadecenoic acid (Z)-, methyl ester	2.943
Heptasiloxane, 1,1,3,3,5,5,7,7,9,9,11,11,13,13-tetradecamethyl-	2.111
Methyl tetradecanoate	1.676
Methyl hexadec-9-enoate	1.388
Benzo[h]quinoline, 2,4-dimethyl-	1.078
Total of 35 compounds that less than 1.0 % Others	10.095
Others	2.092
<b>TOTAL</b>	<b>100.000</b>

#### **4.2.4 Model Fitting and Statistical Analysis of Biodiesel Conversion**

Table 4.3 shows the experimental data of transesterification WCO for three levels of collection samples based on time collected to space-time ratio (CSR). Box-Behnken Design (BBD) was used to correlate transesterification variables and response and to identify the contribution of significant variables to regression model regression model for three states, ie time collected to the space-time ratios 1/3, 2/3 and 1. The experiments were performed in random order to avoid bias error, and each of the experiment was conducted in replicate and the average value used.

**Table 4.3 :** Experimental data of waste cooking oil transesterification for three level of time collected to space-time ratio

Molar ratio = 9 Catalyst = Calcined cockle 2.0-4.0 mm  
 Set point temperature = 65 (°C) Bulk Density = 1.99 (g/ml)  
 Volume of Bucket container = 32.1 (ml) Volume of Reactor = 412.3 (ml)

Run	Power Input <i>Pm</i> (W)	Catalyst Weight <i>Wc</i> (g)	Siirrer speed <i>Ns</i> (rpm)	Pump Speed <i>Np</i> (rpm)	Flowrate <i>F</i> (ml/min)	Catalyst vol. <i>Vc</i> (ml)	Mix. Volume <i>V mix</i> (ml)	<i>LHSV</i> (h <sup>-1</sup> )	Space time $\tau$ (min)	CSR=1/3		CSR=2/3		CSR=1	
										Coll. Time (min)	<i>C</i> <sub>CSR=1/3</sub>	Coll. Time (min)	<i>C</i> <sub>CSR=2/3</sub>	Coll. Time (min)	<i>C</i> <sub>CSR=1</sub>
1	450	12.73	400	28	6.098	6.40	373.8	57.194	61.3	20.4	67.83	40.9	71.63	61.3	72.48
2	315	12.73	300	28	6.098	6.40	373.8	57.194	61.3	20.4	71.44	40.9	71.66	61.3	72.09
3	450	10.00	300	32	6.969	5.03	375.2	83.210	53.8	17.9	72.20	35.9	72.17	53.8	72.18
4	315	20.00	400	24	5.227	10.05	370.1	31.204	70.8	23.6	72.19	47.2	72.48	70.8	72.11
5	315	10.00	400	32	6.969	5.03	375.2	83.210	53.8	17.9	72.03	35.9	71.43	53.8	71.77
6	315	20.00	200	24	5.227	10.05	370.1	31.204	70.8	23.6	72.18	47.2	71.54	70.8	71.75
7	450	12.73	200	28	6.098	6.40	373.8	57.194	61.3	20.4	72.47	40.9	72.37	61.3	72.46
8	180	10.00	300	32	6.969	5.03	375.2	83.210	53.8	17.9	64.74	35.9	67.76	53.8	70.05
9	315	12.73	300	28	6.098	6.40	373.8	57.194	61.3	20.4	71.48	40.9	71.98	61.3	71.96
10	180	12.73	200	28	6.098	6.40	373.8	57.194	61.3	20.4	66.18	40.9	70.06	61.3	70.49
11	450	20.00	300	24	5.227	10.05	370.1	31.204	70.8	23.6	72.48	47.2	72.40	70.8	72.48
12	315	12.73	300	28	6.098	6.40	373.8	57.194	61.3	20.4	71.86	40.9	72.19	61.3	71.75
13	180	20.00	300	24	5.227	10.05	370.1	31.204	70.8	23.6	69.09	47.2	71.54	70.8	72.13
14	315	10.00	200	32	6.969	5.03	375.2	83.210	53.8	17.9	70.85	35.9	71.73	53.8	70.43
15	180	12.73	400	28	6.098	6.40	373.8	57.194	61.3	20.4	67.25	40.9	71.69	61.3	71.40

#### 4.2.4.1 ANOVA and mathematical model for time collected to space-time ratio = 1/3

The BBD design matrix of the three-factor-three levels with the experimental result for time collected to space-time = 1/3 is depicted in Table 4.4. To classify the correlation of the research variables with the process variables, Box-Behnken Design (BBD) was used for experimental results for time collected to space-time (CSR)=1/3 as shown in Table 4.4. The results of the experiment for all responses were summarised by using ANOVA in Table 4.5.

**Table 4.4 :** Box-Behnken design matrix of three-factor-three levels with experimental result for time collected to space-time ratio = 1/3

Run	Power Input, <i>P<sub>m</sub></i> (W)	Stirrer Speed, <i>N<sub>s</sub></i> (rpm)	<i>LHSV</i> (h <sup>-1</sup> )	Conversion at CSR=1/3, C <sub>CSR=1/3</sub> (%)
1	450	400	57.194	67.83
2	315	300	57.194	71.44
3	450	300	83.21	72.2
4	315	400	31.204	72.19
5	315	400	83.21	72.03
6	315	200	31.204	72.18
7	450	200	57.194	72.47
8	180	300	83.21	64.74
9	315	300	57.194	71.48
10	180	200	57.194	66.18
11	450	300	31.204	72.48
12	315	300	57.194	71.86
13	180	300	31.204	69.09
14	315	200	83.21	70.85
15	180	400	57.194	67.25

**Table 4.5 :** Table analysis of variance (ANOVA) for response surface quadratic model for conversion at time collected to space-time ratio =1/3

Source	Sum of squares	df	Mean square	F-value	p-value Prob>F	Remarks
Model	87.26	9	9.7	7.86	0.0176	significant
A-Power input ( $P_m$ )	39.29	1	39.29	31.83	0.0024	significant
B-Stirrer speed ( $N_s$ )	0.72	1	0.72	0.58	0.48	
C-LHSV	4.68	1	4.68	3.8	0.1089	
AB	8.14	1	8.14	6.6	0.0501	
AC	4.15	1	4.15	3.36	0.1261	
BC	0.34	1	0.34	0.28	0.6217	
A <sup>2</sup>	26.38	1	26.38	21.38	0.0057	significant
B <sup>2</sup>	0.88	1	0.88	0.71	0.4374	
C <sup>2</sup>	1.85	1	1.85	1.5	0.2749	
Residual	6.17	5	1.23			
Lack of fit	6.17	4	1.54	1449.63	0.0197	significant
Pure error	1.06E-03	1	1.06E-03			
Cor Total	93.43	14				

R-Square= 0.9340, Adj R-squared=0.8151 and Pred R Squared =-0.0413

The proposed model related to the actual factors for the conversion is as follows:

$$\begin{aligned}
 C_{CSR=1/3} = & 54.663 + 0.12392 \times P_m + 0.053129 \times N_s \\
 & - 0.27446 \times LHSV - 1.05679 \times 10^{-4} \times P_m \times N_s \\
 & + 2.90262 \times 10^{-4} P_m \times LHSV + 1.12267 \times 10^{-4} \times N_s \times LHSV \\
 & - 1.4667 \times 10^{-4} P_m^2 - 4.87652 \times 10^{-5} \times N_s^2 \\
 & + 1.0481 \times 10^{-3} \times LHSV^2
 \end{aligned} \quad (4.1)$$

The significance of each coefficient in Eq. (4.1) was evaluated by the P-value as shown in ANOVA result on conversion in Table 4.5. The smaller magnitude of the P-value indicates that the model is significant since Prob> F is less than  $\alpha$  (0.10), which implies 90 % confidence interval significant is the corresponding coefficient. Considering the linear effect, only power input and stirrer speed were found to be significant terms in increasing the conversion in the final product. The power input term had the significant linear effect and quadratic effect is significant at 5% levels,



while others are not significant. This means that at a time where sampling takes one-third of the space-time, only the input power parameter has a significant influence against the biodiesel conversion, while the two parameters have no significant effect. The other interaction terms had no significant effect on the WCOME conversion. The lack of fit (LOF) value of 38.55 implies the Lack of Fit is significant. There is only a 2.54 % chance that a "Lack of Fit F-value" this large could occur due to noise. Although the model is acceptable significantly, lack of fit is significant, then with a significant level of 5%, this model is unacceptable.

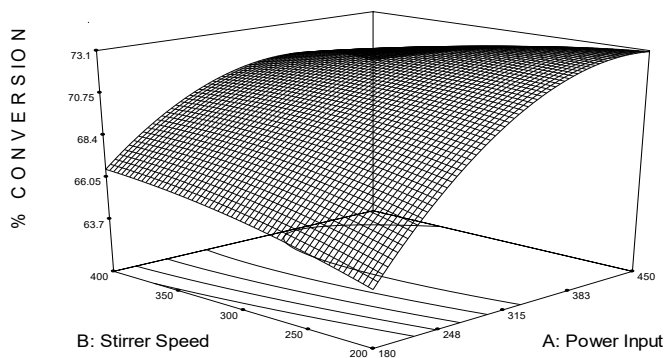
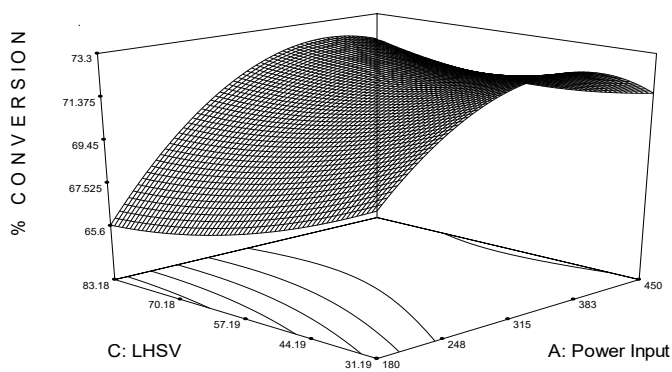
The predicted and actual WCOME conversion (%) given in Table 4.6 shows that the predicted values are quite close to the experimental values. The  $R^2$  value for WCOME is 0.9340; that is, 93.4% of the variability in the data accounted to model, thereby validating the reliability of the model developed for establishing a correlation between the process variables and the WCOME conversion.

Figure 4.4 (a) shows the interaction of power input and stirrer speed at  $LHSV=57.19 \text{ h}^{-1}$  on WCOME conversion at collected time to space-time ratio=1/3. It shows that for low power input, WCOME conversion is increasing with increasing stirrer speed. At the high-power input, WCOME conversion increases with stirrer speed until a certain point and then decreases. The minimum WCOME occurs at minimum power input and minimum stirrer speed. This is due to the fact that both lower agitation and power transmission from microwave to mixture decrease the conversion. The surface and contour plot for the interaction of power input and  $LHSV$  at stirrer speed =300 rpm are shown in Figure 4.4 (b). It is shown that for low power input, WCOME conversion is increasing with decreasing  $LHSV$ . The WCOME conversion increases with power input at the lower  $LHSV$ . The minimum WCOME occurs at maximum  $LHSV$  and minimum power input.

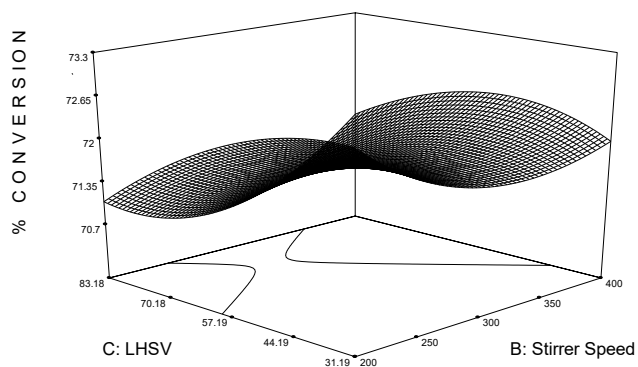
**Table 4.6 :** Responses for transesterification of WCOME at time collected to space-time ratio =1/3

Run	A:Power Input (W)	B:Stirrer speed (rpm)	C:LHSV (h <sup>-1</sup> )	Conversion (%)	
				Experimental Response	Predicted Response
1	450	400	57.173	67.83	68.923
2	315	300	57.173	71.44	71.595
3	450	300	83.179	72.2	72.098
4	315	400	31.192	72.19	71.99
5	315	400	83.179	72.03	71.041
6	315	200	31.192	72.18	73.173
7	450	200	57.173	72.47	72.376
8	180	300	83.179	64.74	65.629
9	315	300	57.173	71.48	71.595
10	180	200	57.173	66.18	65.092
11	450	300	31.192	72.48	71.593
12	315	300	57.173	71.86	71.595
13	180	300	31.192	69.09	69.199
14	315	200	83.179	70.85	71.057
15	180	400	57.173	67.25	67.346

Figure 4.4 (c) shows the effect of stirrer speed and LHSV on WCOME conversion at power input =315 watt. This figure shows that the WCOME conversion decreases with increase *LHSV* until 70 h<sup>-1</sup> and then increases at the lower stirrer speed. The minimum WCOME occurs at maximum *LHSV* and minimum stirrer speed. This is due to the agitation of the catalyst is very low, the amount of catalyst is low and contact time between catalyst and mixture is low.

(a)  $LHSV (C) = 57.19 \text{ h}^{-1}$ 

(b) Stirrer speed (B) = 300 rpm



(c) Power Input (A) = 315 W

**Figure 4.4** 3 D response surface showing the power input speed, stirrer speed and  $LHSV$  on WCOME conversion at time collected to space-time ratio = 1/3

#### 4.2.4.2 ANOVA and Mathematical Model for Time Collected to Space-time Ratio= 2/3

Box-Behnken Design (BBD) design matrix of three-factor-three level with experimental result for time collected to space-time ratio = 2/3 is depicted in Table 4.7, while the results from the experiment for response for time collected to space-time ratio=2/3 was summarized by using ANOVA in Table 4.7.

**Table 4.7 :** Box-Behnken design matrix of three-factor-three level with experimental result for time collected to space-time ratio = 2/3

Run	Power Input, $P_m$ (W)	Stirrer Speed, $N_s$ (rpm)	$LHSV$ (h <sup>-1</sup> )	Conversion at CSR=2/3, C <sub>CSR</sub> =2/3 (%)
1	450	400	57.194	71.63
2	315	300	57.194	71.66
3	450	300	83.21	72.17
4	315	400	31.204	72.48
5	315	400	83.21	71.43
6	315	200	31.204	71.54
7	450	200	57.194	72.37
8	180	300	83.21	67.76
9	315	300	57.194	71.98
10	180	200	57.194	70.06
11	450	300	31.204	72.4
12	315	300	57.194	72.19
13	180	300	31.204	71.54
14	315	200	83.21	71.73
15	180	400	57.194	71.69

**Table 4.8 :** Analysis of variance (ANOVA) for response surface quadratic model for conversion at time collected to space-time ratio =2/3

Source	Sum of squares	df	Mean square	F-value	p-value Prob>F	Remarks
Model	17.54	9	1.95	4.06	0.0686	significant
A-Power input (P <sub>m</sub> )	7.08	1	7.08	14.75	0.0121	significant
B-Stirrer speed (N <sub>s</sub> )	0.23	1	0.23	0.47	0.5214	
C-LHSV	3.2	1	3.2	6.66	0.0494	significant
AB	1.4	1	1.4	2.91	0.1487	
AC	3.16	1	3.16	6.57	0.0504	significant
BC	0.28	1	0.28	0.57	0.4826	
A <sup>2</sup>	1.76	1	1.76	3.67	0.1136	
B <sup>2</sup>	0.13	1	0.13	0.26	0.6308	
C <sup>2</sup>	0.3	1	0.3	0.62	0.4675	
Residual	2.4	5	0.48			
Lack of fit	2.35	4	0.59	10.98	0.2222	not significant
Pure error	0.053	1	0.053			
Cor Total	19.94	14				

R-Square= 0.8796, Adj R-squared=0.6628 and Pred R Squared =-0.8266

The proposed model related to the actual factors for the conversion is as follows:

$$\begin{aligned}
 C_{CSR=2/3} = & 65.84678 + 0.029509 \times P_m + 0.010194 \times N_s + 0.025765 \times LHSV \\
 & - 4.3795 \times 10^{-5} \times P_m \times N_s + 2.5311 \times 10^{-4} P_m \times LHSV - \\
 & 1.0105 \times 10^{-4} \times N_s \times LHSV - 3.78955 \times 10^{-5} P_m^2 + 1.84484 \times 10^{-5} \times N_s^2 \\
 & - 4.19471 \times 10^{-4} \times LHSV^2
 \end{aligned} \quad (4.2)$$

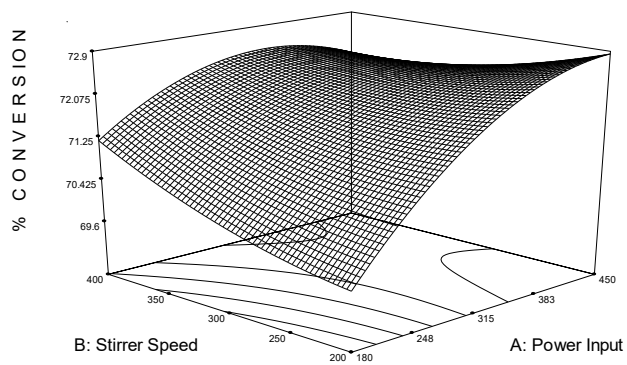
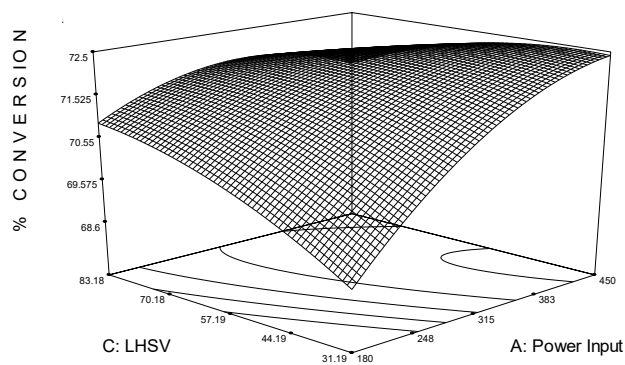
Table 4.9 shows that the selected model is significant with the F-value Model 4.06. There is only a 6.86% chance that this large "F-Value Model" can occur due to noise. There are two linear effects and one significant interaction effect because the value of "Prob> F" is less than 0.1000. In this case, the power input and stirrer speed and interaction effect are only *LHSV* power inputs, other parameters that are greater than 0.1000 indicate the term model is not significant. If there are many insignificant model terms (not including those needed to support the hierarchy), model reductions can improve your model. "Lack of Fit Value" 10.98 implies Lack of Fit is not

significant compared to pure error. There is a 22.22% chance that this "Lack of Fit F-value" can occur due to noise. The absence of an insignificant fit is good enough. With a significant model of lack of fit that is not significant, then this model is acceptable.

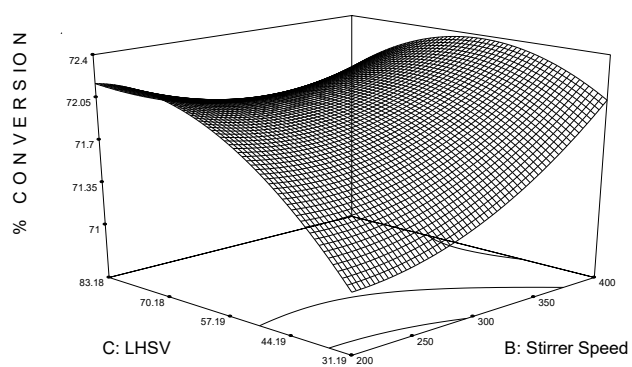
The interaction of power input and stirrer speed at  $LHSV=57.19 \text{ h}^{-1}$  on WCOME conversion at the collected time to space-time ratio= $2/3$  is exhibited in Figure 4.5 (a). It shows that for low power input, WCOME conversion is increasing with increasing stirrer speed. At the high-power input, WCOME conversion increases with stirrer speed until the certain point and then decreases. The minimum WCOME occurs at minimum power input and minimum stirrer speed. This is because both lower agitation and power transmission from microwave to mixture decreases the conversion.

The surface and contour plot for the interaction of power input and  $LHSV$  at stirrer speed =300 rpm are shown in Figure 4.5 (b). It shows that for low power input, WCOME conversion increasing with decreasing  $LHSV$ . The WCOME conversion increases with power input at the lower  $LHSV$ . The minimum WCOME occurs at maximum  $LHSV$  and minimum power input.

Figure 4.5 (c) shows the effect of stirrer speed and  $LHSV$  on WCOME conversion at power input =315 watt. This figure shows that the WCOME conversion decreases with low  $LHSV$  at the lower stirrer speed. The minimum WCOME occurs at maximum  $LHSV$  and minimum stirrer speed. This is due to the agitation of the catalyst is very low, the amount of catalyst is low and contact time between catalyst and mixture is low.

(a)  $LHSV (C) = 57.19 \text{ h}^{-1}$ 

(b) Stirrer speed (B) = 300 rpm



(c) Power Input (A) = 315 W

**Figure 4.5** 3 D response surface showing the power input speed, stirrer speed and  $LHSV$  on WCOME conversion at time collected to space-time ratio =  $2/3$

#### 4.2.4.3 ANOVA and Mathematical Model for Time Collected to Space-time Ratio = 1

The BBD design matrix of three-factor-three level with experimental result for time collected to space-time=1 is depicted in Table 4.9. The results from the experiment for all responses were summarized by using ANOVA in Table 4.10.

**Table 4.9 :** Box Behnken design matrix of three-factor-three level with experimental result for time collected to space-time ratio = 1

Run	Power Input, <i>P<sub>m</sub></i>	Stirrer Speed, <i>N<sub>S</sub></i>	<i>LHSV</i>	Conversion at CSR=1, C <sub>CSR=1</sub>
1	450	400	57.194	72.48
2	315	300	57.194	72.09
3	450	300	83.210	72.18
4	315	400	31.204	72.11
5	315	400	83.210	71.77
6	315	200	31.204	71.75
7	450	200	57.194	72.46
8	180	300	83.210	70.05
9	315	300	57.194	71.96
10	180	200	57.194	70.49
11	450	300	31.204	72.48
12	315	300	57.194	71.75
13	180	300	31.204	72.13
14	315	200	83.210	70.43
15	180	400	57.194	71.40



**Table 4.10 :** Table analysis of variance for response surface quadratic model for conversion at time collected to space-time ratio =1

Source	Sum of squares	df	Mean square	F-value	p-value Prob>F	Remarks
Model	8.26	9	0.92	19.23	0.0023	significant
A-Power input (Pm)	3.83	1	3.83	80.13	0.0003	significant
B-Stirrer speed (Ns)	0.86	1	0.86	18.01	0.0081	significant
C-LHSV	2.04	1	2.04	42.78	0.0013	significant
AB	0.2	1	0.2	4.13	0.0979	
AC	0.79	1	0.79	16.54	0.0097	significant
BC	0.24	1	0.24	5.07	0.0741	
A <sup>2</sup>	1.09E-03	1	1.09E-03	0.023	0.8858	
B <sup>2</sup>	0.16	1	0.16	3.35	0.1266	
C <sup>2</sup>	0.16	1	0.16	3.34	0.1271	
Residual	0.24	5	0.048			
Lack of fit	0.18	3	0.06	2.11	0.337	not significant
Pure error	0.057	2	0.029			
Cor Total	8.5	14				

R-Square= 0.9719, Adj R-squared=0.9214and Pred R Squared =0.6433

The proposed model related to the actual factors for the conversion is as follows:

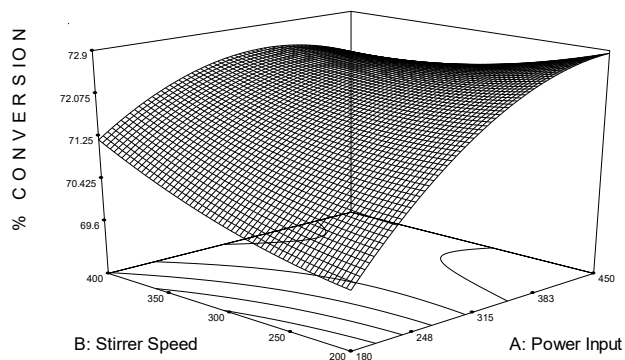
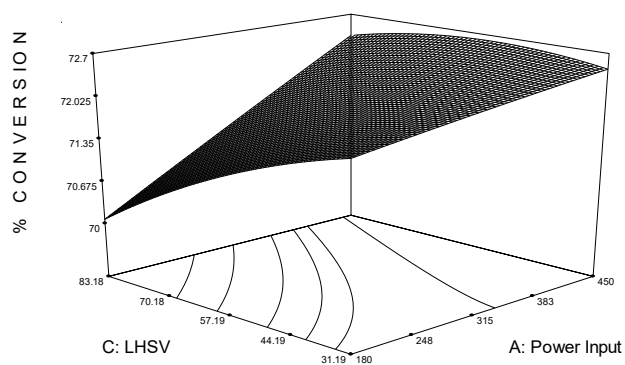
$$\begin{aligned}
 C_{CSR=1} = & 69.8236637 + 0.00341229 \times P_m + 0.0155426 \times N_s \\
 & - 0.95253203 \times LHSV - 1.644414 \times 10^{-5} \times P_m \times N_s \\
 & + 1.0001266 \times P_m \times LHSV + 9.4621 \times 10^{-5} \times N_s \times LHSV \\
 & - 9.4299 \times 10^{-7} P_m^2 - 2.08229 \times 10^{-5} \times N_s^2 \\
 & - 0.000307651 \times LHSV^2
 \end{aligned} \tag{4.3}$$

The significance of each coefficient in Eq. (4.3) was evaluated by the P-value as shown in Table 4.10. The smaller magnitude of the P-value, the more significant is the corresponding coefficient. There are only two operating parameters found to be significant terms in increasing conversions in the final product in a linear equation. The power input term had the most significant linear effect, followed by *LHSV* and stirrer speed, respectively. In terms of the quadratic effect, no parameter was significant at 5% levels. However, for the interaction effect, it was found that only

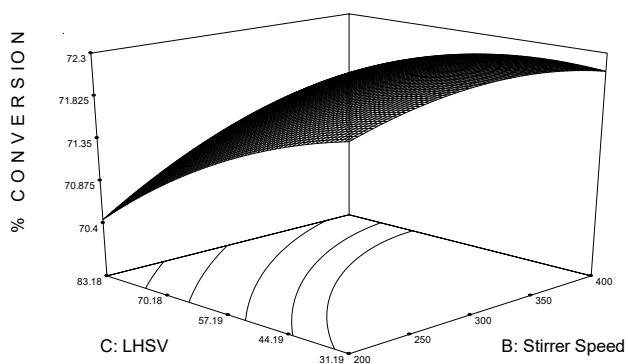
power input-LHSV interaction was significant at 5% level. The other interaction terms had no significant effect on the % conversion.

Table 4.10 shows that the value of Model F-value 19.23 means the model is significant. There is only a 0.23% chance that this large "F-Value Model" can occur due to noise. Under this condition, the "Prob> F" value of less than 0.0500 indicates a significant model term three of which are the main parameters of power input, stirrer speed and *LHSV*. The interaction effect power input- *LHSV* is also significant. If there are many insignificant model terms, model reductions can improve your model. The "Lack of Fit Value" of 2.11 implies Lack of Fit is insignificant compared to pure error. There is a possibility of 33.70% that this "Lack of Fit F-value" could be due to noise. The absence of an insignificant fit is good enough. The result of Table 4.11 also shows that this model is acceptable because the model is significant and lack of fit is not significant. In addition to the power input parameters, stirrer speed, *LHSV*, and (power input x *LHSV*) are also significant.

The interaction of power input and stirrer speed at *LHSV*=57.28 h<sup>-1</sup> on WCOME conversion at a collected time to space-time ratio=1 is exhibited in Figure 4.6 (a). It shows that for low power input, WCOME conversion increasing with increasing stirrer speed. At the high-power input WCOME conversion increases with stirrer speed until the certain point and then decreases. The minimum WCOME occurs at minimum power input and minimum stirrer speed. This is because both lower agitation and power transmission from microwave to mixture decrease the conversion. The surface and contour plot for the interaction of power input and *LHSV* at stirrer speed =300 rpm are shown in Figure 4.6 (b). It shows that for low power input, WCOME conversion is increasing with decreasing *LHSV*. The WCOME conversion increases with power input at the lower *LHSV*. The minimum WCOME occurs at maximum *LHSV* and minimum power input.

(a)  $LHSV (C) = 57.28 \text{ h}^{-1}$ 

(b) Stirrer speed (B) = 300 rpm



(c) Power Input (A) = 315 W

**Figure 4.6** 3 D response surface showing the power input speed, stirrer speed and  $LHSV$  on WCOME conversion at time collected to space-time ratio = 1

Figure 4.6 (c) shows the effect of stirrer speed and *LHSV* on WCOME conversion at power input =300 watt. This figure shows that the WCOME conversion decreases with low *LHSV* at the lower stirrer speed. The minimum WCOME occurs at maximum *LHSV* and minimum stirrer speed. This is because the agitation of the catalyst and oil-methanol mixture is very low, the amount of catalyst is low and contact time between catalyst and the oil-methanol mixture is low.

#### 4.2.5 Optimisation and Validation

The objective of optimisation is to find the best setting value conditions based on the power input, stirrer speed and *LHSV* that convert the highest conversion value. The optimum conversion is obtained by setting the lower and upper limits of variable process namely power input, stirrer speed and *LHSV*. The percentage of conversion was set to maximum.

Based on the model associated with the actual factors for the conversion indicates that the model is significant and the lack of an insignificant F-fit value used on the model, then only conditions on at collected time to space-time = 1 is good, hence indicates that the model can be used to predict the conversion.

The response was optimised to maximise the WCOME conversion conditions for collected time to space-time = 1 based on the mathematical equation. The optimum value of the WCOME conversion 72.52% was achieved with power input of 445 W, stirrer speed of 380 rpm and *LHSV* of 71.5 h<sup>-1</sup>.

The experiment was then re-run at optimisation condition on power input of 450 W, stirrer speed of 353 rpm and *LHSV* of 59.4 h<sup>-1</sup>. The result of WCOME conversion of this condition is 71.9%.

### 4.3 Diesel Engine Test

The following sub-sections discuss the results of engine performance and exhaust gas emission of the single diesel engine using WCOME blends and POME blends. The discussion includes the comparison of BSFC and BTE, the measurement of exhaust gas emission such CO, CO<sub>2</sub>, HC and NO<sub>x</sub>. In addition, measurement in-cylinder pressure traces and heat release rate (HRR) are used to represent the combustion analysis.

#### 4.3.1 Fuel Test

The result of chemical and physical properties of fuel test are shown in Table 4.11. The density and kinematic viscosity of both blended fuel increase with an increased content of biodiesel. Conversely, the calorific value decreases with increasing biodiesel content.

**Table 4.11** : Properties of test fuels

<b>Properties</b>	<b>PDM</b>	<b>BP10</b>	<b>BP20</b>	<b>BW10</b>	<b>BW20</b>
Carbon (wt %)	85.43	85.04	84.98	84.53	83.09
Hydrogen (wt%)	13.98	13.99	14.04	13.97	14.00
Nitrogen (wt%)	0.36	0.38	0.36	0.38	0.34
Sulphur (wt%)	0.10	0.02	0.02	0.04	0.04
Oxygen (wt%)	0.13	0.57	0.59	1.08	2.53
Calorific value (MJ/kg)	45.488	45.311	44.624	44.016	43.801
Density at 15 °C, (kg/l)	0.830	0.832	0.835	0.835	0.855
Kinematic viscosity at 40°C (mm <sup>2</sup> /s)	3.020	3.054	3.134	3.105	3.426

### 4.3.2 Diesel Engine Performance

In this experiment, all data were taken at the engine speed of 2500 rpm. The fuel used in this test are PDM and PDM mixed with two different biodiesels. PDM and POME mixture are symbolised by BP10 and BP20, while the PDM mixture with WCOME are symbolised by BW10 and BW20. For each fuel, five different engine loads were applied for 2500 rpm speed engine. Kumar and Jaikumar (2014) performed their experiment with variation of brake mean effective pressure (BMEP) at constant speed to investigate performance, emission and combustion of diesel engine fuelled with WCO emulsion as fuel. The influence of fuel type usage on parameters related to the performance engine is described in the following sub-sub sections.

#### 4.3.2.1 Brake Specific Fuel Consumption

Figure 4.7 shows the effect of brake mean effective pressure (BMEP) on brake specific fuel consumption (BSFC) for PDM, POME blends and WCOME blends at 2500 rpm engine speed. It is observed that all biodiesel blends were higher than PDM for all loads. For the same BMEP, higher consumption is needed for the biodiesel blends compared to PDM. It is caused by the lower heating values of both biodiesel blends being lower than the PDM. The energy content per unit mass of BP10, BP20, BW10 and BW20 are 45,311, 44,624, 44,016 and 43,801 kJ/kg, respectively, whilst that of PDM is 45,488 kJ/kg. For BW20, fuel could be operated on two loads only, because the engine stopped on the load 7 Nm and 2500 rpm. The engine stopped due to poor combustion of the injected fuel as a result of high viscosity and density (Senthil Kumar and Jaikumar, 2014). Calorific value of the biodiesel blends is lower than PDM due to its oxygenated nature. Therefore, the amount of the expected increments on the BSFC results also can be explained by the low calorific value of the biodiesel blends (Can *et al.*, 2017).

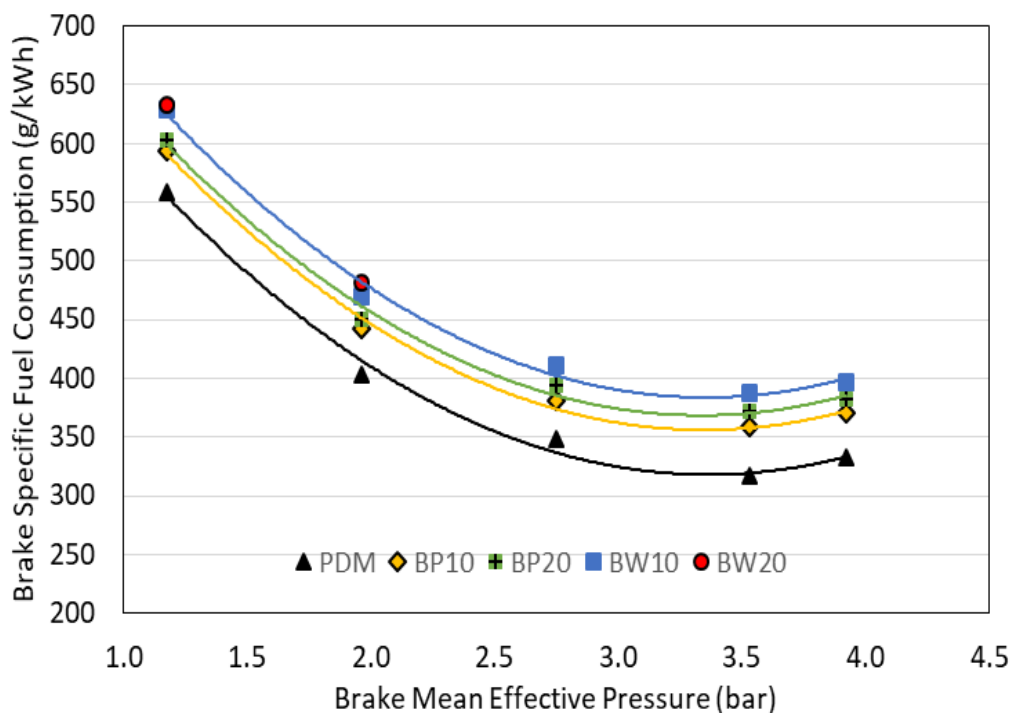


**Figure 4.7** The variation of brake specific fuel consumption with brake mean effective pressure at five different loads

The minimum BSFC for all loads are 316.4, 358.7, 371.6, and 387.9 g/kWh for fuel of PDM, BP10, BP20 and BW10, respectively. All of the minimum BSFC was obtained at BMEP 3.53 bar.

#### 4.3.2.2 Brake Thermal Efficiency

Figure 4.8 shows the effect of BMEP on brake thermal efficiency (BTE) for constant speed. This graph is a good parameter to assess the fuels ability to convert their energy into mechanical energy outputs. As this figure shows, the maximum brake thermal efficiencies for all loads are 22.93%, 22.15%, 21.17% and 21.08% for fuel of PDM, BP10, BP20 and BW10, respectively. All of the maximum BTE was obtained at BMEP 3.53 bar. The BW10 fuel decreased by 13.8% compared to the PDM at BMEP 3.53 bar. This reduction was mainly due to poor combustion of the injected fuel as a result of high viscosity and density. In addition, biodiesel blends have lower

calorific value and poor volatility compared to PDM fuel (Gad *et al.*, 2017; Senthil Kumar and Jaikumar, 2014).

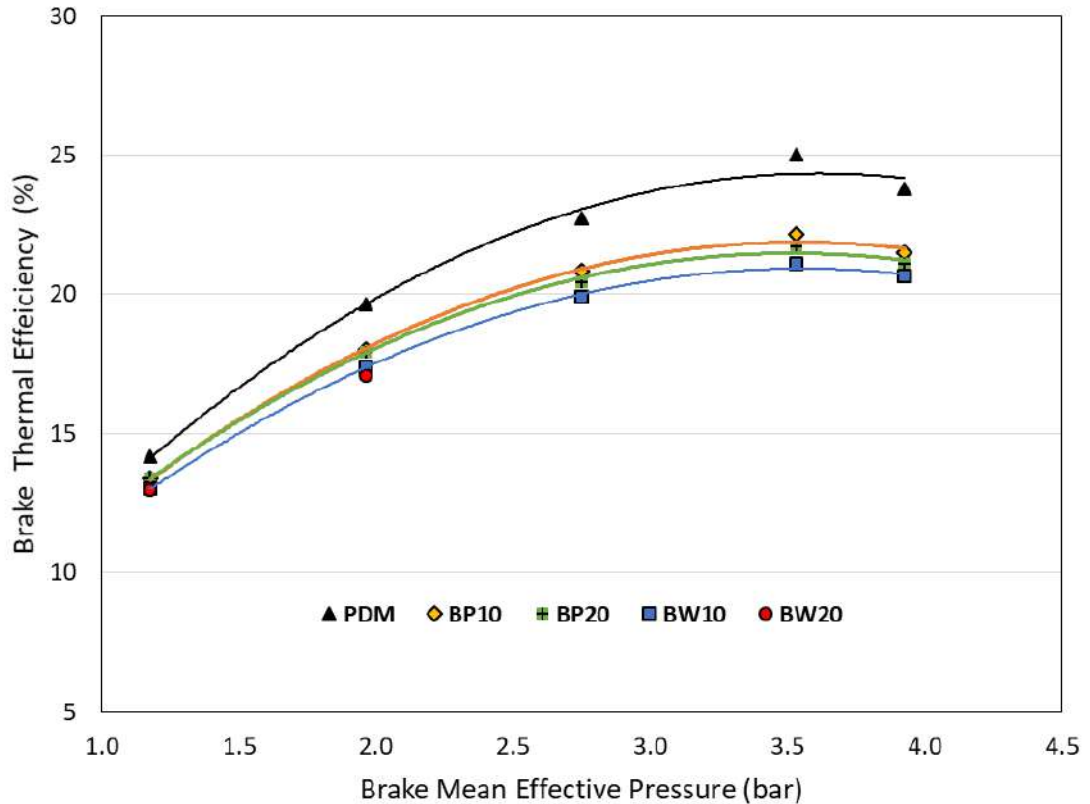


**Figure 4.8** The variation of brake mean effective pressure with engine brake thermal efficiency

#### 4.3.2.3 Engine Performance Statistical Analysis

The BSFC and BTE statistical analysis were conducted on the collected experimental data for loads at constant speed. The analysis of variance (ANOVA) was used to indicate the level of significance of the load effects on the BSFC and BTE. In this analysis, DF represents the degree of freedom, F value represents the probability distribution in repeated sampling, and p-value represents the weight of significance (Ott and Longnecker, 2010). From the ANOVA analysis result, p-value maximum for all fuels is 0.00803, and since p-value is less than 5%, the BMEP has a significant



effect on BSFC. Similarly, BTE, p-value maximum is 0.00972. This means that BMEP is having a significant effect on BTE.

A quadratic polynomial regression model has been applied using the characterisation of the relationship between BMEP and BSFC, and also BMEP and BTE. Parameters of the model were estimated using a least square method. The data were analysed using computer program OriginPro that performs these calculations.

The output statistic indicated that  $R^2$  (COD) minimum of the relationship between BMEP and BSFC for all fuels is 0.99078. Similarly, for BMEP and BTE,  $R^2$  minimum is 0.99028. This value indicates that a quadratic regression model can be used.

#### **4.3.2.4 Air Fuel Ratio**

Figure 4.9 shows effect of BMEP on air-fuel ratio (AFR) for constant speed. As this figure shows, air-fuel ratio decreases with increase in BMEP for all fuels. AFR for PDM is higher than three biodiesel blends fuel test. This is due to the oxygen content of both biodiesel blends being higher than PDM fuel (Gad *et al.*, 2017). Compared with PDM, the average decrease in AFR for each blend biodiesel to PDM is 8.1% for BP10, 10.6% for BP20 and 14.1% for BW10.

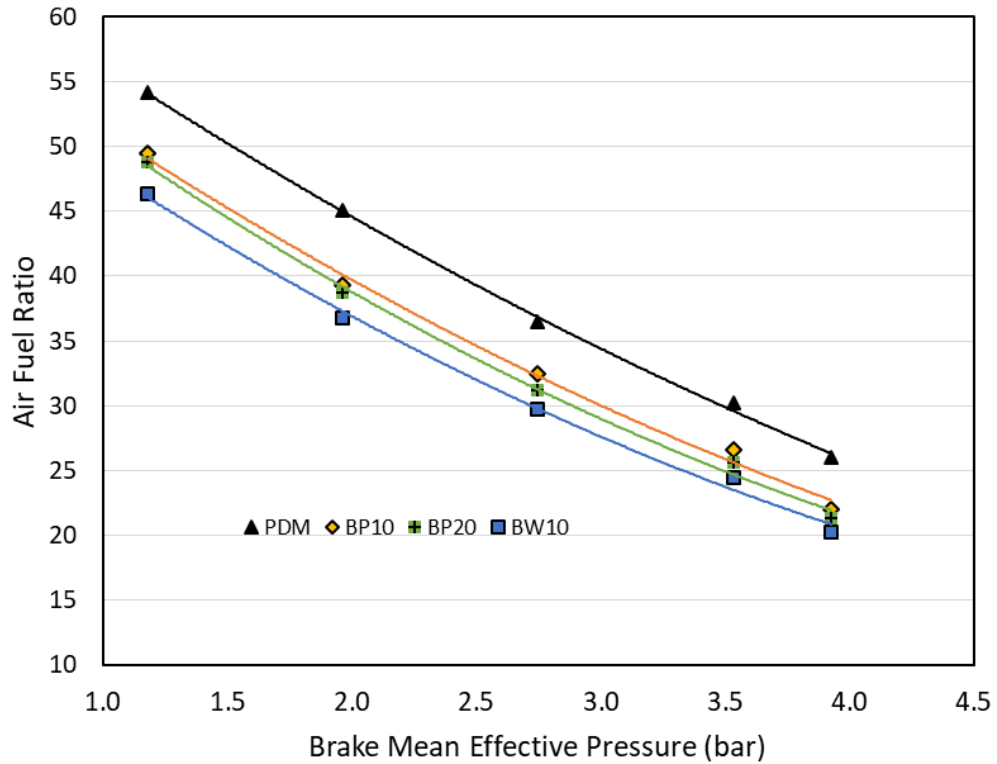


**Figure 4.9** The variation of brake mean effective pressure with air fuel ratio

### 4.3.3 Diesel Engine Exhaust Emissions

The influence of fuel type usage on parameters related to exhaust emission such carbon dioxide ( $\text{CO}_2$ ), carbon monoxide (CO), unburned hydrocarbon (uHC) and nitrogen oxides ( $\text{NO}_x$ ) is described in following sub-subsections. All of the emissions concentrations were expressed in per cent or ppm and in terms of brake specific (g/kWh) basis.

#### 4.3.3.1 Carbon Monoxide Emissions

Figure 4.10 and Figure 4.11 show the CO and BSCO emissions for biodiesel blends decreased compared with PDM for all loads.

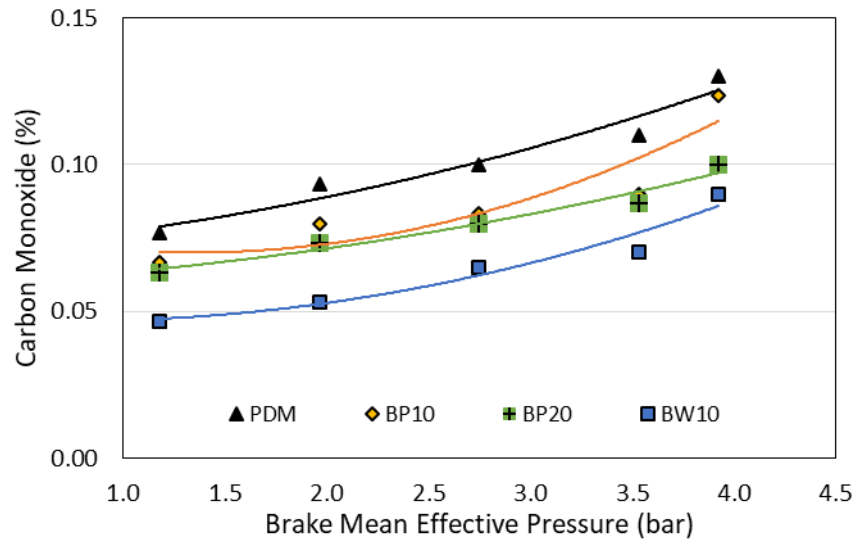


**Figure 4.10** The variation of carbon monoxide with brake mean effective pressure

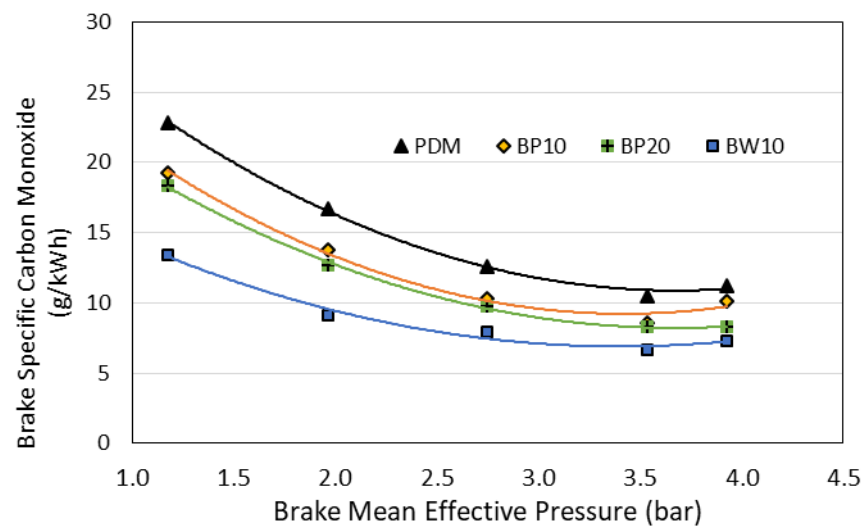


**Figure 4.11** The variation of brake specific carbon monoxide with brake mean effective pressure

It can be seen that the lowest CO and BSCO emissions for all loads are found for BW10 followed by BP20, BP10 and PDM. The CO emissions increase along with increasing load for all fuels due to the decreasing air fuel ratio for higher BMEP. In this condition, the amount of air intake remains constant due to constant engine speed and the amount of fuel continues to increase. Shahid *et al.*(2012) also reported similar results. The lowest CO emissions were found for BW10 fuel on average. This decrease

in emission values may be due to the additional oxygen content in the fuel, which increases the combustion of the fuel perfectly, thereby reducing CO emissions, while the low oxygen content in PDM results in the greatest CO emissions. This agrees with Ilkilic *et al.* (2011). In contrast, the BSCO emissions decrease with increasing load. The decrease of BSCO was caused by significant oxygen in the biodiesel blend (Rao *et al.*, 2008; Said, 2006).

#### 4.3.3.2 Carbon Dioxide Emissions

The carbon dioxide (CO<sub>2</sub>) emission and brake specific carbon dioxide (BSCO<sub>2</sub>) concentration for PDM and biodiesel blends at 2500 rpm and loads were shown in Figure 4.12 and Figure 4.13, respectively. These figures show that the CO<sub>2</sub> and BSCO<sub>2</sub> emission for biodiesel blends are greater than the PDM for all loads. The lowest CO and BSCO<sub>2</sub> occurred in the fuel BW10 caused by the low content of carbon in the fuel.

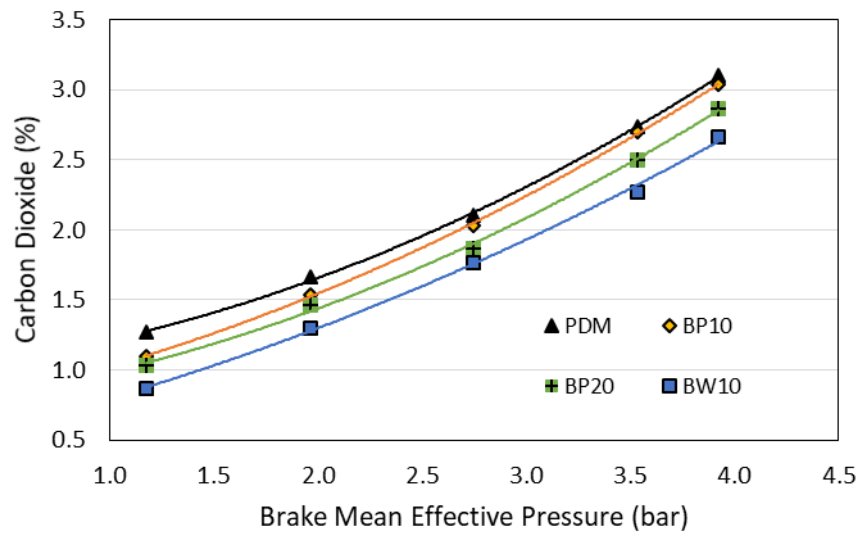


**Figure 4.12** The variation of carbon dioxide with brake mean effective pressure

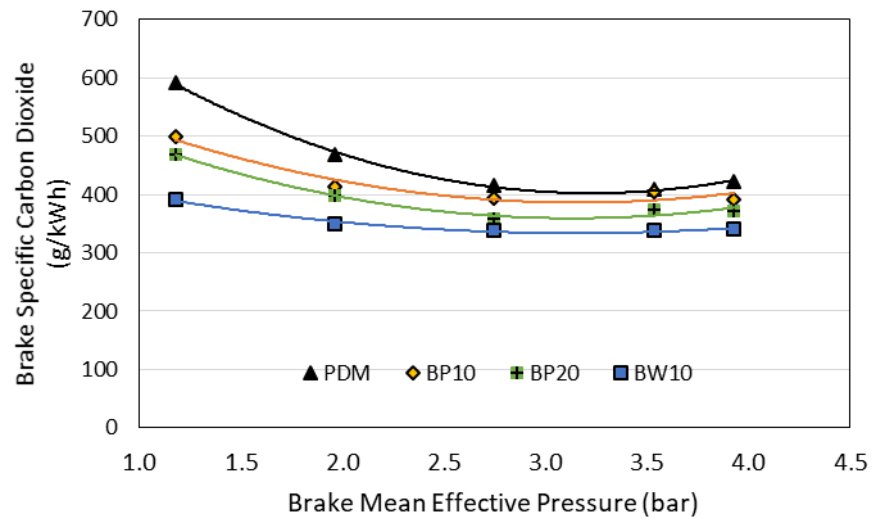


**Figure 4.13** The variation of brake specific carbon dioxide with brake mean effective pressure

#### 4.3.3.3 Unburned Hydrocarbon Emissions

The unburned hydrocarbon (uHC) emission and brake specific hydrocarbon (BSHC) emissions for all tested fuels are shown in Figure 4.14 and Figure 4.15. For all engine loads, all biodiesel blends show higher uHC than PDM, whereas BSHC is lower than that of PDM. Compared to the PDM fuel, the BSHC for the reduction of BW10 is 13.0% to 16.7%. Some studies have found that uHC emissions for biodiesel are higher than diesel. This can be attributed to the oxygen content in the biodiesel molecule, which leads to more complete and cleaner combustion (Ilkılıç *et al.*, 2011), besides relatively poor atomization and lower volatility of biodiesel blends (Banapurmath *et al.*, 2008).

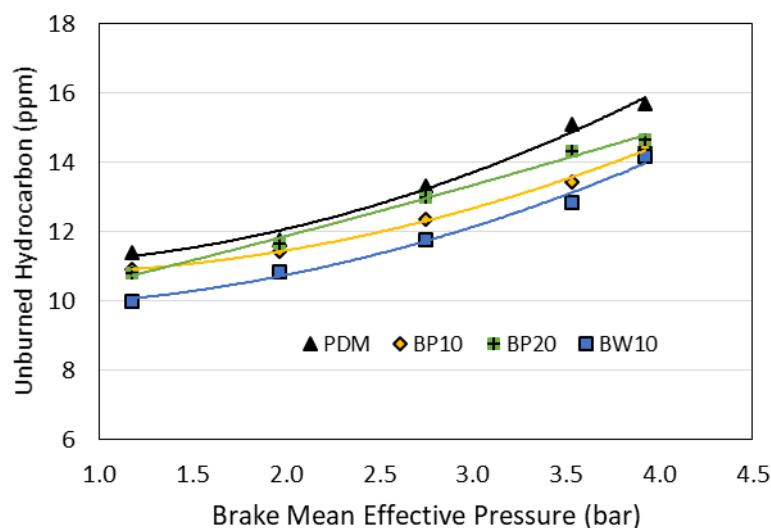


**Figure 4.14** The variation of unburned hydrocarbon with engine brake mean effective pressure

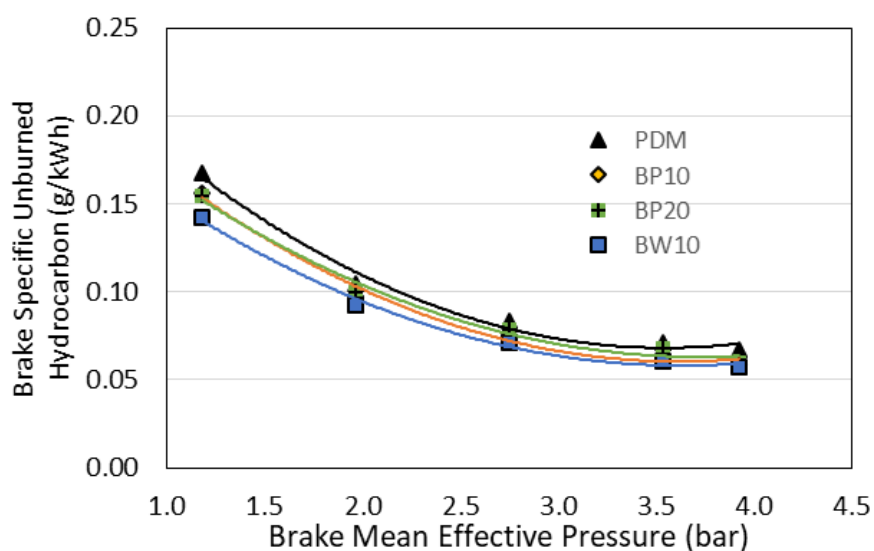


**Figure 4.15** The variation of brake specific unburned hydrocarbon with engine brake mean effective pressure

#### 4.3.3.4 Oxides of Nitrogen Emissions

The variation of  $\text{NO}_x$  and  $\text{BSNO}_x$  with engine BMEP at 2500 rpm engine speed for all tested fuels is shown in Figure 4.16 and Figure 4.17, respectively. Figure 4.16 shows the increase in the emission of nitrogen oxides ( $\text{NO}_x$ ) with increase in

percentage of biodiesel in the PDM fuel. The  $\text{NO}_x$  increase for biodiesel blends may be associated with the oxygen content of the biodiesel blends, since the oxygen present in the fuel may provide additional oxygen for  $\text{NO}_x$  formation. Another factor causing the increase in  $\text{NO}_x$  could be the possibility of higher combustion temperatures arising from combustion (Rao *et al.*, 2008; Shahid *et al.*, 2012), higher proportion of blends viscosity of fuel (Kalam *et al.*, 2011). The  $\text{BSNO}_x$  emissions for biodiesel blends were higher than for the PDM fuel, which is caused by oxygen content in fuel increasing significantly (Said, 2006).

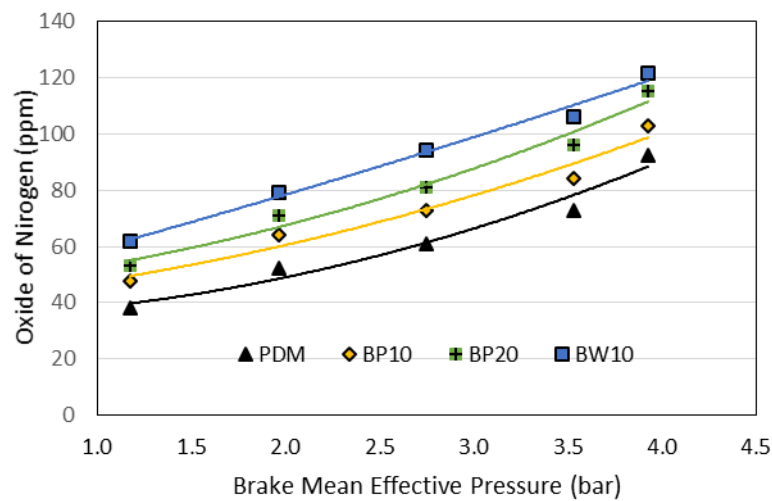


**Figure 4.16** The variation of oxide of nitrogen with engine brake mean effective pressure

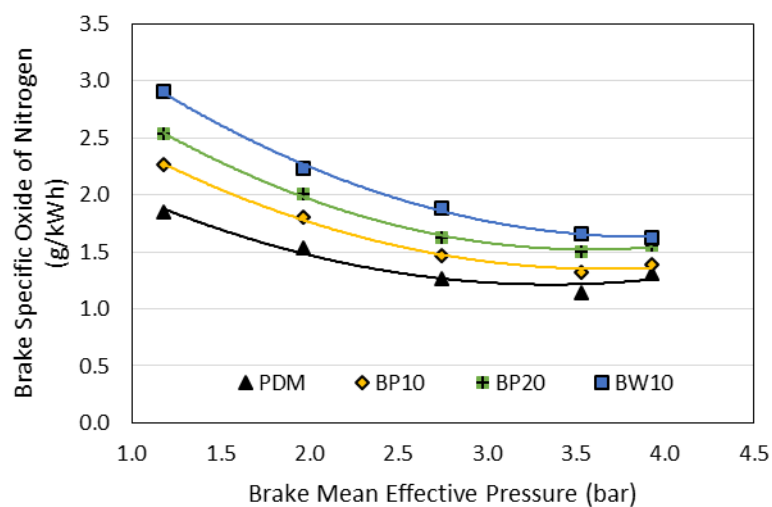


**Figure 4.17** The variation of brake specific oxide of nitrogen with engine brake mean effective pressure

The diesel engine using both biodiesel blends increase the NO<sub>x</sub> emission on average by 55% compared to PDM fuel. The oxygen content of both biodiesel blends are the main reason for higher NO<sub>x</sub> emissions because the oxygen in these biodiesel blends can react easily with nitrogen during the of combustion process, thus causing higher emissions of NO<sub>x</sub> (Abuhabaya *et al.*, 2011).

#### 4.3.4 Combustion Characteristics

##### 4.3.4.1 Pressure in Cylinder and Heat Release Rate

In this section comparison of the combustion characteristics for all fuels were presented and discussed. The profile of cylinder pressure against cranks angle are shown in Figure 4.18 to Figure 4.22 for all loads and all fuels, while the variation of peak cylinder pressures with respect to BMEP at 2500 rpm for all fuel tests are shown in Figure 4.23. This graph indicates that the peak cylinder pressure increases slightly with increasing load. The peak cylinders pressure of biodiesel blends BP10, BP20 and BW10 are lower than PDM for all loads. Compared to PDM, the average pressure drop in the cylinder when using POME blends is 1.59%, while for WCOME blends the average pressure drop in the cylinder is about 3.88%. The contributing factors to this decline is the oxygen content of both biodiesel blends, which results in better combustion, may also result in lower peak pressure compared to PDM (Can *et al.*, 2017; Rao *et al.*, 2008) and it might be attributed to the lower calorific value of biodiesel relative to PDM (Zheng, 2010). In addition, peak cylinder pressure is heavily dependent on the combustion rate at the first stage, which is fuel taking part in the premixed combustion phase (Hwang *et al.*, 2014).

Figure 4.18 depicts the profiles of pressure cylinder against crank angle at low load (BMEP=1.177 bar). For the PDM fuel, the peak pressure of 59.499 bar occurs at 10 °CA. Under the same load, maximum pressure slightly decreased an average of 0.72% for POME blends and 2.28% for WCOME blends. Its crank angle location value were observed slightly earlier for POME blends and BW10 compared to PDM fuel. As for BW20, the crank angle location is 2 °CA slower than PDM.



Figure 4.18 shows that peak pressure occurs at some degree of crank angle after TDC. This corresponds to the start of combustion in the cylinder. Although fuel has been injected into the preceding cylinder, combustion starts several °CA before TDC, and after that gas pressure and temperature increase rapidly due to combustion. Meanwhile, the piston continues to rise which causes the pressure and temperature of the gas to rise faster. The combination of these two effects then create the highest peak in gas pressure at point 10 °CA after TDC.

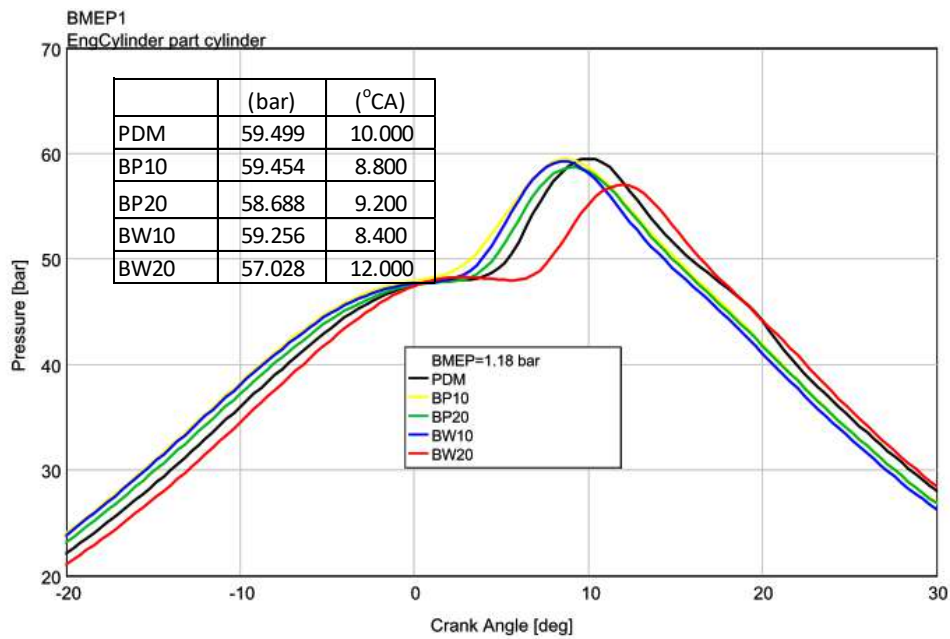
Figure 4.19 depicts the profiles of pressure cylinder against crank angle at load (BMEP=1.96 bar). For the PDM fuel, the peak pressure of 60.425 bar occurs at 9.6 °CA. Under the same load, maximum pressure for BP10 blend is 59.178 bar and BP20 is 58.77 bar. The crank angle location value were observed slightly earlier for POME blends and BW10 compared to PDM fuel.

Figure 4.20 shows the profiles of pressure cylinder against crank angle at BMEP=3.75 bar. At this load, the peak pressure for PDM fuel reaches the highest for all loads of 60.865 bar with 9.2 °CA crank angle. The peak pressure for POME blends decreased by 2.19% and WCOME blends decreased by 1.70% compared to PDM. The peak angle location of all blends are slower 1.2 °CA on average for POME blends and 2.0 °CA compared to PDM.

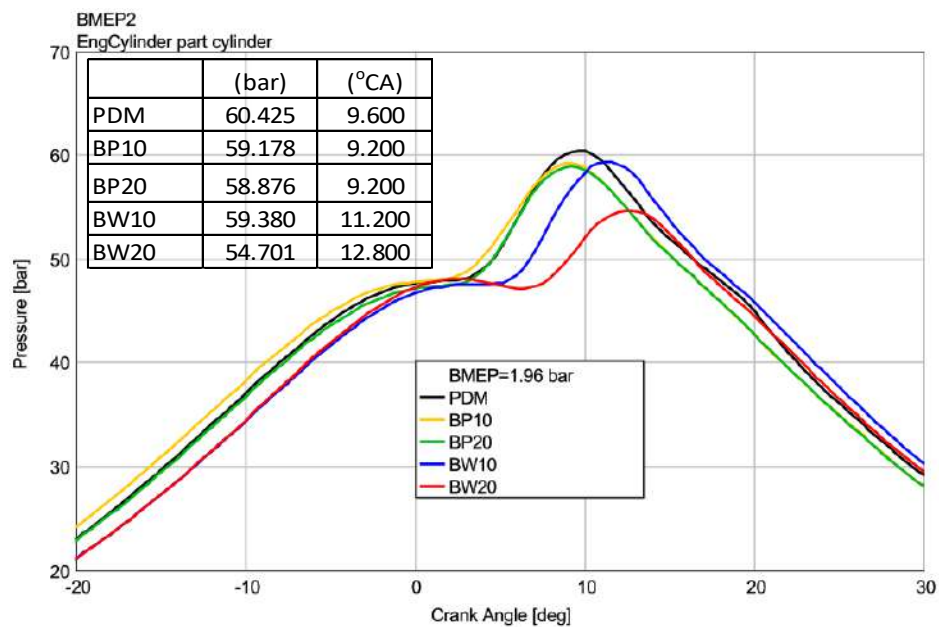
Figure 4.21 shows the profiles of pressure cylinder against crank angle at BMEP=3.533 bar. At this load, the peak pressure for PDM fuel reaches the highest for all loads of 61.07 bar with 7.6 °CA crank angle. The peak pressure for POME blends decreased by 1.67% and WCOME blends decreased by 0.61% compared to PDM. The peak angle location of all blends are slower 0.4 °CA on average for POME blends and 3.6 °CA compared to PDM.

Figure 4.22 depicts the profiles of pressure cylinder against crank angle at high load (BMEP=3.925 bar). For the PDM fuel, the peak pressure of 60.434 bar occurs at 9.6 °CA. Under the same load, maximum pressure decreased an average of 1.04% for POME blends and 0.94% for BW10 compared to PDM. Its crank angle location value

were observed slightly earlier for POME blends compared to PDM fuel. As for BW10, its crank angle location is 10.4 °CA or slower than PDM of 8.3%.



**Figure 4.18** The profiles of pressure cylinder against crank angle for all fuels at brake mean effective pressure 1.18 bar



**Figure 4.19** The profiles of pressure cylinder against crank angle for all fuels at brake mean effective pressure 1.96 bar

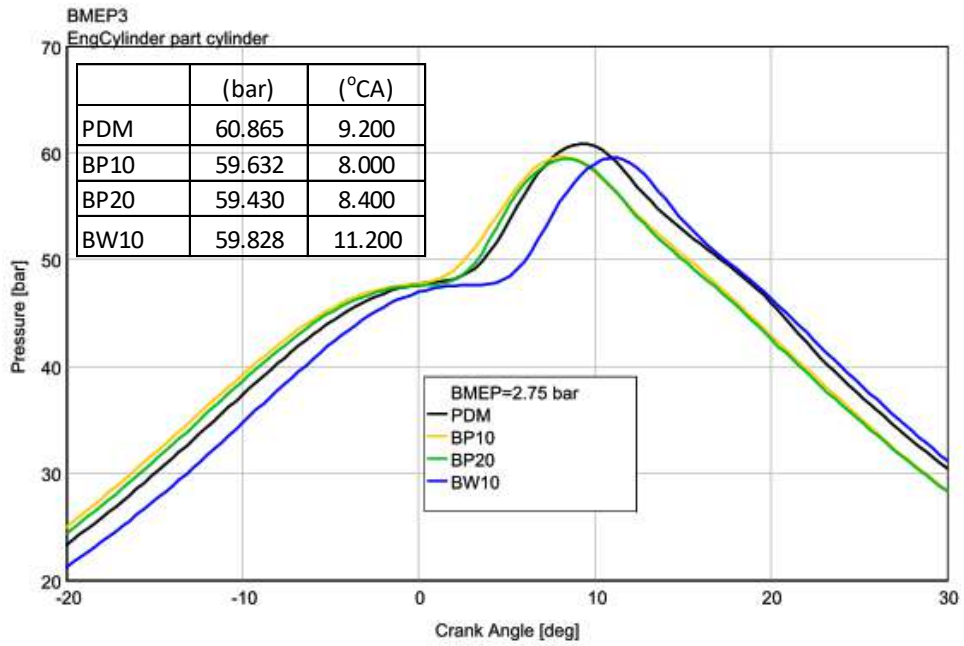


**Figure 4.20** The profiles of pressure cylinder against crank angle for all fuels at brake mean effective pressure 2.75 bar

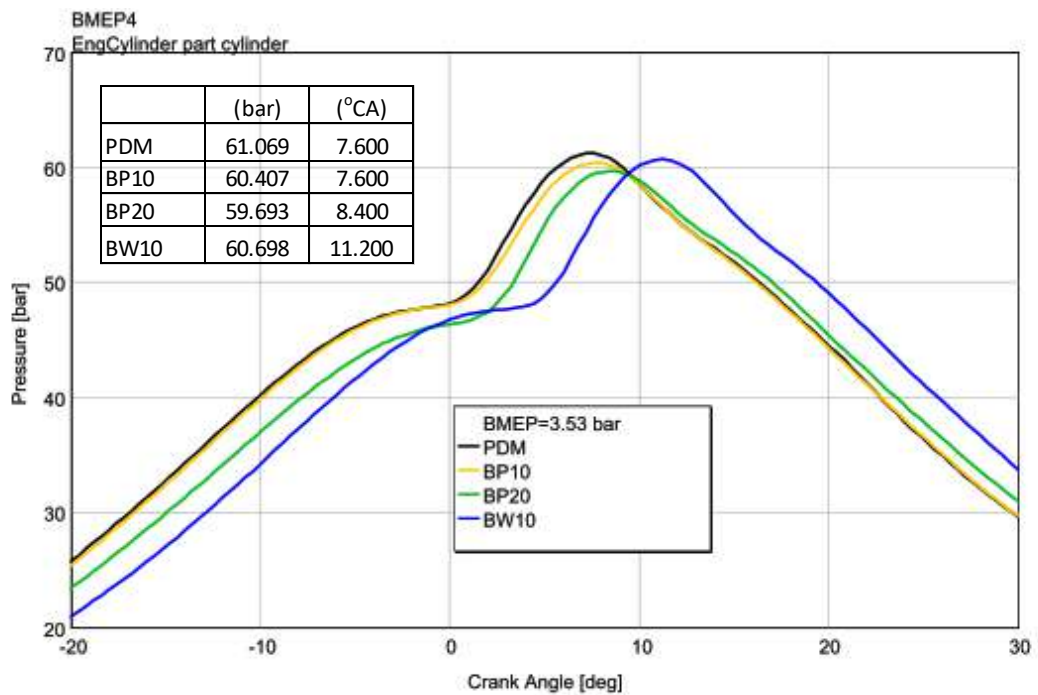


**Figure 4.21** The profiles of pressure cylinder against crank angle for all fuels at brake mean effective pressure 3.53 bar

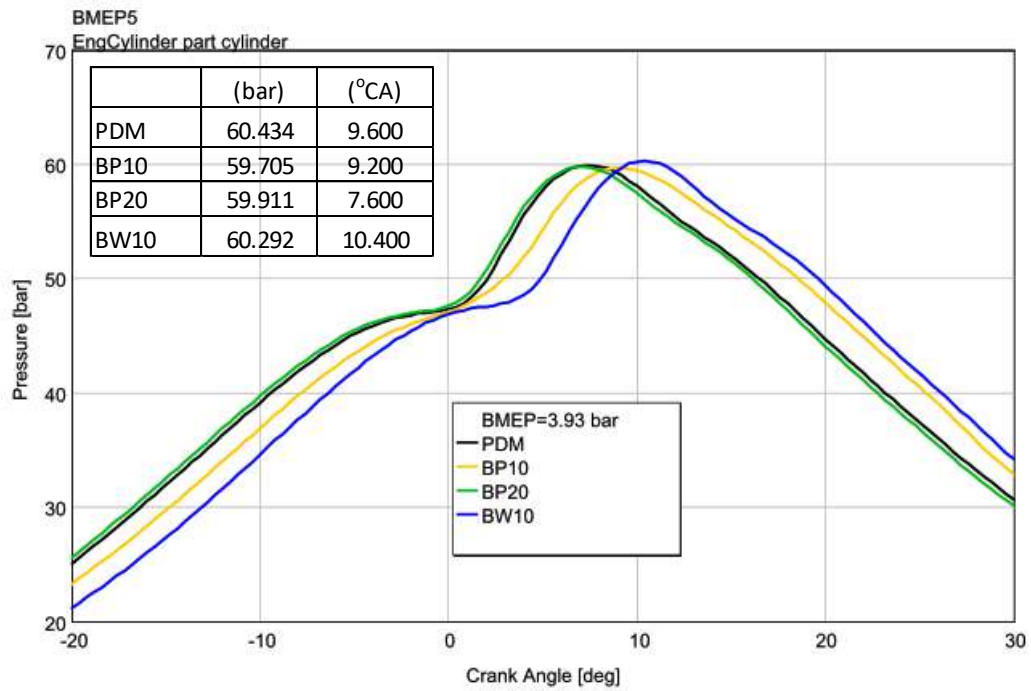


**Figure 4.22** The profiles of pressure cylinder against crank angle for all fuels at brake mean effective pressure 3.93 bar

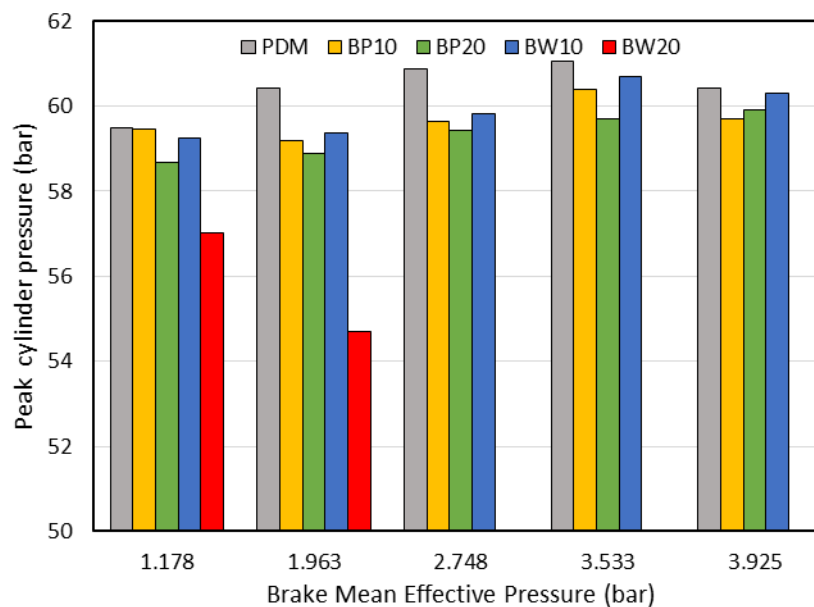


**Figure 4.23** The comparison Petron Diesel Max and biodiesel blends on peak cylinder pressure

The profiles of heat release rate against the crank angle are shown in the Figure 4.24 to Figure 4.28 while Figure 4.29 shows the peak heat release rate for all loads and

all fuels. The heat release rate (HRR) was calculated based on the in-cylinder pressure data using Eq. (3.24) in sub-sub section 3.3.4.3.

Figure 4.24 depicts the profiles of heat release rate against crank angle at low load (BMEP=1.18 bar). For the PDM fuel, the peak heat release rate of 25.43 J/°CA occurs at 6.01 °CA. Under the same load, the peak heat release rate slightly decreased an average of 16.2% for POME blends and 4.71% for WCOME blends. Its crank angle location value were observed slightly slower for POME blends of 6.2 °CA (on average) and for WCOME blends of 7.2 °CA (on average) compared to PDM fuel.

The profiles of heat release rate against crank angle at low BMEP=1.96 bar is shown in Figure 4.25. For the PDM fuel, the peak heat release rate of 24.03 J/°CA occurs at 5.60 °CA. Under the same load, the peak heat release rate decreased an average of 9.73% for POME blends, while for WCOME increased 6.20% compared to peak heat release rate of PDM. Its crank angle location value were observed slightly slower for POME blends of 6.0 °CA (on average) and for WCOME blends of 8.8 °CA (on average) compared to PDM fuel.

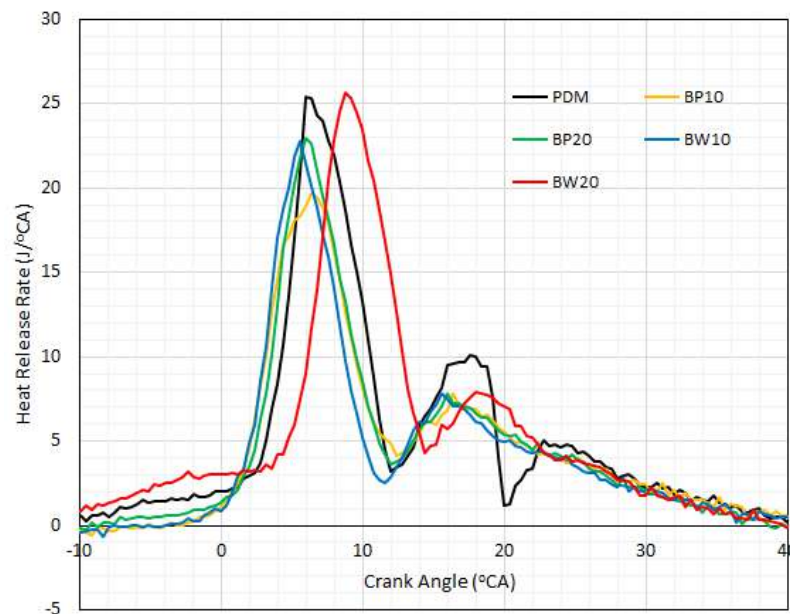
The profiles of heat release rate against crank angle at BMEP=2.74 bar is shown in Figure 4.26. For the PDM fuel, the peak heat release rate of 22.09 J/°CA occurs at 5.20 °CA. In this load, the peak heat release rate decreased 11.0 % for POME blends, while for BW10 increased about 17.82 % compared to peak heat release rate of PDM. The crank angle location value was observed slightly earlier for POME blends of 5.2 °CA (on average), but slower for WCOME blends of 8.0 °CA (on average) as compared to PDM fuel.

Figure 4.27 depicts the profiles of heat release rate against crank angle at BMEP=3.53 bar. For the PDM fuel, the peak heat release rate of 18.81 J/°CA occurs at 3.60 °CA. Under the same load, the peak heat release rate for BP10 slightly decreased only 1.59 %, while BP20 increased 13.14 % and BW10 increased 35.52 % compared to PDM. The crank angle location value were observed slightly slower for POME blends of 3.80 °CA (on average) and for WCOME blends of 7.2 °CA (on average) compared to PDM fuel.

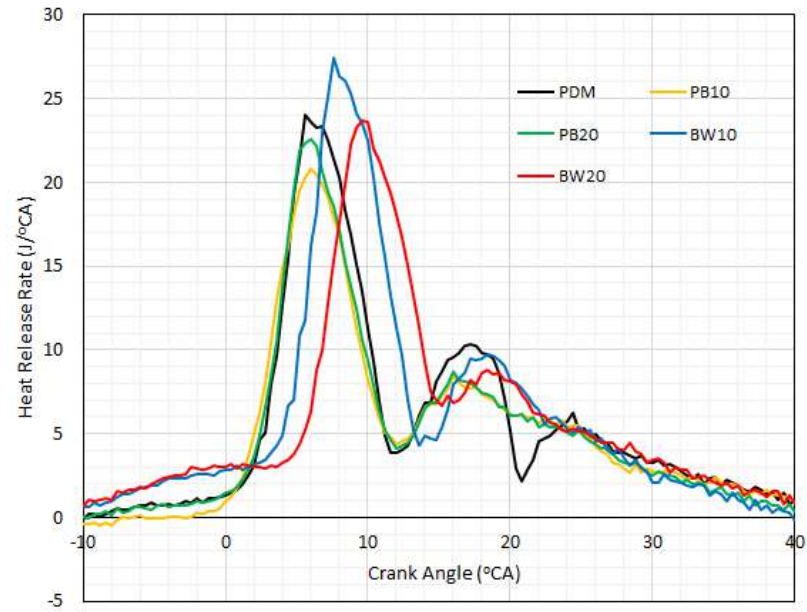
The profiles of heat release rate against crank angle at high load (BMEP=3.923 bar) is shown in Figure 4.28. For the PDM fuel, the peak heat release rate of 20.81 J/°CA occurs at 5.20 °CA. In this load, the peak heat release rate decreased 9.46 % for POME blends, while for BW10 increased about 10.73 % compared to peak heat release rate of PDM. The crank angle location value was observed slightly earlier for BP20 of 2.8 °CA, but slower for BW10 of 6.0 °CA as compared to PDM fuel.

Figure 4.29 shows that peak heat rate release for PDM tends to decrease with increase in loads up to BMEP 3.53 bar and then up again at next load, as well as BP10. The peak heat rate release for BW10 increased up to BMEP 1.96, then decreased. The same tendency is obtained by Can *et al.* (2017).

At the BMEP load of 3.53 bar and 3.93 bar, fluctuation occurs due to the process of a closed loop between the flow, fire and pressure plane of the combustion chamber. The fluctuations of heat dissipation produce acoustic waves that propagate to the wall of the combustion chamber and reflect into the fire zone (Okon *et al.*, 2016).



**Figure 4.24** The profiles of heat release rate against crank angle at brake mean effective pressure at 1.18 bar



**Figure 4.25** The profiles of heat release rate against crank angle at brake mean effective pressure at 1.96 bar

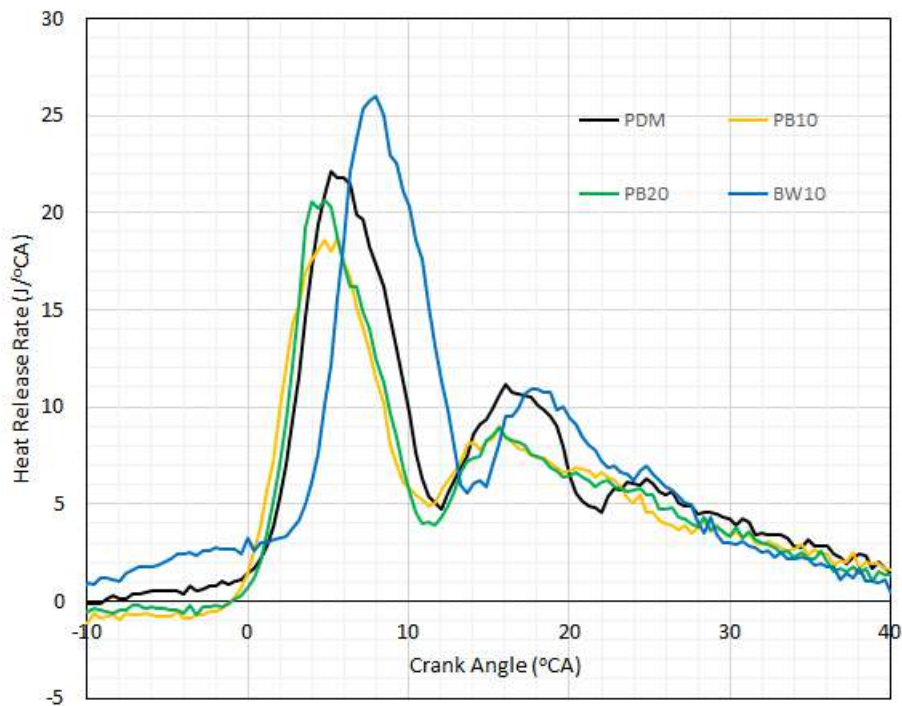


**Figure 4.26** The profiles of heat release rate against crank angle at brake mean effective pressure at 2.75 bar

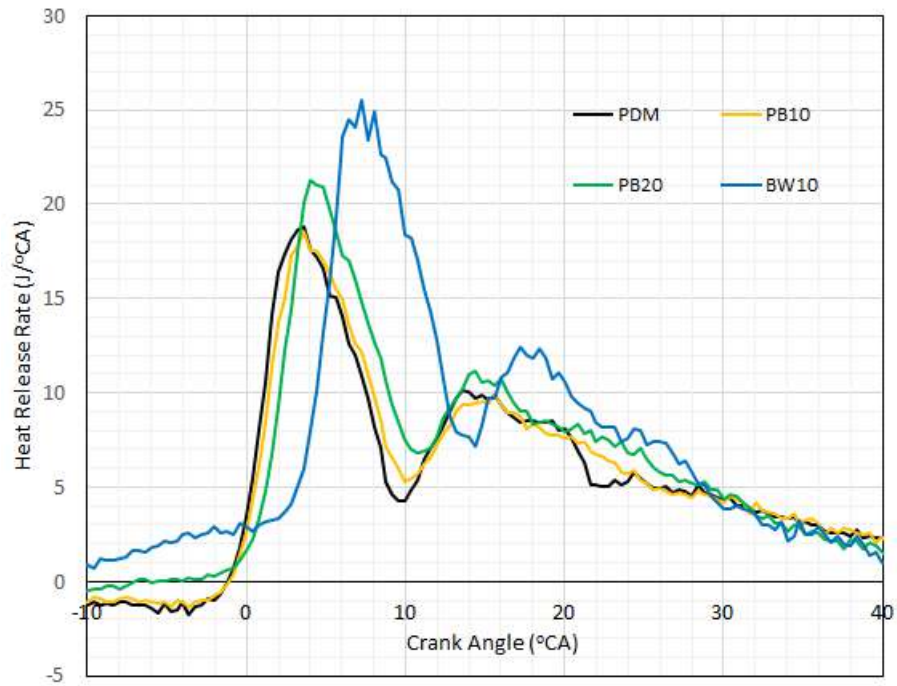


**Figure 4.27** The profiles of heat release rate against crank angle at brake mean effective pressure at 3.53 bar

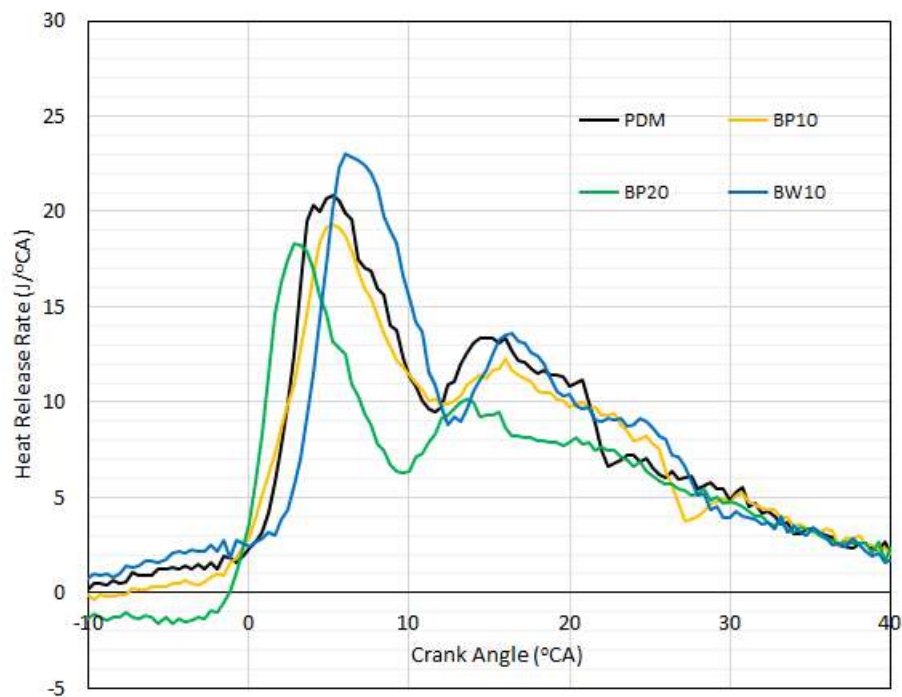


**Figure 4.28** The profiles of heat release rate against crank angle at brake mean effective pressure at 3.93 bar



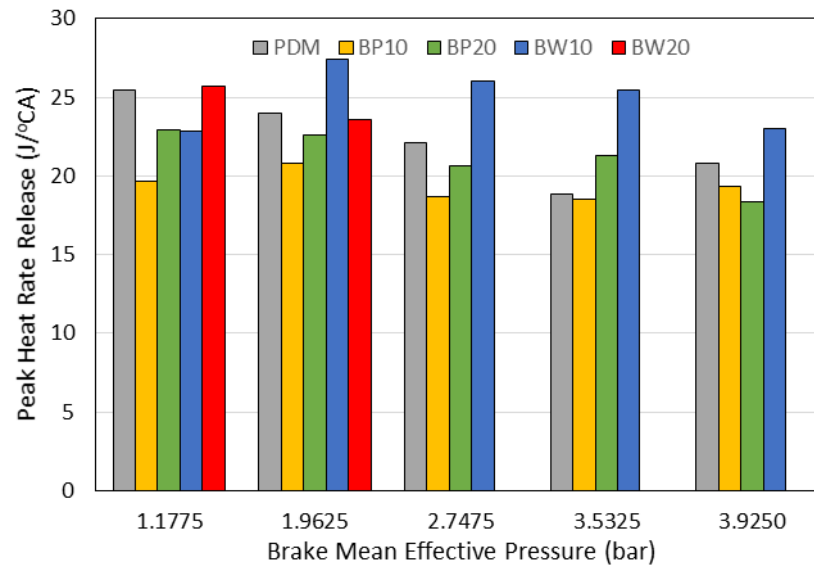


**Figure 4.29** The peak heat release rate against brake mean effective pressure at various fuels

#### 4.3.4.2 Burned Fuel Fraction and Combustion Duration

The relationship between BMEP and the burning fuel fraction obtained from the acquisition of Dewetron data are presented in the graph shown in Figure 4.30 to Figure 4.34, while the duration of combustion is shown in Figure 4.35. Figure 4.30 to Figure 4.34 were fitted with the Wiebe function. These figures show that generally the crank angle location of burned fuel fraction of WCOME blends are earlier than POME blends, while the POME blends are earlier than the PDM fuel (Ozsezen *et al.*, 2009).

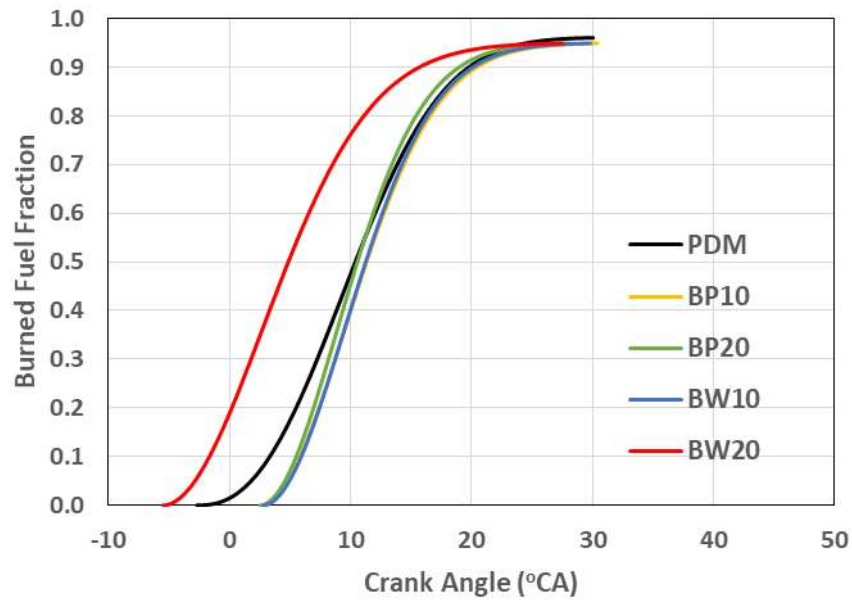


**Figure 4.30** The profile of burned fuel fraction at brake mean effective pressure 1.18 bar

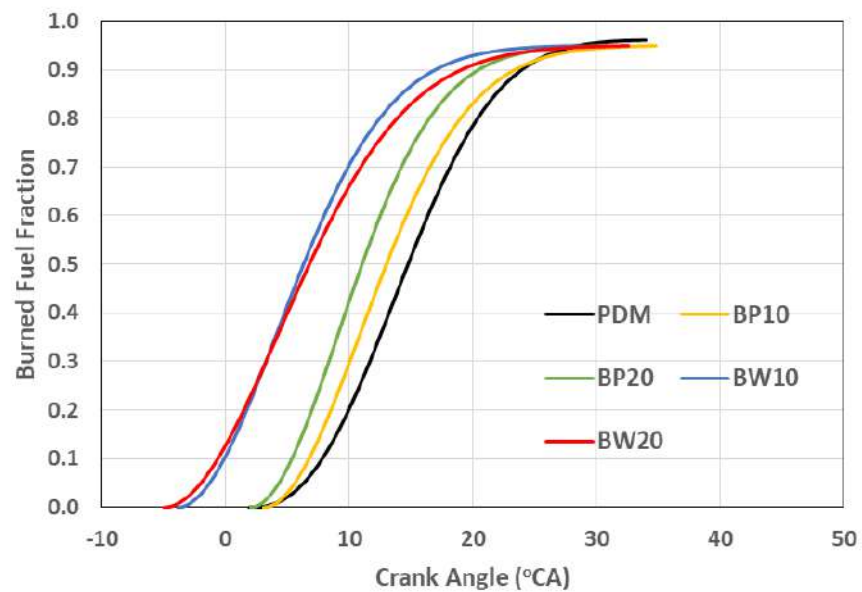


**Figure 4.31** The profile of burned fuel fraction at brake mean effective pressure 1.96 bar

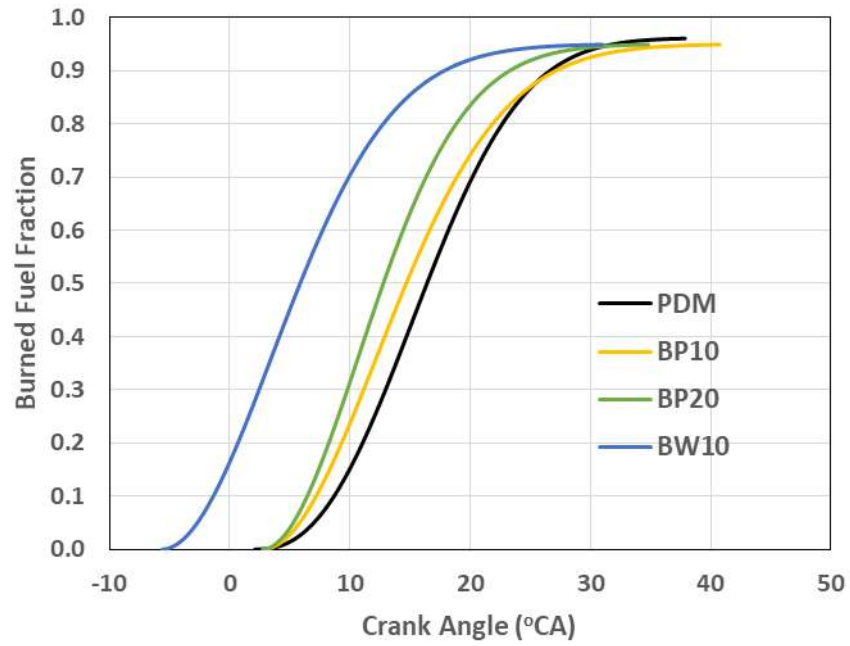


**Figure 4.32** The profile of burned fuel fraction at brake mean effective pressure 2.75 bar

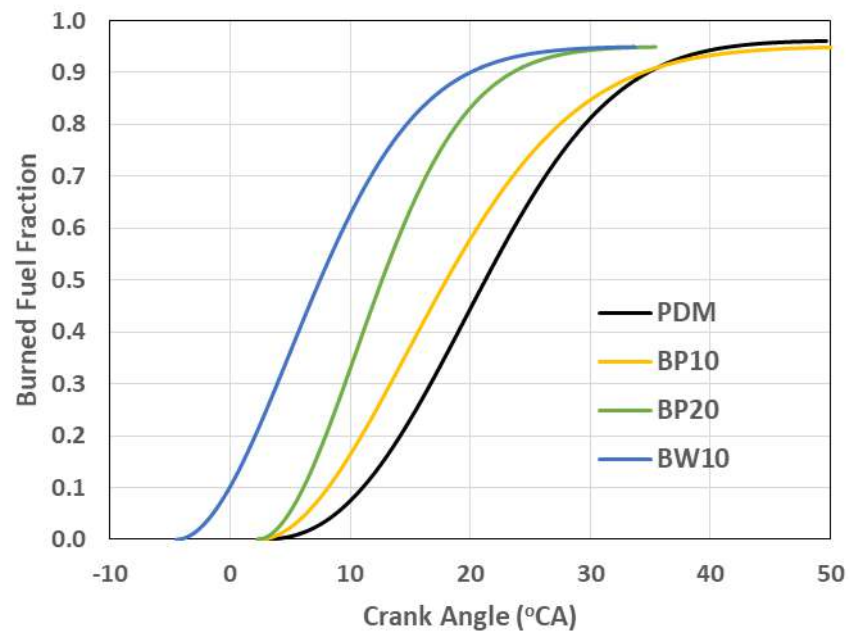


**Figure 4.33** The profile of burned fuel fraction at brake mean effective pressure 3.53 bar

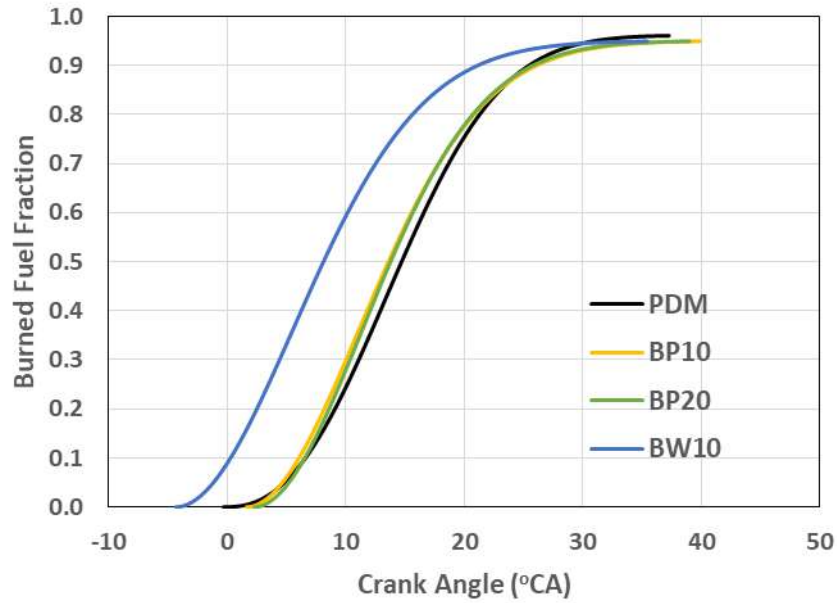


**Figure 4.34** The profile of burned fuel fraction at brake mean effective pressure 3.93 bar

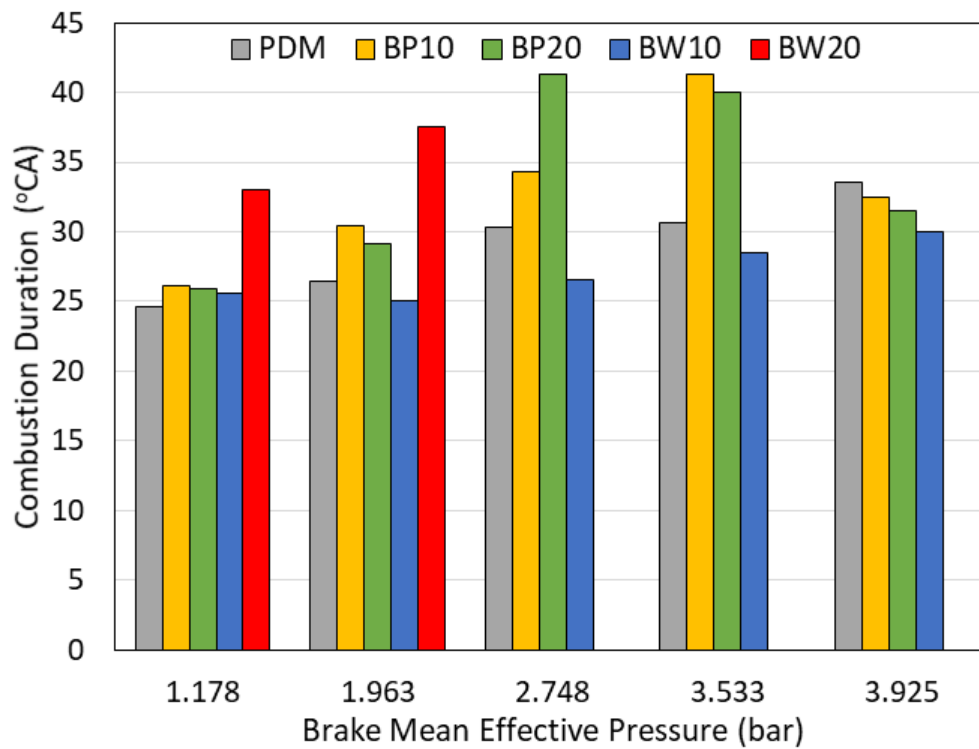


**Figure 4.35** The comparison PDM and biodiesel blends on combustion duration

The combustion duration increases with the increase of BMEP for all PDM and WCOME blends, but not for POME at high BMEP. Higher combustion duration is observed with POME and WCOME blends than PDM due to the longer diffusion combustion phase. This is similar to the results obtained by Banapurmath *et al.* (2008).

Combustion duration for PDM increases with increasing load, while biodiesel blends only increase at BMEP 3.53 bar, then decrease at 3.93 bar BMEP. Generally, the combustion duration of PDM is lower than that of POME blends except at 3.925 bar BMEP. Compared to WCOME, generally the combustion duration of PDM is higher except for BMEP 1.178 and 1.963 bar.

#### 4.3.5 Comparison with Simulation

Figure 4.36 to Figure 4.39 show the comparison between simulation and experiment of BSFC and Brake Thermal Efficiency versus BMEP. Compared to the experimental results, both of the simulations were quite close for all fuel tests. BSFC of experiment was 3.1% higher than BSFC simulation, while BTE of experiment was 2.8% lower than BTE simulation. All the simulation graphs indicate the similar pattern with the experiment.

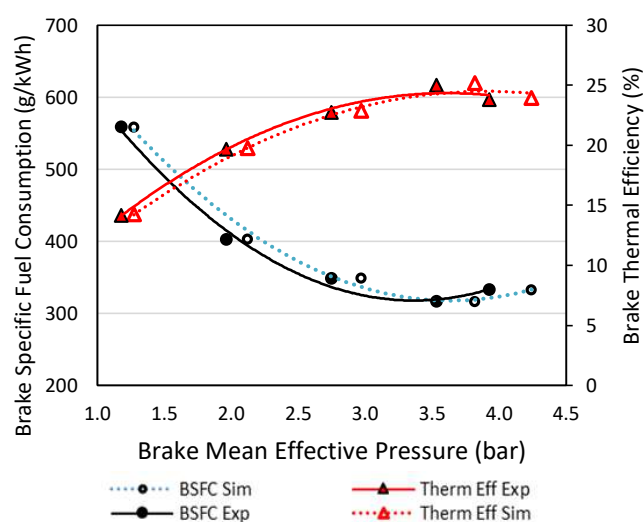


**Figure 4.36** Experiment and simulated data of brake specific fuel consumption and brake thermal efficiency versus brake mean effective pressure for PDM fuel

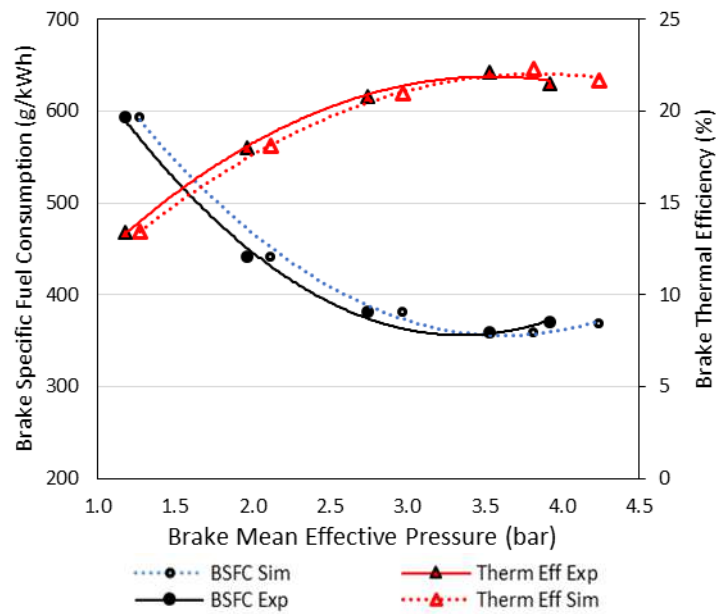


**Figure 4.37** Experiment and simulated data of brake specific fuel consumption and brake thermal efficiency versus brake mean effective pressure for BP10 fuel

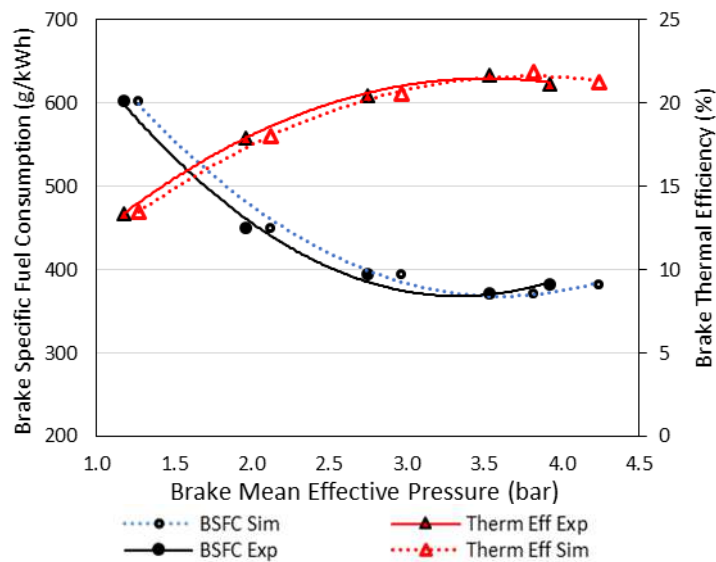


**Figure 4.38** Experiment and simulated data of brake specific fuel consumption and brake thermal efficiency versus brake mean effective pressure for BP20 fuel

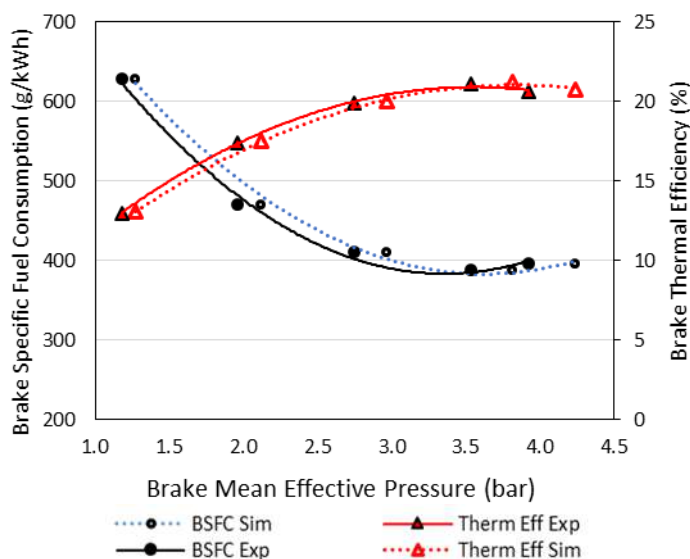


**Figure 4.39** Experiment and simulated data of brake specific fuel consumption and brake thermal efficiency versus brake mean effective pressure for BW10 fuel

In the validation process, the results of the simulations were compared with the experiment data. Simulation performed with the SOC data were varied, while the SOI remained constant. The results of simulation profile of heat release rate (HHR) were matched with experiment profile to find the SOC value.

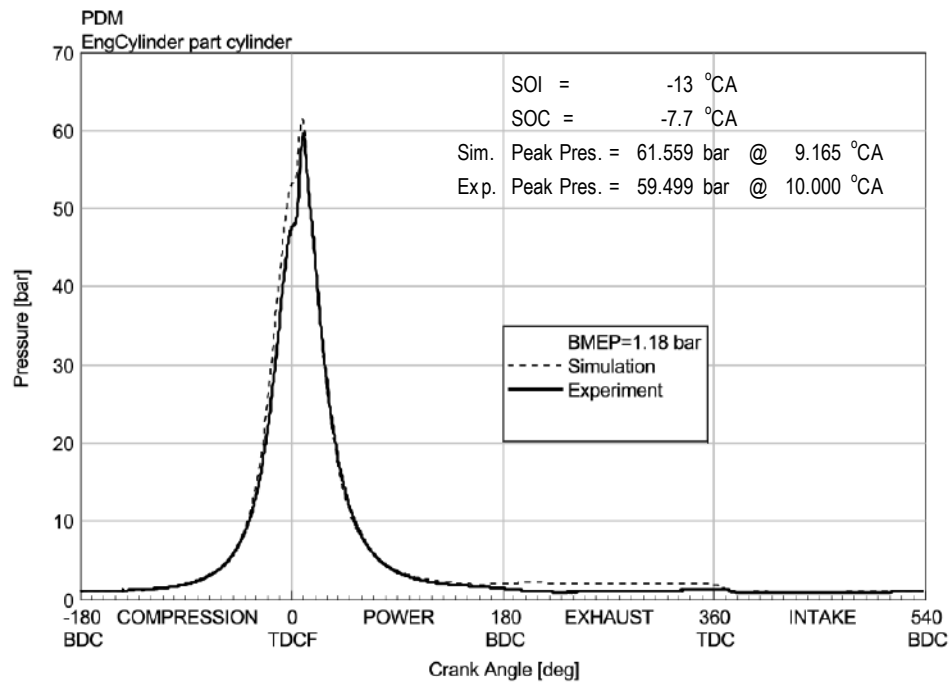
Figure 4.40 to Figure 4.61 illustrate the comparison of pressure in cylinder for all fuels at 2500 rpm for all loads. These figures show that peak pressure occurs at some degree of crank angle after TDC. This effect can be attributed to the start of combustion in the cylinder. If fuel is injected into the cylinder earlier, combustion begins during the compression step, and afterwards gas pressure and temperature increase rapidly due to combustion. Meanwhile, the piston continues to rise which causes the pressure and temperature of the gas to rise faster. These two effects merge together and then create a high peak in gas pressure. Tracing the pressure in the cylinder will show two peaks rather than one. The first peak is mostly caused by compression of the stroke and the second peak is due to the addition of heat (combustion) (Zheng, 2010).

Figure 4.40 compares pressure simulation and experiment at 2500 rpm and BMEP of 1.18 bar. It shows that the pressure diagram matches except for an over-predicted first peak. Simulation result of peak cylinder pressure is higher by around 3.4 % than experiment. This discrepancy might come from an approximated injection pressure which is taken as input for the simulation (Zheng, 2010).

The simulation results of maximum pressure on the cylinder indicate the peak cylinder pressure of the simulation results are all greater than the experimental results. The magnitude of the difference increases with increasing load. At low load (BMEP = 1.18 bar), the average difference obtained is about 8.35%, while at high load (BMEP = 3.93 bar) a difference of 22.36% is obtained. For the average PDM fuel the difference is 10.01%, BP10 is 16.1%, BP20 is 18.6%, BW10 is 16.9% and BW20 is 12.8%.

Many engine operating factors could affect the profiles of pressure in cylinder against crank angle prediction, such as compression ratio, injection timing, and injection profile. Also many calibration factors affect the pressure diagram significantly, such as combustion rate multiplier, breakup length multiplier, and wall temperature (Zheng, 2010). But in general, the difference between simulation and experiment results are still in an acceptable range, considering the existence of the uncertainty of the experiments.





**Figure 4.40** Profiles of pressure in cylinder against crank angle using Petron Diesel Max fuel at BMEP=1.18 bar

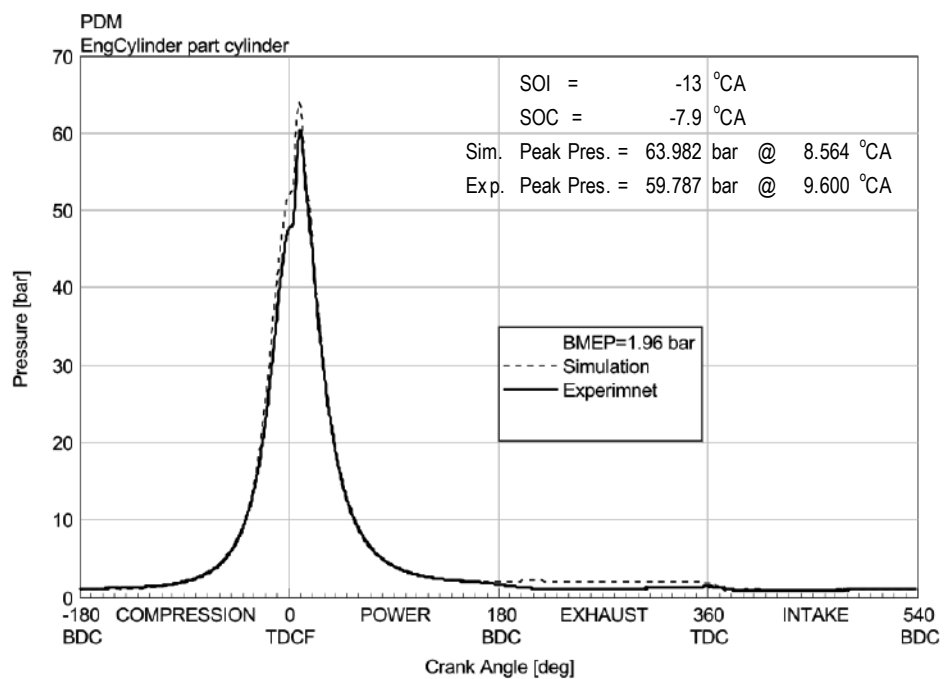


**Figure 4.41** Profiles of pressure in cylinder against crank angle at various brake mean effective pressure using Petron Diesel Max fuel at BMEP=1.96 bar

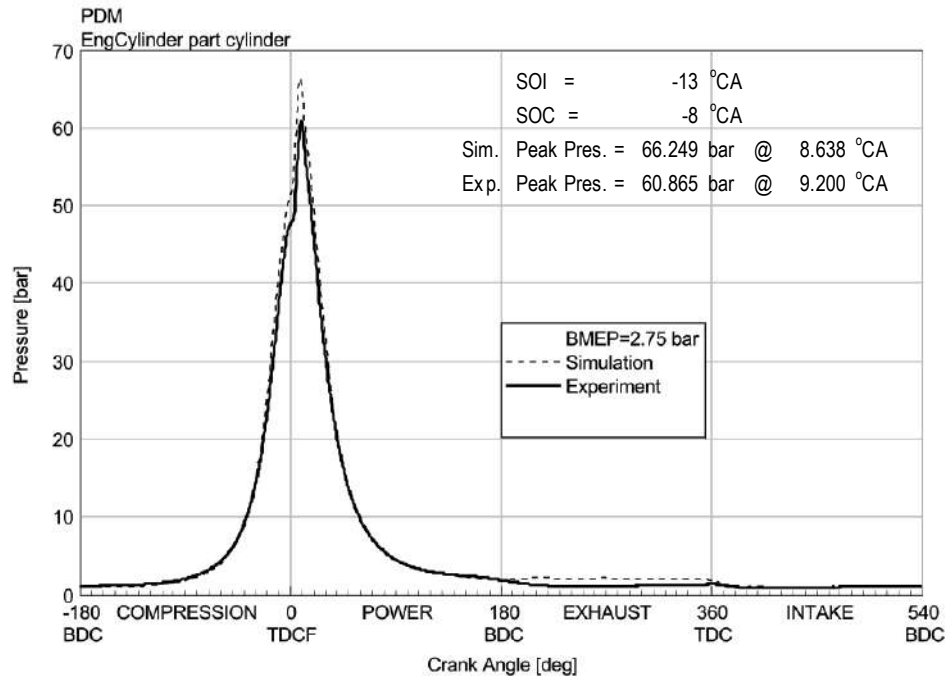


**Figure 4.42** Profiles of pressure in cylinder against crank angle at various brake mean effective pressure using Petron Diesel Max fuel at BMEP= 2.75 bar

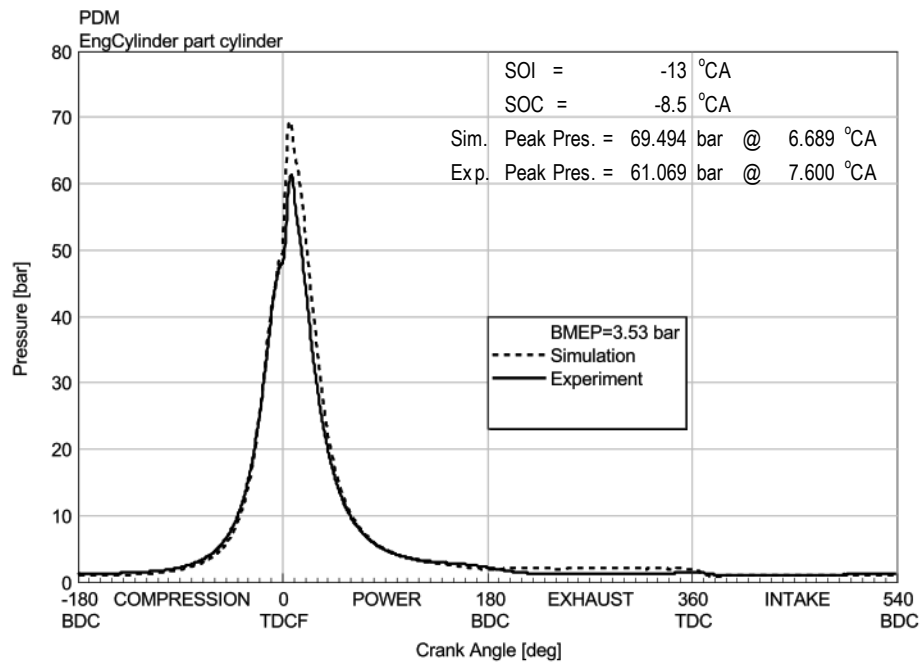


**Figure 4.43** Profiles of pressure in cylinder against crank angle at various brake mean effective pressure using Petron Diesel Max fuel at BMEP= 3.53 bar

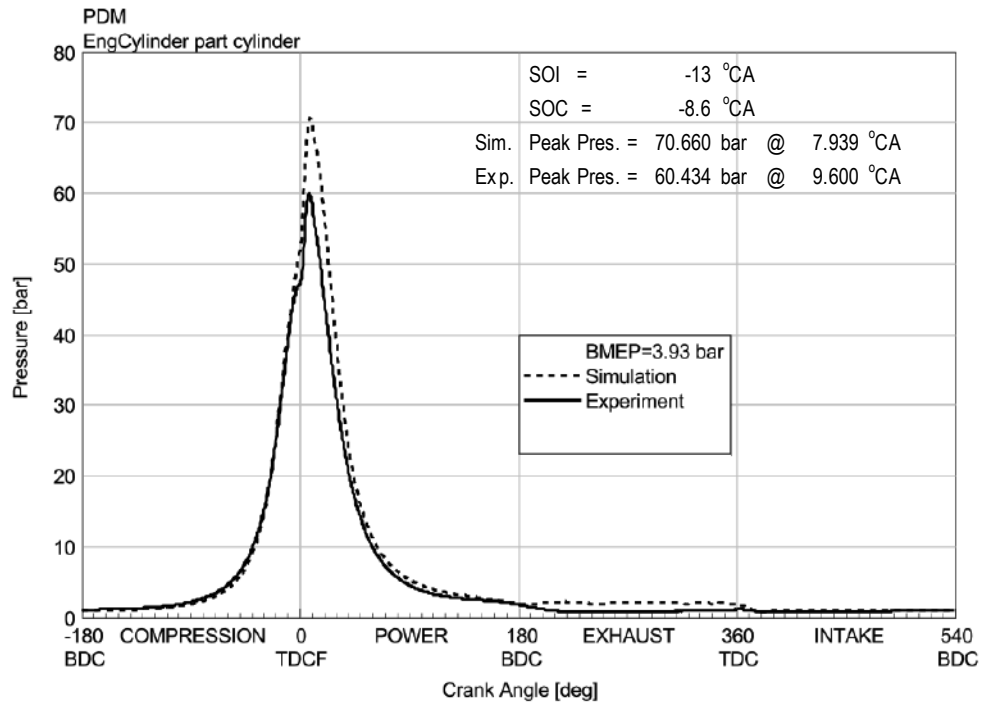


**Figure 4.44** Profiles of pressure in cylinder against crank angle at various brake mean effective pressure using Petron Diesel Max fuel at BMEP=3.93 bar

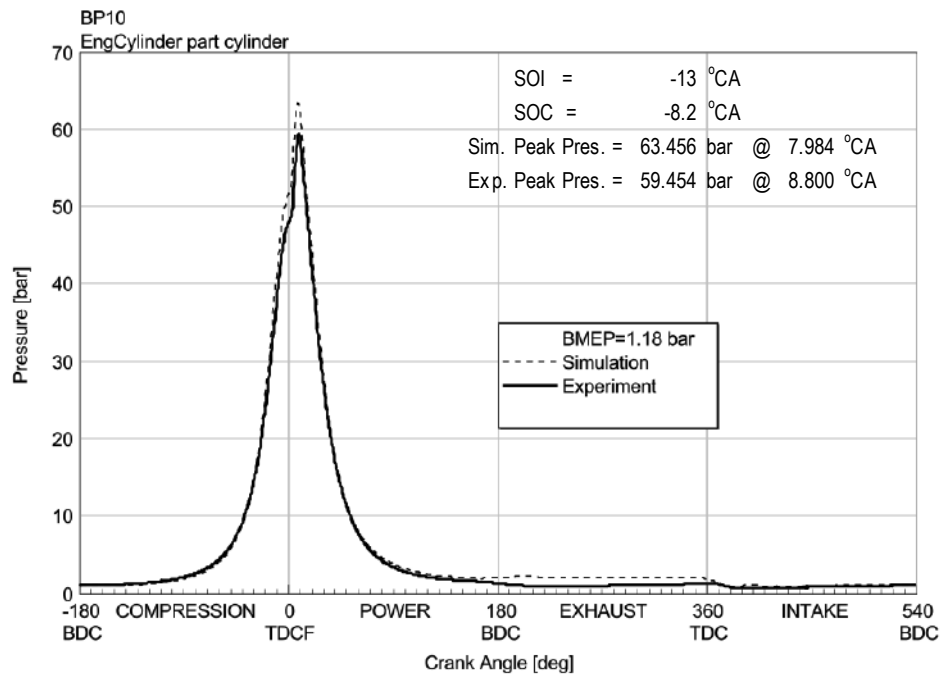


**Figure 4.45** Profiles of pressure in cylinder against crank angle at 1.18 bar brake mean effective pressure using BP10 fuel

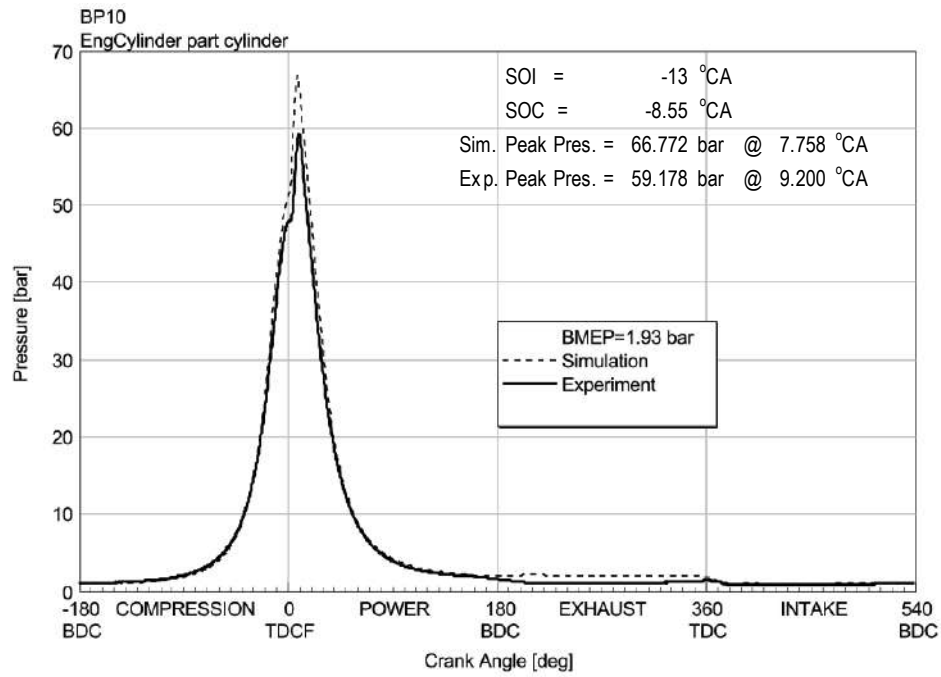


**Figure 4.46** Profiles of pressure in cylinder against crank angle at 1.96 bar brake mean effective pressure using BP10 fuel

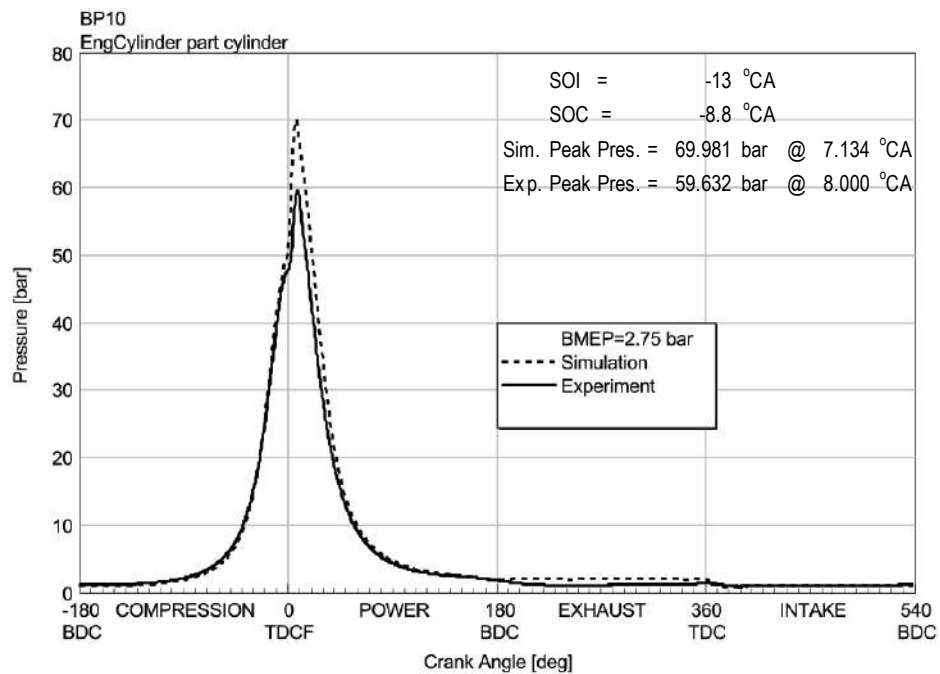


**Figure 4.47** Profiles of pressure in cylinder against crank angle at 2.75 bar brake mean effective pressure using BP10 fuel

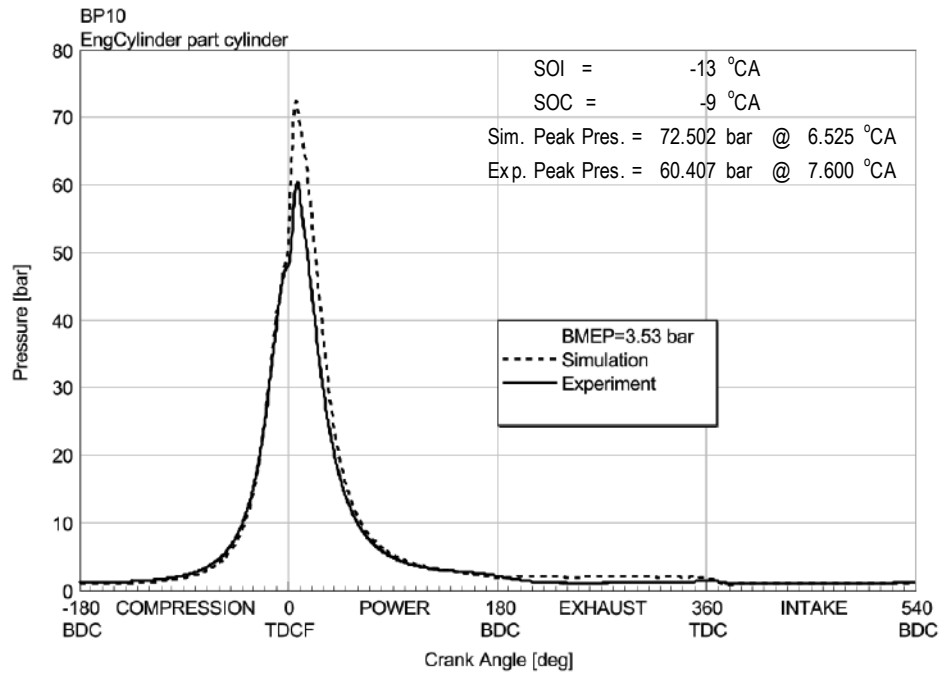


**Figure 4.48** Profiles of pressure in cylinder against crank angle at 3.53 bar brake mean effective pressure using BP10 fuel

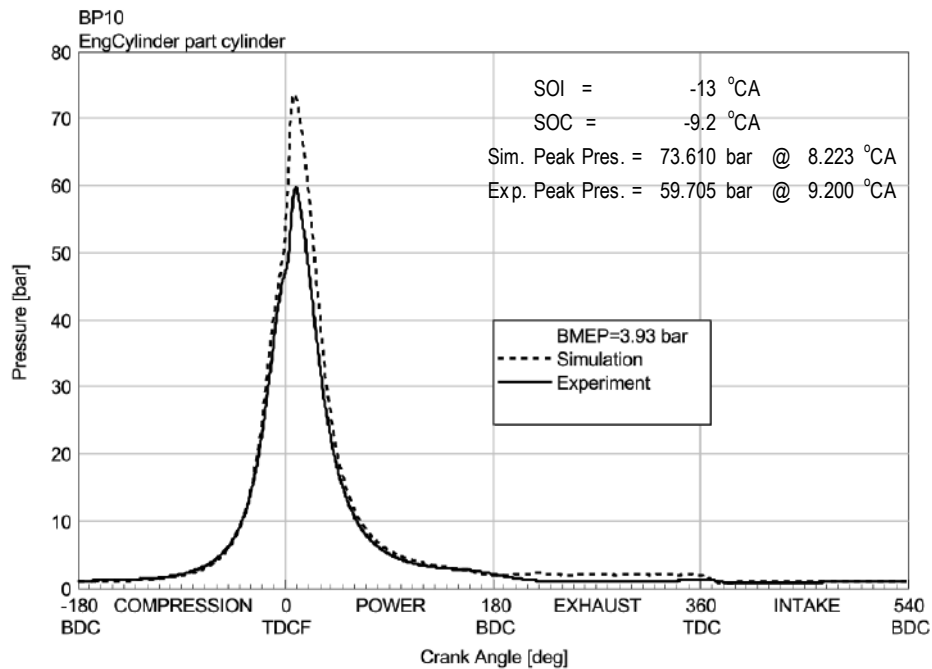


**Figure 4.49** Profiles of pressure in cylinder against crank angle at 3.93 bar brake mean effective pressure using BP10 fuel

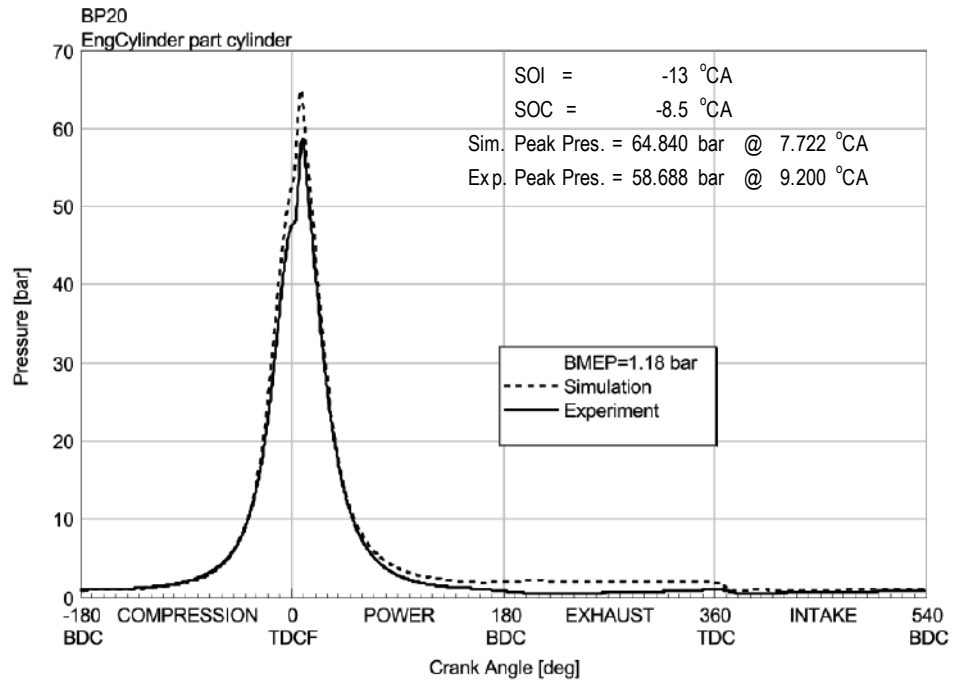


**Figure 4.50** Profiles of pressure in cylinder against crank angle at 1.18 bar brake mean effective pressure using BP20 fuel

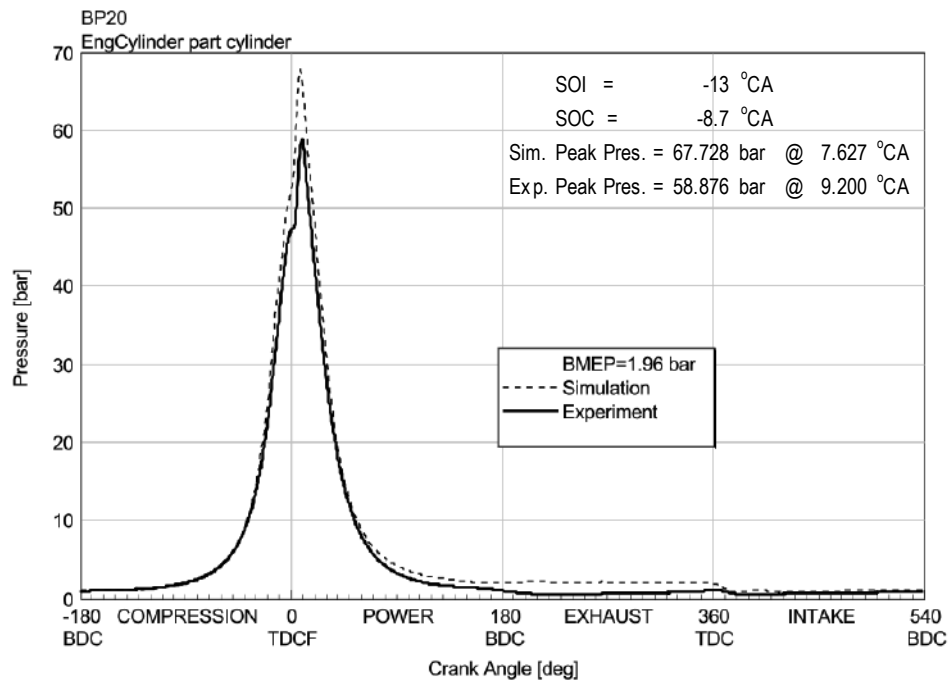


**Figure 4.51** Profiles of pressure in cylinder against crank angle at 1.96 bar brake mean effective pressure using BP20 fuel

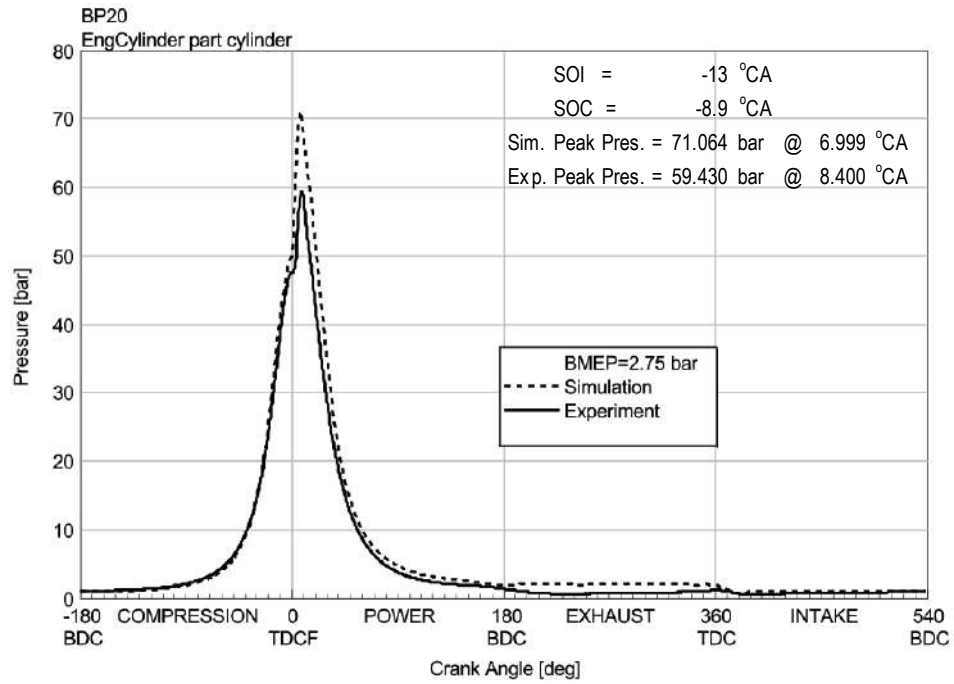


**Figure 4.52** Profiles of pressure in cylinder against crank angle at 2.75 bar brake mean effective pressure using BP20 fuel

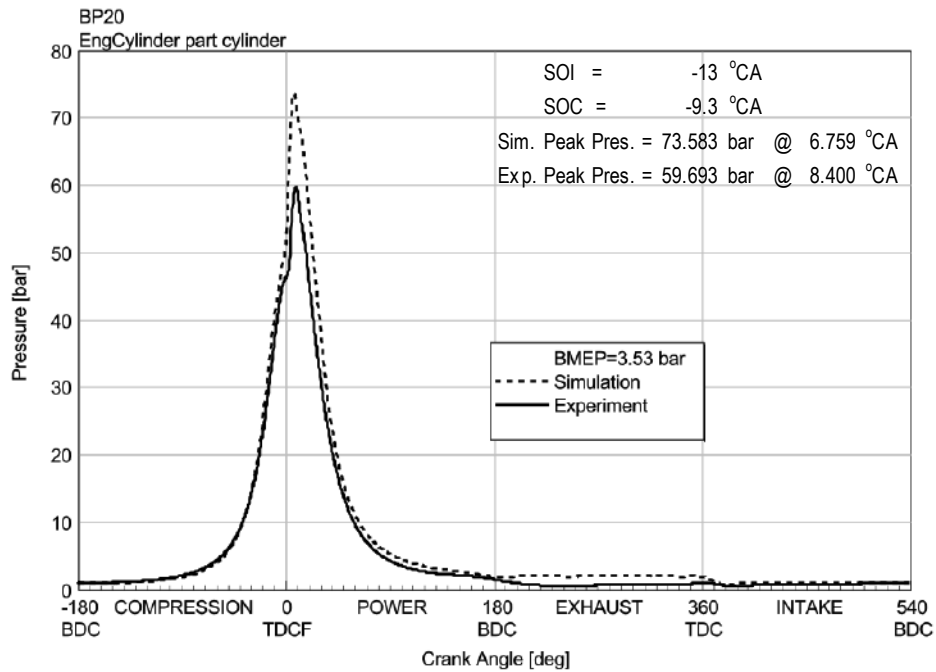


**Figure 4.53** Profiles of pressure in cylinder against crank angle at 3.53 bar brake mean effective pressure using BP20 fuel

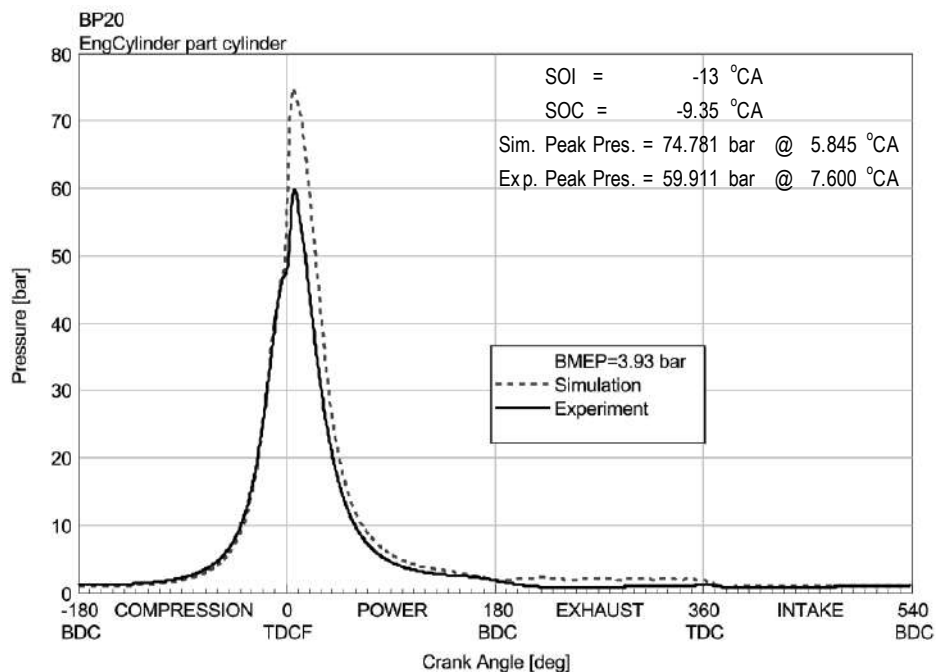


**Figure 4.54** Profiles of pressure in cylinder against crank angle at 3.93 bar brake mean effective pressure using BP20 fuel

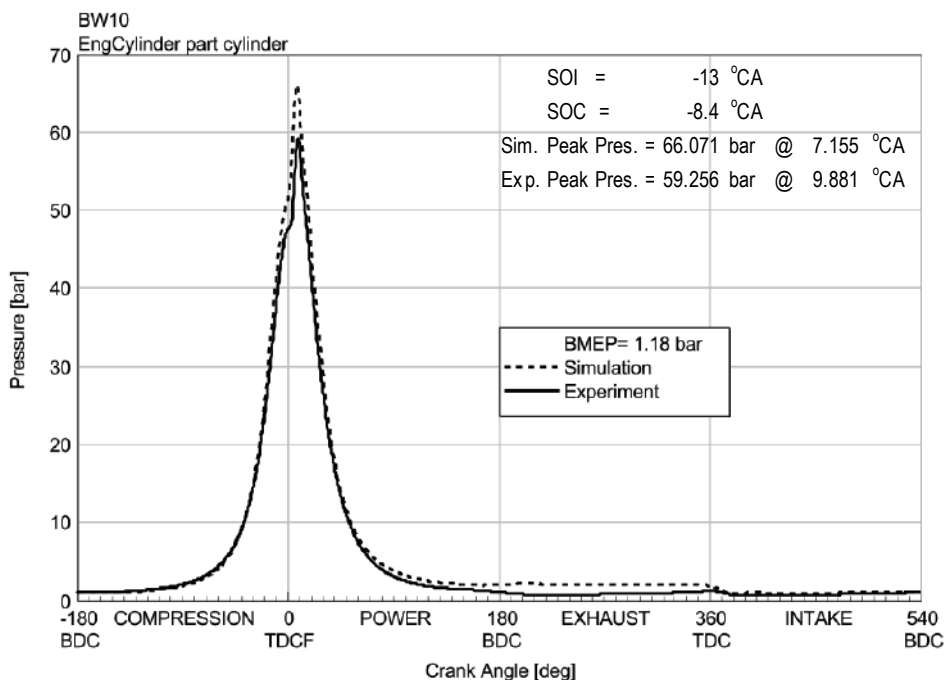


**Figure 4.55** Profiles of pressure in cylinder against crank angle at 1.18 bar brake mean effective pressure using BW10 fuel



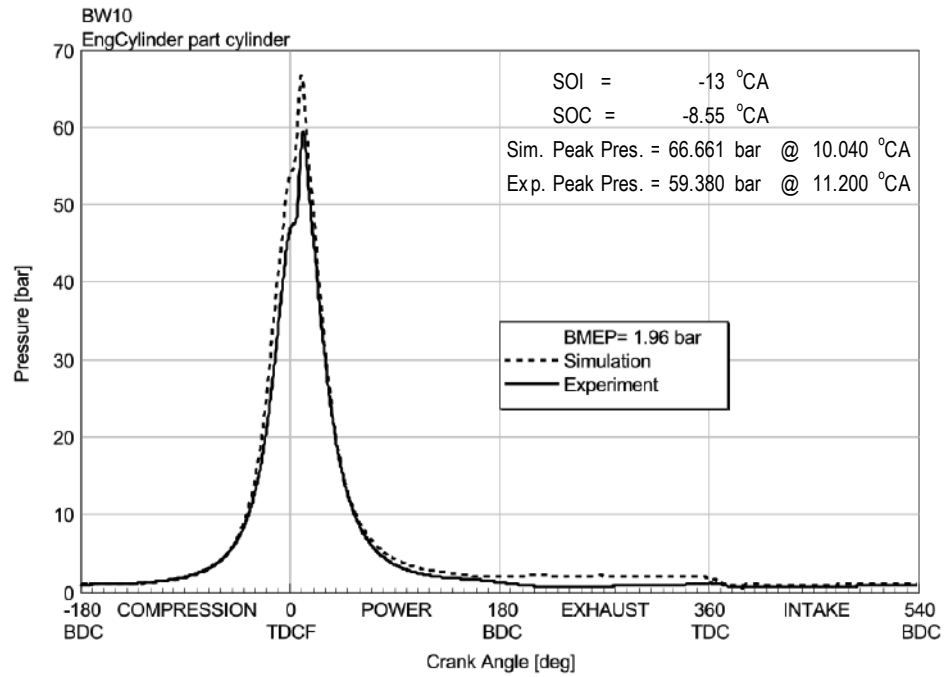


**Figure 4.56** Profiles of pressure in cylinder against crank angle at 1.96 bar brake mean effective pressure using BW10 fuel

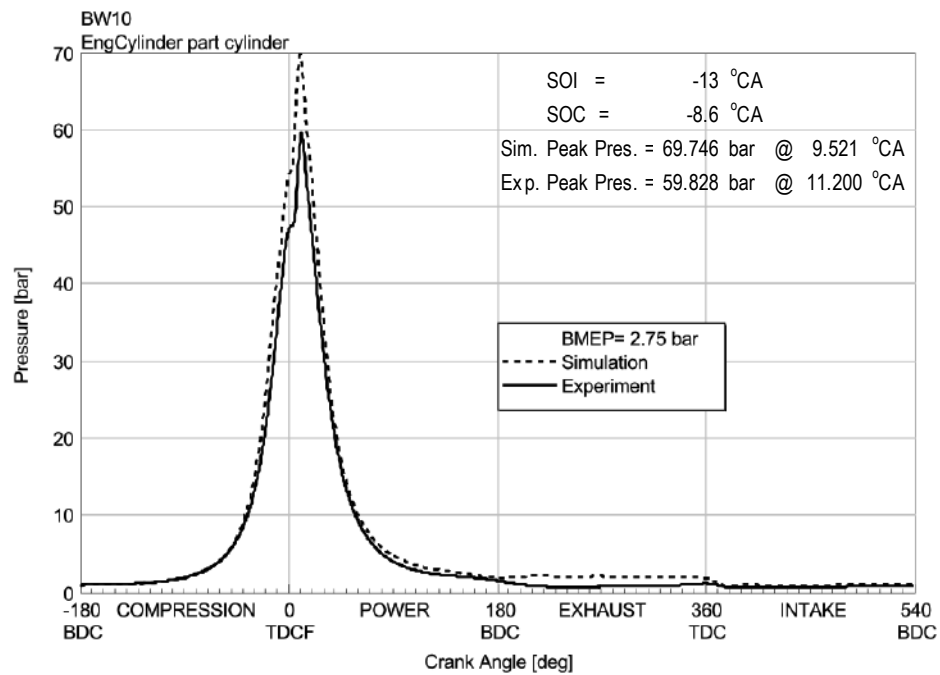


**Figure 4.57** Profiles of pressure in cylinder against crank angle at 2.75 bar brake mean effective pressure using BW10 fuel

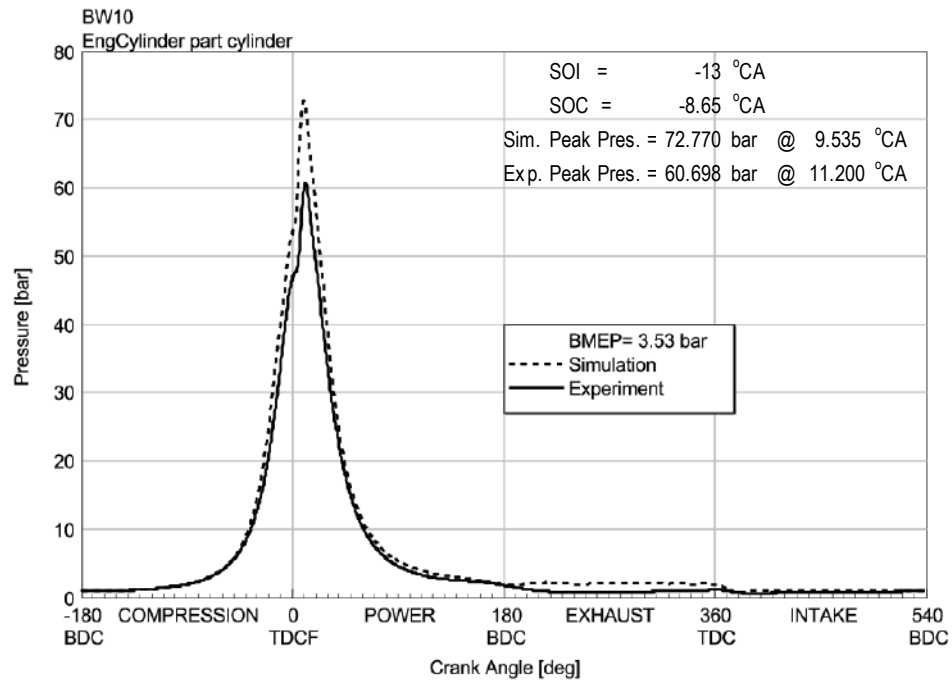


**Figure 4.58** Profiles of pressure in cylinder against crank angle at 3.53 bar brake mean effective pressure using BW10 fuel

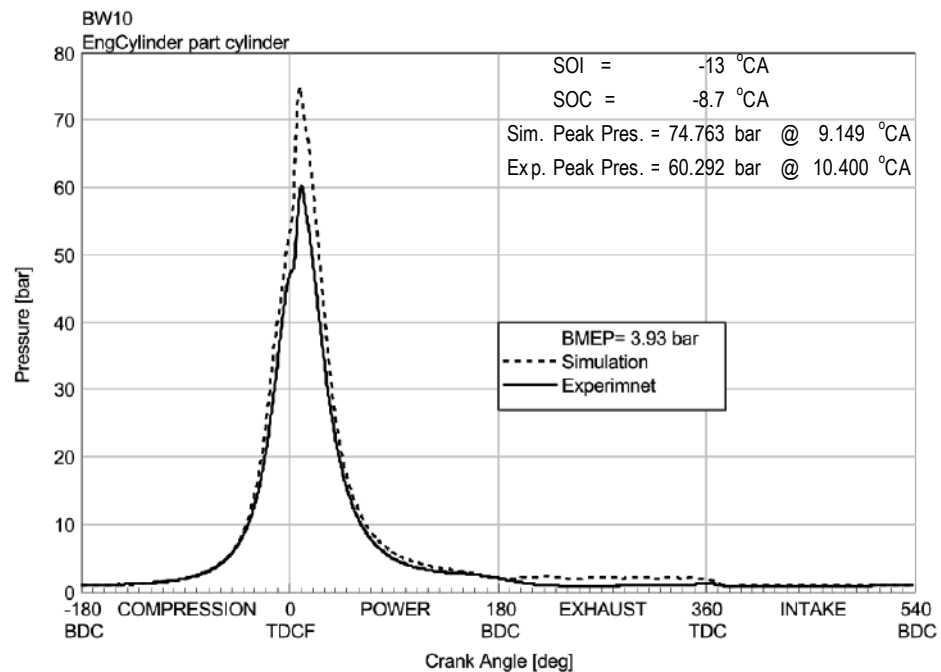


**Figure 4.59** Profiles of pressure in cylinder against crank angle at 3.93 bar brake mean effective pressure using BW10 fuel

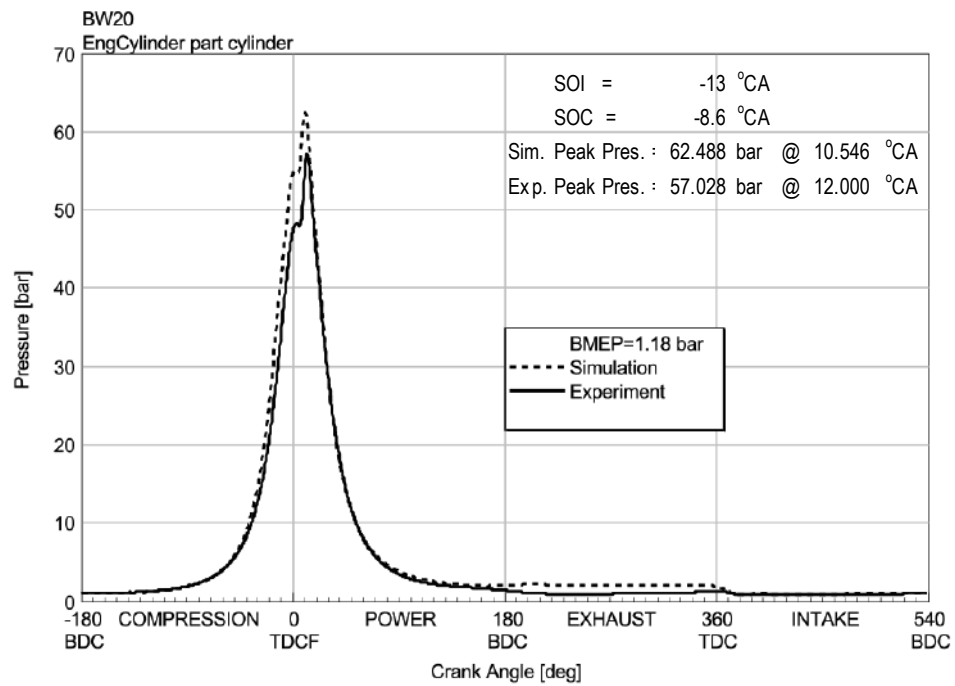


**Figure 4.60** Profiles of pressure in cylinder against crank angle at 1.18 bar brake mean effective pressure using BW20 fuel

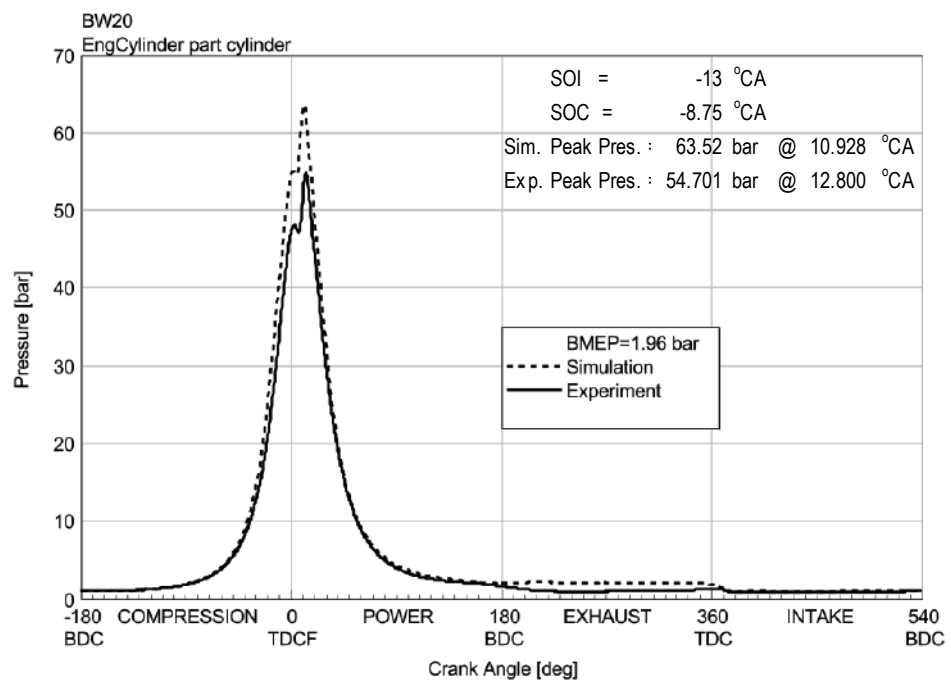


**Figure 4.61** Profiles of pressure in cylinder against crank angle at 1.96 bar brake mean effective pressure using BW20 fuel

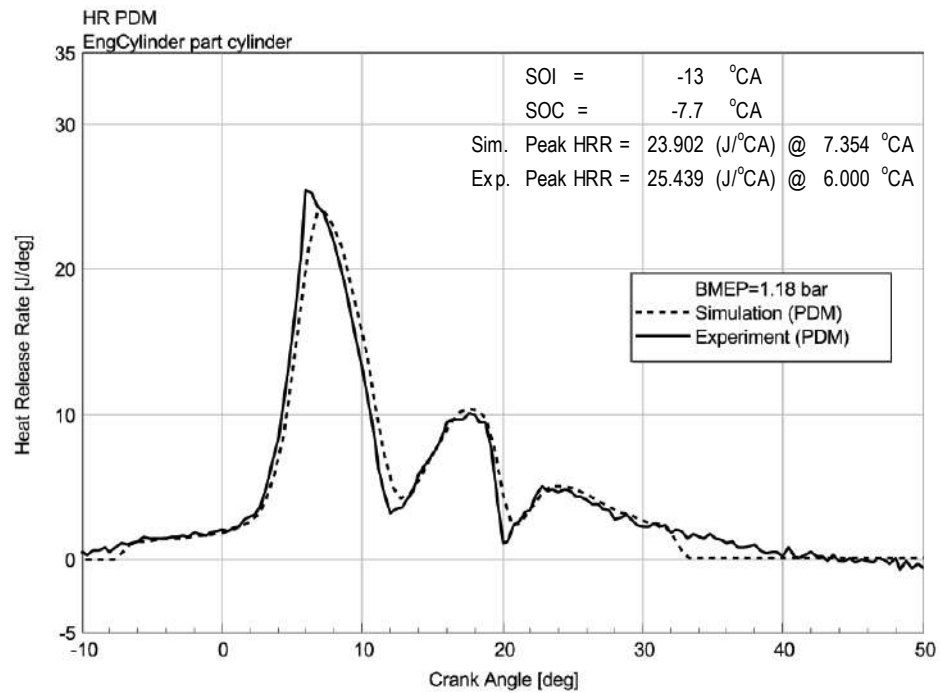
Figure 4.61 to Figure 4.65 show the profile of heat release rate versus crank angle for PDM fuel. These figures show that maximum HRR for simulation is higher than experiment except for BMEP load = 1.18 bar. On average, the maximum HRR for simulation result is higher than experiment by 6.4%. Above this load, the difference between experiment and simulation was increasing from 8.1% to 38.1%. The biggest difference occurred in BMEP = 3.52 bar, which is 52.8%. The average location of peak point of maximum HRR for simulation is slower than experiment of 0.82 °CA or 20.3%.

Figure 4.66 to Figure 4.70 show the profile of heat release rate against crank angle for BP10 fuel. These figures show that HRR maximum for simulation is higher than experiment for all loads. The difference between experiment and simulation is increasing from 15.3% to 58.70%. The biggest difference occurred in BMEP = 3.52 bar, which is 69.2%. The HRR peak point for simulation is slower than the average experiment for BMEP = 1.18 and 1.96 bar, of 1.2 °CA or 2.4%, but for BMEP = 2.75, 3.53 and 3.93 the HRR peak point is faster than the experiment of 4.1 °CA or 27.4%,

From Figure 4.71 to Figure 4.75 show the profile of heat release rate against crank angle for BP20 fuel show that the maximum HRR for simulation is higher than the experiment with the mean difference of 56.3%. The difference between experiment and simulation is increasing from 11.2% in BMEP = 1.18 bar up to 93.4% in BMEP = 3.93 bar. The average HRR peak point location for simulation is faster than experiment by 0.73 °CA or 24.3% for all load except at BMEP of 0.96 °CA or 21.8%.

From Figure 4.76 to Figure 4.80 show the profile of heat release rate against crank angle for BW10 fuel show that the maximum HRR for simulation is higher than the experiment with the mean difference of 29.41%. The minimum difference between experiment and simulation is 9.73% occurs at BMEP of 1.96 bar, while the maximum difference between experiment and simulation is 54.40% occurs at BMEP of 3.93 bar. The HRR peak point for simulation is faster than the average experiment of 0.52 °CA or 15.5%.

For BW20 fuel the HRR profile to crank angle is shown by Figure 4.81 and Figure 4.82. Both of these figures show that the maximum HRR for simulation is higher than the experiment on BMEP of 1.18 bar of 1.8% and at BMEP = 1.96 of 20.8%. The maximum HRR peak point for simulation is slower than the experiment on BMEP of 1.18 bar of 3.2°CA and BMEP of 1.96 bar of 0.41 °CA.



**Figure 4.62** Profiles of heat release rate against crank angle at 1.18 bar brake mean effective pressure using PDM fuel

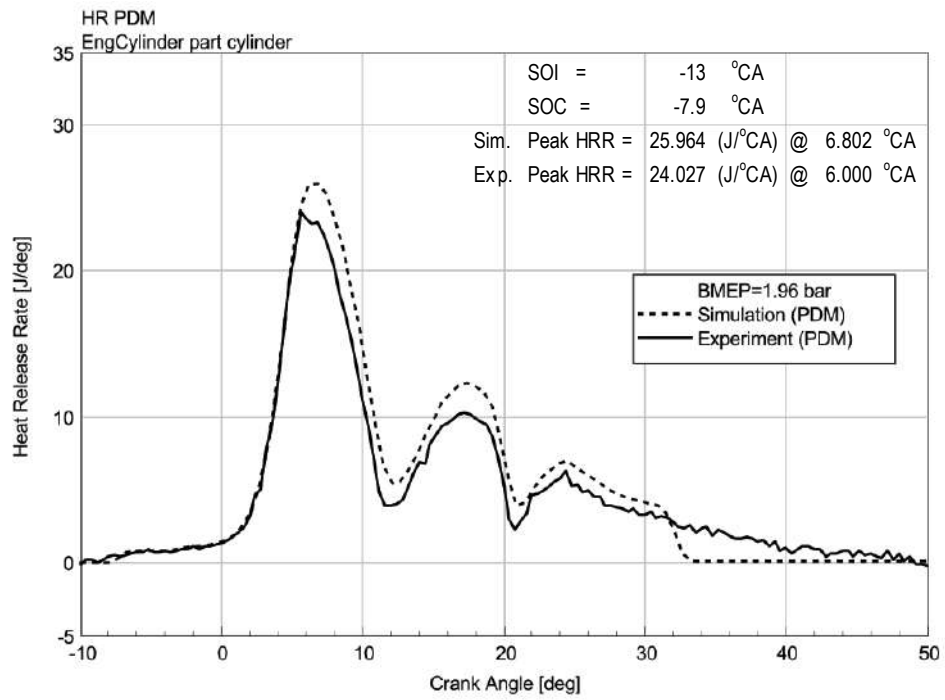


**Figure 4.63** Profiles of heat release rate against crank angle at 1.96 bar brake mean effective pressure using PDM fuel

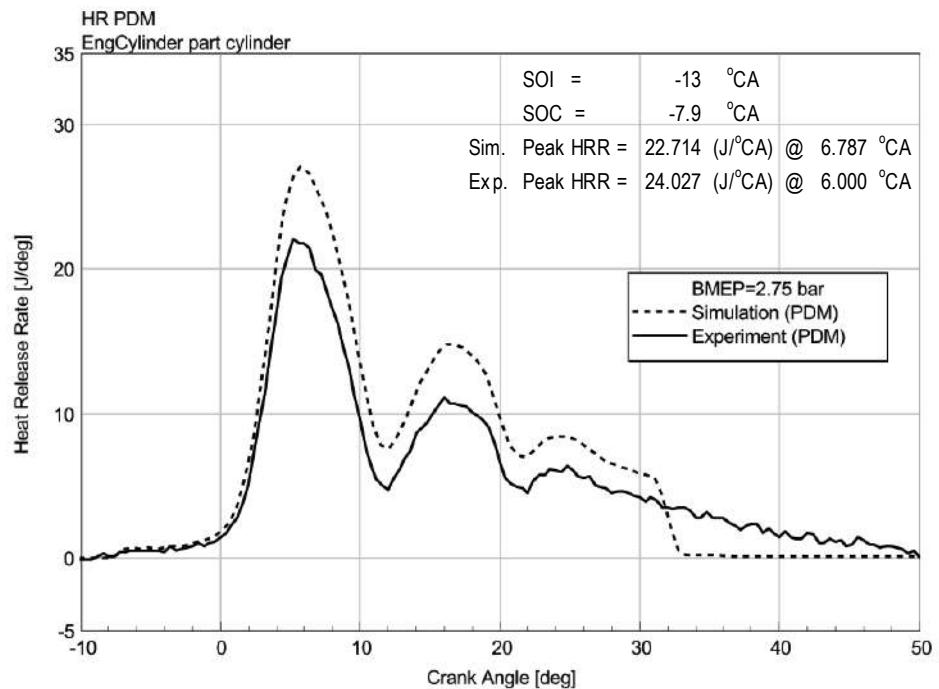


**Figure 4.64** Profiles of heat release rate against crank angle at 2.75 bar brake mean effective pressure using PDM fuel

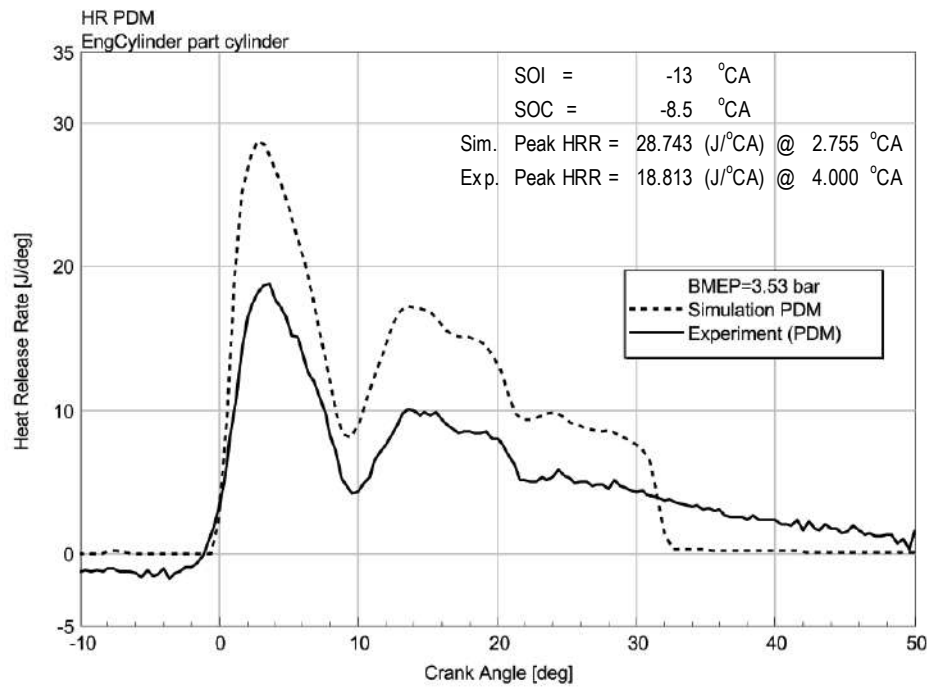


**Figure 4.65** Profiles of heat release rate against crank angle at 3.53 bar brake mean effective pressure using PDM fuel

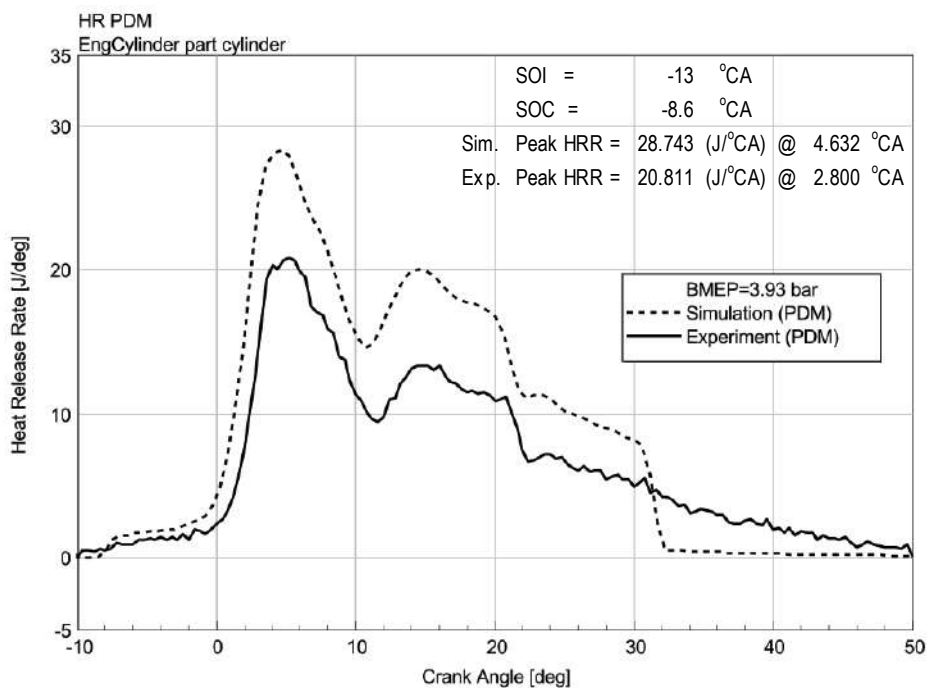


**Figure 4.66** Profiles of heat release rate against crank angle at 3.93 bar brake mean effective pressure using PDM fuel

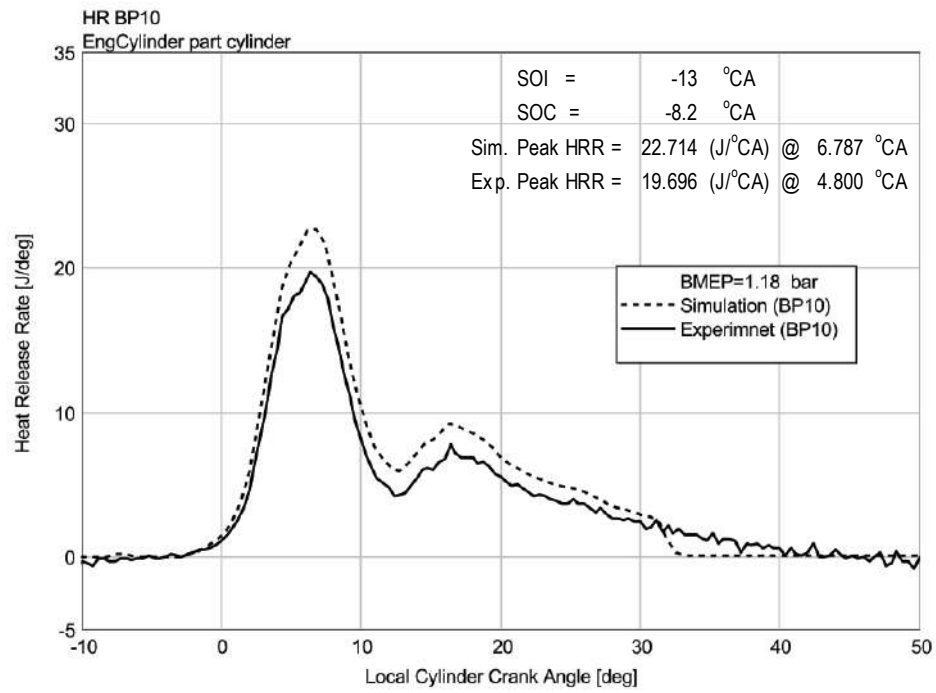


**Figure 4.67** Profiles of heat release rate against crank angle at 1.18 bar brake mean effective pressure using BP10 fuel

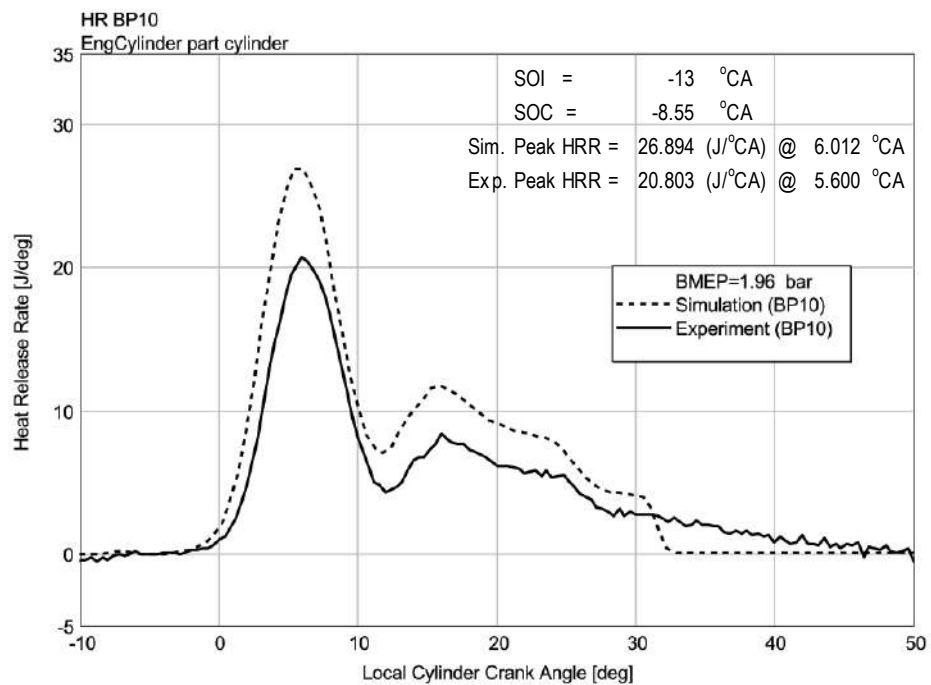


**Figure 4.68** Profiles of heat release rate against crank angle at 1.96 bar brake mean effective pressure using BP10 fuel



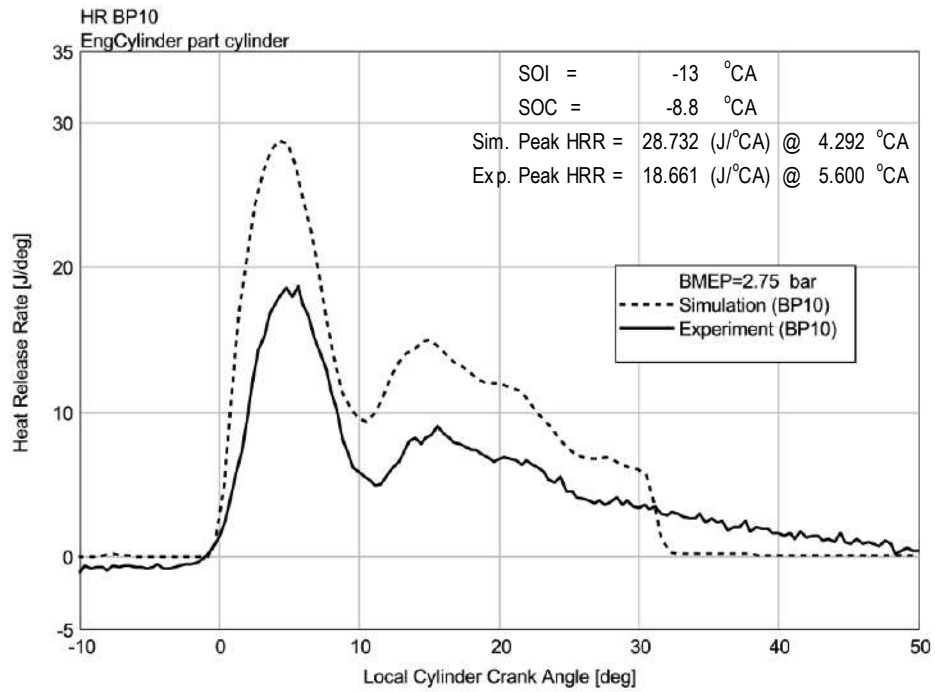


**Figure 4.69** Profiles of heat release rate against crank angle at 2.75 bar brake mean effective pressure using BP10 fuel

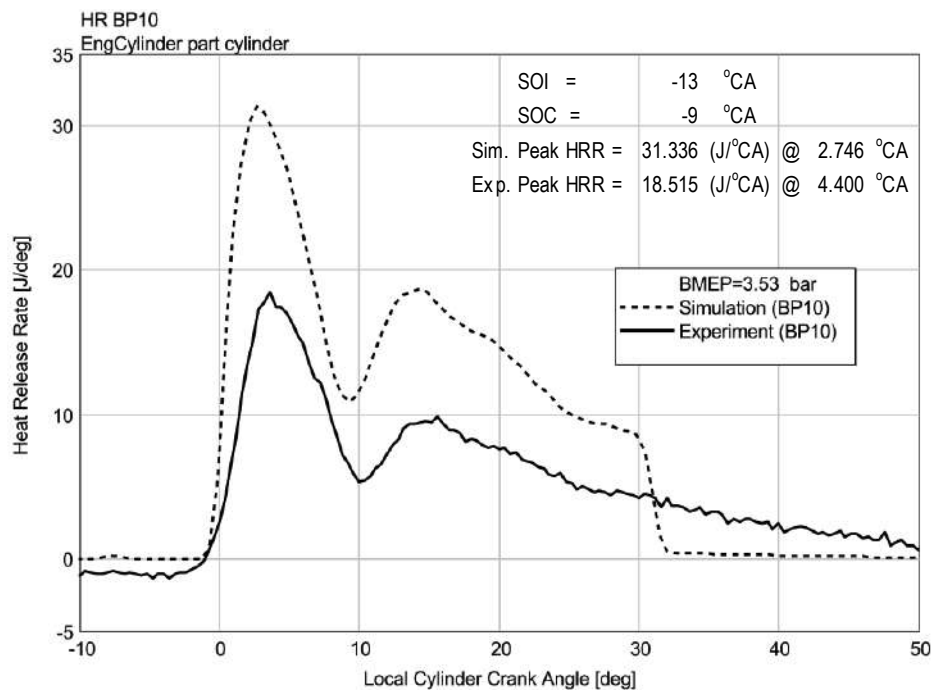


**Figure 4.70** Profiles of heat release rate against crank angle at 3.53 bar brake mean effective pressure using BP10 fuel

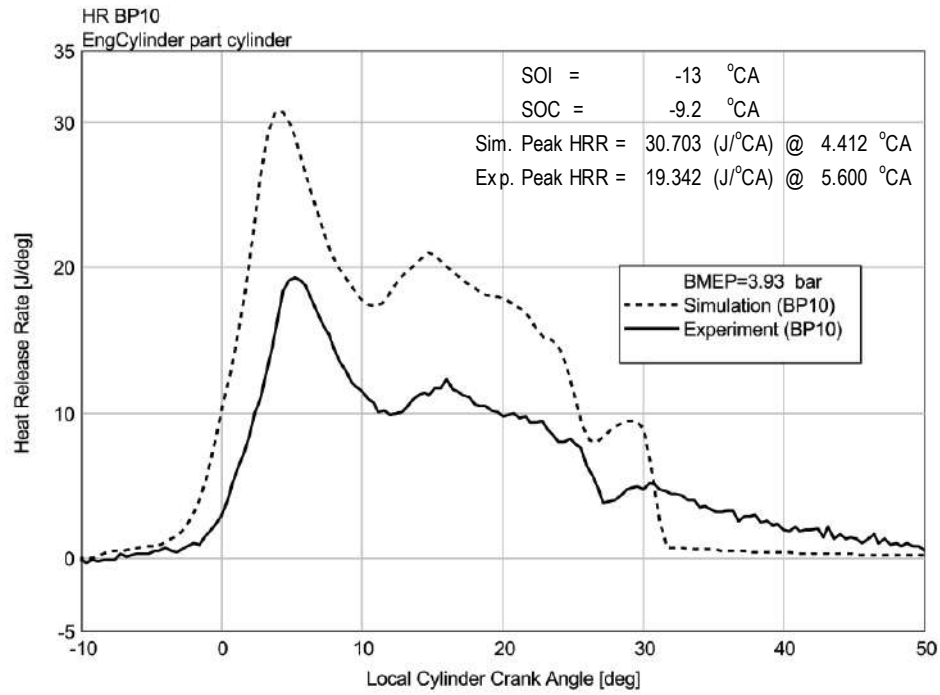


**Figure 4.71** Profiles of heat release rate against crank angle at 3.93 bar brake mean effective pressure using BP10 fuel

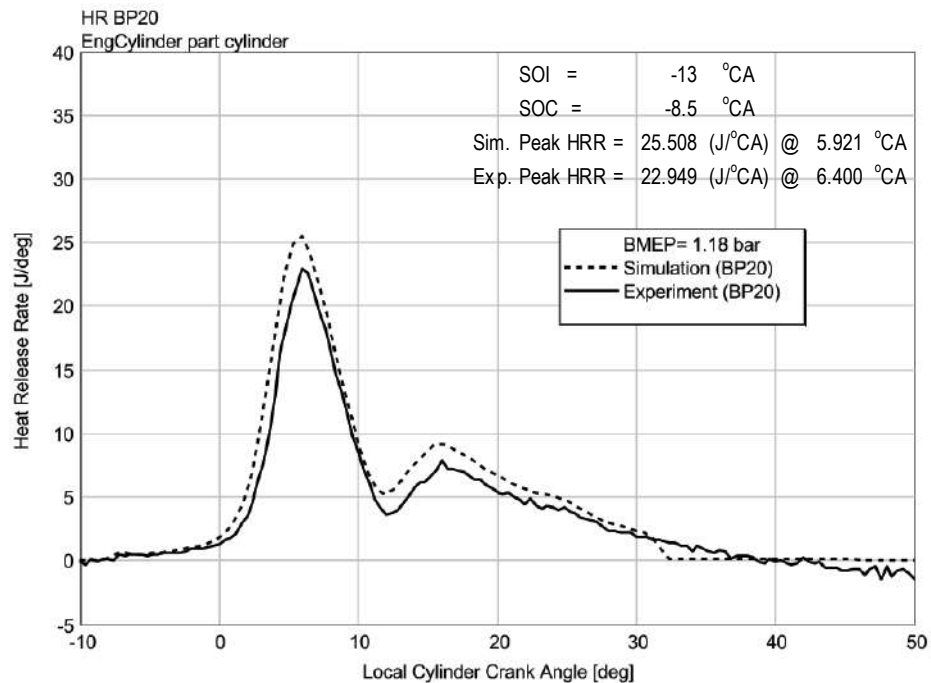


**Figure 4.72** Profiles of heat release rate against crank angle at 1.18 bar brake mean effective pressure using BP20 fuel

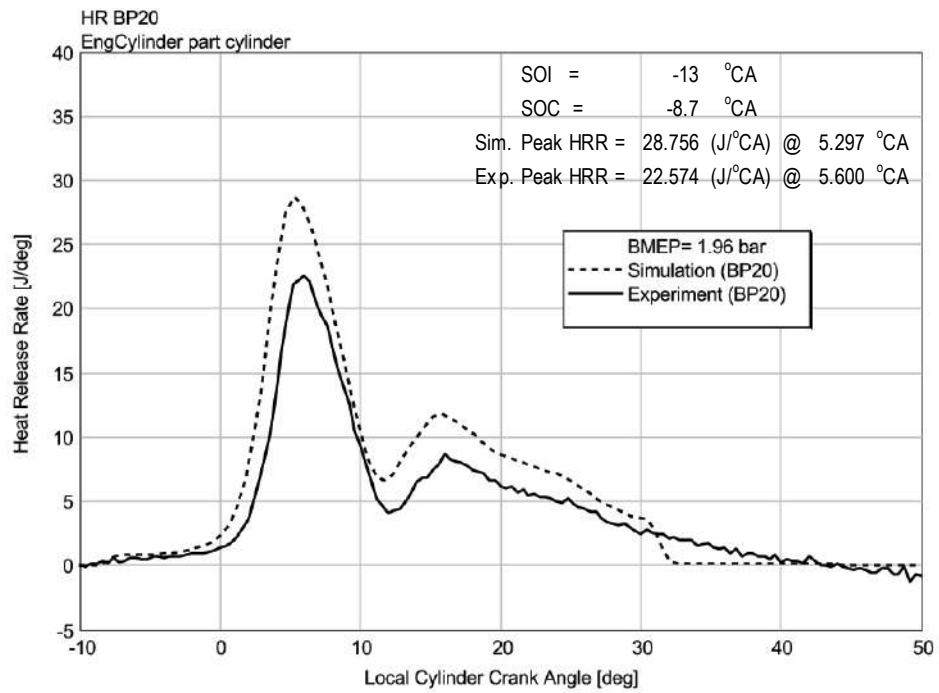


**Figure 4.73** Profiles of heat release rate against crank angle at 1.96 bar brake mean effective pressure using BP20 fuel

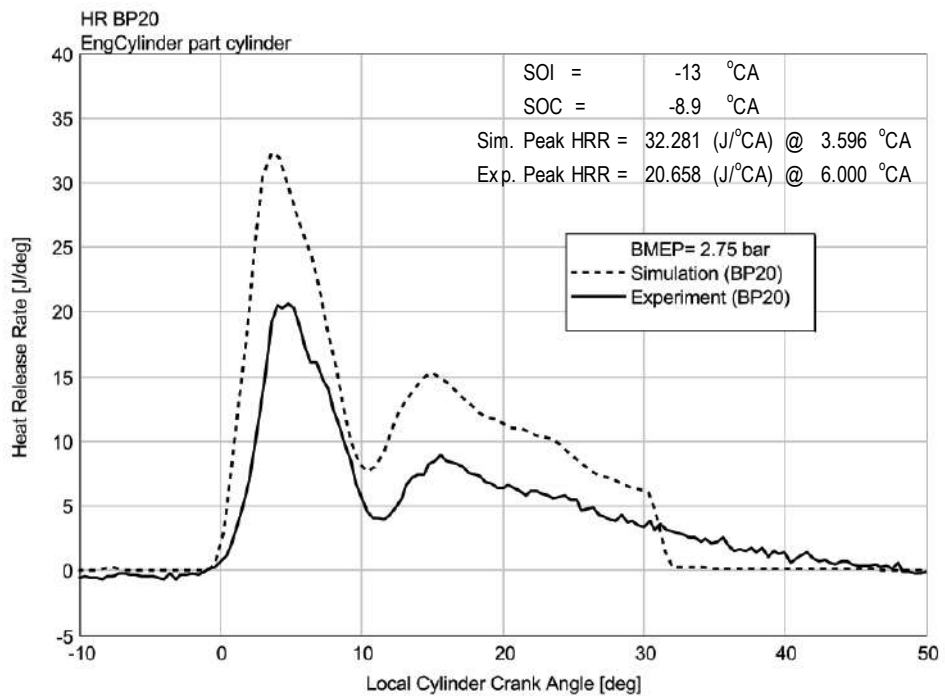


**Figure 4.74** Profiles of heat release rate against crank angle at 2.75 bar brake mean effective pressure using BP20 fuel

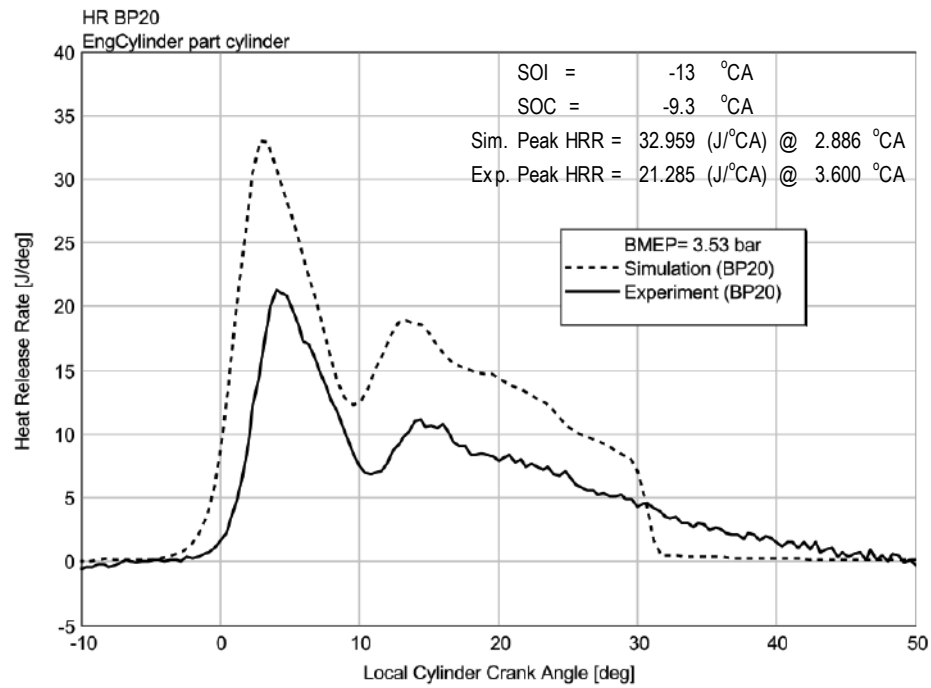


**Figure 4.75** Profiles of heat release rate against crank angle at 3.53 bar brake mean effective pressure using BP20 fuel

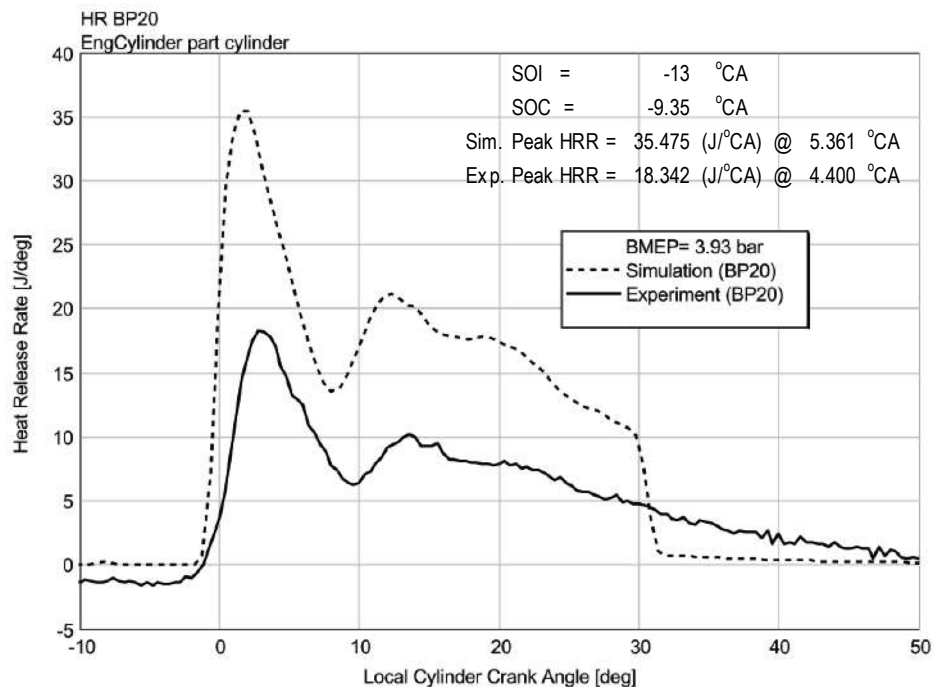


**Figure 4.76** Profiles of heat release rate against crank angle at 3.93 bar brake mean effective pressure using BP20 fuel

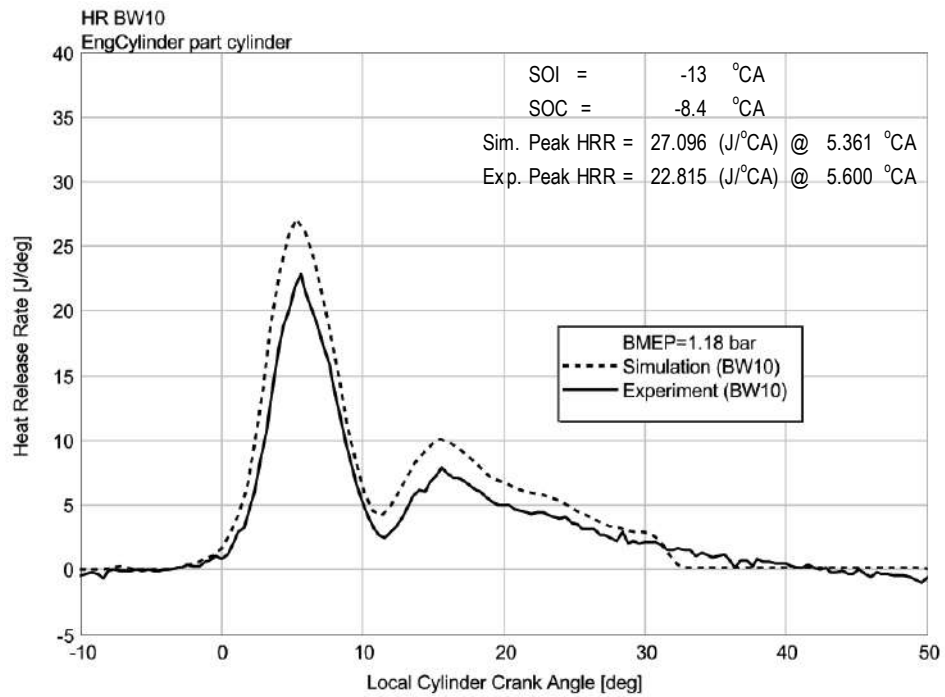


**Figure 4.77** Profiles of heat release rate against crank angle at 1.18 bar brake mean effective pressure using BW10 fuel

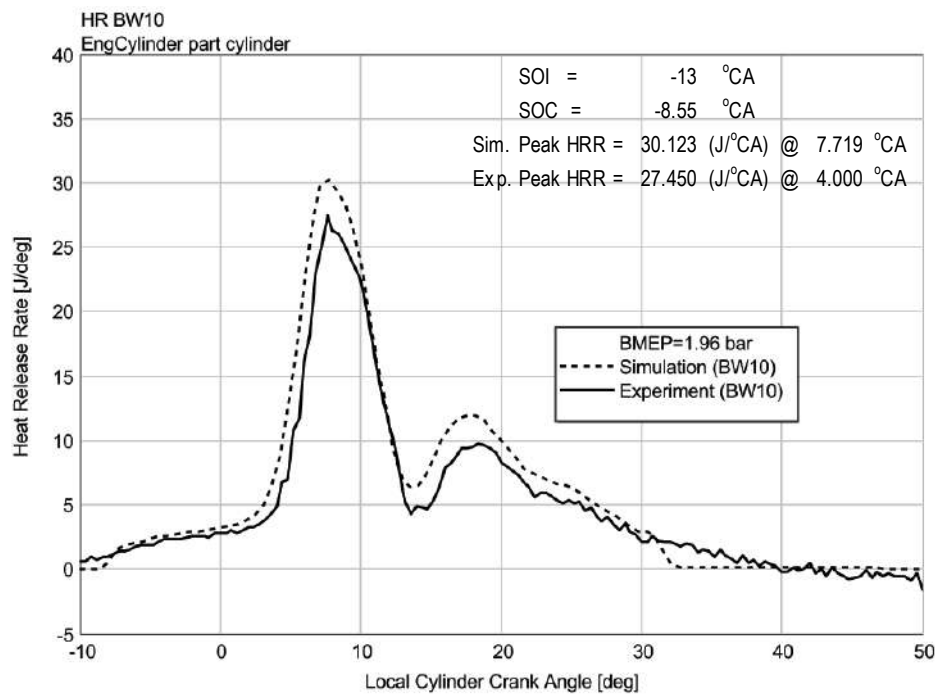


**Figure 4.78** Profiles of heat release rate against crank angle at 1.96 bar brake mean effective pressure using BW10 fuel

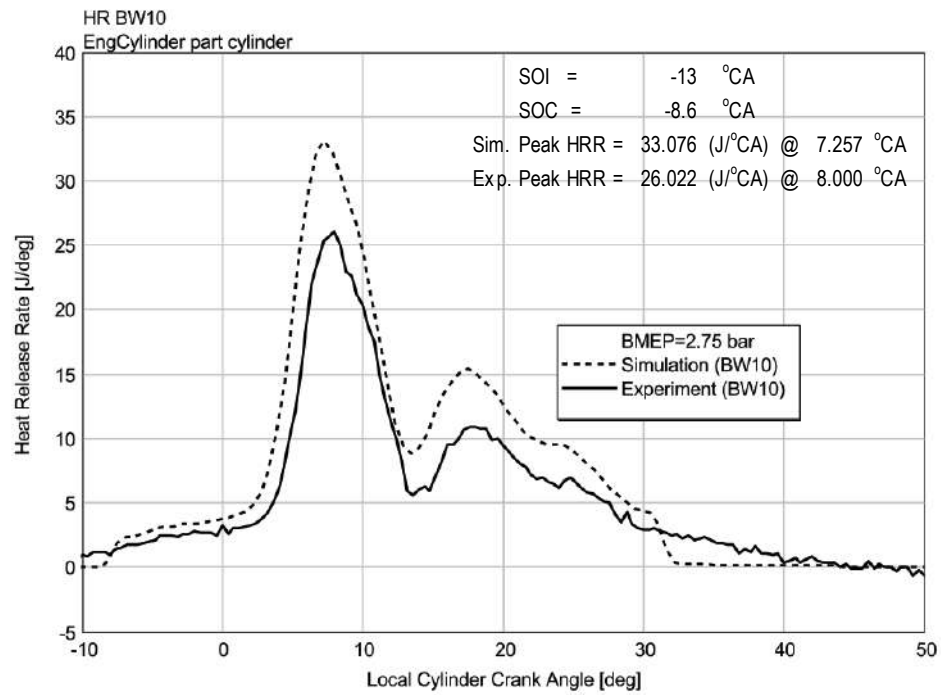


**Figure 4.79** Profiles of heat release rate against crank angle at 2.75 bar brake mean effective pressure using BW10 fuel

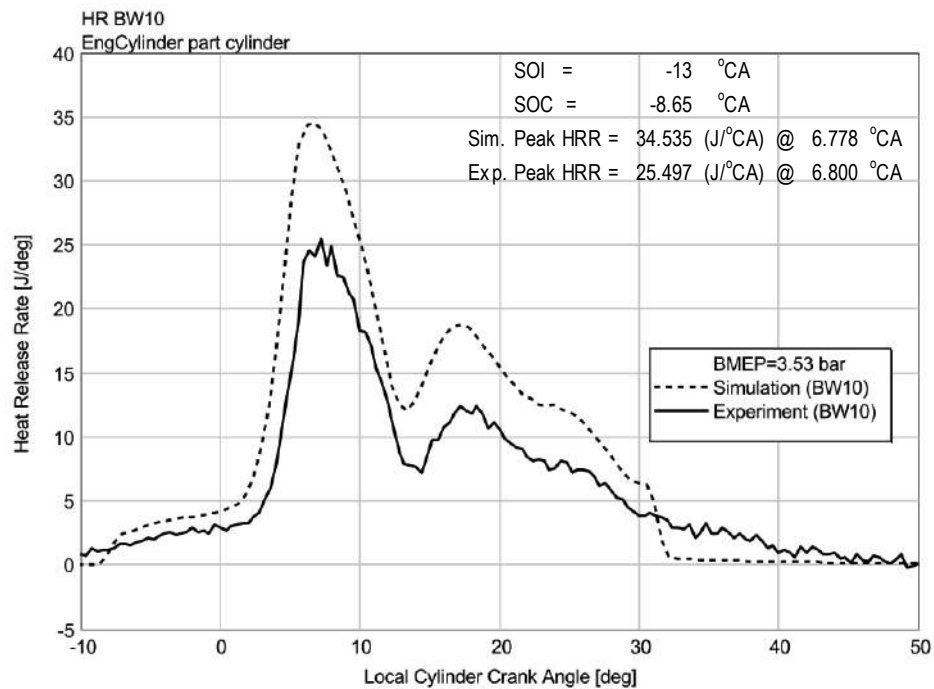


**Figure 4.80** Profiles of heat release rate against crank angle at 3.53 bar brake mean effective pressure using BW10 fuel

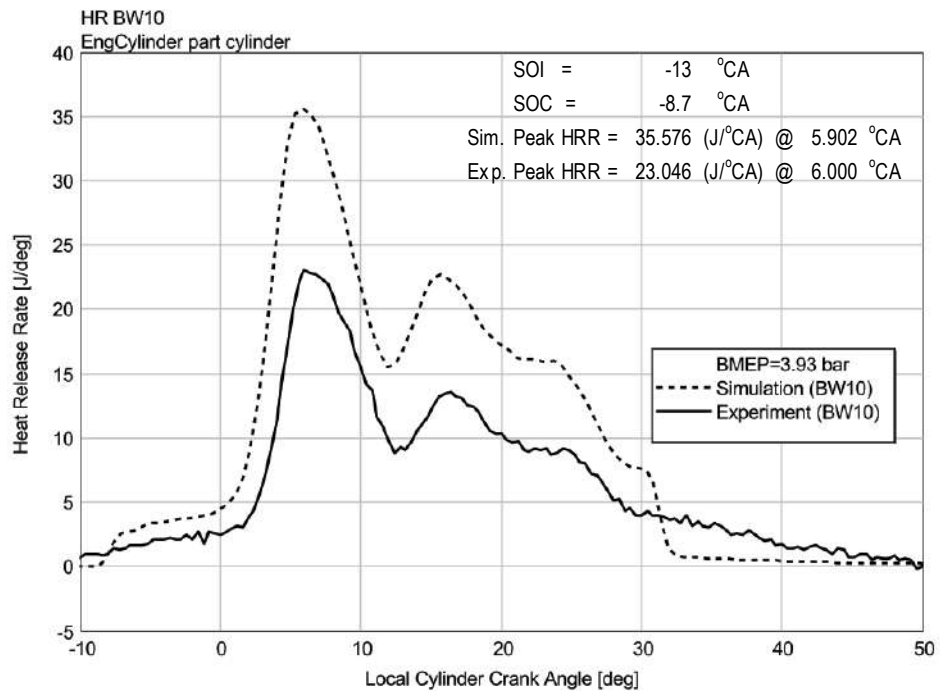


**Figure 4.81** Profiles of heat release rate against crank angle at 3.93 bar brake mean effective pressure using BW10 fuel

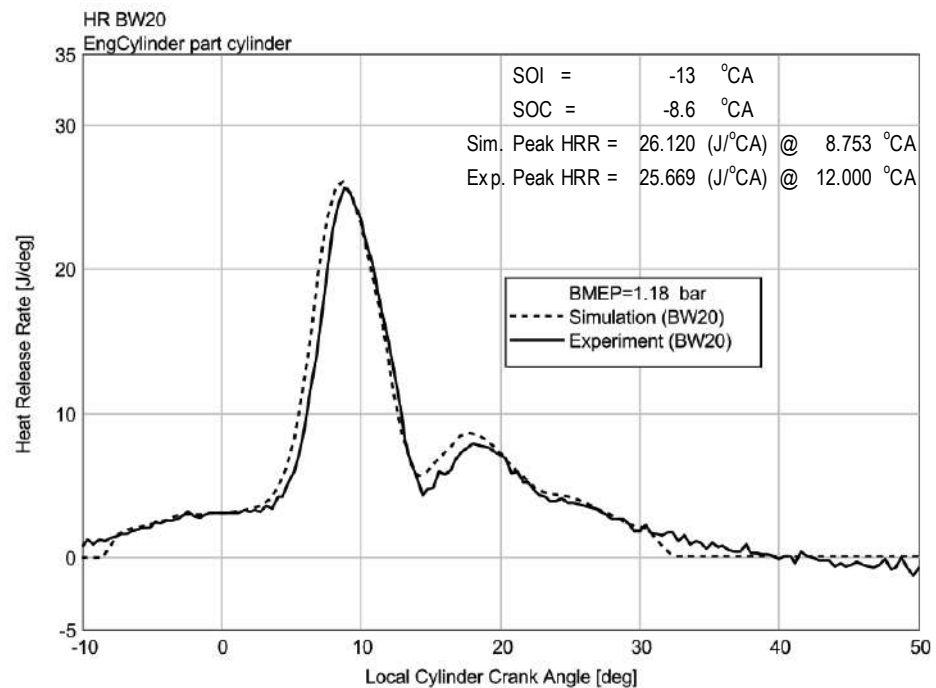


**Figure 4.82** Profiles of heat release rate against crank angle at 1.18 bar brake mean effective pressure using BW20 fuel

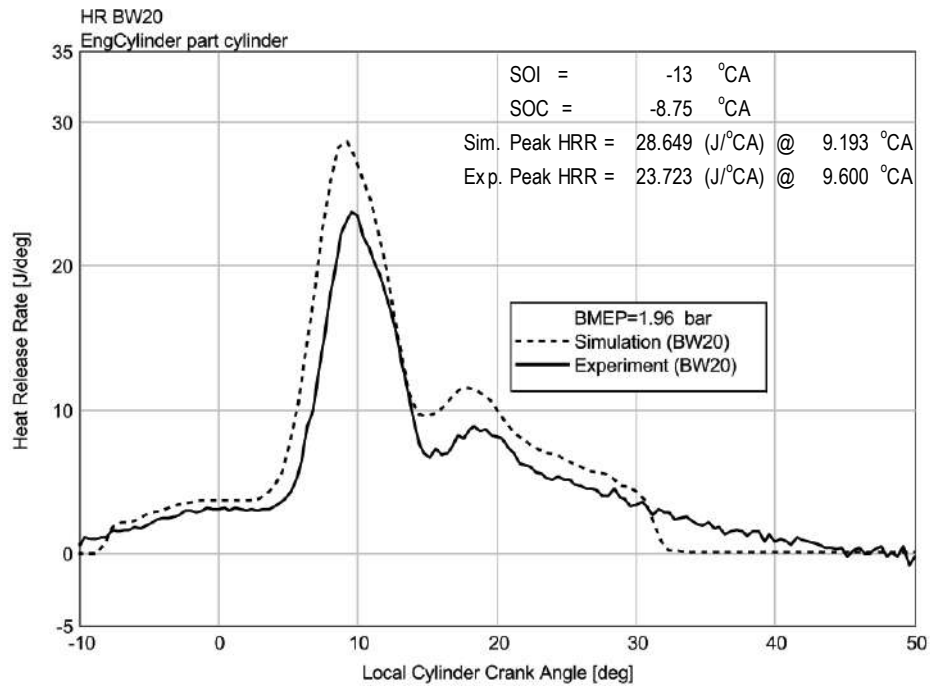


**Figure 4.83** Profiles of heat release rate against crank angle at 1.96 bar brake mean effective pressure using BW20 fuel

The result of simulation and experiment generally indicated conformity, except on the amount of value. This may be due to the absence of consideration on flow phenomena such as turbulence in the simulation process with the GT-SUITE (Hamarashid, 2008).



## CHAPTER 5

### CONCLUSIONS AND RECOMENDATIONS

This chapter summarises the work undertaken in accordance with the stated objectives and recommends immediate action to improve future research.

#### 5.1 Conclusions

The characterisation of CaO catalyst from cockle shell as a raw material has been successfully done by using calcination process in the furnace at 900 °C for 3.5 h. The XRD analysis that was carried out on powder cockle shell calcined for determining their chemical compositions indicated that CaO contains more than 70%.

The application of the continuous flow transesterification of WCO using microwave technology with a perforated plastic container for solid catalyst CaO on stirrer could be used to convert WCO to biodiesel. All the variables such as power input, stirrer speed and LHSV gave a significant effect on the heterogeneous transesterification reaction. The results indicated that RSM based BBD could be used to find the relationships among process variable and response in an efficient manner using a minimum number of experiments. Moreover, the recommended optimum condition of biodiesel production can also be determined via RSM based BBD.

The WCOME blends with commercial diesel fuel (PDM) and POME blends with commercial diesel fuel (PDM) were successfully investigated in DI Diesel engine without any modifications, except BW20 could be loaded with only two of five loads.

The maximum BTE for all loads is obtained in the use of PDM as fuel, then BP10, BP20 and BW10. The minimum BSFC for all loads is obtained in the use of PDM as fuel, then BP10, BP20, BW10 and BW20. Compared to PDM, the biodiesel blends have the tendency to reduce the CO, CO<sub>2</sub> and emissions for all loads. In contrast, NO<sub>x</sub> increased with usage of biodiesel blends. The peak cylinder tends to increase with increasing load. The peak cylinders pressure of biodiesel blends BP10, BP20 and BW10 are lower than PDM for all loads. All the experiment graphs show the similar trend compared to simulation, except on the amount of value. This may be due to the absence of consideration on flow phenomena such as turbulence in the simulation process with the GT-SUITE.

## 5.2 Recommendations for Future Work

It is necessary to test by varying the molar ratio of methanol oil, the reaction temperature, and the time of collection to space-time to obtain more in-depth information about the transesterification process for the future.

Some suggestions can be taken into consideration on the use of biodiesel from WCO and commercial diesel oil blends regarding engine performance and exhaust gas emissions.

- (i) The use of WCOME for particular BW20 that cannot be used at high loads needs should be studied more in depth concerning fuel and regarding used engine.
- (ii) Optimising biodiesel from WCO and commercial diesel oil blends on the performance and emissions generated by diesel engines, and a comprehensive investigation of the effects of other parameters such as injection time, injection pressure, compression ratio effects and the shape of a geometry of the combustion chamber on performance and emissions from the diesel engine.
- (iii) The exhaust emissions generated by the engine need to be studied in-depth to get information on whether WCO biodiesel blends have harmful effects on human health.

## REFERENCES

- Abd Rabu, R., Janajreh, I. and Honnery, D. (2013). Transesterification of waste cooking oil: Process optimization and conversion rate evaluation. *Energy Conversion and Management*, 65(0): 764-769.
- Abu-Jrai, A., Yamin, J. A., Al-Muhtaseb, A. H. and Hararah, M. A. (2011). Combustion characteristics and engine emissions of a diesel engine fueled with diesel and treated waste cooking oil blends. *Chemical Engineering Journal*, 172(1): 129-136.
- Abuhabaya, A., Fieldhouse, J. and Brown, R. (2011). The Effects of Using Bio-diesel as Fuel on Compression Ignition (CI) Engine and Its Production from Vegetable Oils. *International Conference on Environmental, Biomedical and Biotechnology*. 11 March 2011. Singapore. 41-46.
- Ahmad Farid, M. A., Hassan, M. A., Taufiq-Yap, Y. H., Ibrahim, M. L., Othman, M. R., Ali, A. A. M., *et al.* (2017). Production of methyl esters from waste cooking oil using a heterogeneous biomass-based catalyst. *Renewable Energy*, 114: 638-643.
- Altun, Ş., Bulut, H. and Öner, C. (2008). The comparison of engine performance and exhaust emission characteristics of sesame oil–diesel fuel mixture with diesel fuel in a direct injection diesel engine. *Renewable Energy*, 33(8): 1791-1795.
- Amani, H., Ahmad, Z., Asif, M. and Hameed, B. H. (2014). Transesterification of waste cooking palm oil by MnZr with supported alumina as a potential heterogeneous catalyst. *Journal of Industrial and Engineering Chemistry*, 20(6): 4437-4442.
- An, H., Yang, W. M., Maghbouli, A., Li, J., Chou, S. K. and Chua, K. J. (2013). Performance, combustion and emission characteristics of biodiesel derived from waste cooking oils. *Applied Energy*, 112(0): 493-499.
- Anastopoulos, G., Dodos, G. S., Kalligeros, S. and Zannikos, F. (2012). Biodiesel Production by Ethanolysis of Various Vegetable Oils Using Calcium Ethoxide as a Solid Base Catalyst. *International Journal of Green Energy*, 10(5): 468-481.
- Ancheyta, J. (2011). *Modeling and Simulation of Catalytic Reactors for Petroleum Refining*. New Jersey: John Wiley & Sons
- Aworanti, O. A., Agarry, S. E. and Ajani, A. O. (2013). Statistical Optimization of Process Variables for Biodiesel Production from Waste Cooking Oil Using Heterogeneous Base Catalyst. *British Biotechnology Journal*, 3(2): 116-132.
- Bajpai, D. and Tyagi, V. K. (2006). Biodiesel: source, production, composition, properties and its benefits. *Journal of Oleo Science* 55(10): 487-502.

- Balakrishnan, K., Olutoye, M. A. and Hameed, B. H. (2013). Synthesis of methyl esters from waste cooking oil using construction waste material as solid base catalyst. *Bioresource Technology*, 128(0): 788-791.
- Balat, M. and Balat, H. (2008). A critical review of bio-diesel as a vehicular fuel. *Energy Conversion and Management*, 49(10): 2727-2741.
- Balat, M. and Balat, H. (2010). Progress in biodiesel processing. *Applied Energy*, 87(6): 1815-1835.
- Banapurmath, N. R., Tewari, P. G. and Hosmath, R. S. (2008). Performance and emission characteristics of a DI compression ignition engine operated on Honge, Jatropa and sesame oil methyl esters. *Renewable Energy*, 33(9): 1982-1988.
- Banković-Ilić, I. B., Stamenković, O. S. and Veljković, V. B. (2012). Biodiesel production from non-edible plant oils. *Renewable and Sustainable Energy Reviews*, 16(6): 3621-3647.
- Barnard, T. M., Leadbeater, N. E., Boucher, M. B., Stencel, L. M. and Wilhite, B. A. (2007). Continuous-Flow Preparation of Biodiesel Using Microwave Heating. *Energy & Fuels*, 21(3): 1777-1781.
- Basumatary, S. (2013). Heterogeneous Catalyst derived from Natural Resources for Biodiesel Production: A Review *Research Journal of Chemical Sciences*, 3(7): 95101.
- Bezergianni, S. and Dimitriadis, A. (2013). Comparison between different types of renewable diesel. *Renewable and Sustainable Energy Reviews*, 21(0): 110-116.
- Birla, A., Singh, B., Upadhyay, S. N. and Sharma, Y. C. (2012). Kinetics studies of synthesis of biodiesel from waste frying oil using a heterogeneous catalyst derived from snail shell. *Bioresource Technology*, 106(0): 95-100.
- Boey, P.-L., Maniam, G. P. and Hamid, S. A. (2009). Biodiesel production via transesterification of palm olein using waste mud crab (*Scylla serrata*) shell as a heterogeneous catalyst. *Bioresource Technology*, 100(24): 6362-6368.
- Boffito, D. C., Pirola, C., Galli, F., Di Michele, A. and Bianchi, C. L. (2013). Free fatty acids esterification of waste cooking oil and its mixtures with rapeseed oil and diesel. *Fuel*, 108(0): 612-619.
- Borges, M. E. and Díaz, L. (2013). Catalytic packed-bed reactor configuration for biodiesel production using waste oil as feedstock. *BioEnergy Research*, 6(1): 222-228.
- Brito, A., Borges, M. E., Garin, M. and Hernandez, A. (2009). Biodiesel production from waste oil using Mg-Al layered double hydroxide catalysts. *Energy & Fuels* 23: 2952–2958.
- Buasri, A., Chaiyut, N., Loryuenyong, V., Worawanitchaphong, P. and Trongyong, S. (2013). Calcium Oxide Derived from Waste Shells of Mussel, Cockle, and Scallop as the Heterogeneous Catalyst for Biodiesel Production. *The Scientific World Journal*, 2013: 1-7.
- Buasri, A., Ksapabutr, B., Panapoy, M. and Chaiyut, N. (2012). Biodiesel production from waste cooking palm oil using calcium oxide supported on activated

- carbon as catalyst in a fixed bed reactor. *Korean Journal of Chemical Engineering*, 29(12): 1708-1712.
- Can, Ö. (2014). Combustion characteristics, performance and exhaust emissions of a diesel engine fueled with a waste cooking oil biodiesel mixture. *Energy Conversion and Management*, 87(0): 676-686.
- Can, Ö., Öztürk, E. and Yücesu, H. S. (2017). Combustion and exhaust emissions of canola biodiesel blends in a single cylinder DI diesel engine. *Renewable Energy*, 109: 73-82.
- Canakci, M. and Sanli, H. (2008). Biodiesel production from various feedstocks and their effects on the fuel properties. *Journal of Industrial Microbiology & Biotechnology*, 35(5): 431-441.
- Cao, F., Chen, Y., Zhai, F., Li, J., Wang, J., Wang, X., *et al.* (2008). Biodiesel production from high acid value waste frying oil catalyzed by superacid heteropolyacid. *Biotechnology and Bioengineering*, 101(1): 93-100.
- Challen, B. and Baranescu, R. (1999). *Diesel Engine Reference Book* (2nd. ed.). Oxford: Butterworth Heinemann
- Charoenchaitrakool, M. and Thienmethangkoon, J. (2011). Statistical optimization for biodiesel production from waste frying oil through two-step catalyzed process. *Fuel Processing Technology* 92: 112-118.
- Chen, K.-S., Lin, Y.-C., Hsu, K.-H. and Wang, H.-K. (2012). Improving biodiesel yields from waste cooking oil by using sodium methoxide and a microwave heating system. *Energy*, 38(1): 151-156.
- Chen, Y.-H., Huang, Y.-H., Lin, R.-H. and Shang, N.-C. (2010). A continuous-flow biodiesel production process using a rotating packed bed. *Bioresource Technology*, 101(2): 668-673.
- Chhetri, A. B., Watts, K. C. and Islam, M. R. (2008). Waste Cooking Oil as an Alternate Feedstock for Biodiesel Production. *Energies*, 1: 3-18.
- Chin, J. (2011). *Characterization of biofuels blends: Emissions, permeation and apportionment of volatile organic compounds*. University of Michigan: Ph. D.
- Chin, L. H., Hameed, B. H. and Ahmad, A. L. (2009). Process optimization for biodiesel production from waste cooking palm oil (*Elaeis guineensis*) using response surface methodology. *Energy & Fuels*, 23(2): 1040-1044.
- Choedkiatsakul, I., Ngaosuwan, K., Assabumrungrat, S., Mantegna, S. and Cravotto, G. (2015). Biodiesel production in a novel continuous flow microwave reactor. *Renewable Energy*, 83(0): 25-29.
- Chouhan, A. P. S. and Sarma, A. K. (2011). Modern heterogeneous catalysts for biodiesel production: A comprehensive review. *Renewable and Sustainable Energy Reviews*, 15(9): 4378-4399.
- Demirbas, A. (2008). *Biodiesel: a realistic fuel alternative for diesel engines*. London: Springer
- Demirbas, A. (2009). Biodiesel from waste cooking oil via base-catalytic and supercritical methanol transesterification. *Energy Conversion and Management*, 50(4): 923-927.

- Dias, J. M., Alvim-Ferraz, M. C. M. and Almeida, M. F. (2008). Comparison of the performance of different homogeneous alkali catalysts during transesterification of waste and virgin oils and evaluation of biodiesel quality. *Fuel*, 87(17–18): 3572-3578.
- Dwivedi, G. and Sharma, M. P. (2015). Application of Box–Behnken design in optimization of biodiesel yield from Pongamia oil and its stability analysis. *Fuel*, 145(0): 256-262.
- Elshaib, A. A., Kamal, M. M. and Elahwany, A. A. (2014). Performance of a diesel engine fueled by waste cooking oil biodiesel. *Journal of the Energy Institute*, 87(1): 11-17.
- Encinar, J., Gonzalez, J., Martinez, G., Sanchez, N. and Pardal, A. (2012). Soybean oil transesterification by the use of a microwave flow system. *Fuel*, 95: 386 - 393.
- Farag, H. A., El-Maghraby, A. and Taha, N. A. (2011). Optimization of factors affecting esterification of mixed oil with high percentage of free fatty acid. *Fuel Processing Technology*, 92(3): 507-510.
- Farooq, M., Ramli, A. and Naeem, A. (2015). Biodiesel production from low FFA waste cooking oil using heterogeneous catalyst derived from chicken bones. *Renewable Energy*, 76(0): 362-368.
- Farooq, M., Ramli, A. and Subbarao, D. (2013). Biodiesel production from waste cooking oil using bifunctional heterogeneous solid catalysts. *Journal of Cleaner Production*, 59(0): 131-140.
- Ferreira, S. L. C., Bruns, R. E., Ferreira, H. S., Matos, G. D., David, J. M., Brandão, G. C., *et al.* (2007). Box-Behnken design: An alternative for the optimization of analytical methods. *Analytica Chimica Acta*, 597(2): 179-186.
- Gad, M. S., El-Araby, R., Abed, K. A., El-Ibiari, N. N., El Morsi, A. K. and El-Diwani, G. I. (2017). Performance and emissions characteristics of C.I. engine fueled with palm oil/palm oil methyl ester blended with diesel fuel. *Egyptian Journal of Petroleum*.
- Gamma Technologies. (2003). *GT-Power User's Manual Version. A GT-Suite-Application for Engine Performance, Acoustics and Control Simulation*. March 2003.
- Graboski, M. S. and McCormick, R. L. (1998). Combustion of fat and vegetable oil derived fuels in diesel engines. *Progress in Energy and Combustion Science*, 24(2): 125-164.
- Guan, G., Kusakabe, K. and Yamasaki, S. (2009). Tri-potassium phosphate as a solid catalyst for biodiesel production from waste cooking oil. *Fuel Processing Technology*, 90: 520 - 524.
- Hamarashid, L. (2008). *GT-Power Modeling of a 6-Cylinder Natural Gas Engine and Investigation of the Possible Performance Improvements by Studying the Miller Cycle*. Lunds University: Master.
- Han, X.-X., Chen, K.-K., Yan, W., Hung, C.-T., Liu, L.-L., Wu, P.-H., *et al.* (2016). Amino acid-functionalized heteropolyacids as efficient and recyclable catalysts for esterification of palmitic acid to biodiesel. *Fuel*, 165: 115-122.

- Heywood, J. B. (1988). *Internal Combustion Engine Fundamentals*. Singapore: McGraw Hill
- Hill, C. G. (1977). *An introduction to chemical engineering kinetics and reactor design*. Wisconsin: John Wiley & Sons, Inc.
- Hillion, G., Delfort, B., Pennec, D. 1., Bournay, L. and Chodorge, J.-A. (2003). Biodiesel production by a continuous process using a heterogeneous catalyst. *American Chemical Society / Division of Gas and Fuel Chemistry: Preprints of papers*, 48(2): 636-638.
- Hindryawati, N. and Maniam, G. P. (2015). Novel utilization of waste marine sponge (*Demospongiae*) as a catalyst in ultrasound-assisted transesterification of waste cooking oil. *Ultrasonics Sonochemistry*, 22(0): 454-462.
- Hwang, J., Qi, D., Jung, Y. and Bae, C. (2014). Effect of injection parameters on the combustion and emission characteristics in a common-rail direct injection diesel engine fueled with waste cooking oil biodiesel. *Renewable Energy*, 63(0): 9-17.
- Ilkılıç, C., Aydın, S., Behcet, R. and Aydın, H. (2011). Biodiesel from safflower oil and its application in a diesel engine. *Fuel Processing Technology*, 92(3): 356-362.
- Jacobson, K., Gopinath, R., Meher, L. C. and Dalai, A. K. (2008). Solid acid catalyzed biodiesel production from waste cooking oil. *Applied Catalysis B: Environmental*, 85(1-2): 86-91.
- Kalam, M. A., Masjuki, H. H., Jayed, M. H. and Liaquat, A. M. (2011). Emission and performance characteristics of an indirect ignition diesel engine fuelled with waste cooking oil. *Energy*, 36(1): 397-402.
- King, A. J. (2002). *A turbocharger unsteady performance model for the GT-Power internal combustion engine simulation*. Purdue University: Ph.D. Thesis.
- Kouzu, M., Kasuno, T., Tajika, M., Sugimoto, Y., Yamanaka, S. and Hidaka, J. (2008). Calcium oxide as a solid base catalyst for transesterification of soybean oil and its application to biodiesel production. *Fuel*, 87(12): 2798-2806.
- Kulkarni, M. G. and Dalai, A. K. (2006). Waste Cooking Oil An Economical Source for Biodiesel: A Review. *Industrial & Engineering Chemistry Research*, 45(9): 2901-2913.
- Lam, M. K., Lee, K. T. and Muhammed, A. R. (2010). Homogeneous, heterogeneous and enzymatic catalysis for transesterification of high free fatty acid oil (waste cooking oil) to biodiesel: A review. *Biotechnology Advances*, 28(4): 500-518.
- Lam, S. S., Russell, A. D. and Chase, H. A. (2010). Pyrolysis Using Microwave Heating: A Sustainable Process for Recycling Used Car Engine Oil. *Industrial & Engineering Chemistry Research*, 49(21): 10845-10851.
- Lapuerta, M., Rodríguez-Fernández, J. and Agudelo, J. R. (2008). Diesel particulate emissions from used cooking oil biodiesel. *Bioresource Technology*, 99(4): 731-740.
- Lee, C. S., Park, S. W. and Kwon, S. I. (2005). An experimental study on the atomization and combustion characteristics of biodiesel-blended fuels. *Energy & Fuels*, 19(5): 2201-2208.

- Levenspiel, O. (1999). *Chemical Reaction Engineering*. New York: John Wiley & Sons, Inc.
- Li, M., Zheng, Y., Chen, Y. and Zhu, X. (2014). Biodiesel production from waste cooking oil using a heterogeneous catalyst from pyrolyzed rice husk. *Bioresource Technology*, 154(0): 345-348.
- Li, Z.-H., Lin, P.-H., Wu, J. C. S., Huang, Y.-T., Lin, K.-S. and Wu, K. C. W. (2013). A stirring packed-bed reactor to enhance the esterification–transesterification in biodiesel production by lowering mass-transfer resistance. *Chemical Engineering Journal*, 234(0): 9-15.
- Liu, H.-P., Strank, S., Werst, M., Hebner, R. and Osara, J. (2010). Combustion Emission Modeling and Testing of Neat Biodiesel Fuels. *Proceedings of the ASME 2010 4th International Conference on Energy Sustainability*. May 17-22, 2010. Phoenix, AZ USA.
- Lloyd, L. (2011). *Handbook of Industrial Catalysts*. London: Springer
- Lou, W.-Y., Zong, M.-H. and Duan, Z.-Q. (2008). Efficient production of biodiesel from high free fatty acid-containing waste oils using various carbohydrate-derived solid acid catalysts. *Bioresource Technology*, 99(18): 8752-8758.
- Ma, F. and Hanna, M. A. (1999). Biodiesel production: a review. *Bioresource Technology*, 70(1): 1-15.
- Maddikeri, G. L., Pandit, A. B. and Gogate, P. R. (2012). Intensification Approaches for Biodiesel Synthesis from Waste Cooking Oil: A Review. *Industrial & Engineering Chemistry Research*, 51(45): 14610-14628.
- Maddikeri, G. L., Pandit, A. B. and Gogate, P. R. (2013). Ultrasound assisted interesterification of waste cooking oil and methyl acetate for biodiesel and triacetin production. *Fuel Processing Technology*, 116(0): 241-249.
- Mahanta, P., Mishra, S. and Kushwah, Y. (2006). A comparative study of pongamia pinnata and jatropha curcus oil as diesel substitute. *International Energy Journal*, 7: 1-7.
- Mahesh, S. E., Ramanathan, A., Begum, K. M. M. S. and Narayanan, A. (2015). Biodiesel production from waste cooking oil using KBr impregnated CaO as catalyst. *Energy Conversion and Management*, 91(0): 442-450.
- Mansourpoor, M. and Shariati, A. (2012). Optimization of Biodiesel Production from Sunflower Oil Using Response Surface Methodology. *J Chem Eng Process Technol*, 3(4): 1-5.
- Marchetti, J. M. (2011). The effect of economic variables over a biodiesel production plant. *Energy Conversion and Management*, 52(10): 3227-3233.
- Mazubert, A., Poux, M. and Aubin, J. (2013). Intensified processes for FAME production from waste cooking oil: A technological review. *Chemical Engineering Journal*, 233(0): 201-223.
- Melero, J. A., Bautista, L. F., Iglesias, J., Morales, G. and Sánchez-Vazquez, R. (2014). Production of biodiesel from waste cooking oil in a continuous packed bed reactor with an agglomerated Zr-SBA-15/bentonite catalyst. *Applied Catalysis B: Environmental*, 145(0): 197-204.



- Menéndez, J. A., Arenillas, A., Fidalgo, B., Fernández, Y., Zubizarreta, L., Calvo, E. G., *et al.* (2010). Microwave heating processes involving carbon materials. *Fuel Processing Technology*, 91(1): 1-8.
- Meyer, J. (2011). *Calibration reduction in internal combustion engine fueling control: modeling, estimation and stability robustness*. The Ohio State University: Ph.D Dissertation.
- Molaei Dehkordi, A. and Ghasemi, M. (2012). Transesterification of waste cooking oil to biodiesel using Ca and Zr mixed oxides as heterogeneous base catalysts. *Fuel Processing Technology*, 97(0): 45-51.
- Moser, B. R. (2011). Biodiesel production, properties, and feedstocks. In D. Tomes, P. Lakshmanan & D. Songstad (Eds.), *Biofuels* (pp. 285-347): Springer New York.
- Motasemi, F. (2011). *Production of Biodiesel from Used Cooking Palm Oil by Using Microwave Irradiation*. Universiti Teknologi Malaysia: Master Thesis.
- Motasemi, F. and Ani, F. N. (2012). A review on microwave-assisted production of biodiesel. *Renewable and Sustainable Energy Reviews*, 16(7): 4719-4733.
- Muciño, G. G., Romero, R., Ramírez, A., Martínez, S. L., Baeza-Jiménez, R. and Natividad, R. (2014). Biodiesel production from used cooking oil and sea sand as heterogeneous catalyst. *Fuel*, (0).
- Mulinari, J., Venturin, B., Sbardelotto, M., Dall Agnol, A., Scapini, T., Camargo, A. F., *et al.* (2017). Ultrasound-assisted hydrolysis of waste cooking oil catalyzed by homemade lipases. *Ultrasonics Sonochemistry*, 35: 313-318.
- Muralidharan, K. and Vasudevan, D. (2011). Performance, emission and combustion characteristics of a variable compression ratio engine using methyl esters of waste cooking oil and diesel blends. *Applied Energy*, 88(11): 3959-3968.
- Nair, P., Singh, B., Upadhyay, S. N. and Sharma, Y. C. (2012). Synthesis of biodiesel from low FFA waste frying oil using calcium oxide derived from Mereterix mereterix as a heterogeneous catalyst. *Journal of Cleaner Production*, 29-30(0): 82-90.
- Niju, S., Begum, K. M. M. S. and Anantharaman, N. (2015). Preparation of biodiesel from waste frying oil using a green and renewable solid catalyst derived from egg shell. *Environmental Progress & Sustainable Energy*, 34(1): 248-254.
- No, S.-Y. (2011). Inedible vegetable oils and their derivatives for alternative diesel fuels in CI engines: A review. *Renewable and Sustainable Energy Reviews* 15: 131-149.
- Noshadi, I., Amin, N. A. S. and Parnas, R. S. (2012). Continuous production of biodiesel from waste cooking oil in a reactive distillation column catalyzed by solid heteropolyacid: Optimization using response surface methodology (RSM). *Fuel*, 94(0): 156-164.
- Okon, A., Kurji, H., Medina, A. and Xue, Y. (2016). Heat release rate and pressure fluctuation of lean premixed flame at different forcing levels. *2016 International Conference for Students on Applied Engineering (ICSAE)*. 20-21 Oct. 2016. 232-236.

- Ott, R. L. and Longnecker, M. (2010). *An Introduction to Statistical Methods and Data Analysis* ( 6th ed. ed.). Belmont, CA, USA: Brooks/Cole, Cengage Learning
- Ozsezen, A. N. and Canakci, M. (2011). Determination of performance and combustion characteristics of a diesel engine fueled with canola and waste palm oil methyl esters. *Energy Conversion and Management*, 52(1): 108-116.
- Ozsezen, A. N., Canakci, M., Turkan, A. and Sayin, C. (2009). Performance and combustion characteristics of a DI diesel engine fueled with waste palm oil and canola oil methyl esters. *Fuel*, 88(4): 629-636.
- Pandey, A. (2009). *Handbook of plant-based biofuels*. New York: CRC Press
- Park, Y.-M., Lee, D.-W., Kim, D.-K., Lee, J.-S. and Lee, K.-Y. (2008). The heterogeneous catalyst system for the continuous conversion of free fatty acids in used vegetable oils for the production of biodiesel. *Catalysis Today*, 131(1-4): 238-243.
- Patil, P., Gude, V., Reddy, H., Muppaneni, T. and Deng, S. (2012). Biodiesel production from waste cooking Oil using sulfuric acid and microwave irradiation processes. *Journal of Environmental Protection*, 3(01): 107 - 113.
- Pugazhivadivu, M. and Jeyachandran, K. (2005). Investigations on the performance and exhaust emissions of a diesel engine using preheated waste frying oil as fuel. *Renewable Energy*, 30(14): 2189-2202.
- Rakopoulos, C. D., Antonopoulos, K. A., Rakopoulos, D. C., Hountalas, D. T. and Giakoumis, E. G. (2006). Comparative performance and emissions study of a direct injection Diesel engine using blends of Diesel fuel with vegetable oils or bio-diesels of various origins. *Energy Conversion and Management*, 47(18-19): 3272-3287.
- Rakopoulos, D. C., Rakopoulos, C. D., Papagiannakis, R. G. and Kyritsis, D. C. (2011). Combustion heat release analysis of ethanol or n-butanol diesel fuel blends in heavy-duty DI diesel engine. *Fuel*, 90(5): 1855-1867.
- Ramadhas, A. S., Jayaraj, S. and Muraleedharan, C. (2004). Use of vegetable oils as I.C. engine fuels—A review. *Renewable Energy*, 29(5): 727-742.
- Rao, G. L. N., Sampath, S. and Rajagopal, K. (2008). Experimental Studies on the Combustion and Emission Characteristics of a Diesel Engine Fuelled with Used Cooking Oil Methyl Ester and its Diesel Blends. *World Academy of Science, Engineering and Technology* 13: 551-557.
- Refaat, A. A. (2011). Biodiesel production using solid metal oxide catalysts. *International Journal of Environmental Science and Technology*, 8(1): 203-221.
- Roschat, W., Kacha, M., Yoosuk, B., Sudyoadsuk, T. and Promarak, V. (2012). Biodiesel production based on heterogeneous process catalyzed by solid waste coral fragment. *Fuel*, 98: 194-202.
- Ross, J. R. H. (2012). Chapter 4 - Catalyst Preparation. In J. R. H. Ross (Ed.), *Heterogeneous Catalysis* (pp. 65-96). Amsterdam: Elsevier.
- Rutz, D. and Janssens, R. (2007). *Biofuel Technology Handbook*. Muenchen: WIP Renewable Energie

- Said, M. F. M. (2006). *Performance and Emission Tests of Biodiesel Fuels using a Conventional Diesel Engine*. Universiti Teknologi Malaysia: Master Thesis.
- Sanjid, A., Masjuki, H. H., Kalam, M. A., Rahman, S. M. A., Abedin, M. J. and Palash, S. M. (2013). Impact of palm, mustard, waste cooking oil and Calophyllum inophyllum biofuels on performance and emission of CI engine. *Renewable and Sustainable Energy Reviews*, 27(0): 664-682.
- Senthil Kumar, M. and Jaikumar, M. (2014). A comprehensive study on performance, emission and combustion behavior of a compression ignition engine fuelled with WCO (waste cooking oil) emulsion as fuel. *Journal of the Energy Institute*, 87(3): 263-271.
- Serrano-Ruiz, J. C., Ramos-Fernandez, E. V. and Sepulveda-Escribano, A. (2012). From biodiesel and bioethanol to liquid hydrocarbon fuels: new hydrotreating and advanced microbial technologies. *Energy & Environmental Science*, 5(2): 5638-5652.
- Shah, A. N., Shah, F. H., Shahid, E. M. and Gardezi, S. A. R. (2014). Prediction of an Optimum Biodiesel-Diesel Blended Fuel for Compression Ignition Engine Using GT-Power. *Pakistan Journal Engineering & Applied Science*, 14: 102-114.
- Shahid, E. M., Y. Jamal, Shah, A. N., Rumzan, N. and Munsha, M. (2012). Effect of used cooking oil methyl ester on compression ignition engine. *Journal of Quality and Technology Management*, VIII(II): 91-104.
- Sharma, Y. C., Sing, B., Korstad, J. and Roberts, O. (2011). Advancements in solid acid catalysts for ecofriendly and economically viable synthesis of biodiesel. *Biofuels, Bioprod. Bioref.*, 5: 69-92.
- Sharma, Y. C., Singh, B. and Upadhyay, S. N. (2008). Advancements in development and characterization of biodiesel: A review. *Fuel*, 87(12): 2355-2373.
- Sirisomboonchai, S., Abuduwayiti, M., Guan, G., Samart, C., Abliz, S., Hao, X., et al. (2015). Biodiesel production from waste cooking oil using calcined scallop shell as catalyst. *Energy Conversion and Management*, 95(0): 242-247.
- Stoytcheva, M. and Montero, G. (Eds.). (2011). *Biodiesel – Feedstocks and Processing Technologies*. Rijeka, Croatia: InTech.
- Sultania, M., Rai, J. S. P. and Srivastava, D. (2011). Process modeling, optimization and analysis of esterification reaction of cashew nut shell liquid (CNSL)-derived epoxy resin using response surface methodology. *Journal of Hazardous Materials*, 185(2-3): 1198-1204.
- Talebian-Kiakalaieh, A., Amin, N. A. S. and Mazaheri, H. (2013). A review on novel processes of biodiesel production from waste cooking oil. *Applied Energy*, 104(0): 683-710.
- United State Department of Energy. 2006, (2016, March 8). Biodiesel handling and use guideline. *Energy Efficiency and Renewable Energy* Retrieved From <http://www.osti.gov/bridge>
- United States Environmental Protection Agency (EPA). 2002, (2016, October 2). A Comprehensive Analysis of Biodiesel Impacts on Exhaust Emissions. Retrieved From <http://www.epa.gov/otaq/models/analysis/biodsl/p02001.pdf>

- Uzun, B. B., Kılıç, M., Özbay, N., Pütün, A. E. and Pütün, E. (2012). Biodiesel production from waste frying oils: Optimization of reaction parameters and determination of fuel properties. *Energy*, 44(1): 347-351.
- Wan Nor Nadyaini, W. O. and Nor Aishah, S. A. (2011). Optimization of heterogeneous biodiesel production from waste cooking palm oil via response surface methodology. *Biomass and Bioenergy*, 35(3): 1329-1338.
- Wan Omar, W. N. N. and Amin, N. A. S. (2011). Biodiesel production from waste cooking oil over alkaline modified zirconia catalyst. *Fuel Processing Technology*, 92(12): 2397-2405.
- Wen, Z., Yu, X., Tu, S.-T., Yan, J. and Dahlquist, E. (2010). Biodiesel production from waste cooking oil catalyzed by TiO<sub>2</sub>-MgO mixed oxides. *Bioresource Technology*, 101(24): 9570-9576.
- Yaakob, Z., Mohammad, M., Alherbawi, M., Alam, Z. and Sopian, K. (2013). Overview of the production of biodiesel from waste cooking oil. *Renewable and Sustainable Energy Reviews*, 18(0): 184-193.
- Yang, X. (2011). *Modeling and control of SI and SI-HCCI hybrid combustion engines*. Michigan State University: Ph.D Dissertation.
- Zabeti, M., Wan Daud, W. M. A. and Aroua, M. K. (2009). Activity of solid catalysts for biodiesel production: A review. *Fuel Processing Technology*, 90(6): 770-777.
- Zheng, J. (2010). *Use of an Engine Cycle Simulation to Study a Biodiesel Fueled Engine*. Texas A&M University: Master Thesis.
- Zhou, Z. F., Kumar, R., Thakur, S. T., Rudnick, L. R., Schobert, H. and Lvov, S. N. (2007). Direct oxidation of waste vegetable oil in solid-oxide fuel cells. *Journal of Power Sources*, 171(2): 856-860.

## APPENDIX A

### Titration of waste cooking oil

KOH Purity =	90
KOH Base =	7.78
Normality of KOH =	0.1
Weight of sample (gram) =	5

Sample	Repeat	V1,ml of KOH	V2,ml of KOH	AV (mg KOH)	FFA (%)
WCO1	1	5.6	6.3	0.78	0.39
	2	6.3	6.9	0.67	0.34
	3	6.9	7.6	0.78	0.39
	Average			0.75	0.38
WCO2	1	20.0	20.6	0.67	0.34
	2	20.6	21.3	0.78	0.39
	3	21.3	22.1	0.90	0.45
	Average			0.78	0.39
WCO3	1	30.0	30.5	0.56	0.31
	2	30.5	31.3	0.90	0.50
	3	31.3	32.4	1.23	0.68
	Average			0.90	0.50
WCO4	1	40.0	40.7	0.78	0.44
	2	40.7	41.5	0.90	0.50
	3	42.0	42.3	0.34	0.19
	Average			0.67	0.37

Note :

V1 = Initial volume in burette

V2 = Final volume in burette

## APPENDIX B

## Test report of waste cooking oil

 <b>UTM</b> <small>UNIVERSITI TEKNOLOGI MALAYSIA</small> <b>UNIPEM</b> <small>UNIT PERKHIDMATAN MAKMAL</small>	<b>UNIT PERKHIDMATAN MAKMAL (UNIPEM)</b> Laboratory Services Unit Fakulti Kej. Petroleum & Kej. Tenaga Diperbaharui Faculty of Petroleum & Renewable Energy Engineering Universiti Teknologi Malaysia 81310 UTM Johor Bahru, Johor Darul Ta'zim
	tel: 07-5535461      email: unipen2u@petroleum.utm.my      fax: 07-5581463

## TEST REPORT

Report Number: **PTG/2013/22**Page: **1 of 1**

## SAMPLE DESCRIPTIONS

Date: **3.5.2013**

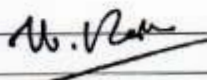
Sample:	Waste Cooking Oil (WCO)
Customer's sample id.:	
Customer Name & Address:	No.4, Jalan Ara 3 Taman Sri Pulai 81110, Johor Attn: Nur Hamzah Said

Job No:	UNIPEM/2013/22
Date Received:	17.4.2013

## TEST REPORT:

No.	Parameter, units	Results	Test Method	Remarks#
1.	Kinematic Viscosity @ 40°C cst	47.51	ASTM D445-94	
	Density @ 15°C, kg/L	917.5	ASTM D1298-85	
	Flash Point (COC), °C	318.0	ASTM D92-90	

Signatory :



Name:

Dr. Mohd. Rashid Bin Mohd. Yusof

No part of this report can be reproduced in any form or by any means, electronic or mechanical including photocopying and recording except in full without the written permission of the issuing laboratory.  
 N.B. # Test method (s) is /are not included under SAMM Scope of Accreditation. Please refer attachment for detail information (if any). This report is strictly limited to the above-mentioned sample.

## APPENDIX C

### Biodiesel production experimental apparatus



## APPENDIX C

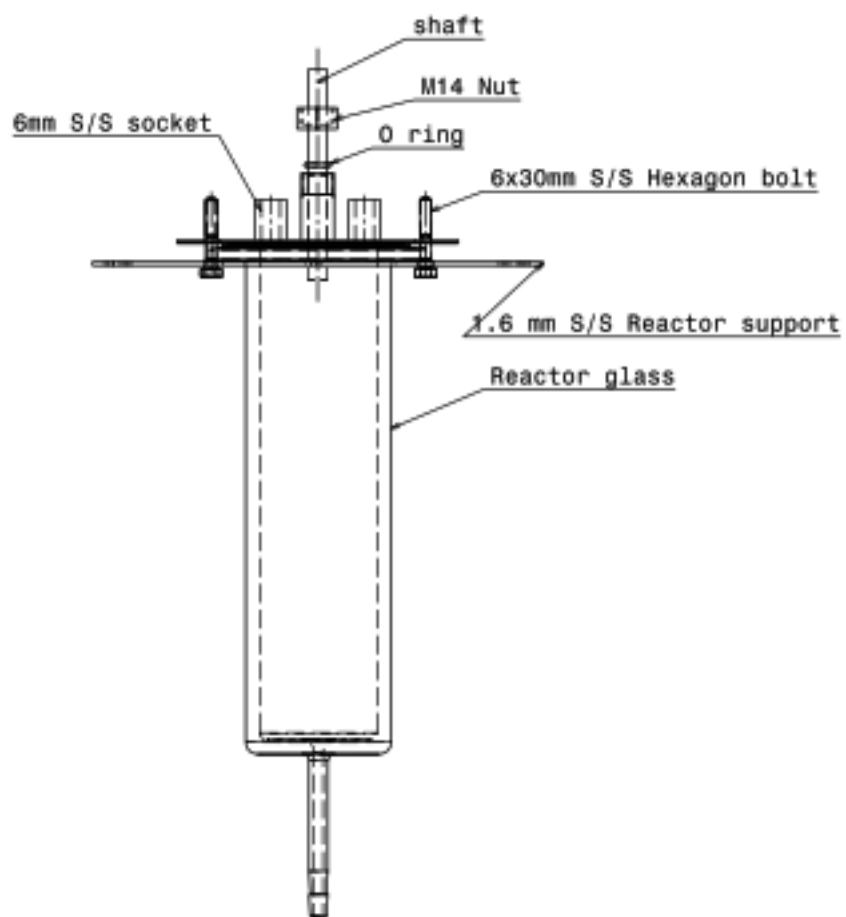
**Biodiesel production experimental apparatus (cont'd)****Table C.1.** Specifications of the reactor and packed-bed stirrer used in this study.

Item	Unit	Value
<b>Reactor</b>		
Material : Borosilicate		
Inner diameter of reactor (di)	mm	50
Outer diameter of reactor (do)	mm	62
Length of reactor , L	mm	210
<b>Bucket</b>		
Material : Plastic		
2 layers plastic net dimension	mm	2 and 4
Shape Ellipse, with 3 fins		
Major radius	mm	20
Minor radius	mm	12.5
Length of packed bed	mm	85



## APPENDIX D

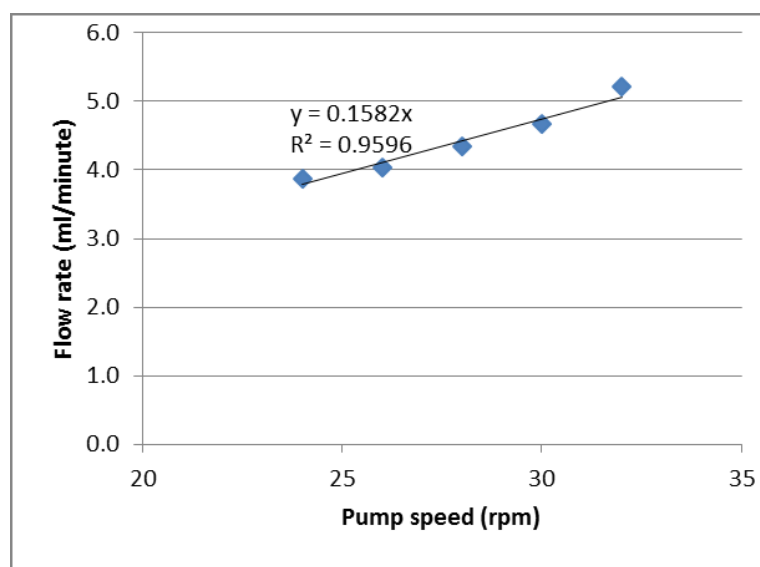
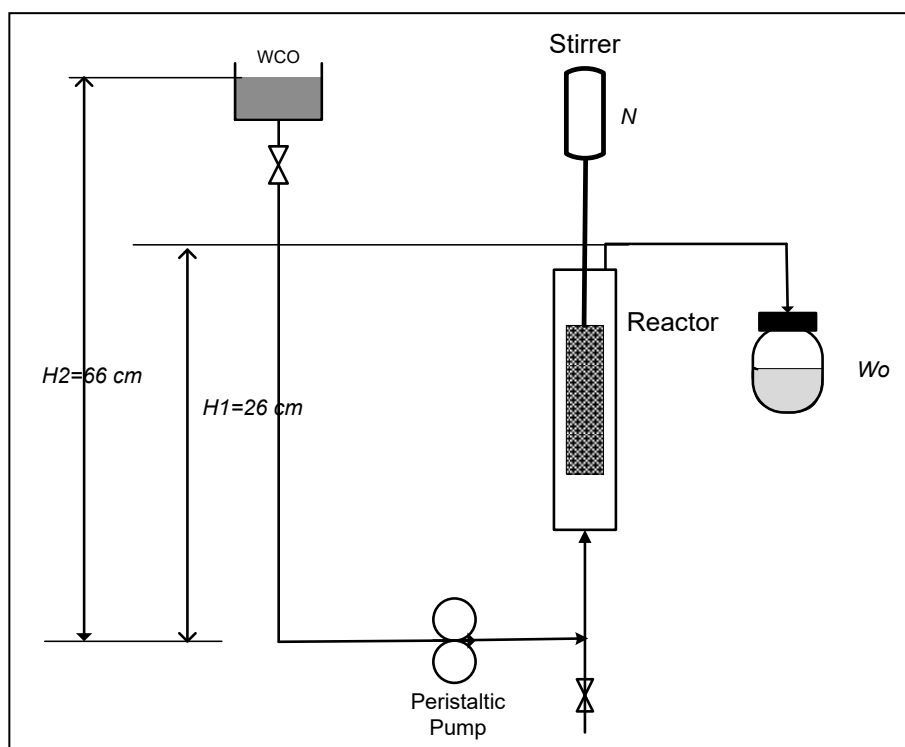
## Reactor and Stirrer Drawing



Front view  
Scale: 1:2



## APPENDIX E

## Peristaltic pump calibration





## APPENDIX F

### Equipment used for biodiesel processing and measuring properties of the raw materials and biodiesel product

Equipment used	Specification and place
	<p>Furnace Carbolite</p> <p>Purpose: Calcination of Catalyst raw material.</p> <p>Maximum temperature = 1200 °C</p> <p>Faculty Mechanical Engineering UTM</p>
	<p>Scale Precision : Precisa Model XT 220A</p> <p>Purpose: Density of Catalyst measurement</p> <p>Science Laboratory Faculty Science, Department Physic UTM</p>

**APPENDIX F****Equipment used for biodiesel processing and measuring properties of raw materials and biodiesel product (Cont'd)**

<b>Equipment used</b>	<b>Specification and place</b>
 A photograph of an Agilent GCMS apparatus. It consists of a large, light-colored main unit with a control panel on the right side featuring a small screen and numerous buttons. To the left of the main unit is a smaller, white, boxy component, likely a detector or part of the gas flow system. The equipment is situated on a dark laboratory bench.	<p>GCMS Apparatus Agilent Technology</p> <p>Analysis Laboratory Faculty Chemical Engineering UTM</p>
 A photograph of a Perkin Elmer GC apparatus. It is a large, grey, rectangular machine with a control panel on top that includes a small display screen and several buttons. The machine is placed on a dark laboratory bench.	<p>GC Apparatus Perkin Elmer Auto system GS FID</p> <p>Analysis Laboratory Faculty Chemical Engineering UTM</p>

## APPENDIX F

**Equipment used for biodiesel processing and measuring properties of  
raw materials and biodiesel product (cont'd)**

Equipment used	Specification and place
	<p>Viscometer Brookfield type DV-II+ Pro.</p> <p>Analysis Laboratory Faculty Chemical Engineering UTM</p>
	<p><b>X-ray Diffraction (XRD)</b> X-ray diffractometer is used to analyse the phase and compound of catalyst.</p> <p>Faculty Mechanical Engineering UTM</p>

## APPENDIX F

### Equipment used for biodiesel processing and measuring properties of raw materials and biodiesel product (cont'd)

Equipment used	Specification and place
	<p>Field emission scanning electron microscope</p> <p>Optical microscopy (Zeiss Axiotech, Germany), Field Emission Electron Microscope (FESEM, VP35 Zeiss Supra, Germany) attached with Dispersive X-ray spectroscope (EDX/EDS)</p> <p>Faculty Mechanical Engineering UTM</p>
	<p>Bomb Calorimeter (IKA C2000 Calorimeter).</p> <p>Faculty Mechanical Engineering UTM</p>

**Appendix G**  
**Standards JCPDS card No. 00-021-0917**

00-021-0917

Mar 20, 2017 4:22 PM (Rigaku)

**Status:** Primary **GM:** Star **Pressure/Temperature:** Ambient **Chemical Formula:** Ca Fe O2  
**Structural Formula:** Fe O · Ca O **Empirical Formula:** Ca Fe O2 **Weight %:** Ca31.33 Fe43.66 O25.01  
**Atomic %:** Ca25.00 Fe25.00 O50.00 **Compound Name:** Calcium Iron Oxide

**Radiation:** CoKα **λ:** 1.7902 Å **Filter:** Fe Beta **Intensity:** Diffractometer

**SY:** Cubic **SPGR:** Fm-3m (225) **Author's Cell [ AuthCell a: 4.762 Å AuthCell Vol: 107.99 Å³ ]**  
**SIPOW:** F(5) = 42.7(0.023, 5) **Temp:** 298.0 K (Ambient temperature assigned by ICDD editor)

**Space Group:** Fm-3m (225) **Molecular Weight:** 127.93  
**Crystal Data [ XlCell a: 4.762 Å XlCell b: 4.762 Å XlCell c: 4.762 Å XlCell : 90.00° XlCell : 90.00°**  
**XlCell : 90.00° XlCell Vol: 107.99 Å³ ] Crystal Data Axial Ratio [ a/b: 1.000 c/b: 1.000 ]**  
**Reduced Cell [ RedCell a: 3.367 Å RedCell b: 3.367 Å RedCell c: 3.367 Å RedCell : 90.00°**  
**RedCell : 90.00° RedCell : 90.00° RedCell Vol: 37.00 Å³ ]**

**Crystal (Symmetry Allowed):** Centrosymmetric

**Subst(s):** Cement and Hydration Product, Common Phase, Inorganic **Pearson Symbol:** cF7 **Entry Date:** 09/01/1971  
**Last Modification Date:** 09/01/2003 **Last Modification:** Quality

**References:**

Type	DOI	Reference
Primary Reference		Allen, U.S. Steel Fundamental Res. Lab. Private Communication.

**Database Comments:** Analysis: Sample contains 10% FeO in solid solution. Composition (%): 72.6 CaO, 21.5 FeO, 4.9 "Fe2 O3".  
 General Comments: Crystals are rounded under microscope. Unit Cell Data Source: Powder Diffraction.

**d-Spacings (θ) - Ca Fe O2 - 00-021-0917 (Std, Fixed SR Intensity) - Cu Kα 1.54060 Å**

2 (°)	d (Å)	I	h	k	l	2 (°)	d (Å)	I	h	k	l	2 (°)	d (Å)	I	h	k	l
32.5326	2.750000	40	1	1	1	54.4754	1.663000	80	2	2	0	68.1962	1.374000	30	2	2	2
37.7673	2.340000	100	2	0	0	64.8787	1.438000	30	2	1	1						

## APPENDIX H

## Fatty acid composition from biodiesel waste cooking oil

Compound Name (CAS)	Compound Name (CAS)	Percentage
Hexadecanoic acid, methyl ester	Palmitic acid C16:0	51.569
6-Octadecenoic acid, methyl ester		12.924
11-Octadecenoic acid, methyl ester		7.708
Pentadecanoic acid, 14-methyl-, methyl ester	C15:0	4.629
Octasiloxane, 1,1,3,3,5,5,7,7,9,9,11,11,13,13,15,15- hexadecamethyl-		3.856
9-Octadecenoic acid (Z)-, methyl ester		2.943
Heptasiloxane, 1,1,3,3,5,5,7,7,9,9,11,11,13,13- tetradecamethyl-		2.111
Methyl tetradecanoate	Myristic acid	1.676
Methyl hexadec-9-enoate		1.388
Benzo[h]quinoline, 2,4-dimethyl-		1.078
1,2-Benzenediol, 3,5-bis(1,1-dimethylethyl)		0.893
Nonanoic acid, 9-oxo-, methyl ester		0.769
Methyl 10-methyl-dodecanoate		0.687
Dodecanoic acid, methyl ester	Lauric acid C12:0	0.631
Tetradecanoic acid, 10,13-dimethyl-, methyl ester		0.588
2,4-Cyclohexadien-1-one, 3,5-bis(1,1- dimethylethyl)-4-hydroxy-		0.530



## APPENDIX H

## Fatty acid composition from biodiesel waste cooking oil (cont'd)

Compound Name (CAS)	Compound Name (CAS)	Percentage
Tridecanoic acid, methyl ester		0.427
Indole-2-one, 2,3-dihydro-N-hydroxy-4-methoxy-3,3-dimethyl-		0.378
Cyclotrisiloxane, hexamethyl-		0.300
Tetradecanoic acid, 5,9,13-trimethyl-, methyl ester		0.282
3-Octadecenoic acid, methyl ester		0.253
9H-Fluorene-2-carboxylic acid, 9-oxo-, (2-hydroxyethyl)(methyl)amide		0.228
Hexadecanoic acid, 15-methyl-, methyl ester		0.219
Cyclopentaneundecanoic acid, methyl ester		0.192
Cyclopentanetridecanoic acid, methyl ester		0.166
Pyridine, 1,2,3,6-tetrahydro-1-methyl-4-[4-chlorophenyl]-		0.159
Silicic acid, diethyl bis(trimethylsilyl) ester		0.154
Tetradecanoic acid, 12-methyl-, methyl ester	C14:0	0.150
Octanoic acid, methyl ester		0.121
Tridecanoic acid, 12-methyl-, methyl ester		0.107
5-Octadecenoic acid, methyl ester		0.097
2-Methyl-7-phenylindole		0.093
2-(Acetoxymethyl)-3-(methoxycarbonyl)biphenylene		0.083

## APPENDIX H

## Fatty acid composition from biodiesel waste cooking oil (cont'd)

Compound Name (CAS)	Compound Name (CAS)	Percentage
Heptadecanoic acid, 16-methyl-, methyl ester		0.082
Acetamide, N-[4-(trimethylsilyl)phenyl]-		0.076
trans-13-Octadecenoic acid, methyl ester		0.068
Decanoic acid, methyl ester		0.061
10-Undecenoic acid, methyl ester		0.050
Methyl 13-cyclopentyltridecanoate		0.044
1H-Indole, 1-methyl-2-phenyl-		0.036
Heneicosanoic acid, methyl ester		0.030
Phenol, 2,4-bis(1,1-dimethylethyl)-		0.024
6-Octadecenoic acid, methyl ester, (Z)-		0.018
Heptadecanoic acid, 14-methyl-, methyl ester, (.+/-.)-		0.016
cis-13-Octadecenoic acid, methyl ester		0.014
<b>TOTAL</b>		<b>97.908</b>

## APPENDIX I

## Petron Diesel Max (PDM) specification



## Product Data Sheet

# PETRON Diesel Max

## DESCRIPTION

Petron B7 Diesel Max is a premium diesel fuel with 7% Palm Oil Methyl Ester (POME). It contains robust and multifunctional detergent additive and a smoke reducing agent to provide improved fuel economy and reduced exhaust emissions.

It also has the ability to maintain and improve fuel injection system cleanliness through unsurpassed detergency characteristics

Petron Diesel with its advanced additive technology provides the following performance benefits:

- Optimum cleaning action
- Power loss control
- Improved fuel economy
- Reduced exhaust emissions
- Improved oxidation stability
- Excellent protection against corrosion

## APPLICATION

- For high-speed automotive diesel engines

## TYPE/QUALITY LEVEL

- Distillate fuel with additive

## AVAILABLE PACKAGES


- Bulk

## TYPICAL CHARACTERISTICS

Density at 15°C, kg/l	0.8314
Color, ASTM	L 1.0
Kinematic Viscosity at 40°C, cSt	2.900
Flash Point, °C, PMCC	63.0
Sediments & Water, Vol. %	0.00
Sulfur, ppm	330
Cetane Number	54.0
Copper Corrosion, 3 hrs. at 100°C	1a
Lubricity, HFRR @ 60°C	
Wear Scar diameter, microns	240
CCR on 10% Bottoms, Mass %	0.04
Ash, Mass %	<0.01
Distillation: °C	
95% Recovery	369.0
FAME Content, % vol.	7.0
Cloud Point	13
Oxidation Stability, mg/100ml	0.9
Electrical Conductivity, PS/M	243

## APPENDIX J


## Biodiesel from palm oil specification



[HOME](#)
[CORPORATE PROFILE](#)
[PRODUCTS](#)
[OUR FACILITY](#)

[PRODUCTS](#)
[VANCE BIODIESEL](#)

EN 14214 Specifications




- [Vance Biodiesel](#)
- [Information on Biodiesel](#)
- [EN 14214 Specifications](#)
- [Vance's Profile in Biofuels International Magazine](#)



✿

### Vance Biodiesel EN 14214:2012

Property	Unit	Test Method	Specification
Ester content	% (m/m)	EN 14103-03	96.5 min
Density at 15°C	kg/m <sup>3</sup>	EN ISO 12185-96 EN ISO 3675	860 – 900
Kinematic viscosity at 40°C	mm <sup>2</sup> /s	EN ISO 3104-94	3.5 – 5.0
Flash point	°C	EN ISO 2719-02 EN ISO 3679	101 min
Sulfur content	mg/kg	EN ISO 20846-04 EN ISO 20884 EN ISO 13032	10 max
Cetane Number	–	EN ISO 5165	51 min
Sulfated ash content	% (m/m)	ISO 3987-94	0.02 max
Water content	mg/kg	EN ISO 12937-00	500 max
Total Contamination	mg/kg	EN 12662-98	24 max
Copper Strip Corrosion (3 hours at 50°C)	Rating	EN ISO 2160-98	Class 1 max
Oxidation stability , 110°C (accelerated oxidation)	hours	EN 14112-03	8 min
Acid value	mg KOH/g	EN 14104-03	0.5 max
Iodine value	g iodine/100g	EN 14111-03 EN 16300	120 max
Linolenic acid methyl ester	% (m/m)	EN 14103-03	12 max
Polyunsaturated (>= 4 Double bonds) methyl ester	% (m/m)	EN 15779	1 max
Methanol content	% (m/m)	EN 14110-03	0.2 max
Monoglyceride content	% (m/m)	EN 14105-03	0.7 max
Diglyceride content	% (m/m)	EN 14105-03	0.2 max
Triglyceride content	% (m/m)	EN 14105-03	0.2 max
Free glycerine	% (m/m)	EN 14105-03	0.02 max
Total glycerine	% (m/m)	EN 14105-03	0.25 max
Group I metals (Na + K)	mg/kg	EN 14108/9 EN 14538	5 max
Group II metals (Ca + Mg)	mg/kg	EN 14538	5 max
Phosphorus content	mg/kg	EN 14107 FprEN 16294	4 max
Cold Filter Plugging Point	°C	EN 116	+15 max



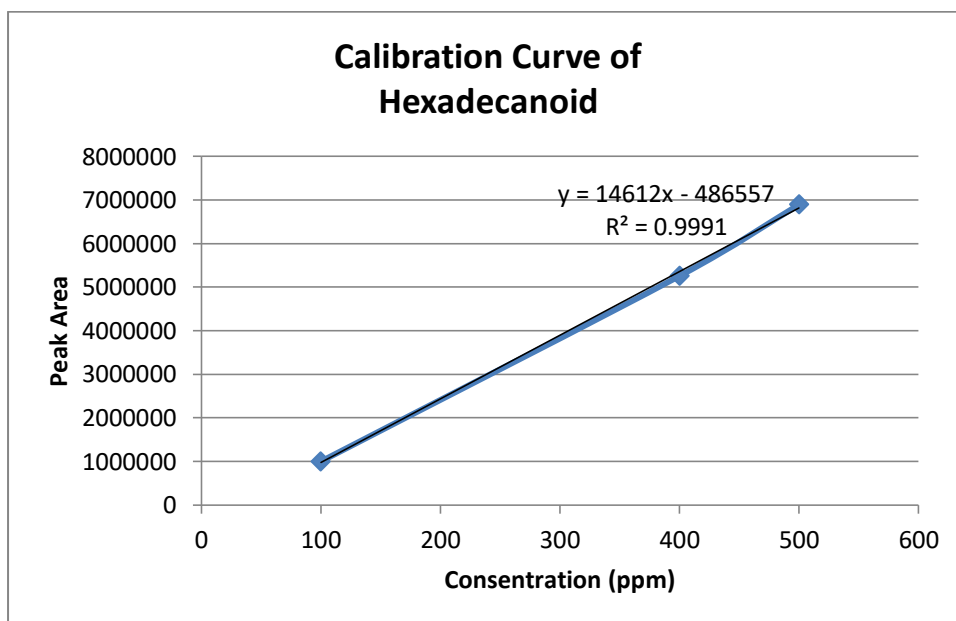
Roundtable on Sustainable Palm Oil

## APPENDIX K

### Standard hexadecanoid calibration

The standard preparation for this technique consists of the dilution of the FAME standard into 4 mL of n-heptane. The sample preparation is also quite simple with 100  $\mu\text{L}$  of biodiesel feedstock into 4 mL of n-heptane. In both cases, a 1- $\mu\text{L}$  injection at a split of 50:1 was performed.



#### Conversion Calculation

$$\text{Concentration} = \frac{\text{Peak Area} + 486557}{14612}$$

## APPENDIX L

### Experimental Procedures of Diesel Engine Test

To complete the experiment successfully, some procedures must be performed such as preparation before running the engine, running the engine and perform the experiment.

Several items are checked prior before run the engine. They are:

- (i). The fan blower in engine room is switched on during the engine tests.
- (ii). Fill the test fuel about 1.2 litres into the fuel tank. Make sure the tank valve and burette valve are opened so the test fuel flow to the fuel pump.
- (iii). Ensure the oil level of lubricating oil is within the range.
- (iv). Water is fed to the dynamometer by opening the dynamometer supply valve.
- (v). Water is supplied to the pressure transducer in cylinder head by opening the in-cylinder pressure transducer cooling valve. This is very important to prevent damage to pressure transducer due to overheating.
- (vi). The exhaust ventilation system is switched on to vent out the exhaust gases.
- (vii). Warm up the exhaust emission analyser for 10 minutes by switch on this equipment.
- (viii). Switch on the computers for the data acquisition system.
- (ix). Adjust the dynamometer controller to zero load.

The following procedures are strictly followed to run the engine:

- (i). The engine is switched on.
- (ii). Warm the engine at idling speed of 850 rpm at least 3 minutes according to the manufacturer's recommendation. Check the controller

of dynamometer and make sure it was set to zero load by the warming period.

To measure the performance and emission of a diesel engine, it must use a constant speed mode, while for testing the engine performed the following procedures:

- (i). After the engine is warmed, the engine speed is raised slowly until it reaches the round of 2500 rpm.
- (ii). Allow the engine to run at 2500 rpm for a few minutes before the loading process is carried on the engine.
- (iii). Perform the load with 3 N.m brake torque on to the engine by adjusting the load adjustor on the dynamometer controller. In this process, the engine speed will slow down, so that engine speed should be increased to 2500 rpm by adjusting the throttle adjustor.
- (iv). After reaching the speed of 2500 rpm and torque of 3 Nm, then according to the SAE standard, the speed and torque conditions are maintained within 1% and the exhaust gas temperature is maintained within  $\pm 2$  °C for at least 1 minute.
- (v). Once the engine is stabilized, adjust the valve on the burette so that the fuel flows into the engine only from the burette. Record time used to consume fuel volume of 5 cc. Record the readings of atmospheric pressure, ambient temperature and humidity, differential pressure on the manometer, and temperature scanner reading such as intake air, engine block, exhaust manifold and exhaust gas.
- (vi). Exhaust emission readings are recorded.
- (vii). After the procedure (i) to (vi) is completed, perform step (iii) to (vi) for the next engine torque. After the engine test is complete, reduce the load and rotation by adjusting the load adjustor and throttle adjustor, respectively to achieve idling speed and zero load for 5 minutes.
- (viii). Switch off the engine.

The pressure inside cylinder and cylinder volume is recorded using a data acquisition system connected to a computer using DeweCA software. The following procedure is used to record pressure data on the cylinder:

- (i). Double clicking the icon *DeweCA* on the computer desktop to open DeweCA software.
- (ii). Clicking the 'Record' button to record all the measured data.
- (iii). The 'Stop' button is clicked after recording process is finished.
- (iv). The data of combustion in-cylinder such as pressure against the crank angle and cylinder volume versus the crank angle are exported to the *MS Excel* software for data analysis.

The exhaust emission analyser and smoke meter are used to measure exhaust gas constituents and smoke density. The following procedures are strictly followed:

- (i). The emission analyser probe is inserted into the end of the exhaust tail pipe.
- (ii). All the measured emissions data are recorded after the readings become stable. The duration of measurement takes about 2 minutes.
- (iii). After the exhaust gas sampling is finished, the emission analyser probe is removed from the tail pipe.
- (iv). Subsequently, the *BOSCH* smoke meter probe is positioned into the end of the exhaust tail pipe (i.e. the same location as emission analyser probe).
- (v). Only one sample of measurements is taken using smoke meter sampling pump type.
- (vi). After the smoke measurements are finished, the *BOSCH* smoke meter probe is removed from the tail pipe. Then the filter paper filter are matched with the colour standards for indexing smoke number.



**APPENDIX M. Experimental data of diesel engine testing**

Engine Performance Test								Date	28-Feb-17				Fuel :		Petron Diesel Max			
								Time	10:00 AM				Engine Speed :		2500 rpm			
Torque Actual (N.m)	Torque Display (N.m)	Fuel Consumption		Air Consumption				Temperature Display (°C)				Gas Emission						
		Volume (ml)	Time (s)	Amb. Press. (mbar)	Amb. Temp. (°C)	Δ H (mmH <sub>2</sub> O)	Humi- dity (% RH)	T1	T2	T3	T4	HC (ppm)	CO <sub>2</sub> (%)	NO <sub>x</sub> (ppm)	CO (%)	O <sub>2</sub> (%)	Smoke No.	
3.0	1.2	5	34.76	1006	26.5	10.54	80	25	61	277	75	11.4	1.2	36	0.08	3.4	3	
		5	34.13	1006	26.5	10.55	80	26	61	277	75	11.3	1.3	38	0.07	3.4		
		5	33.33	1006	26.5	10.54	80	26	61	278	76	11.5	1.3	40	0.08	3.5		
Average		5	34.07	1006	26.5	10.54	80	26	61	277	75	11.4	1.3	38	0.08	3.4	3	
5.0	2.0	5	27.94	1005	26.7	10.58	80	29	64	331	83	11.8	1.5	49	0.09	3.3	5	
		5	27.87	1005	26.7	10.60	80	27	64	332	83	11.6	1.7	53	0.1	3.2		
		5	29.23	1005	26.7	10.50	80	28	64	330	82	11.9	1.8	55	0.09	3.4		
Average		5	28.35	1005	26.7	10.56	80	28	64	331	83	11.8	1.7	52	0.09	3.3	5	
7.0	2.8	5	24.15	1005	27.1	10.16	79	30	70	398	98	13.0	2.1	58	0.1	3.1	7	
		5	23.14	1005	27.1	10.16	79	30	70	398	98	14.0	2.2	62	0.1	3.2		
		5	22.94	1005	27.1	10.16	79	30	70	398	98	13.0	2.0	63	0.1	3.1		
Average		5	23.41	1005	27.1	10.16	79	30	70	398	98	13.3	2.1	61	0.1	3.1	7	
9.0	3.6	5	20.64	1005	27.3	9.55	79	30	78	458	122	15.1	2.8	70	0.11	2.9	7	
		5	20.90	1005	27.3	9.55	79	30	78	458	123	15.0	2.6	73	0.12	2.8		
		5	18.61	1005	27.3	9.55	79	30	78	458	122	15.2	2.8	75	0.1	2.9		
Average		5	20.05	1005	27.3	9.55	79	30	78	458	122	15.1	2.7	73	0.11	2.9	7	
10.0	4.0	5	16.91	1005	27.7	9.61	79	30	92	484	129	15.7	3.1	90	0.14	2.5	9	
		5	18.10	1005	27.7	9.61	79	30	92	484	129	15.7	3.2	91	0.12	2.6		
		5	16.47	1005	27.7	9.61	79	30	92	484	130	15.7	3.0	96	0.13	2.4		
Average		5	17.16	1005	27.7	9.61	79	30	92	484	129	15.7	3.1	92	0.13	2.5	9	

Note : TDC = 109.6

T1 = Intake Air Temperature    T3 = Exhaust Manifold Temperature  
T2 = Engine Block Temperature    T4 = Exhaust Gas Temperature

**APPENDIX M. Experimental data of diesel engine testing (cont'd)**

Engine Performance Test								Date	1-Mar-17				Fuel :	BP10				
								Time	10:10 AM				Engine Speed :	2500 rpm				
Torque Actual (N.m)	Torque Display (N.m)	Fuel Consumption		Air Consumption				Temperature Display (°C)				Gas Emission						
		Volume (ml)	Time (s)	Amb. Press. (mbar)	Amb. Temp. (°C)	Δ H (mmH <sub>2</sub> O)	Humidity (% RH)	T1	T2	T3	T4	HC (ppm)	CO <sub>2</sub> (%)	NO <sub>x</sub> (ppm)	CO (%)	O <sub>2</sub> (%)	Smoke No.	
3.0	1.2	5	31.90	1006	25	9.80	80	26	54	256	64	10.9	1.0	47	0.06	3.87	3	
		5	32.19	1006	25	9.86	80	26	54	254	65	10.8	1.1	48	0.07	3.88		
		5	32.32	1006	25	9.99	80	26	54	255	64	11	1.2	48	0.07	3.86		
Average		5	32.14	1006	25	9.88	80	26	54	255	64.3	10.9	1.1	47.7	0.07	3.87	3	
5.0	2.0	5	25.83	1006	26	9.40	80	27	63	326	87	11.4	1.6	60	0.08	3.7	6	
		5	25.94	1006	26	9.71	80	27	63	323	88	11.5	1.4	67	0.09	3.3		
		5	26.01	1006	26	9.83	80	27	63	326	93	11.4	1.6	65	0.07	3.9		
Average		5	25.92	1006	26	9.65	80	27	63	325	89.3	11.4	1.53	64.0	0.08	3.63	6	
7.0	2.8	5	21.81	1006	25	9.50	80	27	65	389	99	11.8	1.9	72	0.08	3.6	7	
		5	21.31	1006	26	9.50	80	27	66	390	100	12.2	2.1	72	0.09	3.6		
		5	21.18	1006	26	9.80	80	27	66	390	100	13.1	2.1	74	0.08	3.7		
Average		5	21.43	1006	25.67	9.60	80	27	65.7	390	99.7	12.4	2.03	72.7	0.08	3.63	7	
9.0	3.6	5	17.84	1006	26	9.30	80	28	70	456	113	13.5	2.6	81	0.09	3.4	8	
		5	18.01	1006	26	9.40	80	28	71	459	113	13.6	2.8	85	0.09	3.2		
		5	17.34	1006	26	9.56	80	28	71	459	116	13.2	2.7	86		3.6		
Average		5	17.73	1006	26	9.42	80	28	70.7	458	114	13.4	2.7	84	0.09	3.4	8	
10.0	4.0	5	15.51	1006	26	8.70	80	28	76	493	129	14.8	3.1	101	0.12	3.2	9	
		5	15.50	1006	26	8.80	80	28	78	535	491	14.4	3	103	0.14	3.1		
		5	15.41	1006	26	8.00	80	29	77	535	328	14.1	3	104	0.11	3.3		
Average		5	15.47	1006	26	8.50	80	28	77	521	316	14.4	3.03	103	0.12	3.2	9	

Note :

T1 = Intake Air Temperature  
T2 = Engine Block Temperature

T3 = Exhaust Manifold Temperature  
T4 = Exhaust Gas Temperature

**APPENDIX M. Experimental data of diesel engine testing (cont'd)**

Engine Performance Test								Date	1-Mar-17				Fuel :	BP20			
								Time	11:35 AM				Engine Speed :	2500 rpm			
Torque Actual (N.m)	Torque Display (N.m)	Fuel Consumption		Air Consumption				Temperature Display (°C)				Gas Emission					
		Volume (ml)	Time (s)	Amb. Press. (mbar)	Amb. Temp. (°C)	Δ H (mmH <sub>2</sub> O)	Humidity (% RH)	T1	T2	T3	T4	HC (ppm)	CO <sub>2</sub> (%)	NO <sub>x</sub> (ppm)	CO (%)	O <sub>2</sub> (%)	Smoke No.
3.0	1.2	5	31.23	1006	26	10.01	80	26	54	253	64	11	1.0	54	0.06	4.2	3
		5	32.096	1006	26	9.81	80	26	54	253	65	10	1.0	53	0.07	4.3	
		5	32.007	1006	26	9.96	80	26	54	235	64	11	1.1	53	0.06	4.1	
Average		5	31.778	1006	26	9.93	80	26	54	247	64	11	1.0	53	0.06	4.2	3
5.0	2.0	5	25.23	1006	25.5	9.62	80	27	63	321	82	12	1.4	69	0.07	4.1	6
		5	25.21	1006	25.9	9.40	80	27	64	323	88	11	1.5	73	0.08	4.1	
		5	26.14	1006	25	10.10	80	27	63	324	82	12	1.5	71	0.07	4.0	
Average		5	25.527	1006	25.47	9.71	80	27	63	323	84	12	1.5	71	0.07	4.1	6
7.0	2.8	5	20.67	1006	27	9.90	80	27	66	387	99	12	2.0	80	0.07	3.9	7
		5	20.37	1006	27	9.10	80	27	66	388	100	14	1.9	81	0.08	3.7	
		5	21.398	1006	27	9.50	80	27	66	388	99	13	1.7	82	0.09	4.0	
Average		5	20.813	1006	27	9.50	80	27	66	388	113	13	1.9	81	0.08	3.9	7
9.0	3.6	5	17.16	1006	27	9.70	80	28	70	453	103	14	2.4	96	0.08	3.7	8
		5	17.24	1006	26.9	9.10	80	28	71	453	105	14	2.5	95	0.09	3.7	
		5	17.12	1006	27.3	9.40	80	28	71	454	109	15	2.6	97	0.09	3.8	
Average		5	17.173	1006	27.07	9.40	80	28	71	453	106	14	2.5	96	0.09	3.7	8
10.0	4.0	5	15	1006	27	8.31	80	28	76	493	129	15	2.9	112	0.10	3.4	8
		5	15.02	1006	28	8.82	80	29	78	512	491	15	2.9	115	0.10	3.5	
		5	15.04	1006	27.1	8.57	80	29	78	513	328	14	2.8	118		3.3	
Average		5	15.02	1006	27.37	8.57	80	29	77	506	316	15	2.9	115	0.10	3.4	8

Note :

T1 = Intake Air Temperature    T3 = Exhaust Manifold Temperature  
T2 = Engine Block Temperature    T4 = Exhaust Gas Temperature

**APPENDIX M. Experimental data of diesel engine testing (cont'd)**

Engine Performance Test								Date	1-Mar-17				Fuel :	BW10			
								Time	10:20 AM				Engine Speed :	2500 rpm			
Torque Actual (N.m)	Torque Display (N.m)	Fuel Consumption		Air Consumption				Temperature Display (°C)				Gas Emission					
		Volume (ml)	Time (s)	Amb. Press. (mbar)	Amb. Temp. (°C)	Δ H (mmH <sub>2</sub> O)	Humidity (% RH)	T1	T2	T3	T4	HC (ppm)	CO <sub>2</sub> (%)	NO <sub>x</sub> (ppm)	CO (%)	O <sub>2</sub> (%)	
3.0	1.2	5	30.32	1006	25.9	9.70	85	27	51	254	67	9	0.9	60	0.05	3.9	4
		5	30.85	1006	26.1	9.82	85	27	51	260	68	11	0.9	62	0.04	3.9	
		5	30.20	1006	26.2	9.80	85	27	53	266	81	10	0.8	63	0.05	3.9	
Average		5	30.46	1006	26.07	9.77	85	27	52	260	72	10	0.9	62	0.05	3.9	4
5.0	2.0	5	24.52	1006	26.2	9.60	85	28	58	322	83	12	1.2	78	0.06	3.8	5
		5	24.31	1006	26.2	9.70	85	27	59	322	85	10	1.3	80	0.05	3.7	
		5	24.50	1006	26.3	9.40	85	28	59	323	86	11	1.4	80	0.05	3.5	
Average		5	24.44	1006	26.23	9.57	85	28	59	322	85	11	1.3	79	0.05	3.7	5
7.0	2.8	5	19.87	1006	26.5	9.40	85	28	66	441	98	12	1.6	93	0.06	3.7	7
		5	20.02	1006	26.5	9.20	85	28	66	442	100	11	1.9	95	0.07	3.5	
		5	20.01	1006	26.5	9.50	85	28	67	443	100	12	1.8	95		3.7	
Average		5	19.97	1006	26.5	9.37	85	28	66	442	99	12	1.8	94	0.07	3.6	7
9.0	3.6	5	16.21	1006	26.6	9.12	85	28	68	449	125	14	2.2	104	0.07	3.4	8
		5	16.16	1006	26.6	9.26	85	28	68	458	132	12	2.3	107	0.07	3.5	
		5	16.99	1006	26.6	9.61	85	28	67	460	135	13	2.3	107		3.2	
Average		5	16.45	1006	26.6	9.33	85	28	68	456	131	13	2.3	106	0.07	3.4	8
10.0	4.0	5	14.00	1006	27.5	8.11	85	28	72	470	125	14	2.6	121	0.09	3.3	8
		5	14.50	1006	27.5	8.45	85	28	72	472	129	14	2.7	121	0.09	3.6	
		5	15.00	1006	27.5	8.23	85	28	72	501	148	15	2.7	123		3.1	
Average		5	14.50	1006	27.5	8.26	85	28	72	481	134	14	2.7	122	0.09	3.3	8

Note :

T1 = Intake Air Temperature

T2 = Engine Block Temperature

T3 = Exhaust Manifold Temperature

T4 = Exhaust Gas Temperature

**APPENDIX M. Experimental data of diesel engine testing (cont'd)**

Engine Performance Test								Date	1-Mar-17				Fuel :	BW20				
								Time	11:35 AM				Engine Speed :	2500 rpm				
Torque Actual (N.m)	Torque Display (N.m)	Fuel Consumption		Air Consumption				Temperature Display (°C)				Gas Emission						
		Volume (ml)	Time (s)	Amb. Press. (mbar)	Amb. Temp. (°C)	Δ H (mmH <sub>2</sub> O)	Humidit (% RH)	T1	T2	T3	T4	HC (ppm)	CO <sub>2</sub> (%)	NO <sub>x</sub> (ppm)	CO (%)	O <sub>2</sub> (%)		
3.0	1.2	5	31.23	1006	27	9.87	80	28	54	281	396	7	2.5	67	0.03	3.3	4	
		5	30.77	1006	27.2	9.88	79	29	59	283	397	9	2.4	68	0.05	3.7		
		5	30.99	1006		9.86	79	29	63	295	396	10	2.6	70	0.04	3.6		
Average		5	31.00	1006	27.1	9.87	79.3	29	59	286	396	8.7	2.5	68.3	0.04	3.53	4	
5.0	2.0	5	24.50	1006	27.4	9.74	79	29	59	357	359	8	3.3	85	0.04	3.6	6	
		5	24.43	1006	27.4	9.71	79	29	63	358	360	6	3.3	81	0.03	3.5		
		5	24.46	1006	27.4	9.78	79	29	61	356	359	9	3.4	88	0.04	3.3		
Average		5	24.46	1006	27.4	9.7433	79	29	61	357	359	7.7	3.33	84.7	0.04	3.47	6	
7.0	2.8			<b>Engine shut down at 2300 rpm</b>														
Average																		

Note :                    T1 = Intake Air Temperature                    T3 = Exhaust Manifold Temperature  
                                   T2 = Engine Block Temperature                    T4 = Exhaust Gas Temperature

**APPENDIX M. Experimental data of diesel engine testing (cont'd)**

FUEL	TOR	N	Max_1	AMax_1	dpMax_1	AdpMax_1	Pcorr_1	E05_1	E10_1	E50_1	E90_1	EX_1	EXave_1
		Rpm	bar	°CA	dp/d°CA	°CA	bar	°CA	°CA	°CA	°CA	°CA	°CA
PDM	3	2552.328	59.49853	10.00001	0.401715	12.80001	-9.89348	3.363431	4.589311	9.412642	25.81126	9.412642	9.423798
	5	2505.285	60.42465	9.600005	0.368863	12.40001	-8.09982	4.026039	4.802843	10.77161	29.08846	10.77161	10.93426
	7	2517.57	60.86513	9.200006	0.323382	12.80001	-10.2322	3.724259	4.533462	13.64853	32.22537	13.64853	13.58969
	9	2515.347	61.06866	7.600006	0.321546	2.000005	-10.4055	3.427768	4.225998	16.05237	40.01556	16.05237	16.10128
	10	2303.957	60.43389	9.600005	0.284285	3.200006	-10.2272	2.997408	4.019063	14.05454	31.50764	14.05454	14.08043
BP10	3	2521.489	59.45427	8.800006	0.224408	2.400005	-10.2709	3.616304	4.263681	9.758104	26.13326	9.758104	10.58114
	5	2514.168	59.1775	9.200006	0.239073	3.600005	-10.08	4.2472	4.918778	12.37899	29.61604	12.37899	12.48557
	7	2491.495	59.63186	8.000006	0.228404	10.40001	-10.1993	3.877298	4.573778	14.69269	34.25486	14.69269	14.79698
	9	2527.296	60.4066	7.600006	0.282802	1.600005	-10.4717	3.556001	4.379925	16.43103	41.30279	16.43103	16.56214
	10	2420.875	59.70483	9.200006	0.121028	1.200005	-10.3804	3.491592	4.513689	15.00032	33.59795	15.00032	15.29113
BP20	3	2502.486	58.68777	9.200006	0.326195	4.400005	-10.7721	3.84549	4.533984	9.289516	24.63356	9.289516	9.323485
	5	2499.97	58.87574	9.200006	0.301776	4.400005	-10.0264	3.761334	4.519757	10.29256	26.68639	10.29256	10.52572
	7	2532.705	59.42996	8.400005	0.322059	3.600005	-10.3713	3.743018	4.356682	13.73709	30.27969	13.73709	13.69952
	9	2276.056	59.69279	8.400005	0.288701	2.400005	-10.2648	3.477066	4.218179	14.17842	30.65642	14.17842	14.22104
	10	2437.071	59.91058	7.600006	0.348183	2.000005	-10.7226	3.382535	4.19542	15.6607	33.57402	15.6607	15.73448
BW10	3	2492.544	59.25613	8.400005	0.315257	4.000005	-10.2648	3.853851	4.416375	9.288819	25.59093	9.288819	10.09764
	5	2507.443	59.38049	11.20001	0.382425	14.40001	-8.80114	3.104437	5.176565	10.39323	25.0575	10.39323	10.4064
	7	2505.388	59.82833	11.20001	0.343941	14.40001	-10.2621	2.350684	4.819991	10.96205	26.57188	10.96205	10.99804
	9	2508.934	60.69836	11.20001	0.335431	4.800005	-10.5595	3.034685	4.892489	12.12516	28.53783	12.12516	12.16838
	10	2473.471	60.29212	10.40001	0.281014	4.400005	-10.394	3.112581	4.612915	13.70449	29.95955	13.70449	13.70176
BW20	3	2518.512	57.02825	12.00001	0.337342	15.60001	-10.4981	0.776759	4.402721	10.41267	23.75517	10.41267	10.41076
	5	2504.251	54.70133	12.80001	0.299575	15.60001	-10.6294	1.480533	5.479766	12.04836	28.03976	12.04836	12.08175
	7												

**APPENDIX M. Experimental data of diesel engine testing (cont'd)**

FUEL	TORQUE	EXmax_1	EXmin_1	EXstd_1	SOC_1	EOC_1	DOC_1	IMEP_1	PMEP_1	NMEP_1	MF_1	IWork_1	IPower_1	ITorqu_1
		°CA	°CA	°CA	°CA	°CA	°CA	bar	bar	bar		J	kW	Nm
PDM	3	10.23308	8.807532	0.277755	-2.68831	30.05124	32.73956	4.415681	-0.17761	4.238067	0	130.752	2.781016	10.41019
	5	14.19379	9.744236	0.831707	1.935301	34.07354	32.13824	4.858991	-0.17896	4.680027	0	143.8787	3.00381	11.45531
	7	15.29467	11.18483	0.834197	2.111939	37.8714	35.75946	5.441178	-0.19739	5.243784	0	161.1178	3.380211	12.82785
	9	17.63261	14.92857	0.59502	2.332867	49.65688	47.32401	5.283598	-0.18513	5.09847	0	156.4517	3.279419	12.45635
	10	14.98501	13.22018	0.363157	-0.28751	37.26769	37.5552	6.754754	-0.13463	6.620127	0	200.0139	3.840195	15.92467
BP10	3	14.05805	8.245218	1.626324	2.639502	30.41613	27.77663	3.725314	-0.1864	3.53891	0	110.3096	2.317871	8.782614
	5	15.20203	9.841605	1.541628	3.097896	34.83813	31.74023	4.326052	-0.19478	4.131268	0	128.098	2.683832	10.19888
	7	17.5155	11.90402	1.303435	2.802254	40.77183	37.96957	4.568407	-0.19292	4.375487	0	135.2743	2.808628	10.77025
	9	19.25206	13.97591	1.160152	2.374111	52.33425	49.96014	5.145943	-0.20943	4.936508	0	152.3756	3.209153	12.13182
	10	19.2874	13.08972	1.323056	1.655346	39.86557	38.21022	6.327728	-0.16795	6.159776	0	187.3693	3.77998	14.91794
BP20	3	11.2928	8.307227	0.461934	2.546808	28.19777	25.65096	3.463757	-0.00787	3.455887	0	102.5647	2.138889	8.165981
	5	12.82217	9.221385	0.855105	2.0517	30.84909	28.79739	4.08657	-0.00514	4.081435	0	121.0067	2.520944	9.634294
	7	15.17679	11.24576	0.719038	2.745135	34.81117	32.06603	4.287965	-0.03487	4.253094	0	126.9702	2.679817	10.10909
	9	15.63243	12.81019	0.562344	2.266061	35.44442	33.17836	5.277971	0.022786	5.300757	0	156.2851	2.96428	12.44308
	10	16.93079	14.47862	0.511262	2.315811	38.99796	36.68214	5.17234	-0.02941	5.142928	0	153.1573	3.11046	12.19405
BW10	3	12.87522	8.339374	1.430133	2.805583	29.8105	27.00492	3.41129	-0.08918	3.322114	0	101.0111	2.098122	8.042288
	5	11.05201	9.649601	0.26124	-3.8631	28.70272	32.56583	4.935378	-0.10632	4.829058	0	146.1406	3.05366	11.6354
	7	12.21225	10.04635	0.358938	-5.58951	30.99596	36.58547	5.682062	-0.12921	5.552855	0	168.2505	3.512774	13.39574
	9	13.74963	11.35454	0.439634	-4.46317	33.72325	38.18641	6.502767	-0.14269	6.360073	0	192.5523	4.025842	15.3306
	10	15.26264	11.89515	0.576578	-4.28992	35.42658	39.7165	6.760666	-0.15355	6.607114	0	200.1889	4.126346	15.93861
BW20	3	11.5971	9.409948	0.402685	-5.47625	27.55904	33.03529	4.53668	-0.16567	4.371014	0	134.3348	2.819366	10.69545
	5	12.82771	11.0705	0.356638	-4.95795	32.61148	37.56943	5.190574	-0.18407	5.006501	0	153.6972	3.207469	12.23704
	7													

## APPENDIX N. Data analysis result of diesel engine testing

Tested Fuel : Petron Diesel Max      Low Heating value =      45.488 MJ/kg  
 Density =      830 kg/m<sup>3</sup>

Torque (N.m)	Brake Power (kW)	BMEP (bar)	Fuel Consumption			BSFC (g/kWh)	Brake Thermal Eff. (%)	Air Consumption					AFR calculated	
			Vol. (ml)	Time (s)	Flowrate (g/h)			Amb. Press. (mbar)	Amb. Temp. (°C)	Density (kg/m <sup>3</sup> )	Δ H (mmH <sub>2</sub> O)	Flowrate (g/h)		Humidity (% RH)
3.0	0.7850	1.1775	5	34.07	438.47	558.57	14.17	1006	26.5	1.170	10.54	23740.42	80	54.14
5.0	1.3083	1.9625	5	28.35	527.05	402.84	19.64	1005	26.7	1.168	10.56	23739.44	80	45.04
7.0	1.8317	2.7475	5	23.41	638.19	348.42	22.71	1005	27.1	1.166	10.16	23269.96	79	36.46
9.0	2.3550	3.5325	5	20.05	745.14	316.41	25.01	1005	27.3	1.166	9.55	22553.08	79	30.27
10.0	2.6167	3.9250	5	17.16	870.63	332.72	23.78	1005	27.7	1.164	9.61	22608.76	79	25.97

Torque (N.m)	Power (kW)	NO <sub>x</sub> (ppm)	O <sub>2</sub> (%)	CO (%)	CO <sub>2</sub> (%)	HC (ppm)	Smoke Number (BSN)	Exh rate (g/h)	Exh rate (kg/min)	BSNO <sub>x</sub> (g/kWh)	BSCO (g/kWh)	BSCO <sub>2</sub> (g/kWh)	BSHC (g/kWh)
3.0	0.7850	38	3.4	0.08	1.3	11	3	24178.9	0.40298	1.853	22.788	591.074	0.1680
5.0	1.3083	52	3.3	0.09	1.7	12	5	24266.5	0.40444	1.537	16.705	468.328	0.1044
7.0	1.8317	61	3.1	0.10	2.1	13	7	23908.2	0.39847	1.261	12.596	415.271	0.0832
9.0	2.3550	73	2.9	0.11	2.7	15	9	23298.2	0.3883	1.138	10.502	409.673	0.0715
10.0	2.6167	92	2.5	0.13	3.1	16	9	23479.4	0.39132	1.312	11.257	421.418	0.0674

Torque (N.m)	Power (kW)	Temperature (oC)			
		T1	T2	T3	T4
3.0	0.7850	26	61	277	75
5.0	1.3083	28	64	331	83
7.0	1.8317	30	70	398	98
9.0	2.3550	30	78	458	122
10.0	2.6167	30	92	484	129

T1 = Intake Air Temperature  
 T2 = Engine Block Temperature  
 T3 = Exhaust Manifold Temperature  
 T4 = Exhaust Gas Temperature



### APPENDIX N. Data analysis result of diesel engine testing (cont'd)

Tested Fuel : BP10

Low Heating value = 45.311 MJ/kg

Density = 832 kg/m<sup>3</sup>

Torque	Brake Power	BMEP	Fuel Consumption			BSFC	Brake Thermal Eff.	Air Consumption					AFR calculated	
			Vol.	Time	Flowrate			Amb. Press.	Amb. Temp.	Density	Δ H	Flowrate		Humidity
(N.m)	(kW)	(bar)	(ml)	(s)	(g/h)	(g/kWh)	(%)	(mbar)	(°C)	(kg/m <sup>3</sup> )	(mmH <sub>2</sub> O)	(g/h)	(% RH)	
3.0	0.7850	1.1775	5	32.14	465.99	593.62	13.38	1006	25.0	1.176	9.88	23042.35	80	49.45
5.0	1.3083	1.9625	5	25.92	577.71	441.56	17.99	1006	26.0	1.172	9.65	22729.03	80	39.34
7.0	1.8317	2.7475	5	21.43	698.81	381.52	20.82	1006	25.7	1.173	9.60	22685.07	80	32.46
9.0	2.3550	3.5325	5	17.73	844.84	358.75	22.15	1006	26.0	1.172	9.42	22458.86	80	26.58
10.0	2.6167	3.9250	5	15.47	967.80	369.86	21.48	1006	26.0	1.172	8.50	21333.97	80	22.04

Torque	Power	NO <sub>x</sub>	O <sub>2</sub>	CO	CO <sub>2</sub>	HC	Smoke No.	Exh rate	Exh rate	BSNO <sub>x</sub>	BSCO	BSCO <sub>2</sub>	BSHC
(N.m)	(kW)	(ppm)	(%)	(%)	(%)	(ppm)	(BSN)	(g/h)	(kg/min)	(g/kWh)	(g/kWh)	(g/kWh)	(g/kWh)
3.0	0.7850	48	3.9	0.07	1.1	11	3	23508.3	0.39181	2.260	19.266	499.066	0.1561
5.0	1.3083	64	3.6	0.08	1.5	11	6	23306.7	0.38845	1.805	13.752	413.821	0.0974
7.0	1.8317	73	3.6	0.08	2.0	12	7	23383.9	0.38973	1.469	10.266	393.270	0.0755
9.0	2.3550	84	3.4	0.09	2.7	13	9	23303.7	0.3884	1.316	8.594	404.772	0.0636
10.0	2.6167	103	3.2	0.12	3.0	14	9	22301.8	0.3717	1.385	10.144	391.673	0.0588

Torque	Power	Temperature (oC)			
		T1	T2	T3	T4
3.0	0.7850	26	54	255	64
5.0	1.3083	27	63	325	89
7.0	1.8317	27	66	390	100
9.0	2.3550	28	71	458	114
10.0	2.6167	28	77	521	316

T1 = Intake Air Temperature  
 T2 = Engine Block Temperature  
 T3 = Exhaust Manifold Temperature  
 T4 = Exhaust Gas Temperature

### APPENDIX N. Data analysis result of diesel engine testing (cont'd)

Tested Fuel : BP20

Low Heating value = 44.624 MJ/kg

Density = 835 kg/m<sup>3</sup>

Torque	Brake Power	BMEP	Fuel Consumption			BSFC	Brake Thermal Eff.	Air Consumption					AFR calculated	
			Vol.	Time	Flowrate			Amb. Press.	Amb. Temp.	Density	Δ H	Flowrate		Humidity
(N.m)	(kW)	(bar)	(ml)	(s)	(g/h)	(g/kWh)	(%)	(mbar)	(°C)	(kg/m <sup>3</sup> )	(mmH <sub>2</sub> O)	(g/h)	(% RH)	
3.0	0.7850	1.1775	5	31.78	472.97	602.51	13.39	1006	26.0	1.172	9.93	23054.94	80	48.74
5.0	1.3083	1.9625	5	25.53	588.80	450.04	17.92	1006	25.5	1.174	9.71	22818.39	80	38.75
7.0	1.8317	2.7475	5	20.81	722.16	394.26	20.46	1006	27.0	1.168	9.50	22516.40	80	31.18
9.0	2.3550	3.5325	5	17.17	875.19	371.63	21.71	1006	27.1	1.168	9.40	22395.09	80	25.59
10.0	2.6167	3.9250	5	15.02	1000.67	382.42	21.09	1006	27.4	1.167	8.57	21368.69	80	21.35

Torque	Power	NO <sub>x</sub>	O <sub>2</sub>	CO	CO <sub>2</sub>	HC	Smoke Number	Exh rate	Exh rate	BSNO <sub>x</sub>	BSCO	BSCO <sub>2</sub>	BSHC
(N.m)	(kW)	(ppm)	(%)	(%)	(%)	(ppm)	(BSN)	(g/h)	(kg/min)	(g/kWh)	(g/kWh)	(g/kWh)	(g/kWh)
3.0	0.7850	53	4.2	0.06	1.0	11	3	23527.9	0.39213	2.531	18.318	469.209	0.1548
5.0	1.3083	71	4.1	0.07	1.5	12	6	23407.2	0.39012	2.011	12.661	397.534	0.0998
7.0	1.8317	81	3.9	0.08	1.9	13	7	23238.6	0.38731	1.627	9.794	358.791	0.0789
9.0	2.3550	96	3.7	0.09	2.5	14	8	23270.3	0.38784	1.502	8.264	374.251	0.0677
10.0	2.6167	115	3.4	0.10	2.9	15	8	22369.4	0.37282	1.557	8.250	371.274	0.0600

Torque	Power	Temperature (oC)			
		T1	T2	T3	T4
3.0	0.7850	26	54	247	64
5.0	1.3083	27	63	323	84
7.0	1.8317	27	66	388	113
9.0	2.3550	28	71	453	106
10.0	2.6167	29	77	506	316

T1 = Intake Air Temperature

T2 = Engine Block Temperature

T3 = Exhaust Manifold Temperature

T4 = Exhaust Gas Temperature

### APPENDIX N. Data analysis result of diesel engine testing (cont'd)

Tested Fuel : BW10

Low Heating value = 44.016 MJ/kg

Density = 835 kg/m<sup>3</sup>

Torque	Brake Power	BMEP	Fuel Consumption			BSFC	Brake Thermal Eff.	Air Consumption					AFR calculated	
			Vol.	Time	Flowrate			Amb. Press.	Amb. Temp.	Density	Δ H	Flowrate		Humidity
(N.m)	(kW)	(bar)	(ml)	(s)	(g/h)	(g/kWh)	(%)	(mbar)	(°C)	(kg/m <sup>3</sup> )	(mmH <sub>2</sub> O)	(g/h)	(% RH)	
3.0	0.7850	1.1775	5	30.46	493.50	628.66	13.01	1006	26.1	1.172	9.77	22873.63	85	46.35
5.0	1.3083	1.9625	5	24.44	614.88	469.97	17.40	1006	26.2	1.171	9.57	22624.20	85	36.79
7.0	1.8317	2.7475	5	19.97	752.73	410.95	19.90	1006	26.5	1.170	9.37	22376.49	85	29.73
9.0	2.3550	3.5325	5	16.45	913.55	387.92	21.08	1006	26.6	1.170	9.33	22329.72	85	24.44
10.0	2.6167	3.9250	5	14.50	1036.55	396.13	20.64	1006	27.5	1.166	8.26	20981.46	85	20.24

Torque	Power	NO <sub>x</sub>	O <sub>2</sub>	CO	CO <sub>2</sub>	HC	Smoke Number	Exh rate	Exh rate	BSNO <sub>x</sub>	BSCO	BSCO <sub>2</sub>	BSHC
(N.m)	(kW)	(ppm)	(%)	(%)	(%)	(ppm)	(BSN)	(g/h)	(kg/min)	(g/kWh)	(g/kWh)	(g/kWh)	(g/kWh)
3.0	0.7850	62	3.9	0.05	0.9	10	4	23367.1	0.38945	2.906	13.405	390.841	0.1424
5.0	1.3083	79	3.7	0.05	1.3	11	5	23239.1	0.38732	2.231	9.142	349.830	0.0920
7.0	1.8317	94	3.6	0.07	1.8	12	7	23129.2	0.38549	1.886	7.921	337.973	0.0711
9.0	2.3550	106	3.4	0.07	2.3	13	8	23243.3	0.38739	1.656	6.667	338.927	0.0606
10.0	2.6167	122	3.3	0.09	2.7	14	8	22018.0	0.36697	1.621	7.308	339.947	0.0570

Torque	Power	Temperature (oC)			
		T1	T2	T3	T4
3.0	0.7850	27	52	260	72
5.0	1.3083	28	59	322	85
7.0	1.8317	28	66	442	99
9.0	2.3550	28	68	456	131
10.0	2.6167	28	72	481	134

T1 = Intake Air Temperature

T2 = Engine Block Temperature

T3 = Exhaust Manifold Temperature

T4 = Exhaust Gas Temperature

### APPENDIX N. Data analysis result of diesel engine testing (cont'd)

Tested Fuel : BW20

Low Heating value = 43.801 MJ/kg

Density = 855 kg/m<sup>3</sup>

Torque	Brake Power	BMEP	Fuel Consumption			BSFC	Brake Thermal Eff.	Air Consumption					AFR calculated	
			Vol.	Time	Flowrate			Amb. Press.	Amb. Temp.	Density	Δ H	Flowrate		Humidity
(N.m)	(kW)	(bar)	(ml)	(s)	(g/h)	(g/kWh)	(%)	(mbar)	(°C)	(kg/m <sup>3</sup> )	(mmH <sub>2</sub> O)	(g/h)	(% RH)	
3.0	0.7850	1.1775	5	31.00	496.51	632.49	12.99	1006	27.1	1.168	9.87	22946.87	79.3333	46.22
5.0	1.3083	1.9625	5	24.46	629.11	480.85	17.09	1006	27.4	1.166	9.74	22787.76	79	36.22
7.0	<b>Engine shut down at 2300 rpm</b>													

Torque	Power	NO <sub>x</sub>	O <sub>2</sub>	CO	CO <sub>2</sub>	HC	Smoke Number	Exh rate	Exh rate	BSNO <sub>x</sub>	BSCO	BSCO <sub>2</sub>	BSHC
(N.m)	(kW)	(ppm)	(%)	(%)	(%)	(ppm)	(BSN)	(g/h)	(kg/min)	(g/kWh)	(g/kWh)	(g/kWh)	(g/kWh)
3.0	0.7850	68	3.5	0.04	2.5	9	4	23443.4	0.39072	3.231	11.528	1131.105	0.1238
5.0	1.3083	85	3.5	0.04	3.3	8	6	23416.9	0.39028	2.399	6.333	903.861	0.0656
7.0	<b>Engine shut down at 2300 rpm</b>												

Torque	Power	Temperature (oC)			
		T1	T2	T3	T4
3.0	0.7850	29	59	286	396
5.0	1.3083	29	61	357	359
7.0	<b>Engine shut down at 2300 rpm</b>				

T1 = Intake Air Temperature  
 T2 = Engine Block Temperature  
 T3 = Exhaust Manifold Temperature  
 T4 = Exhaust Gas Temperature

**APPENDIX O**  
**List of Publication**

**JOURNALS**

1. **Nur Hamzah Said**, Farid Nasir Ani, Mohd Farid Muhamad Said. (2015). Review of the production of biodiesel from waste cooking oil using solid catalyst. *Journal of Mechanical Engineering and Sciences (JMES)*, 8, 1302-3111.
2. Ani, F.N., **Said, N.H.**, Said, M.F.M. (2018). Optimization of biodiesel production using a stirred packed-bed reactor. *International Journal of Technology*. 9(2), 129-138.
3. **Said, N.H.**, Ani, F.N., Said, M.F.M. (2018). Emission and performance characteristics of waste cooking oil biodiesel blends in a single direct injection Diesel engine. *International Journal of Technology*, 9(2), 148-155.

**CONFERENCES**

4. **Nur Hamzah Said**, Farid Nasir Ani, Mohd Farid Muhamad Said. (2014). A Specific review on production of biodiesel from waste cooking oil using solid catalyst. Presented at *International Conference on Automotive Innovation and Green Energy Vehicle 2014*, Pahang, 26-27 August 2014.
5. **Nur Hamzah Said**, Farid Nasir Ani, Mohd Farid Muhamad Said. (2017). Emission and performance characteristics of waste cooking oil biodiesel blends in a single cylinder DI diesel. Presented at *the 2<sup>nd</sup> International Tropical Renewable Energy (the 2<sup>nd</sup> i-TREC) 2017*, Bali, 3-4 October 2017.